V.M. van Deursen

Long-term creep behavior of CFRP in actively bent grid shells

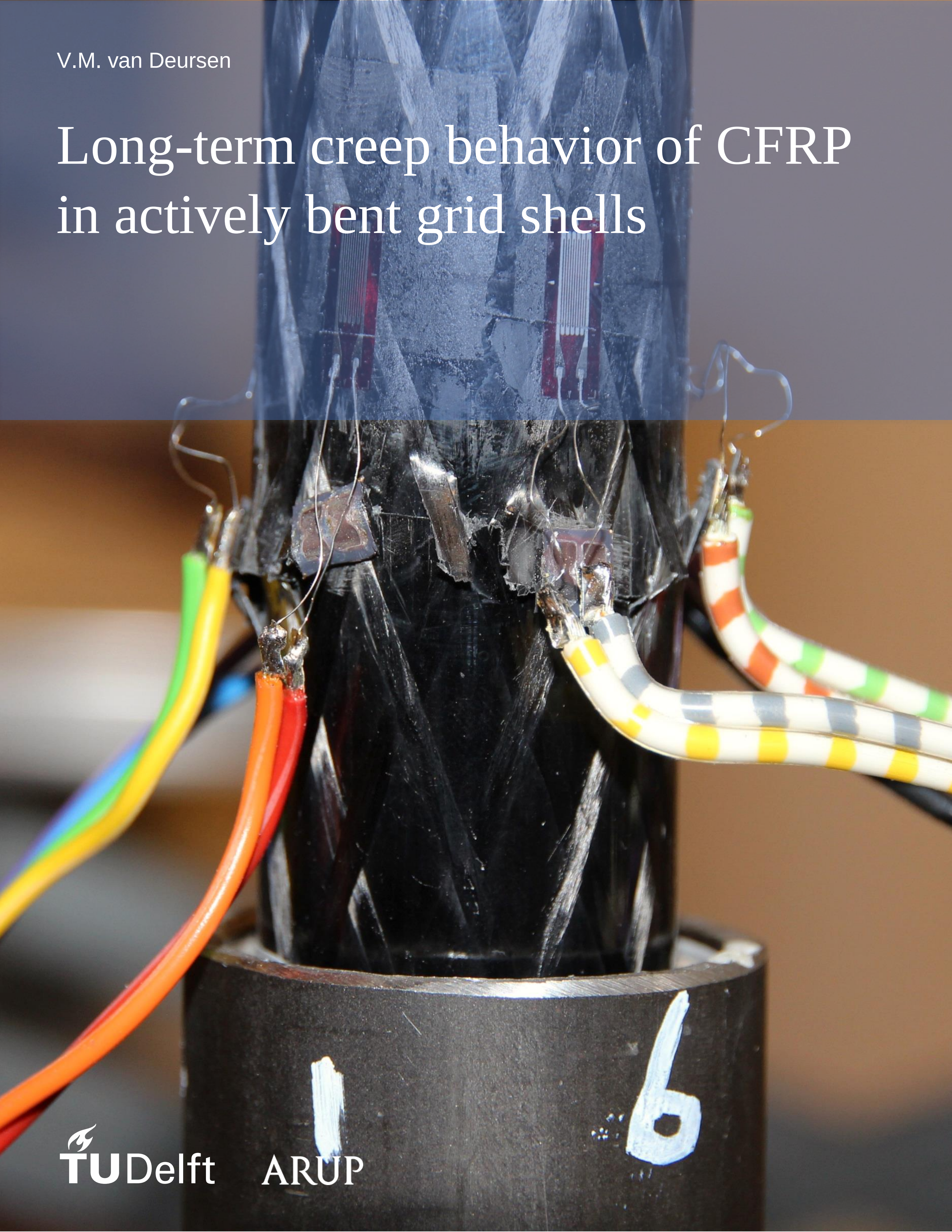

TU Delft ARUP

Long-term creep behavior of CFRP in actively bent grid shells

By

V.M. van Deursen

in partial fulfilment of the requirements for the degree of

Master of Science
in Civil Engineering

at the Delft University of Technology,
to be presented on Friday September 1, 2017 at 14:00 AM.

Student number:	4006283	
Project duration:	October 2016 – August 2017	
Thesis committee:	Prof. dr. M.V. Veljkovic,	TU Delft
	Dr. M. Pavlovic,	TU Delft
	Dr. ir. O.K. Bergsma,	TU Delft
	Ir. R.J. van de Straat,	Arup

Preface

In front of you lies the report of my thesis on long-term creep behavior of Carbon Fiber Reinforced Polymer (CFRP) in actively bent grid shells. This thesis is the final project for the master's degree in Building Engineering at the Faculty of Civil Engineering of the Delft University of Technology.

Most of the thesis has been performed at the office of Arup in Amsterdam. During the period of my research, I have been part of their department for structural engineering. I felt lucky to be surrounded by such ambitious engineers, which all have a strong tendency to strive for high quality work. Personally, I am interested in both architecture and engineering aspects of building design. I believe that a building design is not only about the aesthetics of the design, but primarily about the integration of all the different aspects that have to be considered. This is actually the main reason why I chose to proceed my education in building engineering after I graduated from my degree in architecture.

Enjoying the integration of these different aspects has also led to the subject of my thesis. In addition, I am very interested in the growing use of Fiber Reinforced Polymers (FRP) in the building engineering practice. An innovative solution, such as actively bent grid shells, confirms the usefulness of structures with FRP materials. It has been my aim in this project, to provide more insight for structural engineers into using CFRP as construction material for actively bent grid shells in the field of structural design of buildings.

Acknowledgment

First I would like to thank Arup Amsterdam in general. Within Arup I would like to thank Mathew Vola for getting me on board and for providing me the opportunity to follow my own research path. A special thanks to Roel van de Straat, for his guidance in keeping the overview and setting clear research goals and approach.

From the Delft University of Technology I would like to express my gratitude towards Milan Veljkovic, for chairing the thesis committee. I would like to give a special thanks to Marko Pavlovic, for his willingness to always help me during the thesis and for the helpful discussions regarding my results. I would also like to thank Otto Bergsma for this expertise in FRP materials. Finally, I would like to thank Fred Schilperoort and John Hermsen for their expertise and help related to the experiments.

I would like to thank PFT Profiles in general for providing me with the specimens for the experiments. A special thanks to Paul Olde Bolhaar for managing.

Last but not least, I would like to express my gratitude towards my parents, Hein and Brigitte van Deursen, for their support and the freedom they have given me during my studies and other endeavors. A special thanks to my godmother, Charlotte van Wylick, for encouraging my creativity. Finally, I would like to thank Bart, for his endless support and positivity.

Amsterdam, August 2017
V.M. van Deursen

Summary

Actively bent grid shells are curved structural surfaces made of flexible members. The application is mainly in roof structures. The members, spanning between two supports on the perimeter, are connected at their intersections by joints, and assembled in an initially straight grid. By lifting at a sufficient number of points the straight grid is subsequently transformed into a bent shape and new geometry is preserved by fixing the supports. Subsequently, the curved surface is braced with a third layer of flexible members. According to this specific principle of construction, actively bent grid shells can be built within a short period of time.

ThinkShell, a research team at École des Ponts ParisTech, has developed a number of actively bent Glass Fiber Reinforced (GFRP) grid shells over the last ten years. Due to mechanical properties such as lightweight, high elastic limit strain, and high stiffness, Carbon Fiber Reinforced Polymer (CFRP) becomes an interesting material choice for construction of long-span actively bent grid shells. CFRP is part of a family of fiber reinforced composites and is a relatively new material in the Architecture, Engineering, and Construction (AEC) industry.

In the actively bent members of the grid shells considerable amount of permanent stresses is present. The main source of stress is caused by the transformation of the straight grid into a bent shape during erection. Fiber Reinforced Polymer (FRP) is sensitive to creep behavior, which may lead to possible collapse mechanism due to creep-rupture or creep-buckling as a result of reduced stiffness of the material on a long-term. Limited knowledge is available of the time-dependent long-term creep behavior of CFRP, in the field of structural design of buildings. The main objective of this research was to define stress limits related to time-dependent long-term creep behavior of CFRP in members of actively bent grid shells, using the Stepped Isostress Method (SSM).

Insight into the field of actively bent grid shells has been provided by a literature review of definitions and principles of actively bent grid shell design, analysis, and construction. Literature review was also done to gain insight in creep characteristics of CFRP and methods to study corresponding time-dependent creep behavior on a long-term. Special attention was paid to recommendations for sustained stress limits to avoid creep-rupture.

To analyze the behavior of the actively bent members of the grid shells, an analytic model has been derived with the finite element analysis software SOFiSTiK. The model was used to study structural forms and in-plane buckling resistance of members of actively bent grid shells. Actively bent members in GFRP and CFRP were compared. Assessment was made based on FEM analysis and sustained stress limits to avoid creep-rupture from literature.

To study creep deformation and creep-rupture behavior of CFRP in members of actively bent grid shells, accelerated creep experiments were performed, based on the Stepped Isostress Method (SSM). Creep tests were performed on specimens made of epoxy and carbon fibers, which were loaded in tension, compression, and bending. As part of the SSM experiments, test data from bending experiments was used to construct final creep curves, from which predictions for creep behavior of CFRP on a long-term were made.

With regard to the literature review and the numerical analysis with SOFiSTiK, the following results and conclusions were obtained during the project. The sustained stress limit to avoid creep-rupture for CFRP from CUR96 is not applicable to all design cases, as it has resulted from creep-rupture tests performed on 6 mm diameter FRP bars that were loaded in tension. From the in-plane buckling analysis of an actively bent member it was concluded that the higher the amount of pre-bending, the higher the corresponding critical load. In addition, if the sustained stress in GFRP and CFRP members of equal dimensions, but with different elastic modulus, is below their corresponding stress limit for creep-rupture (0.2 fult and 0.55 fult respectively, based on CUR96), the CFRP member is available for a point load at mid-span which is 11 times larger compared to the GFRP member. This might be of influence in driving the choice for using a material (e.g. CFRP over GFRP) that has better creep-rupture behavior in members of actively bent grid shells.

An important conclusion drawn from the experiments using the SSM is that, in actively bent grid shell design, it is crucially important to stay below the sustained stress limits to avoid creep-rupture, as the CFRP fails in a brittle manner. From the SSM analysis using test data from bending experiments it was concluded that if the permanent load in the CFRP is 55% of the ultimate load, creep-rupture will happen in 40 days. This result does not seem realistic as the sustained stress limit from CUR96 corresponds to a service life of 50 years. Out of the four steps in processing of raw test data using the SSM, the rescaling step is the most critical step. There is strong dependence between the rescaling step and the horizontal shifting step. To determine the rescaling values and horizontal shifting for the bending experiments, a corresponding conventional creep tests as a reference test is proposed.

The SSM represents a promising method for accelerated creep testing and corresponding test data analysis for CFRP in members of actively bent grid shells. Sustained stress limits derived from the SSM may be used as more realistic, i.e. less conservative stress limit values to avoid creep-rupture, compared to the values defined in CUR96, for the specific design parameters.

Contents

1. Introduction

1.1. Motivation

This Master's Thesis focuses on creep behavior of Carbon Fiber Reinforced Polymer (from here stated as CFRP) in members of actively bent grid shells. The geometric shape of this type of grid shells is a result of a combination of material behavior and related structural typology. The thesis will provide insight in the structural characteristics of the system and experimentally investigates the creep phenomenon on CFRP specimens. The problem that structural engineers face at this moment is the limited knowledge available of the time-dependent long-term creep behavior of CFRP. The outcome of this Master's Thesis will provide insight for structural engineers into using CFRP as construction material for actively bent grid shells in the field of structural design of buildings.

Motivation will be discussed under three categories: structural typology (Section 1.1.1), choice of material (Section 1.1.2), and scientific gap (Section 1.1.3).

1.1.1. Structural typology

Actively bent grid shells are curved structural surfaces made of flexible members. The application is mainly in roof structures. The members, spanning between two supports on the perimeter, are connected at their intersections by joints, and assembled in an initially straight grid. By lifting at a sufficient number of points the straight grid is subsequently transformed into a bent shape and new geometry is preserved by fixing the supports. Subsequently, the curved surface is braced with for example a third layer of flexible members. According to this specific principle of construction, actively bent grid shells can be built within a short period of time.

ThinkShell, a research team at École des Ponts ParisTech, has developed a number of actively bent Glass Fiber Reinforced Polymer (GFRP) grid shells over the last ten years. Figure 1.1 presents the lifting of their grid shell of the Ephemeral Cathedral, in which the use of GFRP has resulted in large spans with very little material.

Figure 1.1 Lifting of the initial straight grid of the Ephemeral Cathedral in Paris (THINkSHELL, 2013)

1.1.2. Choice of material

Due to mechanical properties such as lightweight, high elastic limit strain, and high stiffness, CFRP becomes an interesting material choice for construction of actively bent grid shells. CFRP is part of a family of fiber reinforced composites and is a relatively new material in the Architecture, Engineering, and Construction (AEC) industry. CFRP consists of two major ingredients: carbon fibers and a polymeric resin. It has a high-strength to low-weight ratio and a unique high-strength to low-bending stiffness ratio compared to traditional building materials such as concrete and steel. Due to the material's low density and high ultimate limit strain, CFRP embodies great potential for lightweight, long-span actively bent grid shells.

The material's demand is globally growing rapidly as strong and lightweight alternative to for instance metal. It is used by engineers in all different kinds of fields to create complex shapes with double-curved elements. However, the structural engineer is relatively unknown with the implementation of CFRP as construction material in the field of structural design of buildings. Therefore, CFRP deserves further investigation of application in this field.

1.1.3. Scientific gap

In the actively bent members of the grid shells considerable amount of permanent stresses is present. The main source of stress is caused by the transformation of the straight grid into a bent shape during construction. Fiber Reinforced Polymer (FRP) is sensitive to creep behavior, which may lead to possible collapse mechanisms due to creep-rupture or creep-buckling as a result of reduced stiffness of the material on a long-term.

Limited knowledge is available of the time-dependent long-term creep behavior of CFRP, in the field of structural design of buildings. The main objective of this research is to provide more insight in the long-term creep behavior of CFRP in members of actively bent grid shells, an application where the material is subjected a considerable amount of permanent stresses. The Stepped Isostress Method (SSM) is used to perform creep experiments and corresponding test data analysis.

1.2. Aim of the research

This section presents the aim and main research question of this thesis (Section 1.2.1). The accompanying key questions are presented (Section 1.2.2), followed by the explanation of the scope of this thesis (Section 1.2.3).

1.2.1. Aim and main research question

The aim of this thesis is to define recommendations for design stresses for CFRP in members of actively bent grid shells with respect to creep. To achieve this aim, the objective is to define stress limits related to time-dependent long-term creep behavior of CFRP in members of actively bent grid shells, using the <u>S</u>tepped Iso<u>s</u>tress <u>M</u>ethod (SSM).

The accompanying main research question reads:

Which stress limits related to time-dependent long-term creep behavior of CFRP in members of actively bent grid shells can be defined using the Stepped Isostress Method?

1.2.2. Key questions

To answer the main research question, the following key questions are defined:

1. What are general characteristics of actively bent grid shells?

2. What are creep characteristics of CFRP and what are methods to study the time-dependent long-term behavior?

3. What are relevant effects of the creep phenomenon on pultruded CFRP specimens derived from SSM experiments?

4. How to define recommendations for design stresses for CFRP in members of actively bent grid shells, based on the study of long-term creep and experiments?

1.2.3. Scope of the research

The research will be focused on the time-dependent long-term creep behavior of CFRP in members of actively bent grid shells. Investigation of long-term creep behavior of CFRP in actively bent grid shells as a whole, is beyond the scope of this thesis.

To study the structural performance of actively bent members, a two-dimensional in-plane buckling analysis will be performed with FEA software SOFiSTiK. Simple load cases will be performed on a tubular member with constant cross-section. Other analyses of the structural performance of actively bent members are beyond the scope of this thesis. Sustained stress limits to avoid creep-rupture from CUR96 will be used for a creep-rupture analysis with SOFiSTiK. The implementation of stress limits resulting from the performed creep experiments is beyond the scope of this thesis.

Creep experiments will be carried out on pultruded CFRP material at element-scale. Tubular specimens will be tested under tensile, compressive, and flexural loading, according to the Stepped Isostress Method (SSM). The CFRP specimens used for SSM creep experiments have fiber reinforcement which is not purely unidirectional, therefore the results of the bending experiments will not be representative at the material level. Results from bending experiments will therefore be used to present 'apparent' creep behavior. Tensile and compressive creep experiments will be performed to investigate creep behavior in tension and compression respectively. Results from tension and compression experiments could be used to calculate expected creep response in bending, but this is beyond the scope of this thesis.

1.3. Methodology

The methods that will be used to answer the key questions and ultimately, the main research question, are presented in this section. The thesis and its accompanying final report are divided in four parts.

Part I: Literature study

In part I, insight into the field of actively bent grid shells will be provided by a literature study of definitions and principles of actively bent grid shell design, analysis, and construction. Literature study will also be done to gain insight in creep characteristics of CFRP and methods to study corresponding time-dependent creep behavior on a long-term. Special attention will be paid to recommendations for sustained stress limits to avoid creep-rupture.

Part II: Numerical analysis

In part II, to analyze the behavior of the actively bent members of the grid shells, an analytic model will be derived with the finite element analysis software SOFiSTiK. The model will be used to study structural forms and in-plane buckling resistance of members of actively bent grid shells. To study the importance of using a material that has better creep-rupture behavior in members of actively bent grid shells, members in GFRP and CFRP will be compared. Assessment will be made based on FEM analysis and sustained stress limits to avoid creep-rupture from CUR96.

Part III: Experiments

In part III, accelerated creep experiments based on the Stepped Isostress Method (SSM) will be performed on pultruded CFRP specimens made of Epikote epoxy resin and Toho Tenax carbon fibers. Creep deformation and creep-rupture behavior of specimens loaded in tension, compression, and bending will be studied. As part of the SSM experiments, test data will be used to construct final creep curves, from which predictions for design stresses for CFRP in members of actively bent grid shells on a long-term will be made.

Part IV: Reporting

1.4. Outline

For every part the content of each chapter will be explained.

Part I: Literature review

Chapter 2 presents definitions and principles related to shells, grid shells, and actively bent grid shells. Long-term creep characteristics of CFRP and methods to study related time-dependent long-term behavior are presented in Chapter 3.

Part II: Numerical analysis

A two-dimensional in-plane buckling analysis of an actively bent member in SOFiSTiK is presented in Chapter 4. The chapter also presents the importance of using a material has better creep-rupture behavior (e.g. CFRP over GFRP) in members of actively bent grid shells.

Part III: Experiments

Chapter 5 presents the procedure of creep testing and corresponding test data analysis using the Stepped Isostress Method (SSM). Results of experiments using the SSM performed on pultruded CFRP specimens loaded in tension, compression, and bending, are presented in Chapters 6, 7, and 8 respectively. Chapter 9 presents a summary of creep test results using the SSM.

Part IV: Reporting

In the concluding chapter the results of this thesis focusing on creep behavior of CFRP in members of actively bent grid shells are presented. The chapter consists of two parts: the first part provides feedback and answers to the main- and key questions of the research. In the second part recommendations for future research in fields where this research can be further improved and extended are presented.

PART I LITERATURE STUDY

2. General characteristics of actively bent grid shells

This chapter will give the reader an insight into the field of a specific type of grid shells, namely actively bent grid shells. Section 2.1 presents definitions of shells, grid shells, and actively bent grid shells. Section 2.2 presents construction principles related to bracing and detailing of actively bent grid shells. Structural principles of the system are presented in Section 2.3. An overview of the most likely collapse mechanisms of actively bent grid shells is presented in Section 2.4. Six grid shells constructed over time are explored and can be found in Annex A.

2.1. Definitions of shells, grid shells, and actively bent grid shells

A classification of structures can be made in many ways according to their shape, their function and the materials used for construction. This section introduces the definitions of respectively shells, grid shells, and actively bent grid shells.

2.1.1. Shells

A shell is a structure defined by a three-dimensional curved surface. It is defined by its thickness, its dimensions, and material properties. The thickness of shells is significantly smaller compared to the dimensions of the two other directions. A shell might be curved in only in one direction, like a cylinder, or it might be curved in two directions, like a dome. Shells are form-passive and due to their curved surface, they resist external loads predominantly through membrane stresses (Adriaenssens, Block, Veenendaal, & Williams, 2014)

2.1.2. Grid shells

A grid shell can be defined as a structural *grid* following the shape of a double-curved *shell*. The grid surface is made of members which are spaced in a regular manner and form a net of triangles, squares, or other discrete surface geometries. Apart from stresses due to self-weight, these grid shells are free of stresses in their initial configuration (Adriaenssens et al., 2014). The term 'pre-formed' grid shells is used in this thesis to distinguish from actively bent grid shells.

A grid shell derives its strength from its double-curvature and the structural grid often follows a free-curved[1] shape. The geometrical layout of a grid shell can therefore not be defined with standard geometrical shapes. Form-finding (see Chapter 4) is often used to develop the geometrical form of a grid shell, as they are able to define the structural system with conventional mathematical equations (Fritzsche, 2013).

2.1.3. Actively bent grid shells

Actively bent grid shells are to create curved structural surfaces made of flexible members. The members, spanning between two supports on the perimeter, are connected at their intersections by joints, and assembled in an initially straight grid (see Figure 2.1). By lifting at sufficient number of points the straight grid is subsequently transformed into a bent shape and new geometry is preserved by fixing the supports. Subsequently, the curved surface is braced with for example a third layer of flexible members (Section 2.2.1). According to this specific principle of construction, actively bent grid shells can be built within a short period of time.

[1]Free-curved, or freeform shells are generated without taking structural performance into account (Adriaenssens et al., 2014).

Figure 2.1 Members assembled in the initial straight grid of the Ephemeral Cathedral (THINkSHELL, 2013)

2.2. Construction principles of actively bent grid shells

In this section construction principles related to bracing (2.2.1) and detailing (2.2.2) of actively bent grid shells are introduced.

2.2.1. Bracing

According to the specific principle of construction of actively bent grid shells, a straight grid is transformed into a bent shape, by lifting a sufficient number of points. After fixing the supports on the perimeter, the preserved new geometry is braced, to obtain in-plane shear stiffness of the structure. Compared to the short period of time in which the initial straight grid is transformed into a curved surface, the additional bracing of the structure is relatively time consuming.

There are different ways to brace the curved surface, which are still being investigated. Three possibilities of bracing systems are presented in Figures 2.2, 2.3, and 2.4. Figure 2.2 presents bracing of the curved surface with a third layer of flexible members, which are similar to the members used for construction of the initial grid. In Figure 2.3, the surface bracing is regulated per square with tension rods and wooden plates. In Figure 2.4, bracing of the curved surface is done by a thin layer of concrete.

2.2.2. Construction details

The actively bent grid shells studied in this thesis use the bending capability of long and slender members within a specific construction process. Due to the specific principle of construction, the members spanning between two supports on the perimeter, which are assembled in an initially straight grid, are connected at their intersections with relatively simple joints. This is a great advantage, as complex joints connecting short members spanning from node to node, which are often found in pre-formed grid shells, can be avoided.

To provide an overview of construction details of actively bent grid shells, the four main structural details of the Ephemeral Cathedral (2013), developed by ThinkShell, are presented in Figure 2.5. The structural details consist of:

- Standard swivel scaffolding couples (1130 pieces) connecting the members of the grid shell at their intersections;
- Steel sleeves (125 pieces) connecting pieces of tubes to make long members;
- Ground anchorages (123 pieces) fixing the actively bent members of the grid shell to the slab;
- The perimeter lacing the canvas;

Figure 2.2 Bracing of the curved surface with a third layer of flexible members (THINkSHELL, 2013)

Figure 2.3 Bracing of the curved surface with tension rods (THINkSHELL, 2016a)

Figure 2.4 Bracing of the curved surface with a thin layer of concrete (THINkSHELL, 2016b)

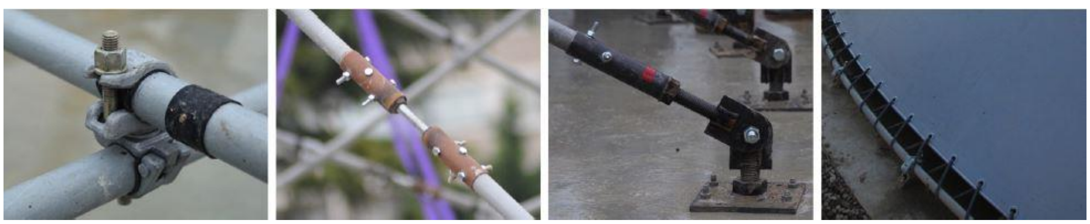

Figure 2.5 Construction details of the Ephemeral Cathedral: swivel scaffolding couplers, steel sleeves, ground anchorages, edge beam (Du Peloux, Tayeb, Caron, & Baverel, 2015)

2.3. Structural principles of shells, pre-formed grid shells, and actively bent grid shells

The structural principles of grid shells correspond to the structural principles of shells. In contrast to a flat plate, a shell is a structure defined by a three-dimensional curved surface. The main difference between grid shells and shells is that grid shells are made of individual members in a curved grid instead of a curved continuous surface. In all three cases corresponding to shells, pre-formed grid shells, and actively bent grid shells, the thickness of the curved surface is significantly smaller than the dimensions of the two other directions.

Structural principles of respectively shells and pre-formed grid shells are presented in Annex B. This section presents the structural principles of actively bent grid shells. With respect to the structural behavior of actively bent grid shells, a distinction is made between membrane behavior and bending behavior.

2.3.1. Membrane behavior

Membrane behavior of shells is characterized by their ability to carry out-of-plane loads by in-plane shear and normal forces, due to their curved surface. The initial straight grid of members of actively bent grid shells is a system with one degree of freedom. According to their specific method of construction, by lifting a sufficient number of points, the straight grid is transformed into a bent shape and new geometry is preserved by fixing the supports. Subsequently, the curved surface is braced with for example a third layer of members (see

Figure 2.2), causing in-plane shear stiffness of the structure. The membrane behavior of the actively bent grid shell is now activated and the system is able to carry shear forces.

2.3.2. Bending behavior

In regions where out-of-plane loads cannot be fully carried by in-plane forces of actively bent grid shells, bending moments are introduced in the system to compensate for this shortcoming. Similar to bending behavior of pre-formed grid shells (see Annex B), bending moments in actively bent grid shells are resisted through the cross-sections of the grid-members.

In actively bent grid shells, the main source of stress is caused by the transformation of the straight grid into a bent shape during construction. The stress in the members of the grid shells is proportional to their curvature, and the curvature is mainly due to the level of bending. The preserved geometry of the grid shell does, even under critical loads, not change significantly. High stiffness is provided, which is the main advantage of the active bending. The general formula for determining the bending stress in a curved member is given by (Tayeb, Lefevre, Baverel, & Peloux, 2015):

$$\sigma_B \frac{E\,y}{R} \tag{1}$$

where

σ_B	bending stress
E	elastic modulus
y	outer radius of member
R	bending radius

A description of non-linear beam theory and related derivation of the moment-curvature relation is presented in Annex B. The formula for the relationship between the member's curvature due to bending and bending moment is given by:

$$\frac{1}{R} = \frac{M}{EI} \tag{2}$$

where:

1/R	curvature
M	bending moment
EI	bending stiffness

ThinkShell has developed a number of Glass Fiber Reinforced Polymer (GFRP) grid shells over the last ten years. The research group states that the maximum stress in each member of the grid shells must not exceed 30% of the strength of the member, to avoid the members to break (Tayeb et al., 2015). Based on eq. 2, this limit stress gives a limit curvature. The minimum bending radius is given by:

$$R_{min} = \frac{E\,y}{\sigma_{Rd}} \tag{3}$$

where:

R_{min}	minimum bending radius
E	elastic modulus
y	outer radius of the member
σ_{Rd}	permissible stress

The formula for the related strain of the members is given by:

$$\varepsilon = \frac{\Delta l}{l} = \frac{y}{R} \quad (4)$$

where:

ε	strain
Δl	difference in length of the member
l	initial length of the member
y	outer radius
R	bending radius

The stresses in the actively bent members of the grid shells can be derived directly from their curvature. The stress rate of a grid which lies on a surface can be indicated by the principal curvatures of the surface, as the principal curvatures give a qualitative measurement of the local curvature of every curve on the surface (Tayeb et al., 2015). ThinkShell developed the following condition, which should be true in the entire grid shell:

$$E = \frac{y}{R_{min}} < \frac{\sigma_{k.flex}}{\gamma_{lt}} \quad (5)$$

where:

E	elastic modulus
y	outer radius of the member
R_{min}	minimum bending radius
$\sigma_{k.flex}$	characteristic flexural strength
γ_{lt}	partial material coefficient (long-term)

2.4. Collapse mechanisms with respect to creep

To gain insight into the possible collapse mechanisms of actively bent grid shells with respect to creep, the Mannheim Multihalle grid shell (1975) and the actively bent GFRP grid shells developed by ThinkShell over the last ten years are studied (see Annex A).

2.4.1. Creep buckling

The Manheim grid shell (see Figure 2.6) is made of timber and as timber will creep, the most likely collapse mechanism for this grid shell would be creep buckling (Adriaenssens et al., 2014). Creep (see Section 3.2.1) is the time dependent deformation of a material or structure under a constant applied load. In case of creep buckling, the structure slowly moves, causing an increase in moments and stresses leading to an increase in creep strain. Due to this progressive deformation, collapse of the axial loaded members will finally occur. The dominant parameter to control creep buckling of actively bent grid shells is the bending stiffness of the structure (Adriaenssens et al., 2014).

2.4.2. Creep-rupture

In addition to creep causing reduction in stiffness, reductions in strength may also occur. These strength reductions may finally lead to a rupture failure of the material, referred to as creep-rupture (EUROCOMP, 1996). ThinkShell, a research team at École des Ponts ParisTech, has developed a number of actively bent Glass Fiber Reinforced Polymer (GFRP) grid shells over the last ten years. A damage mechanism due to progressive rupture of fibers was observed on the actively bent members of the grid shells and is presented in Figure 2.7 (Cyril Douthe, 2007).

The primary determining factors in creep deformation of Fiber Reinforced Polymer (FRP) are the type of resin and the quality of the interface between the fibers and the resin. The dominant parameter to control the long-term behavior of FRP in actively bent grid shells is the level of permanent stress prescribed in the material (C. Douthe, Caron, & Baverel, 2010). This level of stress is addressed by the ultimate strength of the material. In actively bent FRP grid shells, an application where the material is subjected to a considerable amount of permanent stresses, it appears essential to predict the ultimate strength and deflection as functions of loading and time (C. Douthe et al., 2010).

Figure 2.6 Grid shell of the Mannheim Multihalle (1975) (Adriaenssens et al., 2014)

Figure 2.7 Rupture due to combined torsion-compression loading (Cyril Douthe, 2007)

2.5. Conclusion

This chapter has introduced definitions with respect to the structural geometry, and construction- and structural principles of actively bent grid shells. Furthermore, special attention has been paid to most likely collapse mechanisms of actively bent grid shells, with respect to creep.

Actively bent grid shells are curved structural surfaces made of flexible members. The application is mainly in roof structures. The members, spanning between two supports on the perimeter, are connected at their intersections by relatively simple joints, and assembled in an initially straight grid. By lifting at sufficient number of points the straight grid is subsequently transformed into a bent shape and new geometry is preserved by fixing the supports. Then, the surface is braced, to obtain in-plain shear stiffness of the structure. According to this specific principle of construction, actively bent grid shells can be built within a short period of time.

In actively bent members of the grid shells considerable amount of permanent stresses are present. The main source of stress is caused by the transformation of the straight grid into a bent shape during construction. The stress in the members of the grid shells is proportional to their curvature, and the curvature is mainly due to the level of bending. The preserved geometry of the grid shell does, even under critical loads, not change significantly. High stiffness is provided, which is the main advantage of the active bending.

ThinkShell has developed a number of GFRP grid shells over the last ten years. In actively bent members of the GFRP grid shells, creep-rupture was observed. The dominant parameter to control the long-term behavior of actively bent grid shells is the level of permanent stresses prescribed in the material. In actively bent CFRP grid shells, an application where the material is subjected to high permanent stresses, it appears therefore essential to predict the ultimate strength and deflection as functions of loading and time.

3. Creep characteristics of CFRP

Due to mechanical properties such as lightweight, high elastic limit strain, and high stiffness, Carbon Fiber Reinforced Polymer (CFRP) becomes an interesting material choice for construction of actively bent grid shells. In the actively bent members of the grid shells considerable amount of permanent stresses is present. Fiber Reinforced Polymer (FRP) is sensitive to creep, which may lead to creep buckling as a result of reduced stiffness of the material on a long-term (see Section 2.4.1), or possible collapse mechanisms due to creep-rupture (see Section 2.4.2).

Limited knowledge is available of the time-dependent long-term creep behavior of CFRP, in the field of structural design of buildings. In this chapter, long-term creep characteristics of CFRP and methods to study related time-dependent long-term behavior are presented. Section 3.1 presents important material parameters for construction of actively bent grid shells, based on short-term behavior. In Section 3.2, long-term creep characteristics of CFRP are presented. Methods to study long-term creep are discussed in Section 3.3. The chapter is concluded in Section 3.4,

3.1. Short-term material parameters for construction of actively bent grid shells

The first grid shells that were built according to the specific principle of construction related to actively bent grid shells were made of timber materials (see Annex A). Timber is the only traditional building material which allows for transforming the initial straight members combined in a grid into a bent shape to the desired degree of curvature without breaking. Due to the flexibility of timber members, curved structural surfaces can be made.

When looking at other industries, it appears that when a combination of high stiffness and high deformability is required, FRP materials often replace timber . An example of this is found in the development of the tennis racket, illustrated by Figure 3.1 (Cyril Douthe, 2007).

Figure 3.1 CFRP materials used in tennis rackets (Vivian van Deursen, 2017)

ThinkShell has investigated the most suitable materials for the construction of actively bent grid shells, based on the method introduced by Ashby. The research team has defined important material parameters for construction of actively bent grid shells and has compared these for all available construction materials (Douthe, 2010). The defined parameters, which are based on material behavior on a short term, are presented in Table 3.1.

The two most important material parameters for construction of actively bent grid shells are high elastic limit strain and high stiffness. The best materials for actively bent members of the grid shells should have (Cyril Douthe, 2007):

1. Highest elastic limit strain, in order to transform the initial straight grid into a bent shape.
2. Highest stiffness, in order to achieve high final stiffness after bracing and to achieve high buckling resistance.

parameter	**required material behavior**	**descriptor**
deformability – to fit with the construction process	high elastic limit strain	ratio between elastic limit stress and elastic modulus
rigidity – to give the structure its final stiffness and to prevent buckling	high stiffness	elastic modulus
toughness – to ensure on handling on site	high ductility	ratio between toughness and elastic modulus
cost – to know the achievable stiffness per volume unit	low price for a given performance	square root of elastic modulus over price per unit volume
sustainability – to lower life cycle cost	high environmental properties	square root of elastic modulus over embodied energy
durability – to resist against fire or aggressive atmosphere	high durability of the material	square root of elastic modulus over environmental impact

Table 3.1 Parameters important for construction materials of actively bent grid shells

A log-log graph used in Ashby's method is presented in Figure 3.2. The material properties of timber are used as starting points, as timber is the reference material for the construction of actively bent grid shells. The elastic limit stress [MPa] and the Young's modulus [GPa] are represented respectively on the x-axis and y-axis. The limit between building materials having a 'good' and 'bad' elastic limit strain is represented by line l_1. Line l_2 represents the limit between materials having a Young's modulus which is higher or lower than the Young's modulus of timber.

According to this graph, the materials in the upper right corner represent materials that will have a 'better' elastic limit strain and stiffness than timber. From this it can be concluded that the use of Glass Fiber Reinforced Polymers (GFRP), Carbon Fiber Reinforced Polymers (CFRP), technical ceramics and titanium in actively bent grid shells, would be interesting to investigate. In this thesis the use of FRP materials is investigated, so both technical ceramics and titanium drop out. From the graph can also be concluded that traditional building materials such as concrete and steel have much lower elastic limit strain than timber. This may be a reason these materials have not been used for construction of actively bent grid shells (Cyril Douthe, 2007).

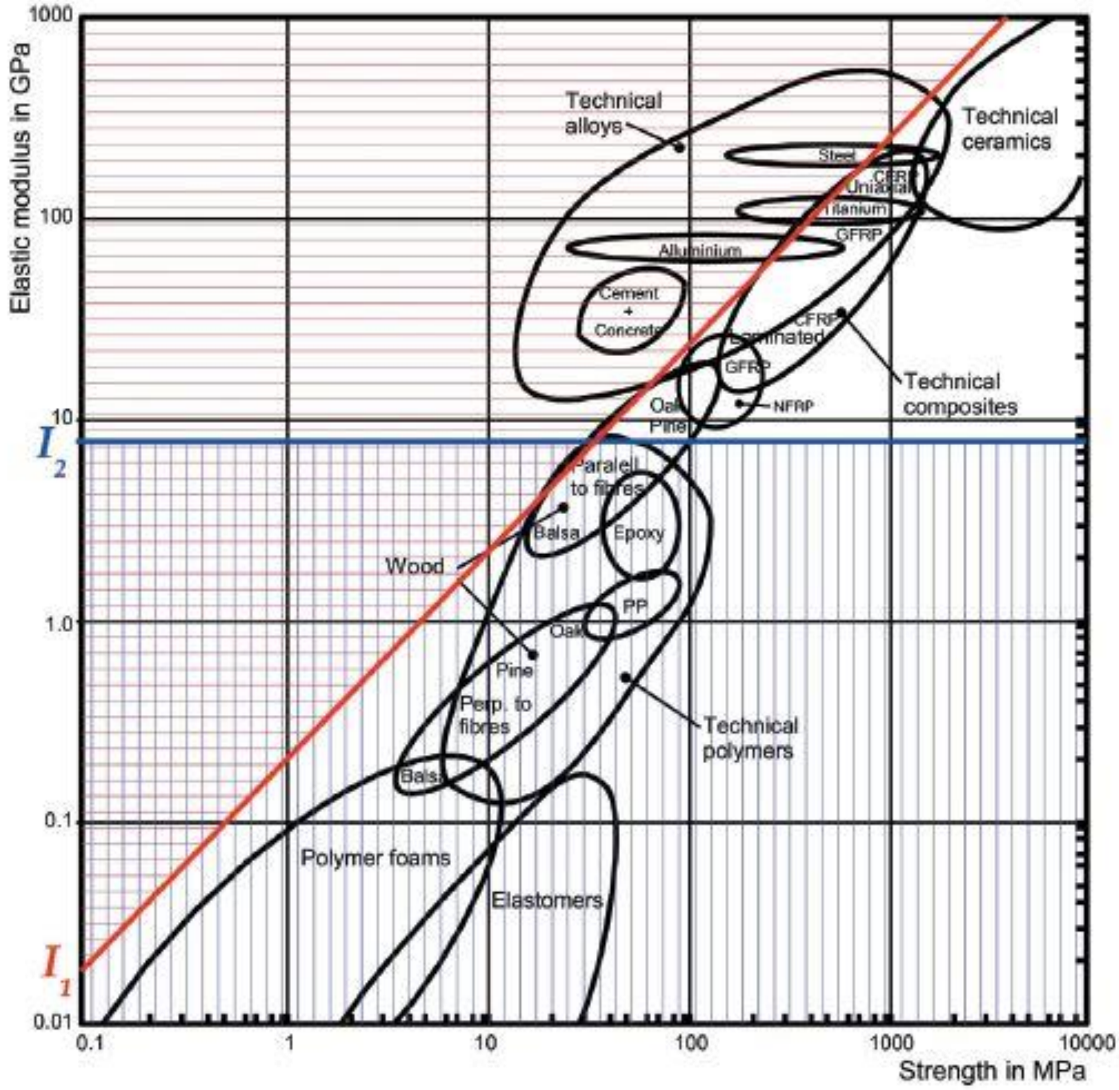

Figure 3.2 Log-log graph representing elastic limit strain and elastic modulus of different materials (Kotelnikova-Weiler et al., 2013)

3.2. Long-term creep characteristics of CFRP

In the actively bent members of the grid shells considerable amount of permanent stresses is present. Fiber Reinforced Polymer (FRP) undergoes creep and creep rupture when subjected to permanent loading. Both of these phenomena were observed on FRP samples, models, and real-scale structures under various circumstances (Kotelnikova-Weiler et al., 2013).

In Section 3.2.1 and 3.2.2, the phenomena of respectively creep and creep-rupture are introduced. Section 3.2.3 presents creep verifications according to (CUR96, 2017). Recommended creep-stress limits by other researchers are presented in Section 3.2.4. Creep testing of CFRP is presented in Section 3.2.5.

3.2.1.Creep

Creep is the time-dependent and permanent deformation of materials (change in strain) due to a constant applied stress. Creep is a phenomenon which is undesired and is often the determining factor in the service life of a material. Fiber Reinforced Polymer (FRP) consists of two major ingredients: fibers and a polymeric resin (e.g. polyester vinyl ester, or epoxy resins). When unidirectional FRP is subjected to a constant load over an extended period of time, its fibers behave elastically while the resin behaves in a viscoelastic manner. The transfer of stress in the resin to the stress in the fibers characterizes creep behavior of FRP (Lee, 2007).

The typical creep response of a material under a constant applied load is presented in Figure 3.3. Creep occurs in three stages:

Stage I referred to as the primary creep stage. This stage is characterized by an instantaneous deformation of the FRP, followed by a deformation where the creep rate decreases with time.

Stage II referred to as the secondary creep stage. This stage is characterized by a constant low creep deformation over a long period of time.

Stage III referred to as the tertiary creep stage. This stage is characterized by a creep rate which is progressively increasing compared to Stage II, and finally results in creep-rupture (see Section 3.2.2). In case of high applied loads, stage III may also directly occur after the primary creep stage.

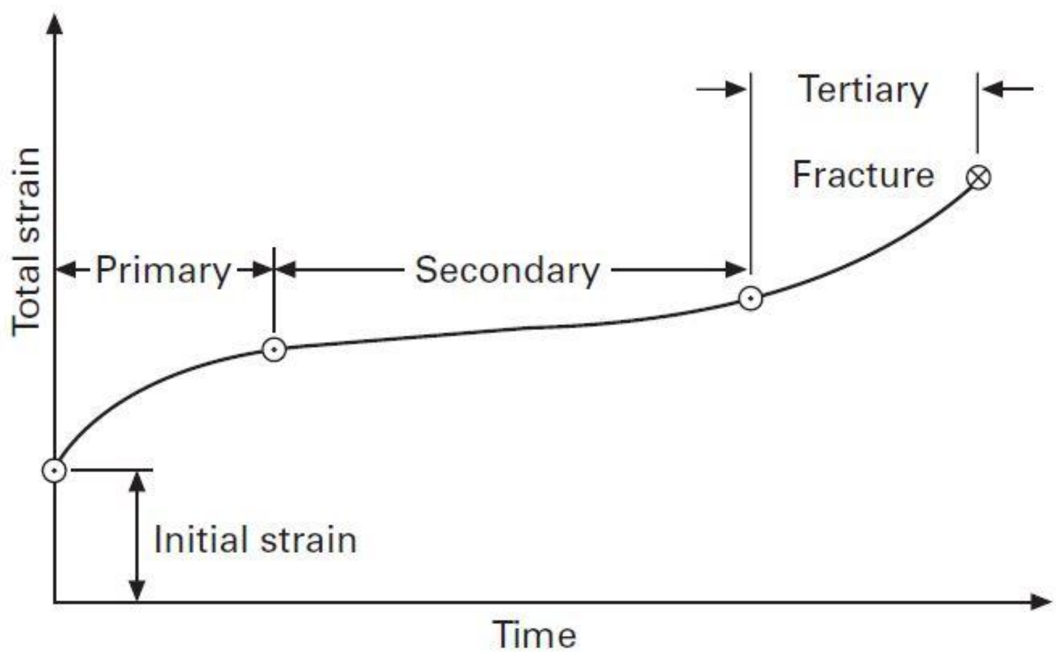

Figure 3.3 Typical creep response of a material under a constant applied load (Lee, 2007)

A. Influencing factors

Creep is a phenomenon which is dominated by the polymeric resin of FRP. The primary determining material factors in creep deformation are the type of resin and the quality of the interface between the fibers and the resin (C. Douthe et al., 2010).

The process of creep in FRP may be described by a time-dependent reduction in modulus, also referred to as creep modulus. The two main external factors that determine creep are stress and temperature. Time-dependent factors, related to material en environment, that determine the extent of creep modulus are presented below (EUROCOMP, 1996):

I. Material related factors:
   - The type of resin and degree of cure;
   - The quality of the interface between the fibers and the resin;
   - The volume fraction of the fibers;
   - The form of reinforcement (e.g. woven, non-woven, mats);
   - The orientation of the fibers with respect to the applied load;

II. Environment related factors
   - The type and duration of loading;
   - The temperature;
   - The presence of aggressive chemicals;
   - The moisture content;

B. Factors influencing creep of the resin

The three main thermosetting resins used in the pultrusion process are polyester, epoxy, and vinyl ester. The listed points below describe factors that influence the extent of creep in the polymeric resin (EUROCOMP, 1996). These factors are compared for the three resins in Table 3.2. It can be concluded that epoxy resins are least sensitive to creep.

- The greater degree of cross-linking in the resin, the smaller the creep. In comparison to thermoplastic resins, thermosetting resins are cross-linked and are therefore, in general, more resistant to creep.

- The higher the Heat Distortion Temperature (HDT) or Glass Transition Temperature T_g of the resin, the greater the creep modulus, so the more resistant to creep. It is advised to select resins that have a T_g, which is at least 20°C higher than the structure’s maximum service temperature.

- The more resistant to moisture (and plasticization behavior), the more resistant to creep.

- The more brittle the resin, the more resistant to creep.

- The stronger the interface between the fibers and the resin, the more resistant to creep. The inter-laminar shear strength ILSS provides a measure for the bonding between the fibers and resin.

	Polyester	Epoxy	Vinyl Ester
Compression strenght	3	1	2
Degree of cross-linking	2	1	3
Glass transition temp.	3	1	2
Moisure resistance	3	1	2
Impact strength	3	1	2
Cost	1	3	2

(Legend: 1=best │2 = better│3= good)

Table 3.2 Comparison of factors influencing the creep resistance of three resin types

3.2.2. Creep-rupture

In addition to creep causing reduction in stiffness, reductions in strength may also occur. These strength reductions may finally lead to a rupture failure of the material, referred to as creep-rupture (EUROCOMP, 1996).

According to CUR96 (2017), creep-rupture should be avoided by limiting the stresses in the resin of the FRP. As stated in Section 2.4.2, the dominant parameter to control the long-term behavior of FRP in actively bent grid shells is the level of permanent stress prescribed in the material. In actively bent FRP grid shells, an application where the material is subjected to a considerable amount of permanent stresses, it appears essential to predict the ultimate strength and deflection as functions of loading and time (C. Douthe et al., 2010).

3.2.3. Creep verifications according to CUR 96

Actively bent grid shells must be verified to both the Ultimate Limit State (ULS) and the Serviceability Limit State (SLS) (see Annex C). In verifications at ULS and SLS, different design situations are considered and different partial safety and conversion factors are used. Table 3.3 presents the applicable conversion factors for every given situation. The general formula for the total conversion factor η_c is given by (JRC, 2016):

$$\eta_c = \eta_{ct} \times \eta_{cm} \times \eta_{cv} \times \eta_{cf} \tag{6}$$

where:

η_c	total conversion factor
η_{ct}	t temperature effects
η_{cm}	the conversion factor for humidity effects
η_{cv}	the conversion factor for creep effects
η_{cf}	the conversion factor considering fatigue effects

Aspect being verified							
Influencing factor	Strength (ULS)	Stability (ULS)	Fatigue (ULS)	Creep (SLS)	Momentary deformation (SLS)	Comfort (vibrations) (SLS)	Damage (SLS)
η_{ct}	√	√	√	√	√	√	√
η_{cm}	√	√	√	√	√	√	√
η_{cv}	√	√		√			√
η_{cf}		√		√	√	√	√

Table 3.3 Conversion factors in ULS and SLS verifications (JRC, 2016)

The conversion factor for creep effects must be used in ULS strength and stability verifications, and SLS verifications of deformations under sustained loads (creep). For FRP laminates with unidirectional (UD) fiber reinforcement, the formula for the conversion factor for creep effects is given by (JRC, 2016):

$$\eta_{cv} = \frac{1}{\varepsilon_v} \times t^n \tag{7}$$

where:

$\Delta\varepsilon_v$	the increase in strain rate of the considered UD ply
t	the duration of the load(s) in hours

n	an exponent depending on the fiber type. If the fiber reinforcement is in the direction of the long-term load[1]: ▪ n = 0,01 for an UD ply; ▪ n = 0,04 for a woven ply; ▪ n = 0,10 for a mat-ply; [1]These factors for n are derived for Glass Fiber Reinforced Polymer (GFRP). For Carbon Fiber Reinforced Polymer (CFRP) these factors are conservative.

For FRP laminates with different fiber directions, the conversion factor for creep effects should be determined based on the method described in CUR 96 (2017) (Section 2.4.5.4) or with the Theory of Findley (see Section 3.3).

In ULS strength verifications of FRP structures subjected to sustained loads, creep-rupture must be considered. Recommendations on sustained stress limits to avoid creep-rupture defined by (ACI440, 2008) may be used as an indication. If the sustained stress in the FRP is below the stress limits for creep-rupture, the FRP's strength is available for non-sustained loads:

$$f_{sus.FRP} \leq f_{sus.limit} \tag{8}$$

where:

$f_{sus.FRP}$	level of stress in the FRP caused by a moment (within the elastic range of member)
$f_{sus.limit}$	sustained stress limit to avoid creep-rupture

The sustained stress limits to avoid creep-rupture are given by:

$$f_{sus.limit} = C \times f_{ult} \tag{9}$$

where:

$f_{sus.limit}$	sustained stress limit to avoid creep-rupture
C	reduction factor (see Table 3.4)
f_{ult}	characteristic value of the initial ultimate tensile strength

type of FRP	C factor
GFRP	0.2
CFRP	0.55
AFRP	0.3

Table 3.4 Reduction factors related to sustained stress limits for different FRPs (CUR, 2017)

3.2.4. Recommended creep-rupture stress limits

The reduction factors related to sustained stress limits for different FRPs presented in Table 3.4 are based on stress limits obtained from creep-rupture tests performed by (Yamaguchi, Nishimura, & Uomoto, 1998), with an imposed safety factor of 1/0.6 (ACI440, 2008). These creep-rupture tests were performed on 6 mm diameter FRP bars reinforced with glass, aramid, and carbon fibers. The bars were loaded in tension to different stress levels at room temperature. Results showed that for all load levels, a linear relationship exists between creep-rupture strength and the logarithmic-time. A long-term extrapolation (50 years) showed that the GFRP, AFRP, and CFRP bars can sustain approximately 0.3, 0.5, and 0.9 times their ultimate strength, before encountering a creep-rupture problem (Yamaguchi et al., 1998).

In case of actively bent grid shells, the reduction factors related to sustained stress limits to avoid creep-rupture (see Table 3.4) should be used for indications only. The members of the grid shells are mainly subjected to sustained bending stresses. In addition, the members have a tubular cross-section with a 40 mm diameter, which is significantly higher diameter compared to the 6 mm bars from creep-rupture experiments performed by Yamaguchi et al., (1998).

The stress-rupture behavior of CFRP has also been examined by (Ando et al., 1998). Creep tests on tendons made from carbon fibers were performed and a critical stress of 0.79 times the ultimate strength was found. The critical stresses of 0.9 f_{ult} and 0.79 f_{ult} from Yamaguchi et al., (1998) and Ando et al., (1998) respectively, are based conventional creep tests which have been performed at ambient conditions at high-load levels. Those circumstances usually result in creep failures in a short period of time (Giannopoulos & Burgoyne, 2009).

ThinkShell has defined a 30% stress limit for actively bent grid shells (see Section 2.3.2). The maximum stress in the members of the grid shells must not exceed 30% of the ultimate strength of the members, in order to prevent severe creep and damage mechanisms such as progressive rupture of fibers. This 30% stress limit was a natural choice, based on proposed safety coefficients for FRP in civil engineering by codes and guidelines (C. Douthe et al., 2010).

In general, there is a lack of knowledge on stress limits related to time-dependent long-term creep behavior of CFRP, in the field of structural design of buildings. The 0.55 f_{ult} design stress defined in CUR is relatively low compared to the obtained critical stresses of 0.9 f_{ult} and 0.79 f_{ult} from Yamaguchi et al. (1997) and Ando et al. (1997) respectively. On the other hand, the 0.3 f_{ult} design stress from ThinkShell, is defined for members in GFRP, and should therefore be used an indication only for the CFRP members investigated in this thesis.

Differences in recommended creep-stress limits and between these limits and related critical stresses obtained from experiments (see Table 3.5), make it difficult to have confidence in predictions of creep behavior of CFRP in actively bent grid shells on a long-term. To ensure that the grid shells' members will perform over time, extensive creep testing is required.

design stress		**critical stress**	
CUR 96 (2017)	ThinkShell (2010)	Yamaguchi (1998)	Ando (1998)
based on critical stress from Yamaguchi with an imposed safety factor of 1/0.6	natural choice, based on safety coefficient for GFRP in CE from codes and guidelines	tests performed on 6 mm diameter FRP bars reinforced with carbon fibers	tests performed on 5 and 12.5 mm diameter CFRP tendons (epoxy resin)
0.55 f_{ult}	**0.3 f_{ult}**	**0.9 f_{ult}**	**0.79 f_{ult}**

Table 3.5 Design- and critical stresses related to creep-rupture

3.2.5. Creep testing of CFRP

To ensure that the members of the grid shells have a long service life, creep tests can be performed to predict their ultimate strength and deflections as functions of loading and time.

In the paper of Giannopoulos & Burgoyne, 2009) the long-term creep behavior of Aramid Fiber Reinforced Polymer (AFRP) was studied. Two methods of testing, respectively the Stepped Isothermal Method (SIM) and the Stepped Isostress Method (SSM), were performed on two different aramid fibers. Test results were compared to results from Conventional Creep

Tests (CCT). The aim of the authors was to predict stress limits of aramid fibers for a service life of 100 years, and avoid overestimating the material use in case of lack of sufficient test data.

From their experiments it was concluded that performing creep tests on aramid fibers, using both SIM and SSM, can be done much more rapidly and at lower stress levels, than with conventional creep tests. In addition, test results using SIM and SSM, can be used to predict long-term creep and creep-rupture behavior of AFRP with confidence, in applications where the material is subjected to high permanent stresses (Giannopoulos & Burgoyne, 2009). Descriptions of successively CCT, SIM, and SSM are given below.

A. Conventional Creep Tests (CCT)

In conventional test methods, the preferred stress mode for creep-rupture measurements is tension, as there are some ductile FRP in which creep-rupture does not occur. D 2990 – 01. To measure creep in bending, three-point loading or four-point loading tests may be performed. Required equipment and test methods for creep and creep-rupture of FRP are described in (D2990-01, 2001).

Material testing should at least be performed in case of lack or inaccurate theoretical models. Material testing should also be performed when design is critical for creep and creep-rupture, for example when subjected to pre-stress and other high permanent loads (CUR96, 2017).

B. Stepped Isothermal Method (SIM)

In testing using the Stepped Isothermal Method (SIM), a single specimen is subjected to constant load, while the temperature is increase in a series of steps. The final temperature step lasts until the specimen ruptures. At each temperature step a creep curve is obtained, which can be modified for the different temperature levels to determine a creep master curve at a starting stress level. From these creep master curves, predictions of the material behavior on a long-term can be made. If both temperature step and step duration are carefully chosen, testing using SIM can be done in 24 hours. This is a great advantage compared with CCT.

C. Stepped Isostress Method (SSM)

In testing using the Stepped Isostress Method (SSM), a single specimen is loaded in steps, from a starting stress level until a final rupture stress. The test ends once the specimen ruptures. Results from SSM tests are used to construct final creep curves at different starting stress levels, from where predictions of the material behavior on a long-term can be made. Similar to SIM, testing using SSM can be done in 24 hours if both the load step and step duration are well chosen.

3.3. Methods to study long-term creep of CFRP

Detailed explanations of analytical models to study the time-dependent long-term creep response of FRP in civil engineering applications is presented in Annex D. In literature, the two most used analytical models to study creep behavior of FRP on a long-term are Findley’s power law and the Boltzmann superposition principle. Both models are based on experimental testing to predict the viscoelastic behavior of FRP (Lee, 2007).

Finley’s power law is a method for curve-fitting of creep data from experiments with a power law equation. The general formula for determining the total creep strain is given by:

$$\varepsilon(t) = \varepsilon_0' + \varepsilon_t' \times t^n \quad (10)$$

where:

ε(t)	total creep strain
ε_0'	stress- and temperature dependent initial elastic strain
t	time after loading
ε_t'	stress independent material constant

Research has indicated that Findley's power law is only valid as long as the material undergoes primary creep. In addition, in order to obtain valid description of creep responses, it has been recommended in creep testing to use sustained stress levels below 33% of the ultimate strength (Lee, 2007).

The Boltzmann superposition principle (BSP) is a method for curve-fitting of creep data from experiments based on a superposition principle. The primary principle of the BSP is that the behavior of a material under a certain load is independent of the behavior of the material under any load, which is already on the material. (Lee, 2007).

3.4. Conclusion

The two most important short-term material parameters for construction of actively bent grid shells are high elastic limit strain and high stiffness. Materials should have high ratio σ_{ult}/E, in order to transform the initial straight grid into a bent shape, and high stiffness E, in order to achieve sufficient final stiffness after bracing and to achieve high buckling resistance.

In the actively bent members of the grid shells considerable amount of permanent stresses is present. Fiber Reinforced Polymer (FRP) undergoes creep and creep-rupture when subjected to permanent loading. Creep is the time-dependent and permanent deformation of materials (change in strain) due to a constant applied stress. Creep-rupture is rupture failure of the material due to creep. Creep response is dominated by the polymeric resin of the FRP, and is highly dependent on the type of resin and the quality of the interface between the fibers and the resin. Other factors that have influence on creep behavior are the orientation of the fibers, the fiber volume fraction, and the form of the FRP reinforcement.Out of the three main thermosetting resins used in the pultrusion process, polyester, epoxy, and vinyl ester, epoxies are least sensitive to creep.

In ULS strength verifications of FRP structures subjected to sustained loads, creep-rupture must be considered. Based on CUR96 (2017), recommendations on sustained stress limits to avoid creep-rupture are 0.2 f_{ult}, 0.3 f_{ult}, and 0.55 f_{ult}, for GFRP, AFRP and CFRP respectively. If the sustained stress in the FRP is below these stress limits for creep-rupture, the FRP's strength is available for non-sustained loads over a period of 50 years. It was concluded that these limits are not applicable to all design cases, as they have resulted from creep-rupture tests performed on 6 mm diameter FRP bards that were loaded in tension.

ThinkShell has defined a 30% stress limit for GFRP members of actively bent grid shells. As this limit was defined for members in GFRP, it can be used as an indication only for the CFRP members investigated in this thesis.

Actively bent grid shell design may be critical for creep and creep-rupture, due to pre-stressing of the members, therefore material testing should be performed. Experimental studies have shown that accelerated creep testing using the Stepped Isothermal Method (SIM) and Stepped Isostress Method (SSM), can be performed to predict long-term creep deformation and creep-rupture times with confidence, in high-stress applications. It was concluded that both methods are interesting for further investigation with respect to actively bent grid shells.

PART II NUMERICAL ANALYSIS

4. 2D buckling analysis of an actively bent member

This chapter presents a two-dimensional in-plane buckling analysis of an actively bent member with constant cross section. The finite element and structural analysis software SOFiSTiK has been used for numerical calculations. The input data to define the SOFiSTiK model of an actively bent member is presented in Annex E.

In Section 4.1, the computational analysis method with SOFiSTiK is validated. In Section 4.2, the influence of pre-bending of members on in-plane buckling and corresponding critical loads is studied. In Section 4.3, a comparison on in-plane buckling response and corresponding critical loads between GFRP and CFRP members is made. In Section 4.4 it is investigated to what extent members of respectively GFRP and CFRP can be bent, not reaching related sustained stress limits to avoid creep-rupture from literature (CUR96, 2017). Section 4.5 presents a 3D SOFiSTiK model of an actively bent grid shell to study the importance of creep-rupture in actively bent grid shells. The chapter is concluded in Section 4.6.

4.1. Validation of 2D analysis method

To validate the computational analysis method used to study effects of the bending of members of actively bent grid shells, a similar approach adopted by (Mesnil, 2013) was used. In this study, form-finding of an actively bent member is performed using the nonlinear solver in SOFiSTiK. To evaluate the 2D analysis method with SOFiSTiK, its numerical solutions to the structural problem of describing the deformed shapes of beams in their post-buckled state, are compared to theoretical values of the Elastica (COURBON, 1984) (see Section 4.1.4).

4.1.1. Structural problem

Starting point is an initially straight member with constant cross section, length (L), moment of inertia (I), and Young's modulus (E). The member is simply supported by end rollers and restrained to lie in a two-dimensional plane. The member is subjected to equal and opposite support forces that cause transformation of the member into a bent shape (see Figure 4.1). Hence it follows that the member is no longer straight, but subjected to a displacement in transverse direction v(x).

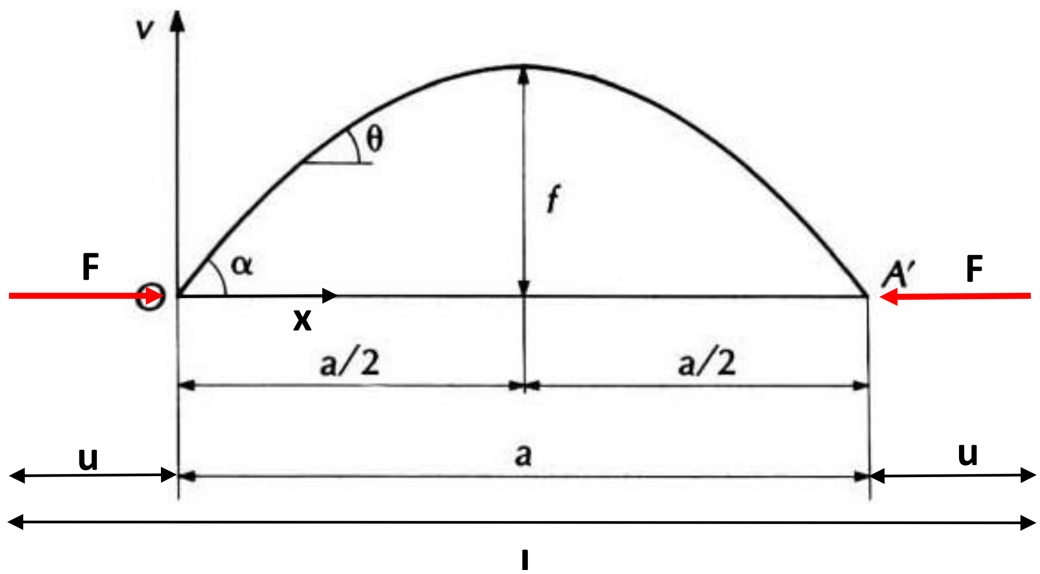

Figure 4.1 Parameters describing the structural problem of a bent member

where:

F	horizontal support force
L	initial length of the member
a	span of the bent member
u	prescribed displacements at supports
f	rise at mid-point
α	angle between the x-axis and tangent of bent member at x = 0
θ	angle between the x-axis and tangent of the bent member at 0 < x < L
v	transverse displacement

4.1.2. Theoretical values describing the structural problem

Theoretical solutions to the structural problem of describing the deformed shapes of beams in their post-buckled state are founded by Jacques Bernoulli and Leonard Euler (Levien, 2008). Corresponding analytical expressions of the bent members taking the shape of curves are known as Elastica (COURBON, 1984).

In Table 4.1, values of F/F_c, f/L, and a/L for different angles (α) are presented. These values can be used to validate a computational analysis method used to study in-plane buckling of a bent member, which is simply supported by end rollers (Mesnil, 2013). Values of a/L from finite element analysis software may be taken to be equal to the values of a/L from Table 4.1. Subsequently, the values of F/F_c and f/L from the table can be used to compare with results for F/F_c and f/L from software.

The critical buckling load is calculated from:

$$F_c = \frac{\pi^2 EI}{L^2} \tag{11}$$

where:

F_c	critical buckling load
E	Young's modulus
I	moment of inertia
L	initial length of the member

α [°]	F/Fc	f/L	a/L
10	1,003818	0,055379	0,992397
20	1,015397	0,109701	0,96973
30	1,035121	0,16195	0,932432
40	1,063663	0,21112	0,881203
50	1,102044	0,256288	0,817004
60	1,151719	0,296604	0,74102
70	1,214723	0,331309	0,654637
80	1,293889	0,359749	0,559396
90	1,393204	0,38138	0,456946
100	1,518389	0,39577	0,348989
110	1,677905	0,402588	0,237205
120	1,884801	0,401585	0,12316
130	2,160369	0,392547	0,008173
140	2,542258	0,375194	-0,106923
150	3,105362	0,348954	-0,222268
160	4,030085	0,312302	-0,340319
170	5,95049	0,259985	-0,471434

Table 4.1 Values of a/L, F/F_c, and f/L as a function of α (COURBON, 1984)

4.1.3. Form-finding with SOFiSTiK

In this study, form-finding of an actively bent member is performed using the non-linear solver of finite element and structural analysis software SOFiSTiK. In the model, one roller end of an initially straight member was subjected to a prescribed displacement to transform the member into a bent shape (see Figure 4.2).

To be able to make a useful comparison between results from theory based on the Elastica (Table 4.1), and SOFiSTiK, a subdivision of the member into straight segments is determined first (see Figure 4.3). Based on the approach adopted by (Mesnil, 2013) starting point was that the polygon division would result in reliable values for both the estimation of the rise at mid-point (f) and horizontal support forces (F).

The initial polygon division in the finite element model was determined for a member with initial length of 6 meters, with tubular cross section of 40 mm diameter and 3 mm wall thickness, and 25 GPa Young's modulus. One roller support of the member was subjected to a 150 mm prescribed displacement, causing transformation of the member into a bent shape.

Results for both the rise at mid-point (f) and horizontal support forces (F) turned out to be reliable for a model consisting of 20 straight segments – 21 nodes (see Figures 4.4 and 4.5). This polygon division was therefore chosen for the comparison of results between theory and SOFiSTiK for validation of the computational analysis method.

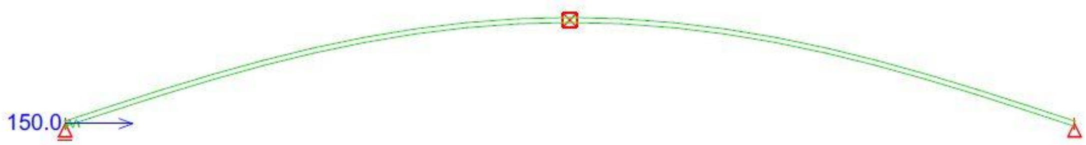

Figure 4.2 Roller support of the member subjected to a 150 mm prescribed displacement

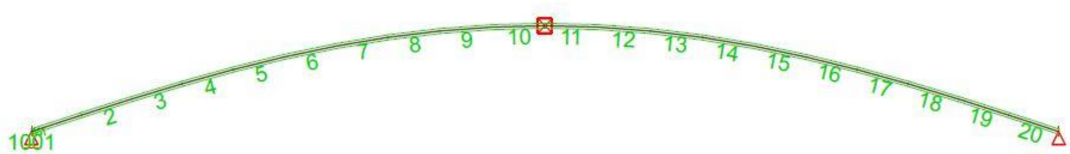

Figure 4.3 Subdivision of the model into straight segments

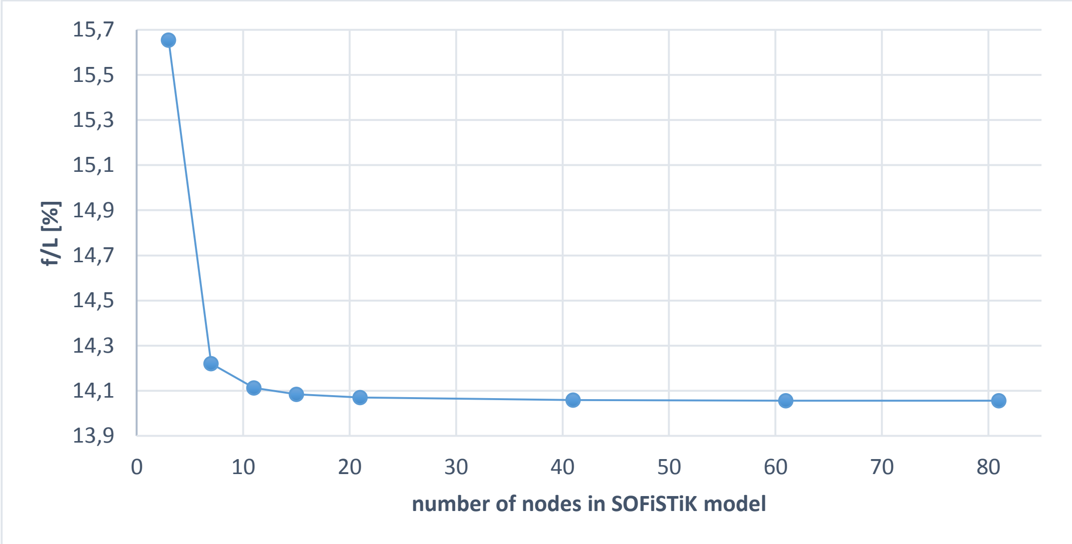

Figure 4.4 Development of f/L for different number of nodes in the finite element model

Figure 4.5 Development of ultimate load for different number of nodes in the finite element model

4.1.4. Comparison between theory and computational analysis method

To validate the computational analysis method used to study the effects of the bending of members of actively bent grid shells, a comparison was made between results from theory and SOFiSTiK. Prescribed displacements were applied to the roller supports of the SOFiSTiK models with 20 elements, equal to values of a/L from Table 4.1. As an example, models with different ratios of a/L are presented in Figure 4.6. To validate the computational analysis method, results for F/F_c and f/L from SOFiSTiK were compared with values for F/F_c and f/L from Table 4.1, and are presented in Table 4.2.

The differences of the rise at mid-point (f) and horizontal forces (F) of the model are relatively small (see Figure 4.7). It is concluded that the model gives an accurate description of the deformed shapes of members in their post buckled state.

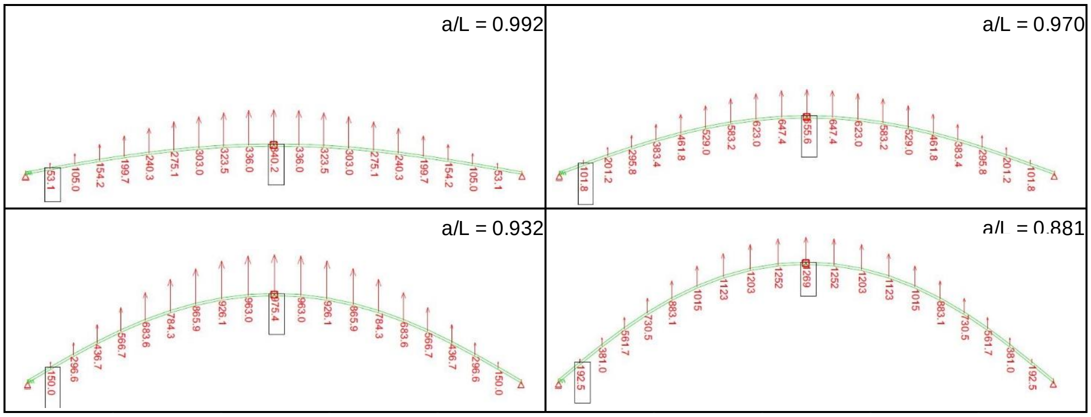

Figures 4.6 SOFiSTiK models with different ratios of a/L (values indicate transverse displacements v)

	theory			SOFiSTiK			difference on F [%]	difference on f [%]
α [°]	a/L	F/Fc	f/L	a/L	F/Fc	f/L		
10	0,992	1,004	0,055	0,992	1,006	0,057	0,18	2,39
20	0,970	1,015	0,110	0,970	1,018	0,109	0,23	-0,40
30	0,932	1,035	0,162	0,932	1,037	0,163	0,20	0,38
40	0,881	1,064	0,211	0,881	1,066	0,212	0,25	0,18

Table 4.2 Comparison between a/L, F/F_c, and f/L results from theory and SOFiSTiK

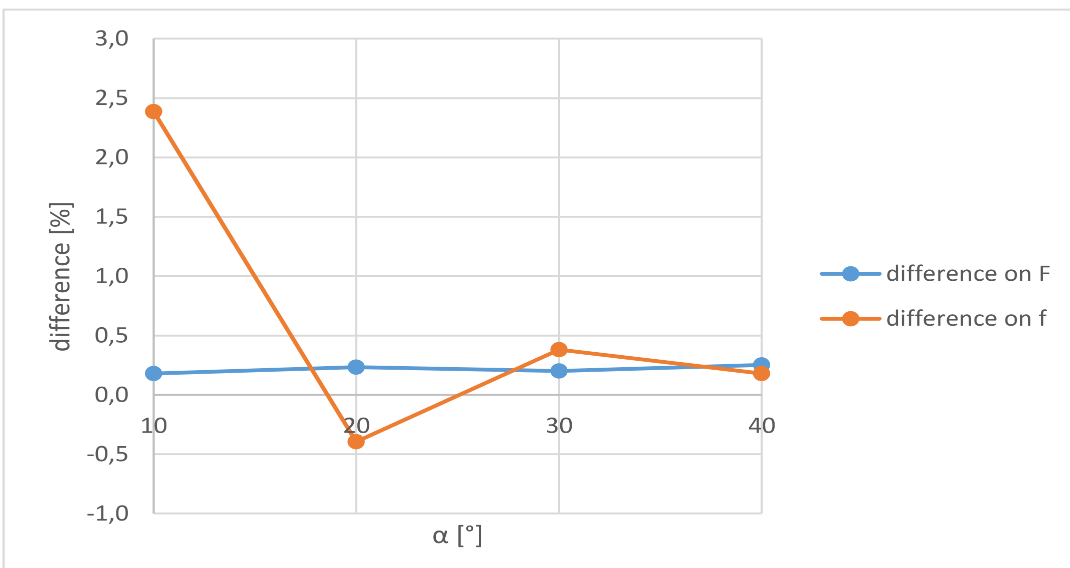

Figure 4.7 Differences on F and f between results from theory and SOFiSTiK

4.2. In-plane buckling analysis of members with constant cross section

In Section 2.1, a classification between pre-formed grid shells and actively bent grid shells is presented. This section presents an in-plane buckling analysis of both pre-formed- and actively bent members of the grid shells. The influence of the pre-bending of the members on in-plane buckling response and corresponding critical loads is studied.

4.2.1. Bifurcation buckling of pre-formed and actively bent members

Bifurcation buckling analysis is performed based on the study of (Chini & Wolde-Tinsae, 1988). The parameters describing the finite element model of a member with initial length of 6 meter, tubular cross section of 40 mm diameter and 3 mm wall thickness, and 25 GPA Young's modulus are presented in Figures 4.8 and 4.9.

A comparison of buckling points of members with f/a = 0.25 between Chini & Wolde-Tinsae (C&W-T) and the SOFiSTiK model is presented in Table 4.3. Relationships between a dimensionless load parameter (PL^2/EI) and the displacement at mid-point (δ/L), bending moment at mid-point (ML/EI), and normal force at mid-point of members with f/a = 0.25 are presented in Figures 4.10-4.12 respectively.

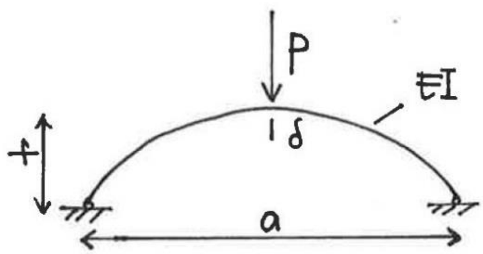

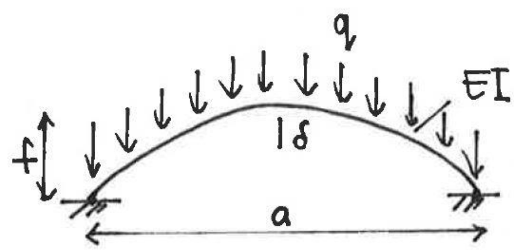

Figures 4.8, 4.9 Parameters describing the analysis models

where:

P	downward point load
q	downward distributed load
a	span of the bent member
f	rise at mid-point
δ	vertical deflection at mid-point
E	elastic modulus
I	moment of inertia

load parameter	C &W-T	SOFiSTiK	difference [%]
$\frac{qL^3}{EI}$, actively bent (AB)	50,7	51,8	2,2
$\frac{qL^3}{EI}$, pre − formed (PF)	69,5	66,2	-4,7
$\frac{PL^2}{EI}$, actively bent (AB)	33,1	33,6	1,5
$\frac{PL^2}{EI}$, pre − formed (PF)	43,7	42,4	-3,0

Table 4.3 Comparison of buckling points for a member with f/a = 0.25 between Chini & Wolde-Tinsae (1988) and SOFiSTiK

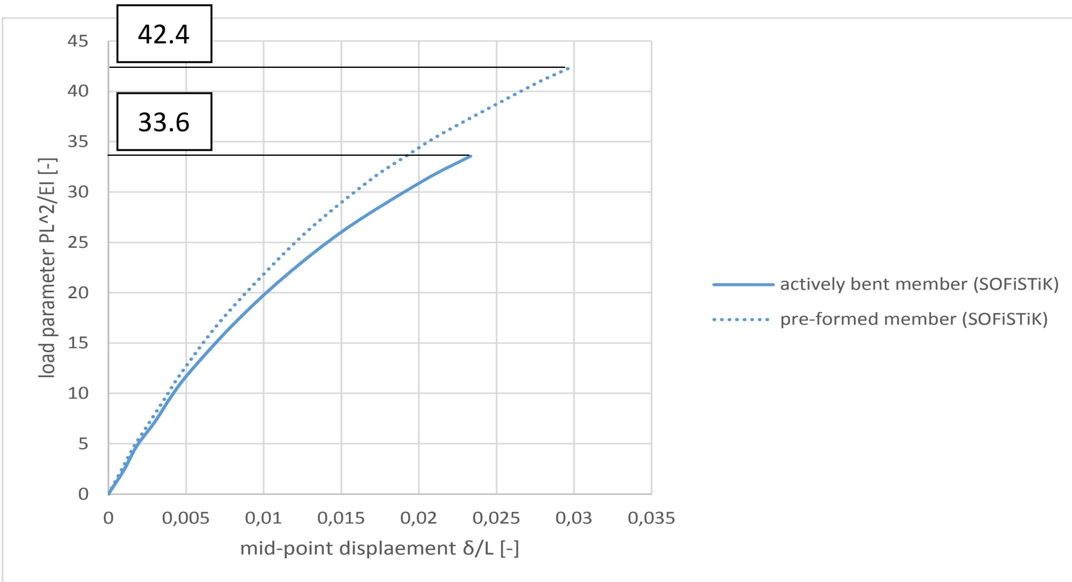

Figure 4.10 Displacement at mid-point due to a dimensionless load parameter of members with f/a = 0.25

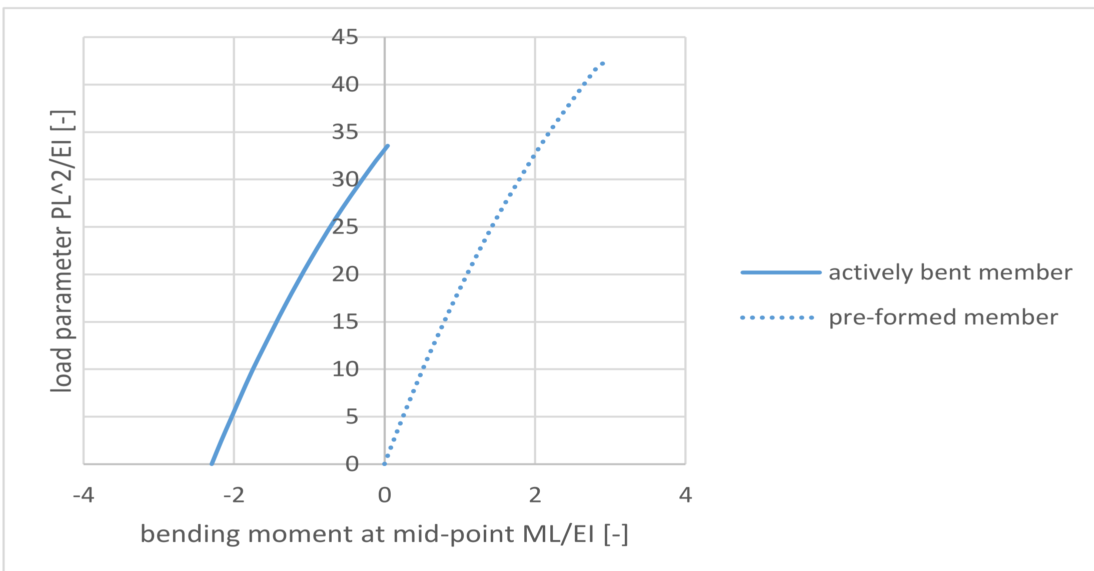

Figure 4.11 Load parameter versus bending moment at mid-point of members with f/a = 0.25

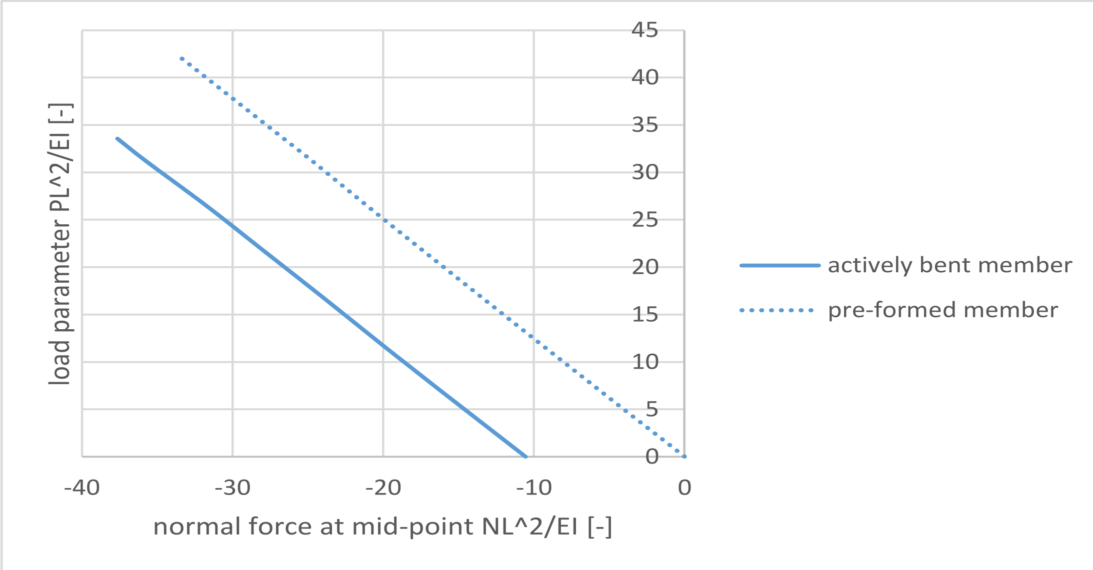

Figure 4.12 Load parameter versus normal force at mid-point of members with f/a = 0.25

4.2.2.The influence of pre-bending on buckling and corresponding critical loads

The development of the vertical displacement at mid-point due to a downward point load P (see Figure 4.8) of members with f/a = 0.25 is presented in Figure 4.13. In this example, the critical buckling load for the pre-formed member (1.77 kN) is 1.26 times greater than the critical buckling load for the actively bent member (1.40 kN). In Figure 4.14, the development of buckling points for a pre-formed member and an actively bent member is presented. In Figure 4.14 can be seen that the higher the amount of pre-bending (f/a), the higher the critical load.

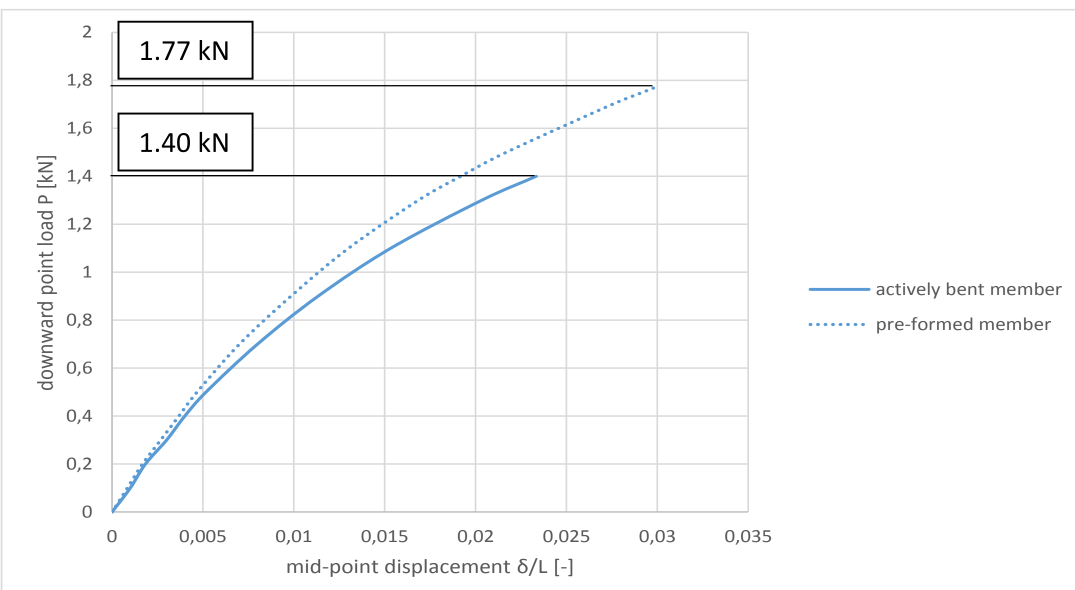

Figure 4.13 Displacement at mid-point due to downward point load P of members with f/a = 0.25

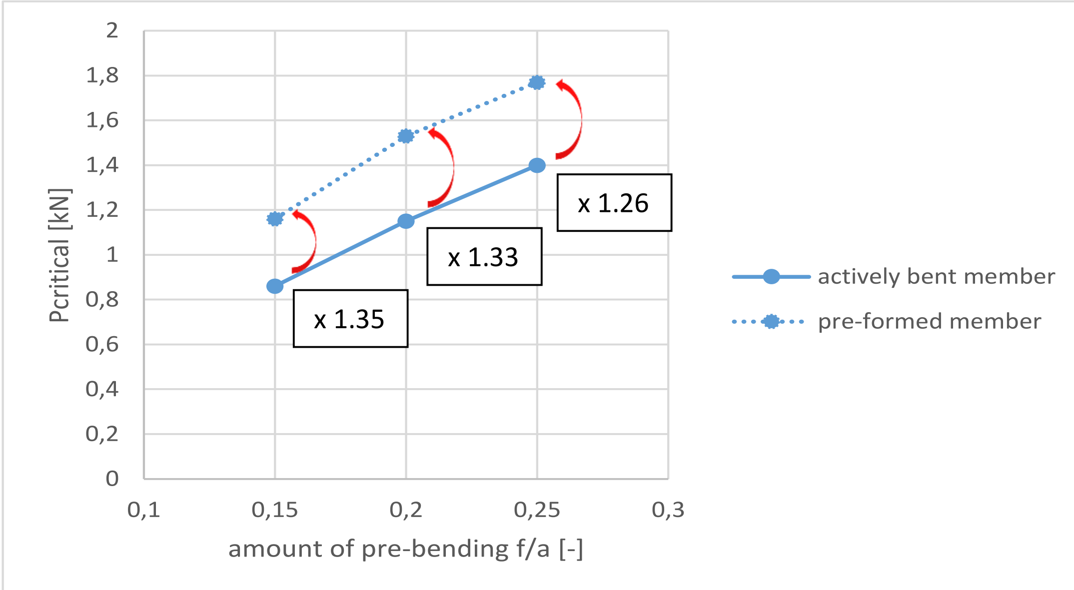

Figure 4.14 Development of buckling points ($P_{critical}$) for different cases

4.3. Comparison of buckling response and critical loads between GFRP and CFRP members

In this section, results of a similar analysis as Section 4.2.2 are presented. A comparison is made between Glass Fiber Reinforced Polymer (GFRP) and Carbon Fiber Reinforced Polymer (CFRP) members with equal dimensions on the influence of pre-bending on buckling and corresponding critical loads. Related parameters are presented in Table 4.4. Figure 4.15 shows the development of displacement at mid-point due to a dimensionless load parameter. It can be seen that in this case both members, which only differ in elastic modulus, show similar buckling response.

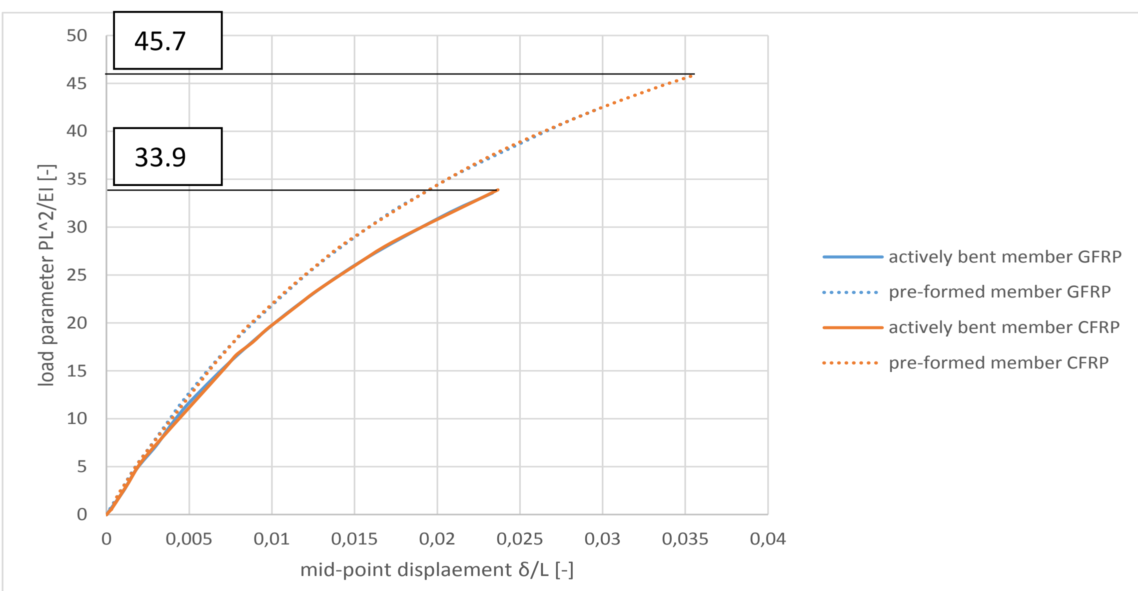

Figure 4.15 Displacement at mid-point due to a dimensionless load parameter of GFRP and CFRP members with f/a = 0.25

Figure 4.16 shows the displacements at mid-point due to downward point load P for members with f/a = 0.25. It can be seen that the critical point load P for the CFRP member is 3.6 times higher than the critical point load for the GFRP member. This can be clarified by the elastic modulus of CFRP (90 GPa) being 3.6 times higher than the elastic modulus of GFRP (25 GPa). From Figure 4.17 can be seen that the more pre-bending is applied, the higher the critical buckling load.

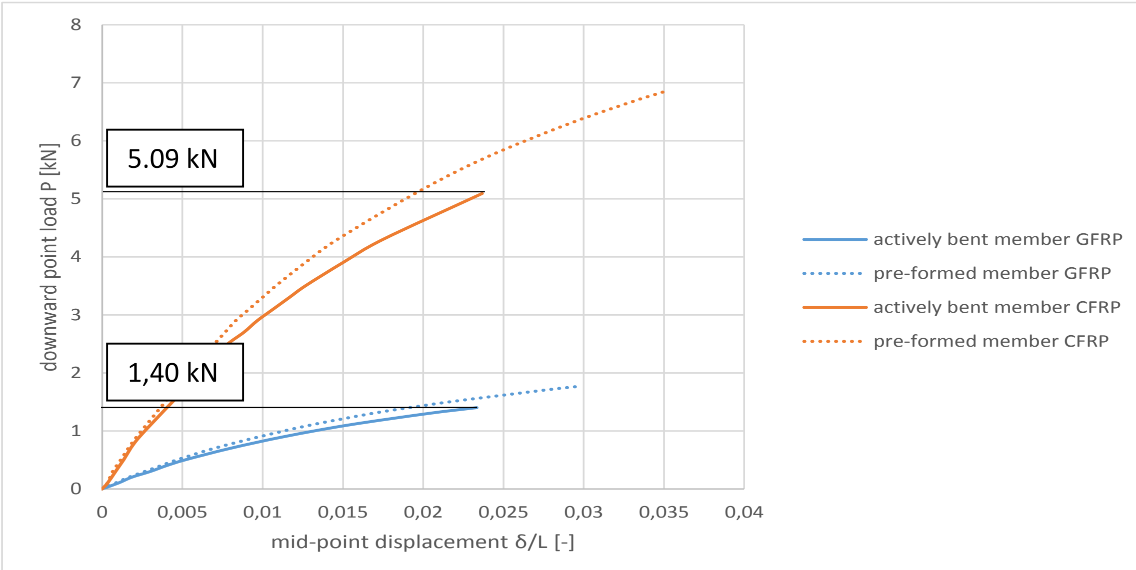

Figure 4.16 Displacement at mid-point due to downward point load P of GFRP and CFRP members with f/a = 0.25

		GFRP	CFRP
L [mm]	initial length	6000	6000
D [mm]	diameter	40	40
t [mm]	wall thickness	3	3
E [Gpa]	elastic modulus	25	90

x 3.6

Table 4.4 Parameters model of members in GFRP and CFRP

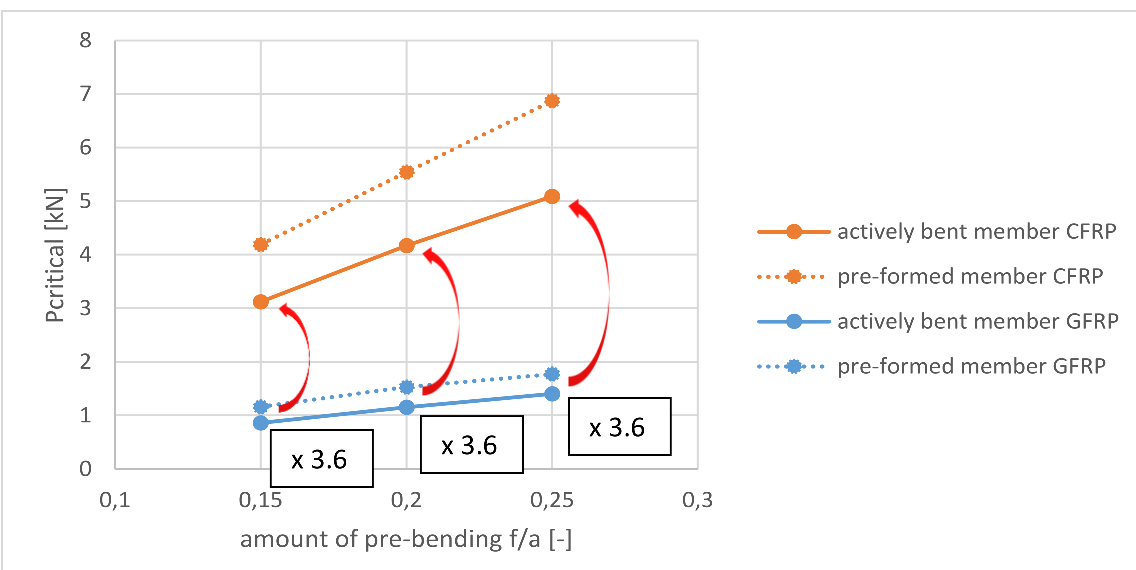

Figure 4.17 Development of buckling points ($P_{critical}$) for different cases

4.4. Creep-rupture analysis

This section presents results from the study about to what extent actively bent members in GFRP and CFRP can be bent, not reaching their related sustained stress limits to avoid creep-rupture. Recommendations on sustained stress limits to avoid creep-rupture defined by ACI440 (2008) are presented in Section 3.2.3. If the sustained stress in the FRP is below the stress limits for creep-rupture, the FRP's strength is available for non-sustained loads (ACI440, 2008).

Based on formula 9, the related 'sustained strain' limits to avoid creep-rupture can be calculated from:

$$\varepsilon_{\mathrm{sus.limit}} = \frac{\mathrm{C} \times \mathrm{f_{ult}}}{\mathrm{E}} \tag{12}$$

where:

$\varepsilon_{sus.limit}$	'sustained strain' limit to avoid creep-rupture
C	reduction factor (see Table 3.4)
f_{ult}	characteristic value of the initial ultimate tensile strength
E	elastic modulus

Sustained strain limits for CFRP and GFRP members can be used to calculate their related maximum radius of curvature. The formula for the radius of curvature of a bent member is given by:

$$\mathrm{R} = \frac{\mathrm{y}}{\varepsilon_{\mathrm{sus.limit}}} \tag{13}$$

where:

R	radius of curvature
y	outer radius of cross-section
$\varepsilon_{sus.limit}$	sustained strain limit to avoid creep-rupture

Figure 4.18 shows a linear extrapolation of the development of buckling points of members in GFRP and CFRP, based on Figure 4.17. The vertical lines indicate sustained strain limits for respectively GFRP and CFRP, based on the reduction factors from Table 3.4. From Figure 4.18 can be seen that if the sustained stress in both FRP members are below their corresponding stress limits for creep-rupture, the CFRP member is available for a point load at mid-span which is 11 times larger compared to the GFRP member.

	GFRP	CFRP
L [mm]	6000	6000
y [mm]	20	20
t [mm]	3	3
I [mm4]	60066	60066
E [MPa]	25000	90000
fult [N/mm2]	1200	2300
C [-]	0,2	0,55

Table 4.6 Parameters model of members in GFRP and CFRP

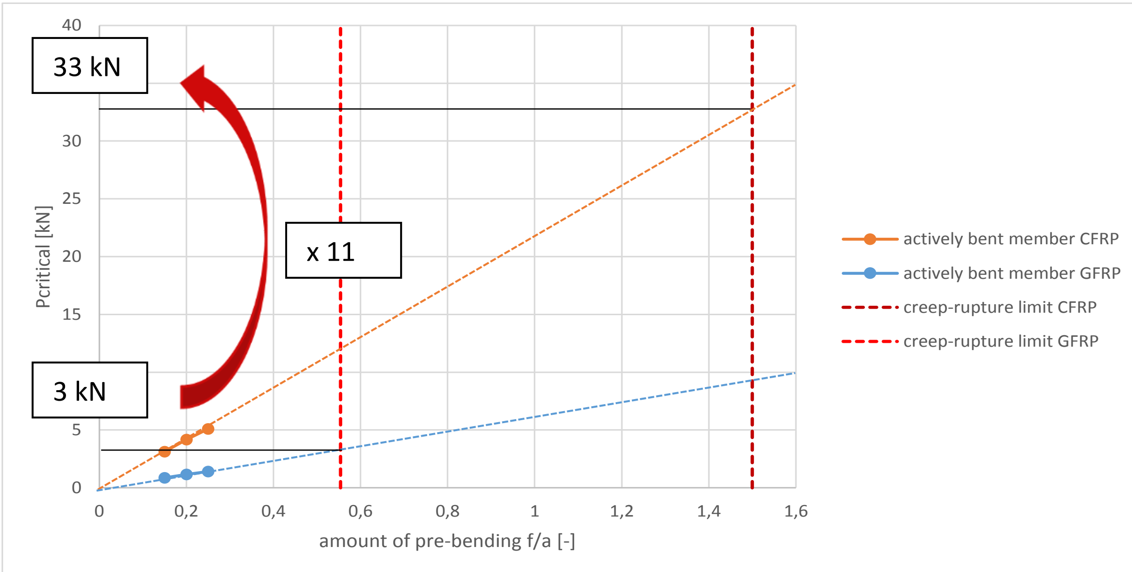

Figure 4.18 Development of buckling points ($P_{critical}$) for different cases against sustained strain limits to avoid creep-rupture

4.5. 3D SOFiSTiK model of an actively bent grid shell

This section presents a 3D model of an actively bent grid shell in SOFiSTiK (see Figure 4.19). As already mentioned in the introduction chapter of this thesis, the investigation of long-term creep behavior of CFRP in actively bent grid shells as a whole, is beyond the scope of this thesis. However, it was concluded that similar buckling- and creep-rupture analyses as performed in 2D, may be performed in 3D to study the importance of creep-rupture in actively bent grid shells. A brief description of the steps performed in the modelling process is presented below:

A.	AutoCAD:	draw the grid in 2D
B.	SOFiSTiK:	lift at two points in the middle
C.	SOFiSTiK:	lock horizontal displacements at the perimeter
D.	SOFiSTiK:	release the two points in the middle

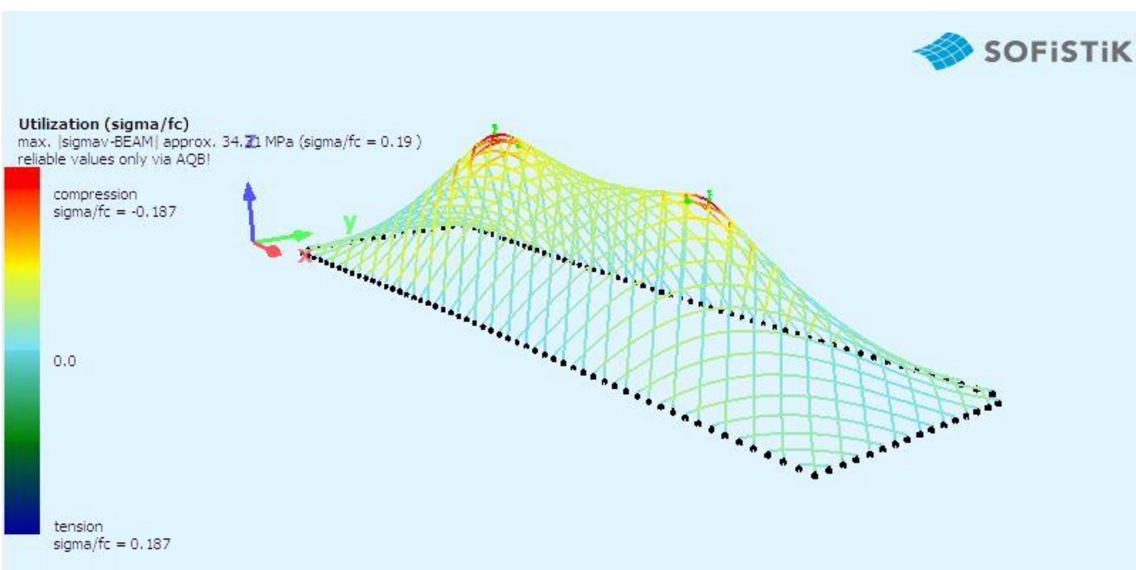

Figure 4.19 3D model of an actively bent grid shell in SOFiSTiK

4.6. Conclusion

In this chapter, a two-dimensional in-plane buckling analysis of an actively bent member with constant cross-section is presented. The finite element model in SOFiSTiK consist of a member with initial length of 6 meter, tubular cross-section of 40 mm diameter, 3 mm wall thickness, and 25 GPa elastic modulus.

From the in-plane buckling analysis (Section 4.2), it was concluded that the higher the amount of pre-bending, the higher the corresponding critical load. In other words, the stiffness of the a member increases when the level of bending increases.

In Section 4.3, the development of the vertical displacement due to a downward point load P between GFRP and CFRP members of equal dimensions was studied (f/a – 0.25). The critical buckling load for the CFRP member is 3.6 times greater compared to the GFRP member. This can be clarified by the elastic modulus taken for CFRP (90 GPa) being 3.6 times higher than the elastic modulus taken for GFRP (25 GPa).

From the creep-rupture analysis (Section 4.4) with SOFiSTiK it was concluded that if the sustained strains in both the GFRP and CFRP members are below their corresponding strain limits for creep-rupture (0.2 fult and 0.55 fult respectively, based on CUR96), the CFRP member is available for a point load at mid-span which is 11 times larger compared to the GFRP member. This might be of influence in driving the choice for using a material (e.g. CFRP over GFRP) that has better creep-rupture behavior in members of actively bent grid shells.

From the 3D analysis of an actively bent grid shell (Section 4.5) it was concluded that similar buckling- and creep-rupture analyses as performed in 2D, may be performed in 3D to study the importance of creep-rupture in actively bent grid shells as a whole.

PART III EXPERIMENTS

5. The Stepped Isostress Method

The Stepped Isostress Method (SSM) was founded by Giannopoulos & Burgoyne (2009) from Cambridge University and allows accelerated testing of materials in order to determine their creep response and creep-rupture behavior. Experimental studies (Giannopoulos & Burgoyne, 2009); (Hadid, Guerira, Bahri, & Zouani, 2014); (Tanks, Rader, Sharp, & Sakai, 2017) have shown that the SSM can be used to study creep behavior of FRP materials on a long-term with confidence, in high-stress applications.

The procedures of creep testing and data analysis using the SSM are presented in Section 5.1 and 5.2 respectively. Section 5.3 presents a comparison of aspects related to the SSM between different researchers. Section 5.4 brings the chapter to a conclusion and presents the SSM procedure utilized in this research.

5.1. Creep testing using the Stepped Isostress Method

The primary principle of creep testing using the SSM is that a single specimen is loaded in steps, from a starting stress level (reference stress) up to a final rupture stress. The test ends once the specimen ruptures. At each stress step a creep curve is obtained, which is then modified for the different stress levels to construct a final creep curve at a reference stress. Subsequently, the final creep curves at different reference stresses can be used to make predictions about the creep behavior of the material on a long-term. If both the stress levels and the duration of the steps are carefully chosen, creep testing using the SSM can be done in 24 hours. This is a great advantage compared to conventional creep testing (CCT).

The steps in the procedure of creep testing using the SSM are presented below:

1. Preliminary testing to determine the average ultimate strength of the specimens and the corresponding initial stress-strain curve.

2. Determination of the reference stresses and corresponding reference strains.

3. Determination of the final rupture stress level, taking into account:
   - The final rupture stress level should be high enough to make sure that creep tests can be done in ~24 hours.
   - The final rupture stress level should not be too high in order to avoid failure during the jump to the final stress level.

4. Division of steps into equal stress increases (see Figure 5.1).

5. Determination of the duration of the stress steps, referred to as creep dwell time, taking into account:
   - Each stress step should be long enough to include sufficient data from secondary creep stages.
   - Enough stress steps are required to represent the range of creep stages in a related long-term creep test. Usually three to five steps are applied until failure of the specimen is reached (Tanks).

6. SSM creep testing at different reference stresses.

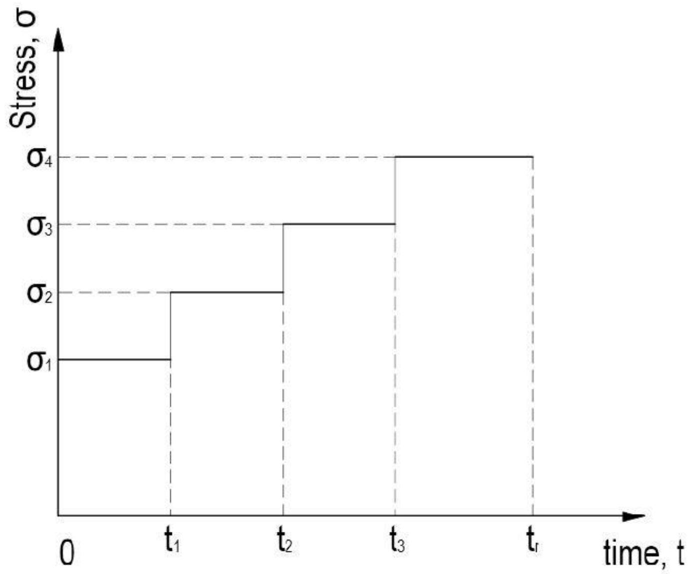

Figure 5.1 Exposures to a timed stepwise increase in stress (Giannopoulos & Burgoyne, 2011)

5.2. Procedure for data analysis using the Stepped Isostress Method

Results from creep testing using the SSM can be used to construct final creep curves, from where predictions of the FRP material on a long-term can be made. Similar to the creep response of FRP presented in Figure 3.3, the general form of a final creep curve based on the SSM is divided into three stages corresponding to primary, secondary, and tertiary creep (Giannopoulos & Burgoyne, 2011).

The procedure of creep testing and data analysis using the SSM is similar to the more traditional Time-Stress Superposition Principle (TSSP). The methods differ in that with SSM testing only one specimen is used for all stress levels instead of individual specimens. In data analysis, a rescaling step is introduced to take stress history into account before a time-stress shift factor is applied to construct the final creep curve (Tanks et al., 2017).

To construct the final creep curves using the SSM, the processing of the raw test data requires four steps corresponding to initial vertical adjustment (Section 5.2.1), vertical shifting (Section 5.2.2), rescaling (Section 5.2.3), and horizontal shifting (Section 5.2.4).

5.2.1. Initial vertical adjustment

The first step in the procedure for SSM data analysis is referred to as initial vertical adjustment. From preliminary testing, the average initial stress-strain curve is determined. This stress-strain curve includes ‘expected’ values for the initial strains at the three reference stresses. In this step, the total strain measured in the SSM test is adjusted by a constant vertical offset in order to match the expected value from the preliminary test (See Figure 5.2a).

5.2.2. Vertical shifting

The second step in the procedure for SSM data analysis is referred to as vertical shifting. Due to the elasticity of the FRP material, each increase in stress in SSM testing causes an instant increase in strain. In this step, these elastic strains are removed by shifting the individual creep curves vertically (see Figure 5.2b). The resulting creep curve includes only creep strains.

5.2.3. Rescaling

The third and most critical step in the procedure for SSM data analysis is referred to as rescaling. Key point is to use only secondary creep data from tests for the rescaling step and for following steps in construction of the creep master curves. The SSM analysis should only include primary creep data of the first stress step, as it relates to the material response on a very short-term (Hadid et al., 2014).

In the rescaling step, data from secondary creep stages of each stress step is extrapolated to the expected initial creep strain (see Section 5.3.1), using a curve-fitting equation. The difference in time between the real start of a step and the projected start time from the curve-fit is the rescaling time (see Figures 5.2c-d). The creep curves corresponding to load steps >1 have to be horizontally shifted over this rescaling time. The rescaling step is considered to be the replacement of the ‘real’ primary creep portion with the ‘virtual’ one, and therefore, to imitate an actual long-term creep test, only the secondary creep portion is rescaled.

Different curve-fitting equations are possible to extrapolate the individual creep curves. The secondary creep portion each step can be fitted with for example a power law (Hadid et al., 2014), a logarithmic function or a Prony series (Tanks et al., 2017). However, these different curve-fitting equations will result in different projected start times from the curve-fits and from that, different rescaling times.

Sub steps of the rescaling using the SSM are presented below:

i. Considering a given creep curve, the primary portion of creep is temporarily deleted from the curve. The limit between the primary and secondary creep portion may be defined based on a certain variation of strain rate of the considered creep curve.

ii. Extrapolation of secondary portion of the creep curve, using a curve-fitting equation.

iii. Determination of the rescaling time corresponding to the difference in time between the real start of the step (including primary and secondary creep portions) and the projected start time from the curve-fit.

iv. Shift of the creep curve (including primary and secondary creep portions) over the rescaling time.

v. Removal of primary creep portion from the curve.

5.2.4. Horizontal shifting

The fourth step in the procedure for SSM data analysis is referred to as horizontal shifting. To obtain a final creep curve at a reference stress, the individual creep curves that have resulted from rescaling should be shifted along the logarithmic time axis (see Figure 5.2e-f). The horizontal shifting corresponds to the rescaling step. The amount of horizontal shifting that is required for a smooth master curve is determined by the slope of the secondary creep curves obtained from rescaling (Tanks et al., 2017).

In the original papers about the SSM (written by Giannopoulos & Burgoyne), it is suggested to use a third order polynomial equation to check the smoothness of the final creep master curve. It is also possible to check it graphically, by ensuring a linear relationship exists between the factors for horizontal shifting and the stress levels related to the steps in the creep test (same slope and overlap as much as possible). A third way is to fit the first creep step of a test with a power law and subsequently compare the projected power law curve that is to fit the first creep step with the obtained creep master curve.

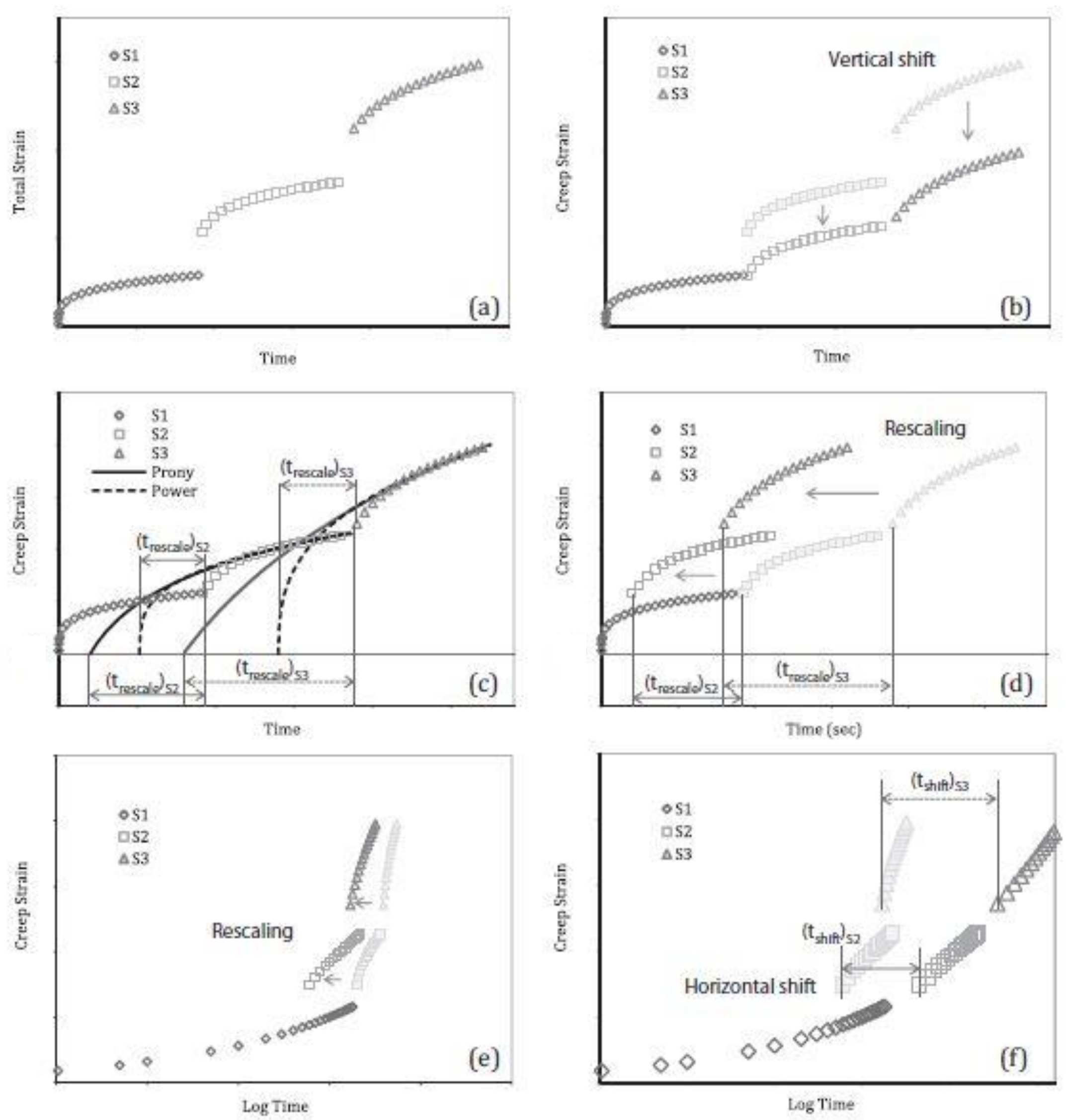

Figure 5.2 Steps in the procedure for SSM data analysis with (a) raw test data, (b) vertical shifting, (c) extrapolation of creep curves using Prony series and power-law equations, (d) rescaling of curves using Prony series, (e) conversion to logarithmic time, (f) horizontal shifting (Tanks et al., 2017)

5.2.5. Creep-rupture

Besides creep deformations, the SSM can also be used to predict creep-rupture behavior of materials. A creep test using the SSM is performed until failure of the specimen. The final creep curve of a related successful creep test is characterized by a stage of tertiary creep. The very last point of such final creep curve is the specimen's rupture time at a constant temperature (Giannopoulos & Burgoyne, 2011). Creep-rupture times corresponding to creep tests at different reference stresses can be plotted in one graph, so that predictions for creep-rupture times on a long term can be made.

5.3. Comparison of SSM aspects between researchers

Up to now, no standard procedure for the processing of the raw test data using the SSM is available (Hadid et al., 2014). In Table 5.1 and Table 5.2, comparisons are made of aspects related to the SSM between different studies. The last column presents SSM aspects for this research.

		research			
		Giannopoulos (2009)	**Hadid (2014)**	**Tanks (2016)**	**this research (2017)**
material and specimen	**material**	aramid yarns (Kevlar 49 and Technora)	polyamide 6 (TECAMID 6) (thermoplastic material)	diglycidyl-ether epoxy and PAN carbon fibers (V_f = 0.68)	epikote epoxy and Toho Tenax STS carbon fibers (V_f = 0.65)
	specimen type	350 mm nominal length, A = 0,17497 / 0,12260 mm^2	specimens cut from extruded 7 mm thick sheets	pultruded laminate with 1.2 mm thickness, 12 mm width, and 50 mm nominal length	pultruded tubes UD with braided outer layer, 30 mm diameter, 1 mm thickness, 300 mm nominal length
preliminary testing	**ultimate strength**	average breaking load (ABL) = 444.6 N (8.2 N st. dev.) / 349.0 N (6.8 N st. dev.)	ultimate tensile strength (UTS) ~ 48 MPa	ultimate tensile strength (UTS) = 41.9 MPa (5.6 MPa st. dev.) – 100% GUTS = 36.3 MPa	ultimate tensile strength (UTS) = 980.3 MPa (17.9 MPa st. dev.) – 100% GUTS = 964 MPa
	type of testing	tension	tension	tension	tension, compression, bending
	loading direction	parallel to fiber direction	-	perpendicular to fiber direction	parallel to fiber direction (tension and compression)
SSM creep testing	**amount of steps**	4 or 5	5 or 6	4	4
	creep dwell time	5 hours	2 and 5 hours	1 (at 85% GUTS) and 5 hours	5 hours
	reference stresses	50, 55, 60, 65, 70, 75% of ABL	1.5 MPa, 2.5 MPa and 4.0 MPa (different stepwise increase of stress)	40, 55, 70, 85% of guaranteed ultimate tensile strength (GUTS)	40, 60, 80% of GUTS, GUCS, GUFS
	final stress level	100% ABL		94% GUTS	96% GUTS, 94% GUCS, 100% GUFS

Table 5.1 Comparison of SSM creep testing aspects between different studies

		research			
		Giannopoulos et al. (2009)	**Hadid et al. (2014)**	**Tanks et al. (2016)**	**this thesis (2017)**
SSM data analysis	**elimination primary creep**	no	yes – not mentioned how	yes – secondary creep region	Yes – secondary creep region

				defined when creep strain rate varies by less than 0.025% from the start of a stress step	defined when creep strain rate is less than 2e-06 (in case of bending creep tests)
	rescaling	graphical procedure based on the Boltzmann superposition principle	power law fit based on the Boltzmann superposition principle	Prony series fit based on Schapery's single integral nonlinear superposition approach	second order polynomial (from EC2) fit
	horizontal shifting	Graphical procedure. Use of a third order polynomial equation to check the smoothness of final master curve. Validation with the Eyring equation.	Determination horizontal shift factor with its magnitude as a function of the stress level. Validation with the Eyring equation.	Determination of time-stress shift factor for each stress level. Use of a power law fit for the first creep step to check the smoothness of final master curve.	Determination of time-stress shift factor. Graphical check of smoothness of final master curve by ensuring that the shift factors of the specimens form the same slope and overlap as much as possible.

Table 5.2 Comparison of SSM data analysis aspects of different studies

5.4. Conclusion

In general, creep testing and data analysis using the Stepped Isostress Method (SSM) consists of three phases:

1. Preliminary testing:
    - To find the average ultimate strength of the FRP material and to determine the stress levels for the SSM creep tests. If both the stress levels and the duration of the stress steps are carefully chosen, creep testing using the SSM can be done in ~24 hours.
2. SSM creep testing:
    - A single specimen is loaded in steps, from a starting stress level up to a final stress level.
    - The procedure of creep testing and data analysis using the SSM is similar to the more traditional Time-Stress Superposition Principle (TSSP). The methods differ in that with SSM testing only one specimen is used for all stress levels instead of individual specimens.
3. SSM data analysis:
    - To make predictions of the FRP material on a long-term:
        - Deformations (strains)
        - Creep-rupture times
    - Processing of raw test data requires four steps: initial vertical adjustment, vertical shifting, rescaling, horizontal shifting.
    - Up to now, no standard procedure for the processing of the raw test data using the SSM is available.
    - The rescaling step is the most critical step in data analysis using the SSM. Key point is to use only secondary creep data from tests for the rescaling step.

6. Tension creep testing using the Stepped Isostress Method

The main objective of this research is to define stress limits related to time-dependent long-term creep behavior of CFRP in members of actively bent grid shells, using the Stepped Isostress Method (see Chapter 5). Creep testing using the SSM is performed on pultruded CFRP specimens made of epoxy and carbon fibers. Specimens were loaded in tension, compression, and bending respectively. Per load type, three creep tests were performed at different reference stresses: 40%, 60%, and 80% of the Guaranteed Ultimate Tensile Strength (GUTS), Guaranteed Ultimate Compressive Strength (GUCS), and Guaranteed Ultimate Flexural strength (GUFS). The final goal of creep testing and data analysis using the SSM, is to construct final creep curves at different reference stresses, from where predictions of the CFRP on a long-term can be made.

This chapter presents the results of tension creep testing and data analysis using the SSM. Test details are presented in Section 6.1. Section 6.2 presents initial results and observations, followed by data processing using the SSM in Section 6.3.

6.1. Test method

This section presents the material and specimen used for tension creep testing (6.1.1), followed by test details of preliminary tensile testing (6.1.2) and SSM creep tests (6.1.3).

6.1.1. Material and specimen

Tensile creep tests were performed on pultruded CFRP specimens made of Epikote epoxy and Toho Tenax STS carbon fibers (V_f = 0.65). The 30 mm x 28 mm tubular specimens are unidirectional with a braided outer layer and have a nominal length of 600 mm. According to the producer, the material has 2300 MPa tensile strength, 130 GPa elastic modulus, and a glass transition temperature of 65°C.

After preliminary experiments (Annex F), it was decided to use Φ28 mm steel bars measuring 300 mm in length as fitting between the specimen and the testing machine. One side of the bar was placed into the tubular specimen over 150 mm height. The other end was clamped with the testing machine. Steel clamps (150 mm x 150 mm x 60 mm) were used at both ends of the specimen to keep the steel bars in place without damaging the CFRP material (see Figure 6.2). On each of the four bolts a torque force of 130 Nm was applied. Figure 6.1 presents the equipment used for tensile tests.

6.1.2. Preliminary tensile tests

Preliminary tensile tests were carried out on three CFRP specimens (TR01-03) to find their average ultimate tensile strength (UTS). The specimens were prepared with steel bars and clamps, leaving a free span of 300 mm. Corresponding clamping detail is presented in Annex G.

Tensile tests were performed on a MTS 647 Hydraulic Wedge Grip with 250 kN capacity (see Figure 6.5). Two LVDTs prepared with the center of the CFRP specimen (gauge length = 130 mm) were used to measure displacements. Strain was measured with three strain gauges, glued to the center of the specimens.

Tensile loading with a speed of 1 mm/sec was applied to the specimens, at room temperature, until rupture had occurred (see Figures 6.6-8). The average ultimate tensile strength was 980.3 MPa with a standard deviation of 17.9 MPa. The average elastic modulus, obtained from the linear elastic region, was 119.3 GPa. Tensile response of the CFRP specimens (TR01-03) is presented in Figures 6.3 and 6.4.

Values found for the average ultimate tensile force (F_{ult}), stress ($\sigma_{T.ult}$), strains (ε_{ult}), and modulus of elasticity (E_T) are presented in Table 6.1. In preparation to the SSM creep tests, the value of the average ultimate tensile strength (980.3 MPa, 100% UTS) is reduced by one standard deviation to avoid premature failure at the high load steps, given the 1,8% coefficient of variation (COV, %) in strength. This results in a value referred to as the Guaranteed Ultimate Tensile Strength (962.4 MPa, 100% GUTS).

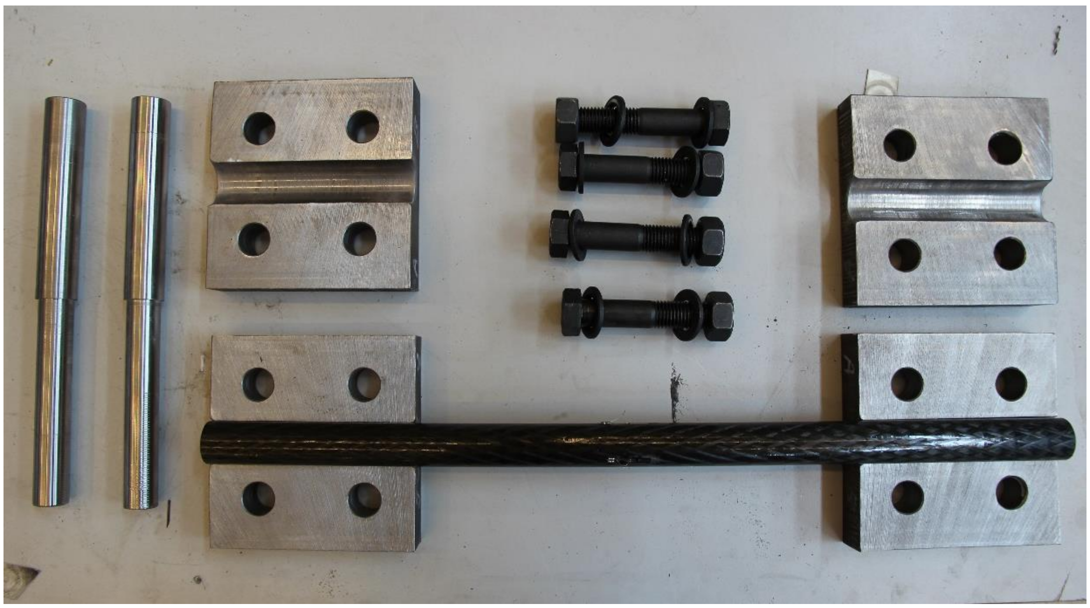

Figure 6.1 Equipment used for tensile testing

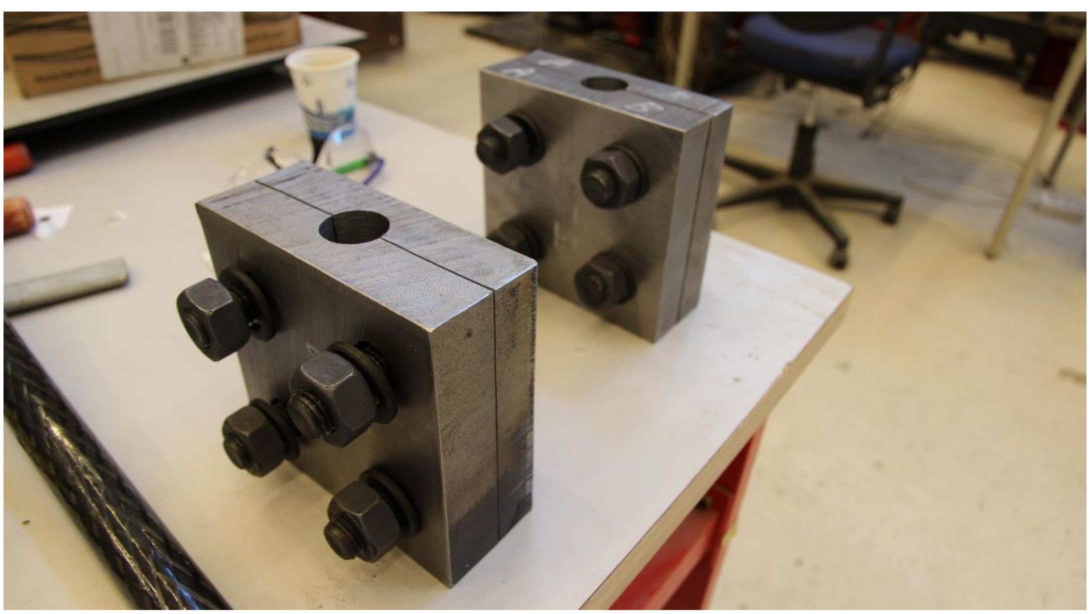

Figure 6.2 Steel clamps used to keep the steel bars in place during tension testing

property	quantity	TR01	TR02	TR03	mean
F_{ult}	kN	89,7	91,1	87,2	89,3
$\sigma_{t,ult}$	MPa	984,5	999,8	956,6	980,3
ε_{ult}	%	0,83	0,82	0,77	0,80
E_T	Gpa	115,8	119,6	122,4	119,3

Table 6.1 Results from preliminary tensile tests (TR01-03)

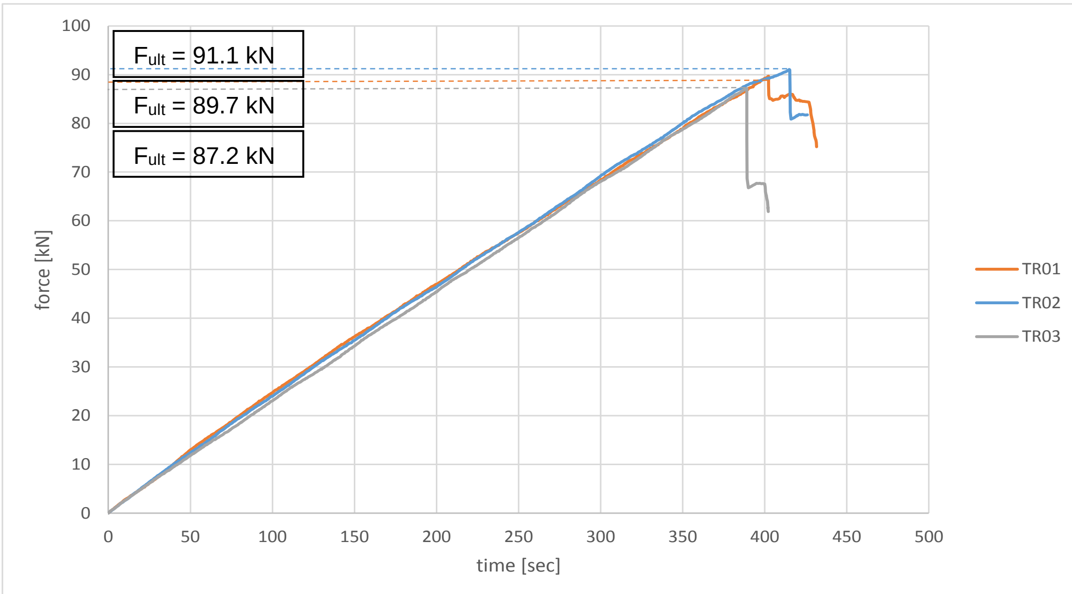

Figure 6.3 Force-time diagram of TR01-03 results

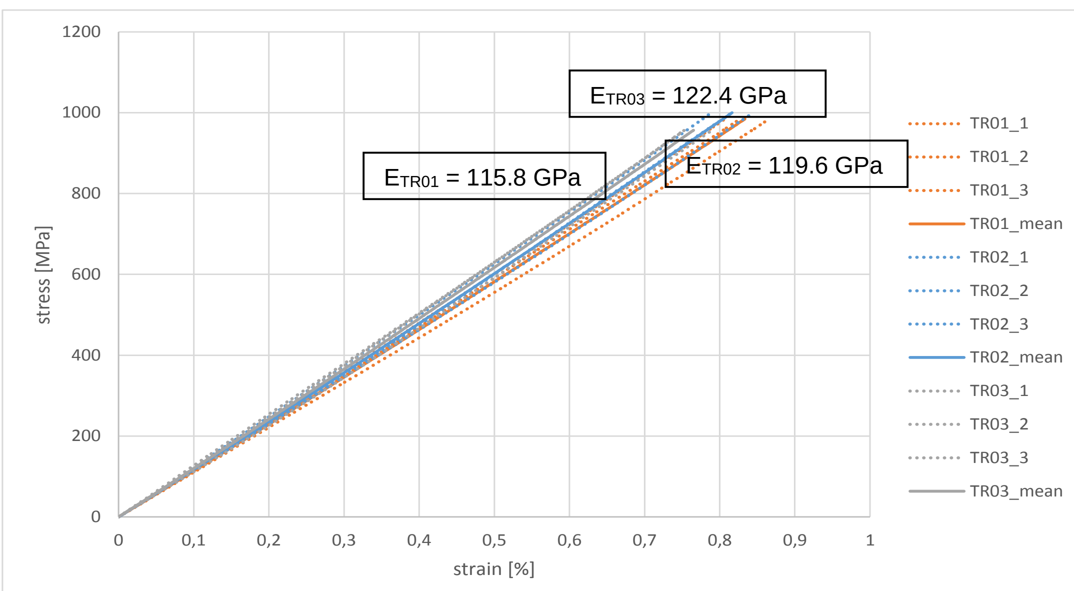

Figure 6.4 Tensile response of CFRP specimens (TR01-03) based on strain gauges

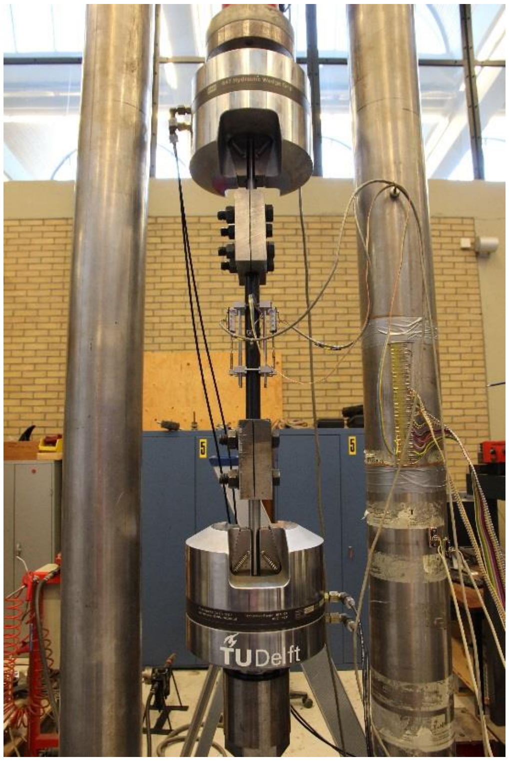

Figure 6.5 CFRP specimen in MTS 647 test machine

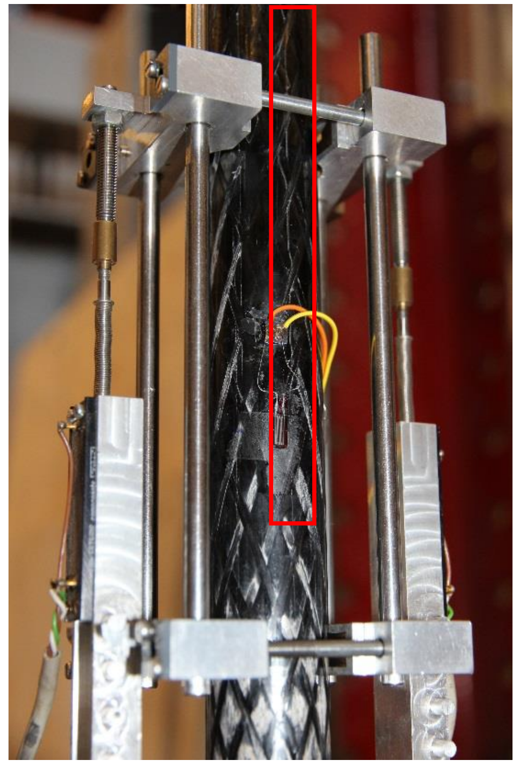

Figure 6.6 Rupture of reference specimen 1 (TR01)

Figure 6.7 Rupture of reference specimen 2 (TR02)

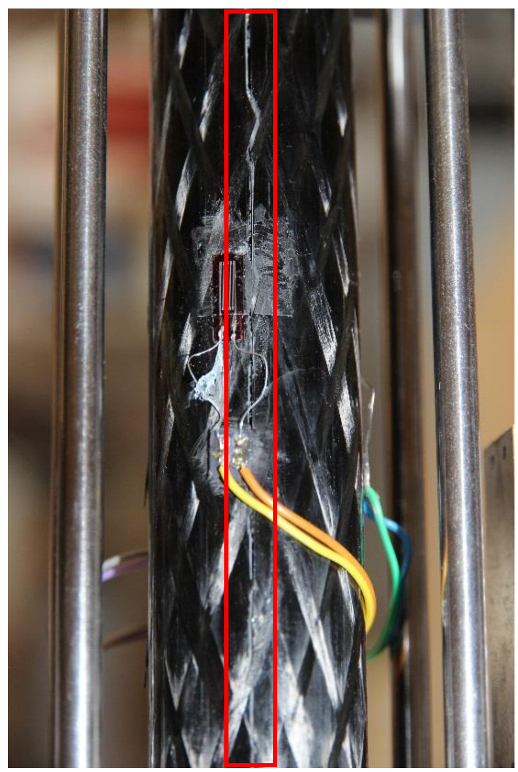

Figure 6.8 Rupture of reference specimen 3 (TR03)

6.1.3.SSM creep tests

SSM creep tests were carried out at constant room temperature on similar specimens and with the same equipment as used for preliminary tensile tests. Three creep tests were performed on specimens loaded in tension (TC01-03) at different starting stress levels (reference stresses); at 40%, 60%, and 80% of the GUTS. For the final load step the stress level was chosen to be 96% GUTS. The specimens were loaded in four to six steps, from their corresponding reference stress until the final rupture stress. Test parameters for the tension creep tests are presented in Table 6.2.

name	**reference stress**			**step parameters**	**load step**					
test	% GUTS	% UTS	MPa		1	2	3	4	5	6
TC01	40	39,3	385,0	stress level [MPa]	385,0	564,6	744,3	923,9		
				step duration [hr]	5	5	5	0,01		
TC02	60	58,9	577,5	stress level [MPa]	577,5	693,0	808,4	923,9		
				step duration [hr]	5	5	5	103,5		
TC03	80	78,5	769,9	stress level [MPa]	769,9	821,3	872,6	923,9	976,3	1026,9
				step duration [hr]	5	5	5	37,7	21,6	90,4

Table 6.2 Test parameters for tension creep tests TC01-03 using the SSM

6.2. Initial results and observations SSM tension creep tests

Detailed results and observation of the SSM creep tests in tension TC01-03 are presented in Annex H. Figures 6.9 and 6.10 present the force versus time diagram and total-strain versus time diagram of TC01-03. The CFRP specimen tested at a reference stress of 40% GUTS (TC01) ruptured after a few seconds in the fourth load step. The specimen failed by brittle splitting vertically along the free span. Only little creep strains were measured during testing of TC01.

The CFRP specimen tested at a reference stress of 60% GUTS (TC02) still had not ruptured after 103.5 hours in the final load step, therefore it was decided to break down the experiment. The specimen was subjected to increasing amount of tensile loading and finally failed at 108 kN of force.

The CFRP specimen tested at a reference stress of 80% GUTS (TC03) still had not failed after 37.7 hours in the final load step, and it was decided to increase the loading with one step (step 5 in Table 6.2). After 21.6 hours it was decided to increase the loading with another step (step 6 in Table 6.2), and finally to break down the experiment. The specimen was subjected to increasing amount of tensile loading, and finally failed at 110.8 kN of force. It is remarkable that of both load levels 1 and 2 the difference in creep strain between the start and end of the load steps is negative. Possible causes: the CFFRP specimen has crept at a cross-section different from its center part / the strain gauges were attached incorrectly to the specimen.

Due to brittle fracture of the specimens, it is difficult to see where the initiation of fracture occurred. It is remarkable that both TC02 and TC03 failed in the creep tests at a final loading of 108.0 kN and 110.8 kN respectively, while the average ultimate tensile strength of TR01-03 was 89.3 kN. The specimens TC02 and TC03 may have had a higher ultimate strength than the ultimate tensile strength of TR01-03 obtained during preliminary testing. Specimens for tension testing were obtained from the producer in two tribes, which may have led to a difference in chemical composition or wall thickness of the specimens, leading to deviate response of TC02 and TC03 in SSM creep tests.

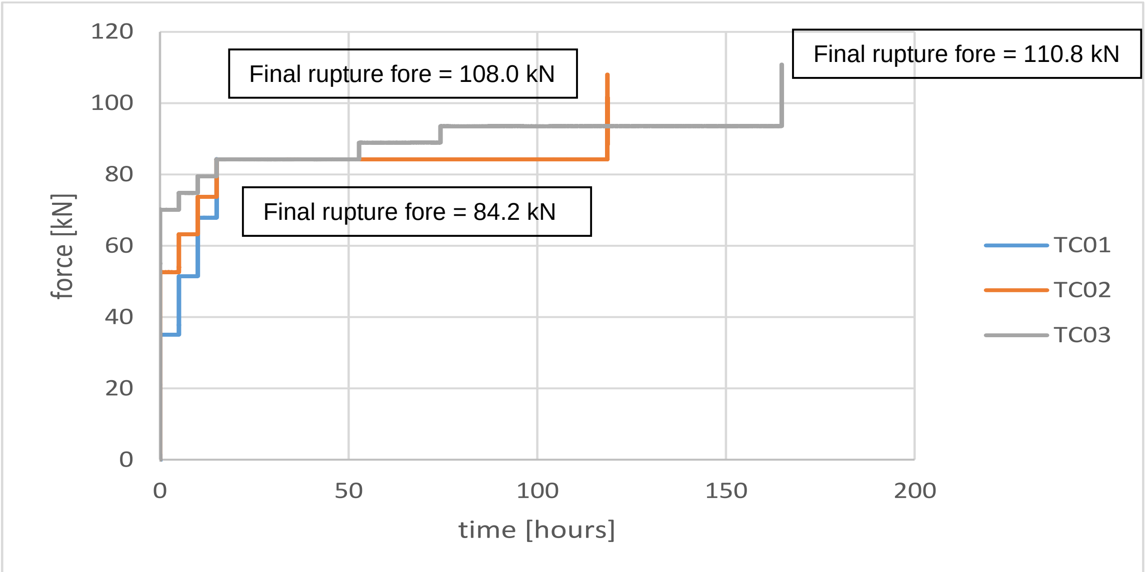

Figure 6.9 Force-time diagram of TC01-03 results

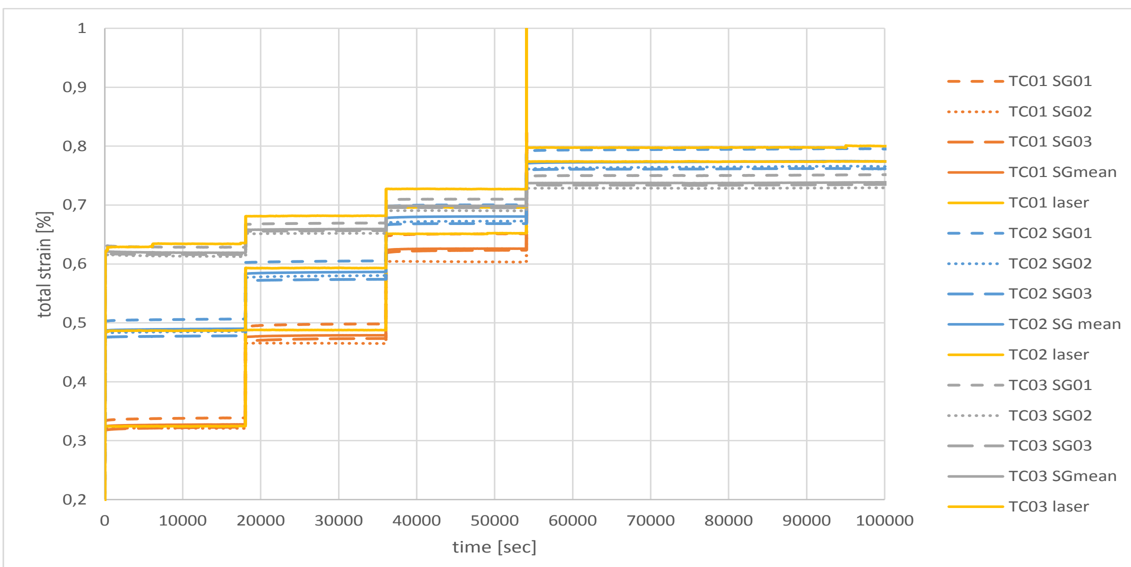

Figure 6.10 Total strain versus time diagram of TC01-03 results (until ~30 hours of testing)

6.3. SSM data analysis

In a successful SSM test of this type, the creep strain-time curve in the final load level is characterized by a stage of tertiary creep. The very last point of a corresponding final creep curve is the specimen's rupture time at a constant temperature. No tertiary creep stages were obtained from test data as the specimens fractured during the jump to the final load level (TC01), or the initiation of facture has not occurred at mid-point (TC02, TC03). Therefore predictions for creep-rupture times cannot be made according to the method described in Section 5.2.5. In addition, as only very little creep strains are measured (TC01 and TC02), and measured creep strains are negative (TC03), it was decided not to perform further analysis using the SSM.

7. Compression creep testing using the Stepped Isostress Method

This chapter presents results of compression creep testing and data analysis using the Stepped Isostress Method (see Chapter 5) carried out on pultruded CFRP specimens made of epoxy and carbon fibers. Test details are presented in Section 7.1. Section 7.2 presents initial results and observations of the SSM creep tests, followed by data processing using the SSM in Section 7.3.

7.1. Test method

This section presents the material and specimen used for compressive creep testing (7.1.1), followed by test details of preliminary compressive tests (7.1.2), and SSM creep tests (7.1.3).

7.1.1. Material and specimen

Compressive creep tests were performed on pultruded CFRP specimens made of Epikote epoxy and Toho Tenax STS carbon fibers ($V_f = 0.65$). The 30 mm x 28 mm tubular specimens are unidirectional with a braided outer layer and have a nominal length of 150 mm.

After preliminary experiments (See Figure 7.1), it was decided to use metal rings, forming a cup, adhesive bonded to the specimens ends. The metal cups control lateral pressure of the CFRP material during compressive testing. The specimens were placed in between two steel plates that distributed the load across the surface area of the specimen's ends. A hinge attachment was used to ensure uniaxial compressive load was applied.

Figure 7.1 CFRP specimens tested in preliminary compression tests

7.1.2. Preliminary compression tests

Preliminary compression tests were carried out on four CFRP specimens (CR01-04) to find their average ultimate compressive strength (UCS). The specimens were prepared with metal cups, leaving a free span of 110 mm. Corresponding detail of the adhesive bonded assembly is presented in Annex G.

Compressive tests were performed on a Schenck test machine with 300 kN capacity (see Figure 7.2). Six strain gauges glued to the center of the specimen were used to measure strains. Compressive loading with a speed of 0.02 mm/sec was applied to the specimens, at room temperature, until rupture had occurred (see Figures 7.6-9). The brittle fracture of CR02 presented in Figure 7.7 aligned with expectations. The average ultimate compressive strength was 517.7 MPa with a standard deviation of 68.1 MPa. The average elastic modulus, obtained from the linear elastic region, was 117.1 GPa. Compressive response of the CFRP specimens (CR01-04) is presented in Figures 7.4 and 7.5.

Values found for the average ultimate tensile force (F_{ult}), stress ($\sigma_{c,ult}$), strains (ε_{ult}), and calculated modulus of elasticity (E_C) are presented in Table 7.1. In preparation to the SSM creep tests, the value of the average ultimate compressive strength (517.7 kN, 100% UCS) is reduced by one standard deviation to avoid premature failure at the high load steps, given the 13.2% COV in strength. This results in a value referred to as the guaranteed ultimate compressive strength (449.7 MPa, 100% GUCS).

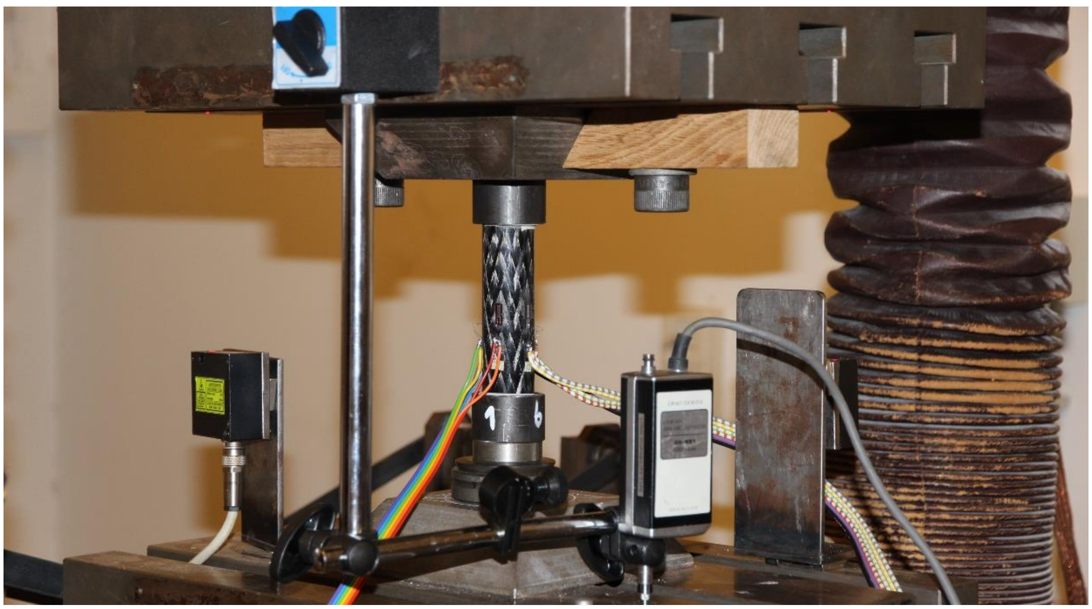

Figure 7.2 Compression test set-up with CFRP specimen

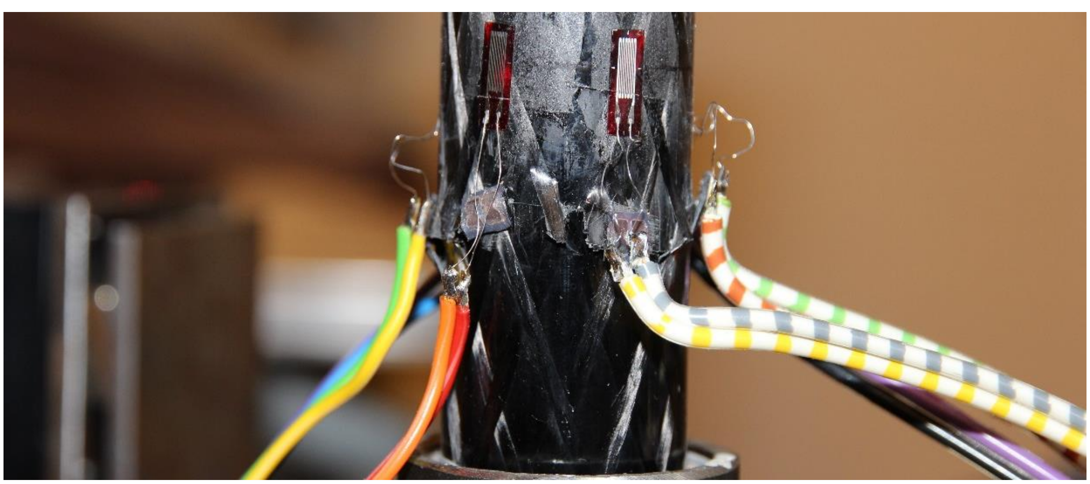

Figure 7.3 Failure of specimen CC02 in SSM compression test

property	quantity	CR01	CR02	CR03	CR04	mean
F_{ult}	kN	39,7	56,9	46,8	45,3	47,2
$\sigma_{c,ult}$	MPa	436,1	624,7	513,2	496,7	517,7
ε_{ult}	%	0,40	0,54	0,41	0,47	0,46
E_C	Gpa	114,0	118,9	121,4	113,9	117,1

Table 7.1 Results from preliminary compressive tests (CR01-04)

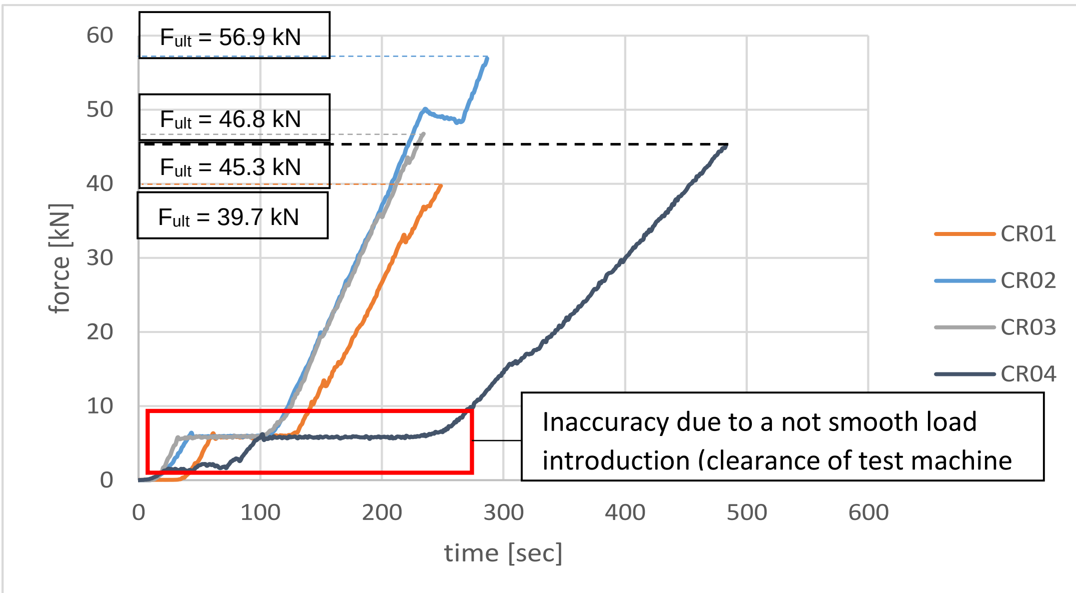

Figure 7.4 Force-time diagram of CR01-04 results

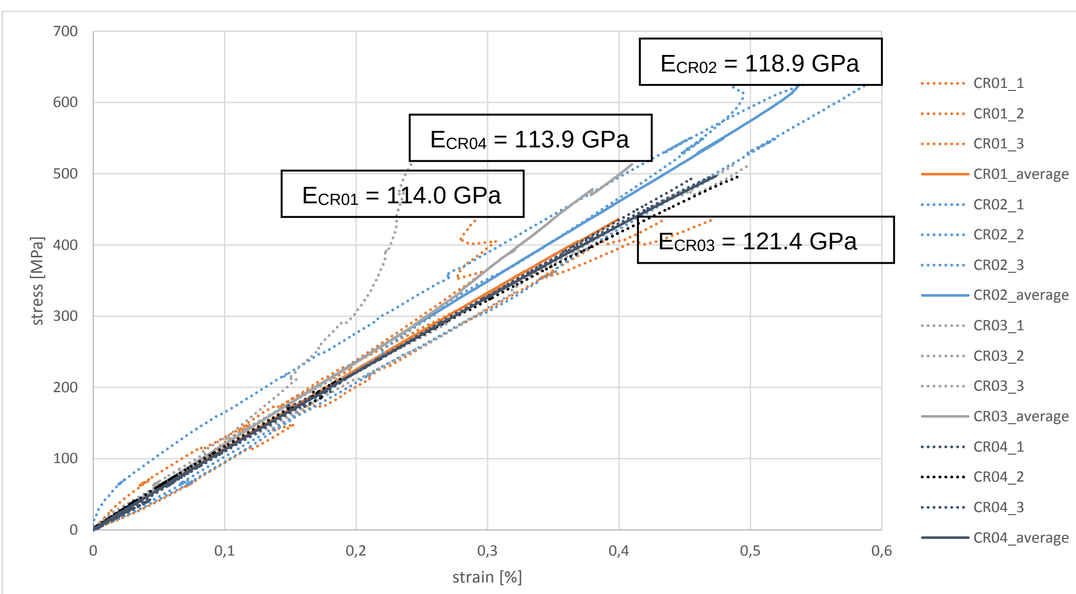

Figure 7.5 Compressive response of CFRP specimens (CR01-04) based on strain gauges

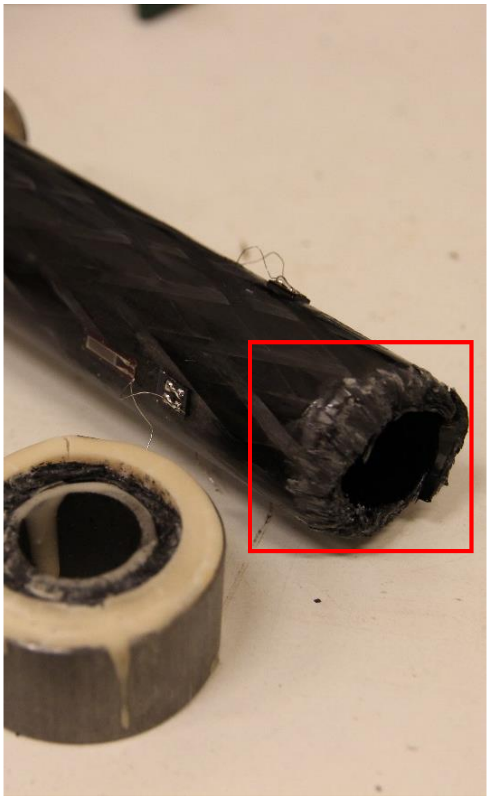

Figure 7.6 Rupture of reference specimen 1 (CR01)

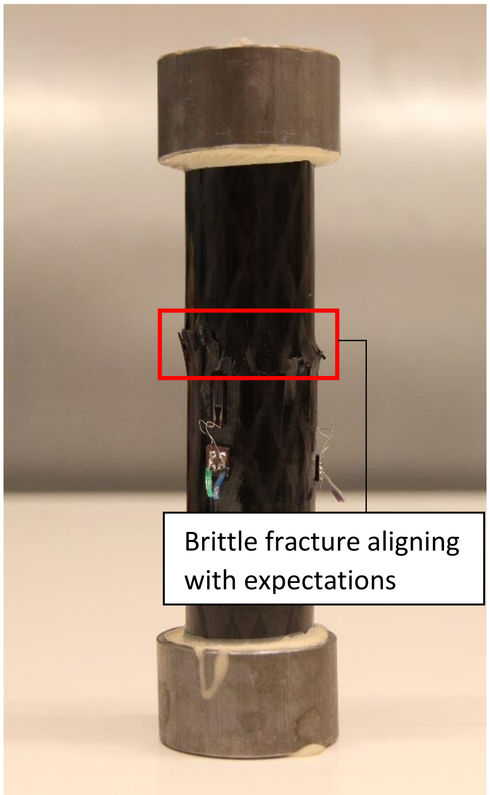

Figure 7.7 Rupture of reference specimen 2 (CR02)

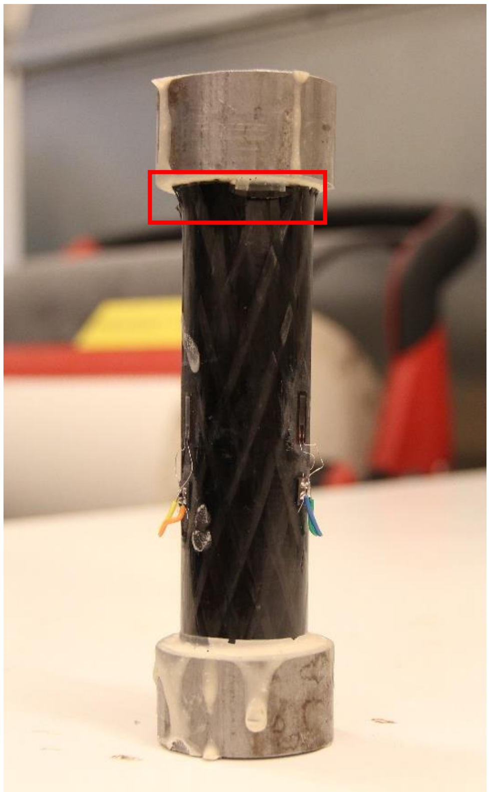

Figure 7.8 Rupture of reference specimen 3 (CR03)

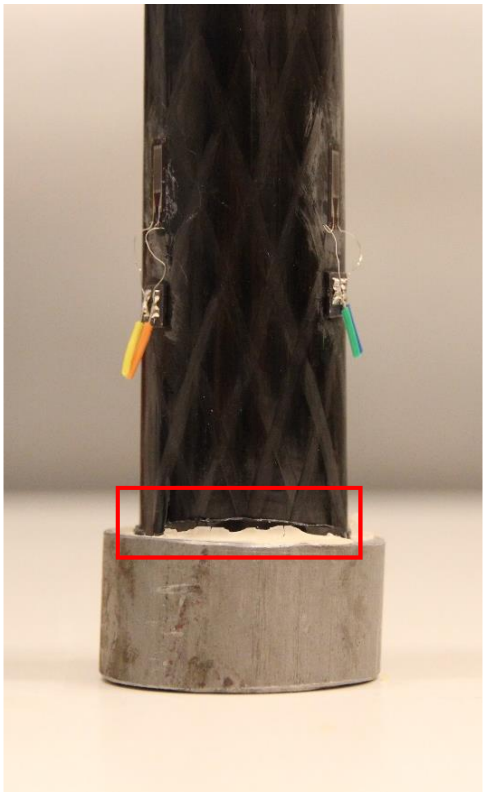

Figure 7.9 Rupture of reference specimen 4 (CR04)

7.1.3. SSM creep tests

SSM creep tests were carried out at constant room temperature on similar specimens and with the same equipment as used for preliminary compressive tests. Three creep tests were performed on specimens loaded in compression (CC01-03) at different starting stress levels (reference stresses) - 40%, 60%, and 80% of the GUCS. For the final load step the stress level was chosen to be 94% GUCS. The specimens were loaded in four to five steps, from their corresponding reference stress until the final rupture stress. Test parameters for the compression creep tests are presented in Table 7.2.

name	**reference stress**			**step parameters**	**load step**				
test	% GUCS	% UCS	MPa		1	2	3	4	5
CC01	40	34,7	179,9	stress level [MPa]	179,9	260,8	341,7	422,7	
				step duration [hr]	5	5	5	8,8	
CC02	60	52,1	269,8	stress level [MPa]	269,8	320,8	371,7	422,7	503,5
				step duration [hr]	5	5	5	11,3	2,7
CC03	80	69,5	359,7	stress level [MPa]	359,7	380,7	401,7	422,7	
				step duration [hr]	5	5	5	failure during jump	

Table 7.2 Test parameters for compression creep tests CC01-03 using the SSM

7.2. Initial results and observations SSM creep tests

Detailed results and observations of the SSM creep tests in compression CC01-03 are presented in Annex I. Figure 7.10 presents the force-time diagram of CC01-03. The CFRP specimen tested at a reference stress of 40% GUCS (CC01) ruptured after 8.8 hours in the fourth load step. The specimens were prepared with metal cups, leaving a free span of 110 mm. No visible damage or deformation appeared on the free span' surface. The specimen did not rupture at the mid-point, but somewhere within the cup area. Remarkable is that the difference of creep strains measured by the laser is significantly higher compared to the (negative) difference of creep strains measured by the strain gauges. This may indicate creep occurred at another location than midpoint, causing decrease in length of the specimen's surface at mid-point.

The CFRP specimen tested at a reference stress of 60% GUCS still had not failed after 11.3 hours in the final load step, and it was decided to increase the loading with a fifth step. After 2.7 hours the specimen failed by brittle circumferential cracking at the center, the preferred mode of delivery for failure in a successful SSM test of this type (see Figure 7.3).

The CFRP specimen tested at a reference stress of 80% GUCS failed during the jump from the third to the fourth load step. No visible damage or deformation appeared on the free span' surface. The specimen did not rupture at mid-point, but somewhere within the cup area. As a large number of points was measured in the third load step, measurements from strain gauges and laser were stopped after 3.7 hours.

For all three tests (CC01-03), during the jump to the first load level, notable amount of elastic strains were measured by the laser, in contrast to the strains from the strain gauges. This may indicate the initiation of fracture, causing a decrease in length of the specimen's surface at mid-span, already occurred during the jump to the first load level.

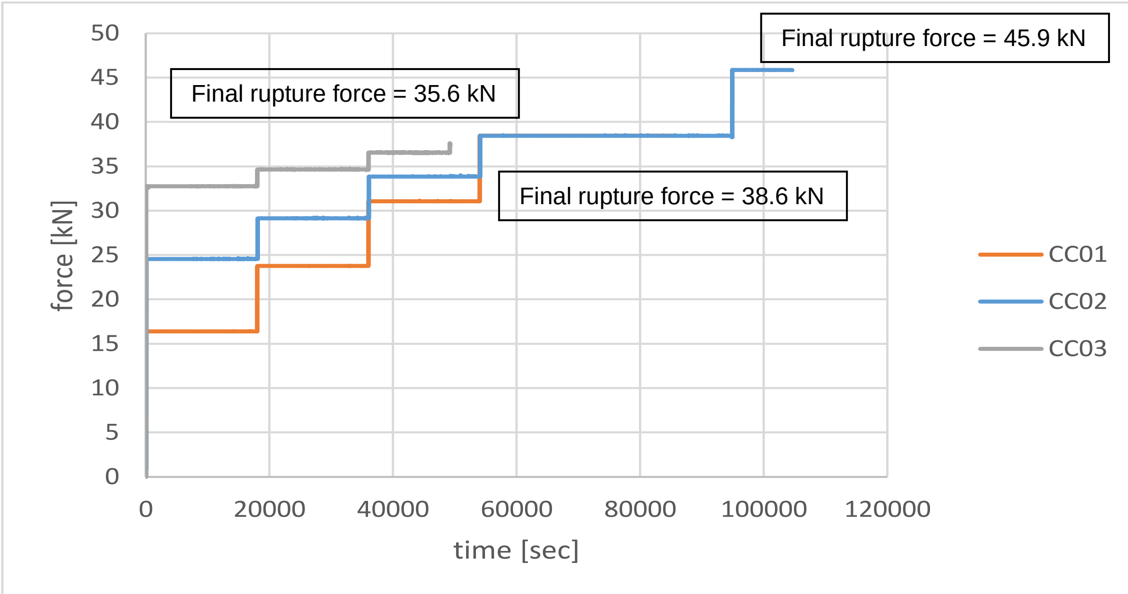

Figure 7.10 Force-time diagram of CC01-03 results

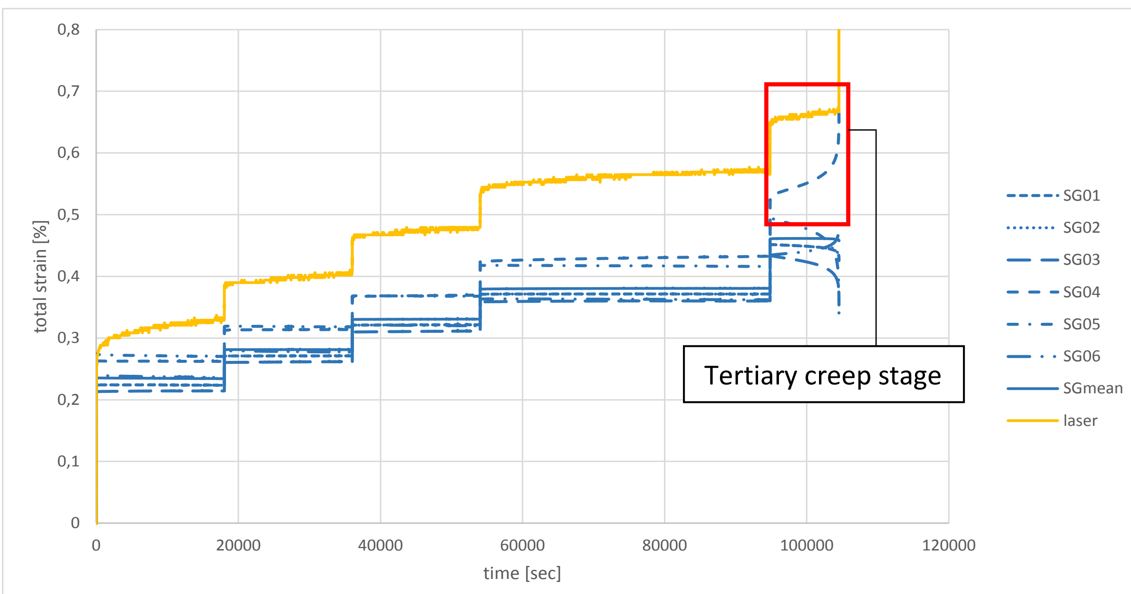

Figure 7.11 Total strains from strain gauges and laser of CC02

7.3. SSM data analysis

In a successful test of this type, the specimen fails by circumferential cracking at the center. This preferred mode of delivery for failure was observed with specimen CC02, which showed brittle fracture behavior at the mid-point. The strain-time curve in the final load level of CC02 is characterized by a stage of tertiary creep (see Figure 7.11). Data from this test may be used for further analysis to predict the creep-rupture times of the specimens on a long-term, using the method described in Section 5.2.5. As almost no creep strains were measured during the SSM creep tests CC01-03, and also negative values of creep strains were measured, it was decided not to perform SSM analysis with data from strain gauges.

8. Bending creep testing using the Stepped Isostress Method

This chapter presents results of bending creep testing and data analysis using the Stepped Isostress Method (see Chapter 5) carried out on pultruded CFRP specimens made of epoxy and carbon fibers. Results from the experiments are used to study creep behavior in bending on a long-term. Test details are presented in Section 8.1. Section 8.2 presents initial results and observations of the SSM creep tests, followed by data processing using the SSM in Section 8.3. The chapter is concluded with end results of the observations in Section 8.4.

8.1. Test method

This section presents the material and specimen used for bending creep tests (8.1.1), followed by test details of preliminary bending tests (8.1.2), and SSM creep tests (8.1.3).

8.1.1. Material and specimen

Bending creep tests were performed on pultruded CFRP specimens made of Epikote epoxy and Toho Tenax STS carbon fibers (V_f = 0.65). The 30 mm x 28 mm tubular specimens are unidirectional with a braided outer layer and have a nominal length of 700 mm.

Steel bars measuring 250 mm in length were used in both ends of the specimens to stiffen locally. The bars had a diameter fitting precisely into the specimens to ensure the specimen would rupture at its center, where the maximum bending moment would be located and shear forces are zero.

To prevent failure at the positions where the load was introduced, metal rings were adhesive bonded to the exterior of the specimens with an PMCA adhesive (see Figure 8.1). Timber blocks were positioned at the height of the supports of a four-point-bending set-up to avoid the specimens moving sideways (see Figure 8.2).

Figure 8.1 Preparation of CFRP specimen with metal rings for bending tests

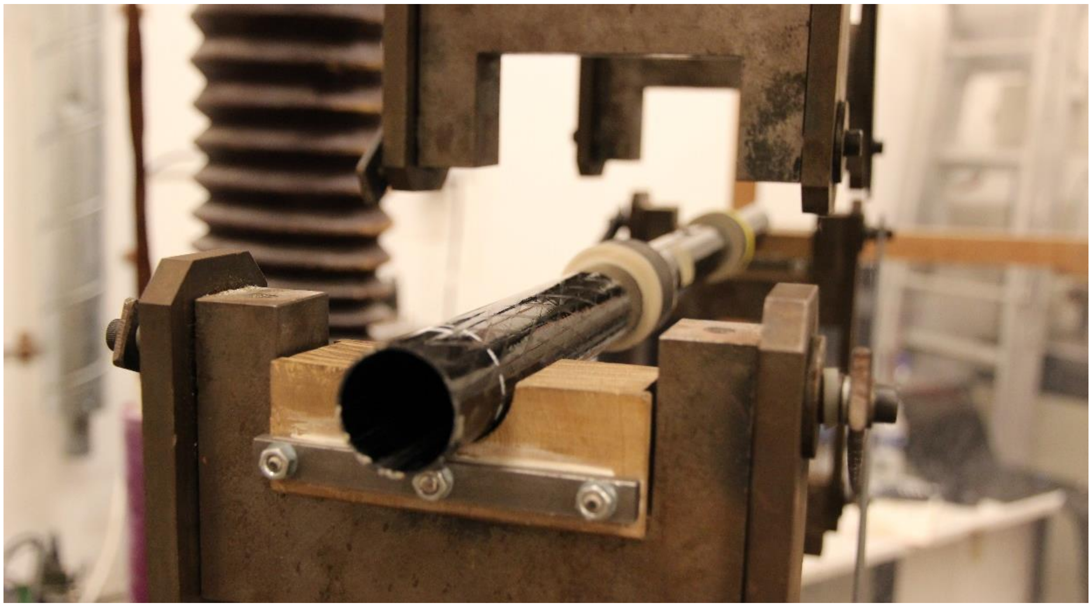

Figure 8.2 Timber blocks in four-point bending set-up (without steel bars inside the specimen)

8.1.2. Preliminary bending tests

Preliminary bending tests were carried out on three specimens (FR01-03) to find their average ultimate bending strength (UFS). The specimens were prepared with metal bars, -rings, and timber blocks, leaving a free span of 602 mm. Corresponding mechanical scheme is presented in Annex K.

Flexural tests were performed on a Schenck test rig with 300 kN capacity, in which a steel four-point bending frame was placed (see Figure 8.3). The static driven ramp of the test rig was used to apply displacement controlled loading to the frame with the specimen, with a speed of 0.02 mm/sec. Two lasers were prepared with the four-point bending frame. Laser I measuring downwards to the top of the specimen was used to calculate strains. Laser II measuring upwards to the bottom of the specimen was used to obtain the vertical deflection of the center of the specimen. Strain was measured with two strain gauges, glued on top and bottom center of the specimens.

The specimens were loaded in bending at room temperature until rupture had occurred (see Figures 8.8, 8.9). The average ultimate bending strength was 632.6 MPa with a standard deviation of 40.5 MPa. The average elastic modulus, calculated from the average from measured strains, was 118.5. Bending response of the CFRP specimens (FR01-03) is presented in Figures 8.5-7. Values found for the average ultimate bending force (F_{ult}), stress ($\sigma_{F.ult}$), deflection (δ_{ult}), strains (ε_{ult}), and elastic modulus (E_F) are presented in Table 8.1. The table shows also corresponding “expected” values which were obtained using the preliminary calculations presented in Annex K.

property	quantity	FR01	FR02	FR03	average	expected	diff. [%]
F_{ult}	kN	4,7	5,2	4,5	4,8	5,1	-5,9
$\sigma_{F.ult}$	MPa	617,1	688,1	592,5	632,6	672,1	-5,9
δ_{ult}	mm	14,8	16,3	13,4	14,8	15,6	-5,0
ε_{ult}	%	0,44	0,67	0,49	0,53	0,58	-8,2
E_F	Gpa	121,5	114,0	120,1	118,5	117,1	1,2

Table 8.1 Results from preliminary bending tests (FR01-03)

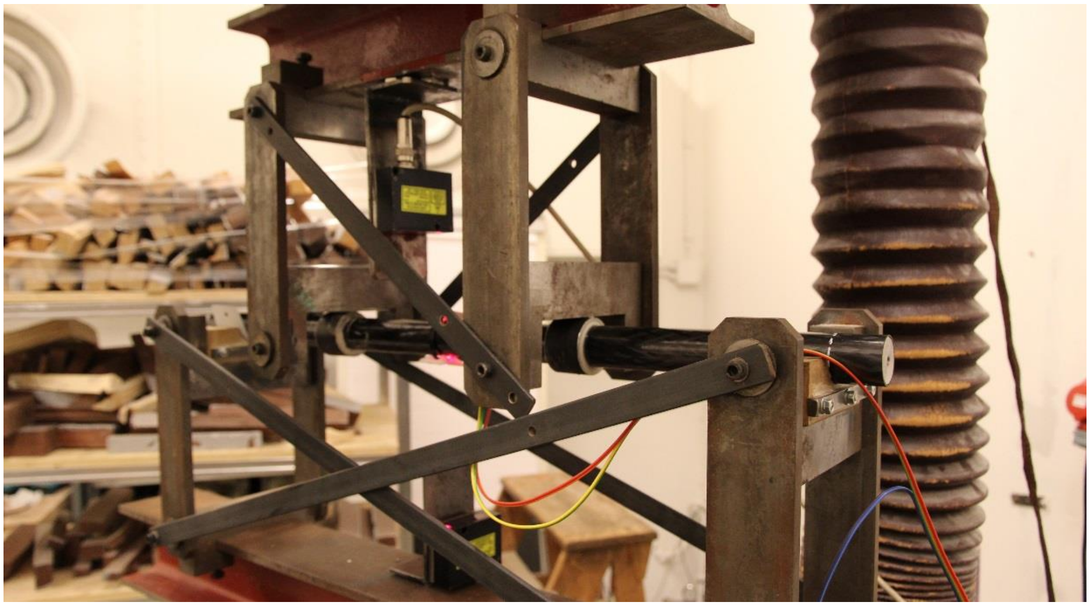

Figure 8.3 Bending test set-up with CFRP specimen

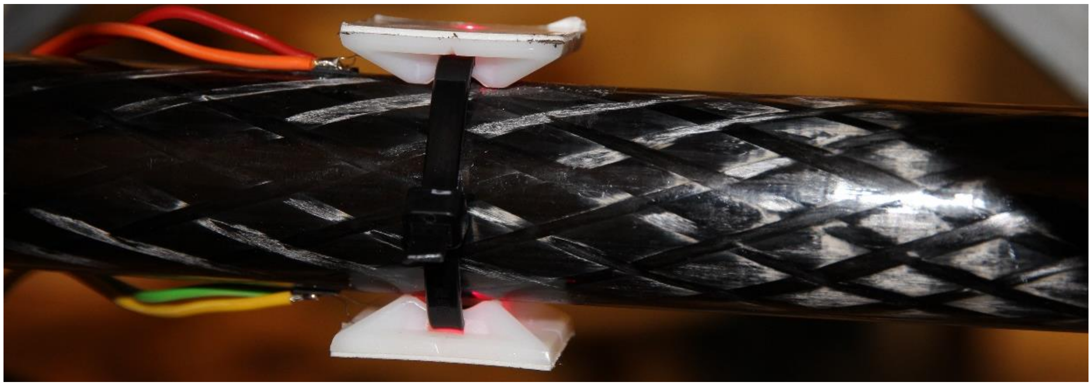

Figure 8.4 Tyrib-assembly to allow for laser measurements at the CFRP specimen's mid-point

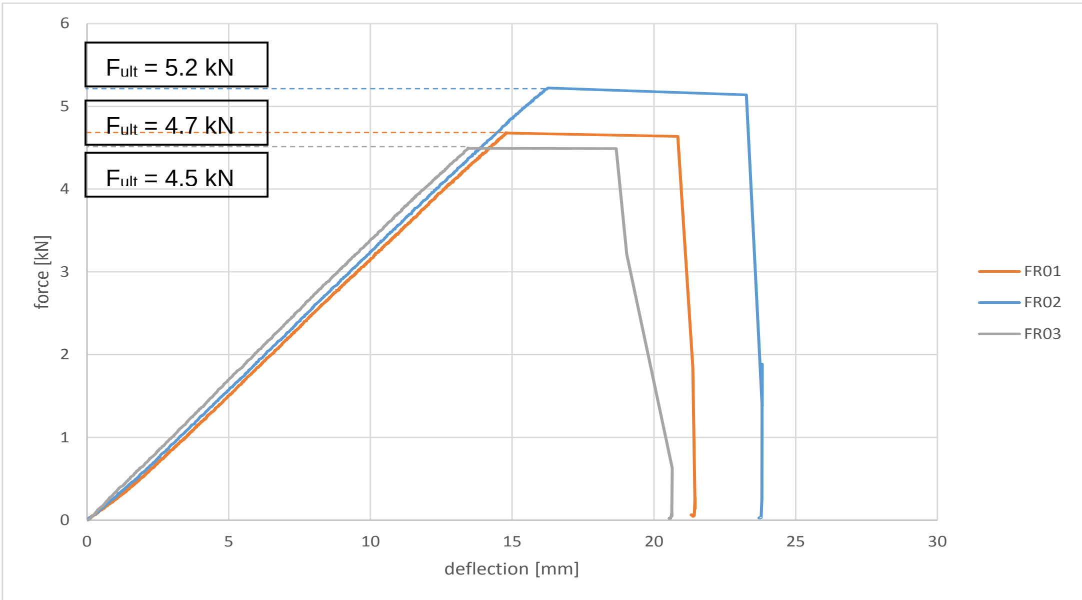

Figure 8.5 Force-displacement diagram of FR01-03 results

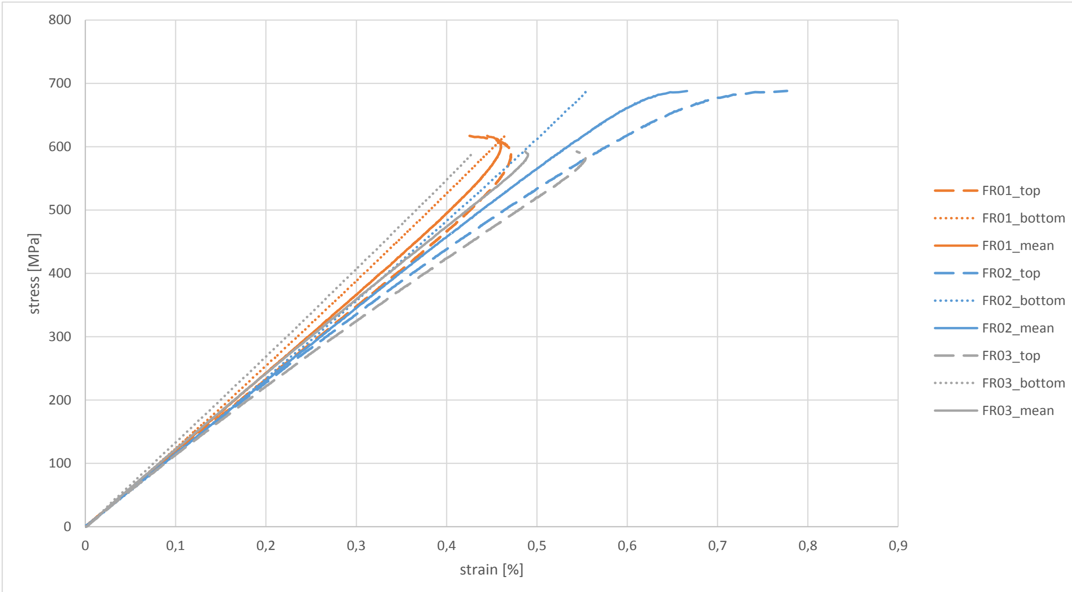

Figure 8.6 Bending response of CFRP specimens (FR01-03) based on strain gauges

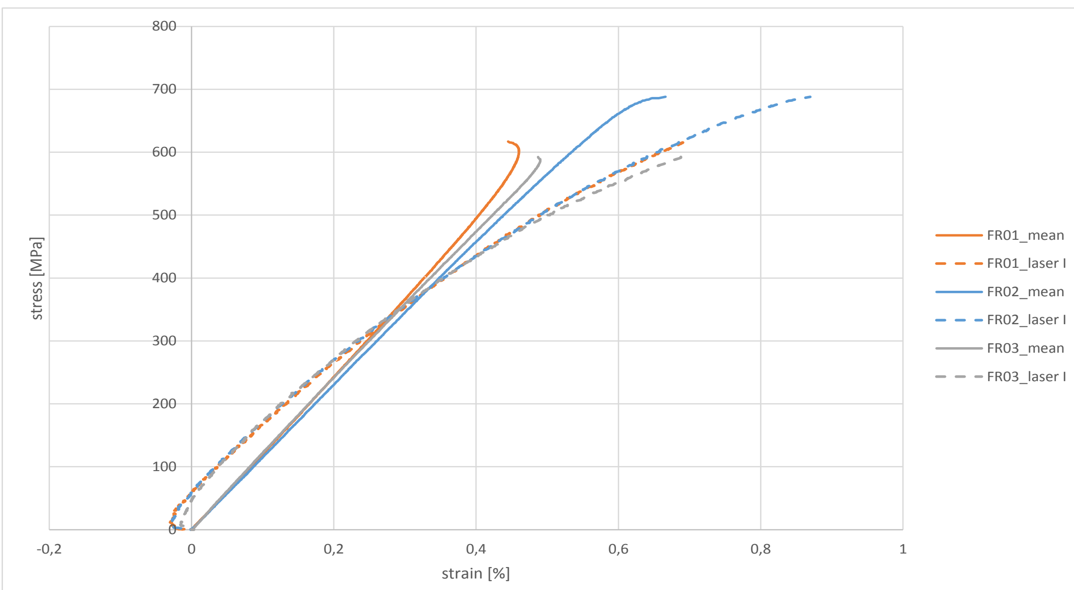

Figure 8.7 Bending response of CFRP specimens (FR01-03) based on strain gauges and laser

8.1.3.SSM creep tests

SSM creep tests were carried out at constant room temperature on similar specimens and with the same equipment as used for preliminary bending tests. Three creep tests were performed on specimens loaded in bending (FC01-03) at different starting stress levels – 40%, 60%, and 80% of the GUFS. For the final load step the stress level was chosen to be 100% GUFS. The specimens were loaded in four steps, from their corresponding reference stress until the final rupture stress. Test parameters for the bending creep tests are presented in Table 8.2.

name	reference stress			step parameters	load step			
test	% GUFS	% UFS	MPa		1	2	3	4
FC01	40	37,4	236,8	stress level [MPa]	236,8	355,2	473,7	592,1
				step duration [hr]	5	5	5	0,3
FC02	60	56,2	355,2	stress level [MPa]	355,2	434,2	513,1	592,1
				step duration [hr]	5	5	5	failure jump
FC03	80	74,9	473,7	stress level [MPa]	473,7	513,1	552,6	592,1
				step duration [hr]	5	5	5	3,5

Table 8.2 Test parameters for bending creep tests FC01-03 using the SSM

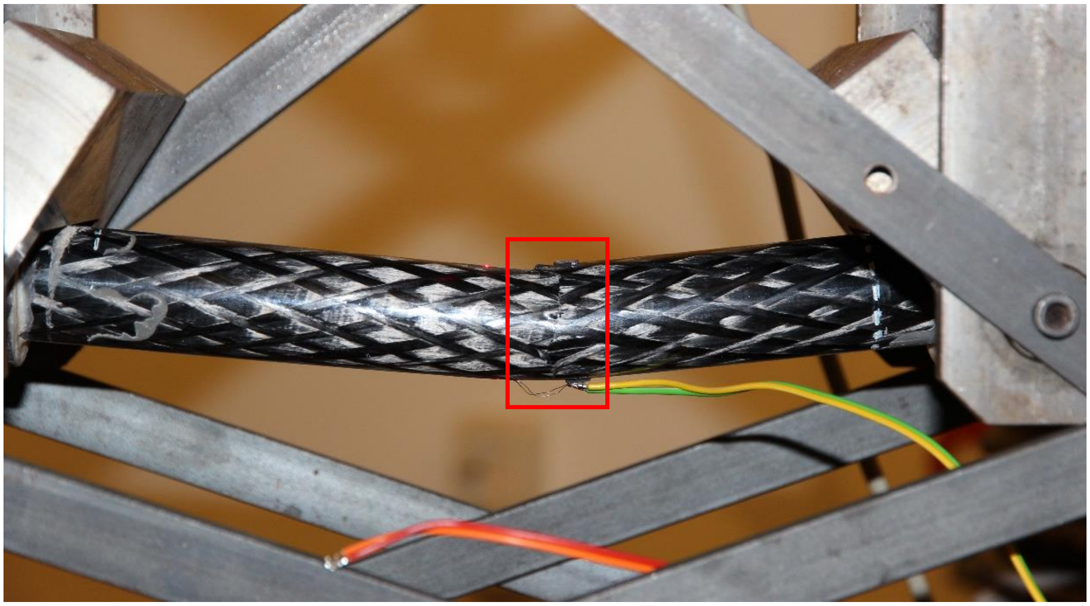

Figure 8.8 Failure of specimen FR01

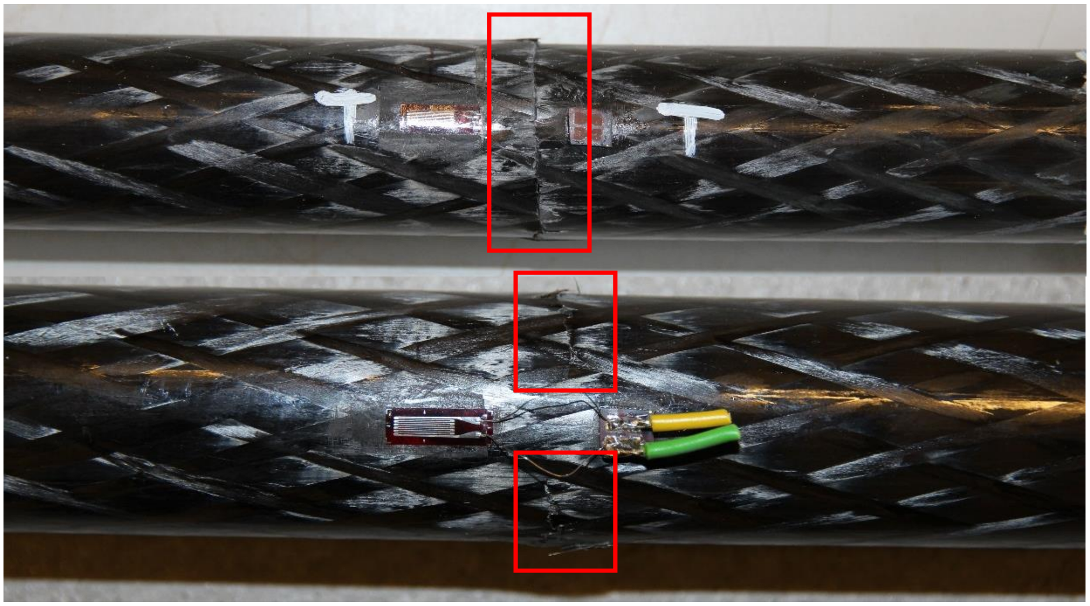

Figure 8.9 Failure of specimen FR01 – top and bottom

8.2. Initial results and observations SSM creep tests

Detailed results and observations of the SSM creep tests in bending FC01-03 are presented in Annex J. The force-time diagram and the total strain-time diagram of FC01-03 are presented in Figure 8.10 and 8.11 respectively. The CFRP specimen tested at a reference stress of 40% GUFS (FC01) ruptured after 0.3 hours in the fourth load step. The specimen did not rupture precisely at the mid-point, but within the central loading span of the specimen. As the stress within the central loading span is constant in a four-point bending test, no correction has to be made. At failure of the specimen, the resulting strain is characterized by a decrease in length of the specimen's top surface (strain gauge top – SGT) and an increase in length of the specimen's bottom surface (strain gauge bottom – SGB). The creep strain-time curve obtained from the strain gauge at the specimen's top surface is characterized by a stage of tertiary creep.

The CFRP specimen tested at a reference stress of 60% GUFS (FC02) ruptured during the jump from the third to the fourth load level. No stage of tertiary creep was observed. The CFRP specimen tested at a reference stress of 80% GUFS (FC03) ruptured after 3.4 hours in the fourth load step. From Figure 8.12 can be seen that the initiation of fracture occurred at the top surface of the specimen, following the rupture of the CFRP. The creep strain-time curve obtained from the strain gauge at the specimen's top surface is characterized by a stage of tertiary creep.

In all three tests FC01-03, the creep strain rate increases when the level of stress increases.

All the specimens tested in bending using the SSM (FR01-03 and FC03-03) exhibited rupture of the CFRP at the top center, i.e. in compression. This can be grounded by CFRP being orthotropic, and having a tensile strength significantly higher than compression strength. The damage mechanism caused brittle fracture of the CFRP without warning. This confirms the importance of making sure that the level of permanent stresses in the CFRP stays below the recommended creep-stress limit, in design of members of actively bent grid shells.

The value found of the average ultimate bending force (4.8 kN) was successively lower than the values found for the average ultimate tension force (89.3 kN) and average ultimate compression force (47.2 kN). This indicates the sensitivity of CFRP being much higher to a load direction that differs from the fiber direction.

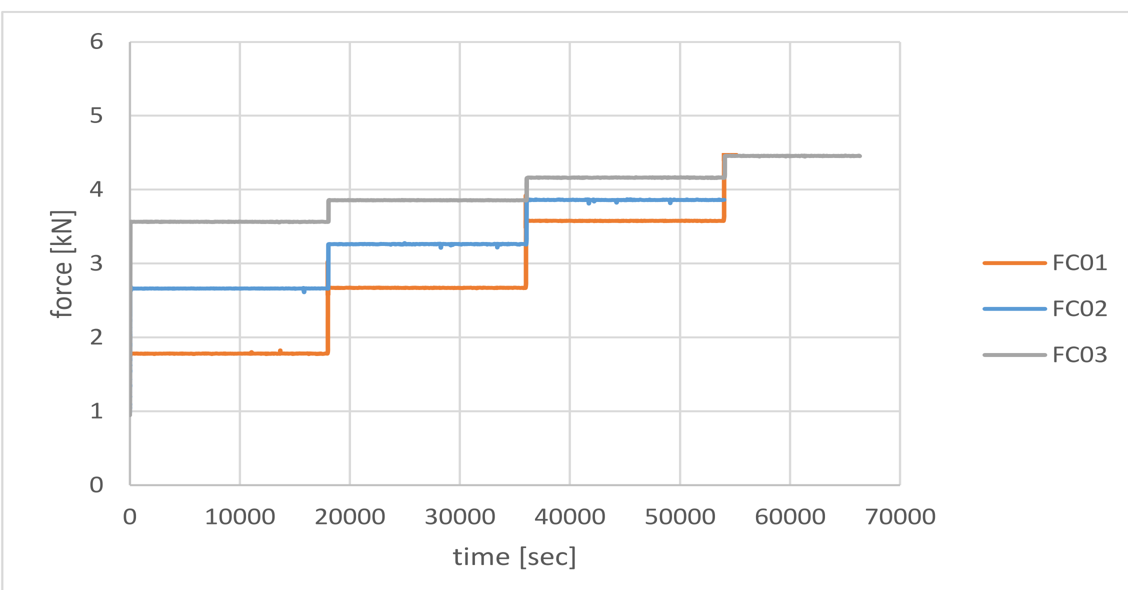

Figure 8.10 Force-time diagram of FC01-03 results

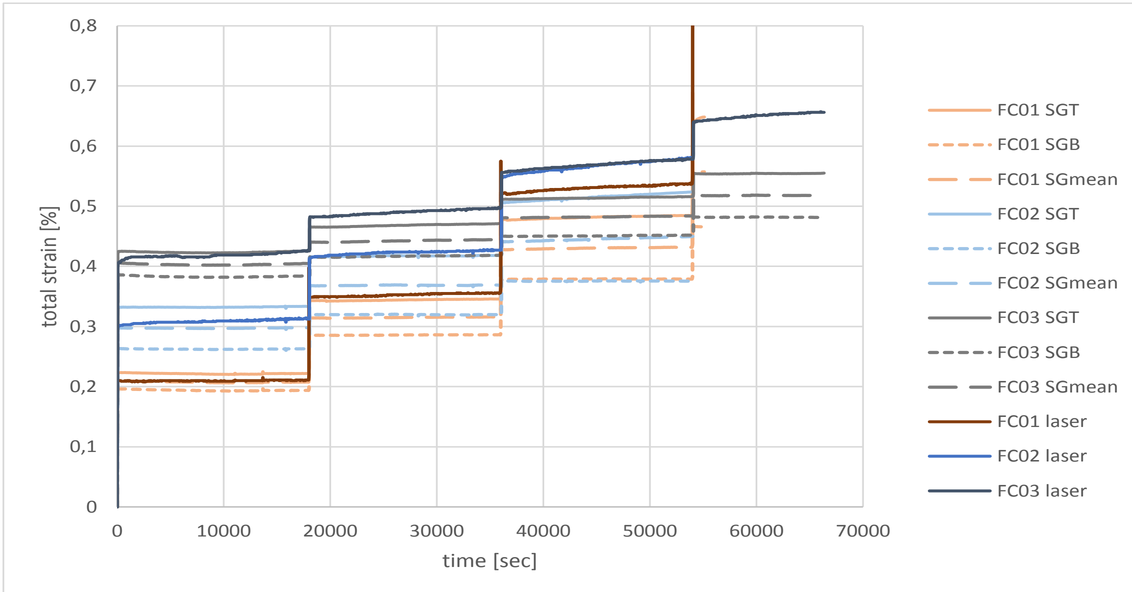

Figure 8.11 Strain-time diagram of FC01-03 results based on strain gauges and laser

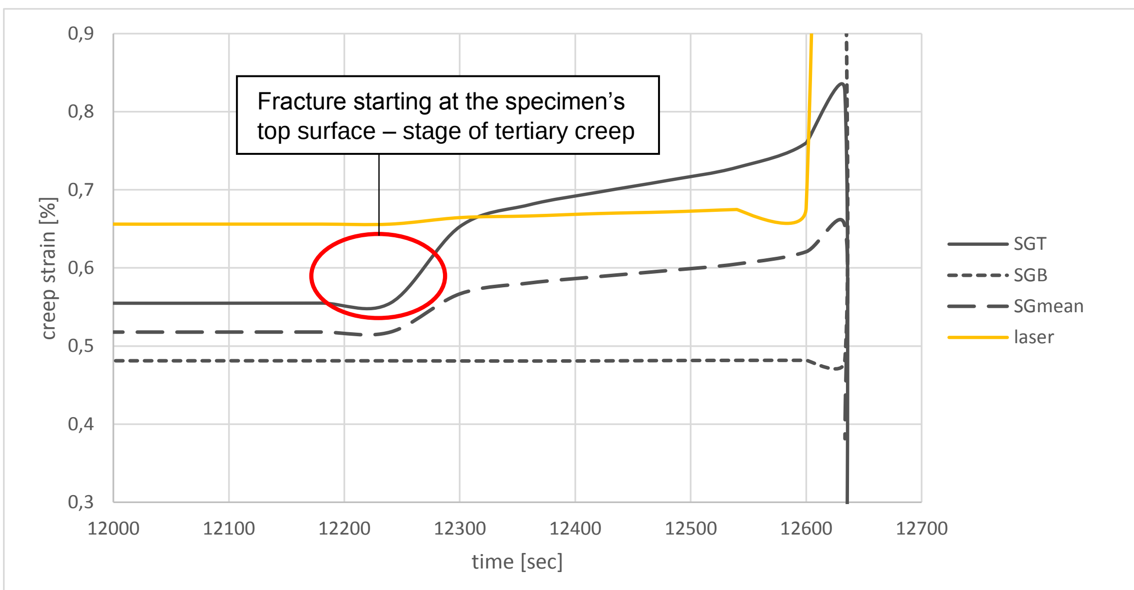

Figure 8.12 Creep strains from strain gauges and laser in final load level – at rupture of the specimen FC03

8.3. SSM data analysis

This section presents the processing of raw test data from bending creep tests using the SSM. Calculated strains from the laser measuring downward to the mid-point on top of the specimens are used to perform the analysis. A detailed description of the procedure for data analysis using the SSM is presented in Section 5.2. The CFRP specimens used for SSM creep tests have fiber reinforcement which is not purely unidirectional. Therefore the results of the bending experiments are not representative at the material level and are used to present 'apparent' creep behavior.

8.3.1. Initial vertical adjustment

From the preliminary bending tests (FR01-03), an average initial stress-strain curve was constructed. From this curve, the 'expected' values for the initial strains at the three reference stresses are determined, which are presented in Table 8.3. The total strains measured in the SSM tests FC01-03 are adjusted by a constant vertical offset in order to match the expected values presented in Table 8.3 (see Figure 8.13).

name test	ref. stress [% GUFS]	exp. ini. ε [%]
FC01	40	0,17
FC02	60	0,3
FC03	80	0,45

Table 8.3 Expected values for initial strains at different reference stresses

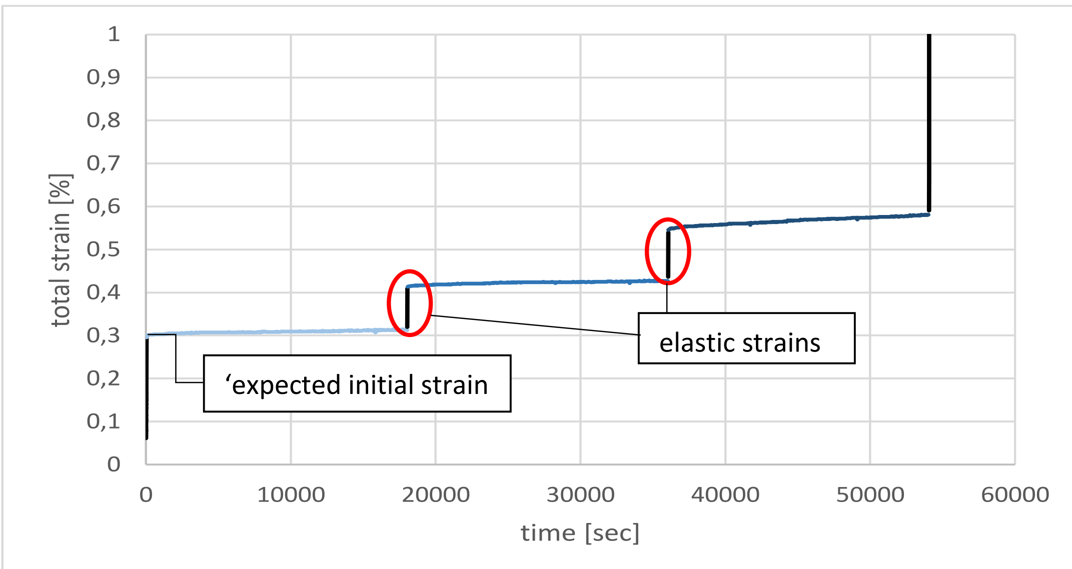

Figure 8.13 Initial vertical adjustment along strain axis (result of bending creep test FC02)

8.3.2. Vertical shifting

The elastic strains (see Figure 8.13) are removed from the total-strain curves of FC01-03, by shifting the creep portions of the curves vertically. The resulting creep curve of FC02, which included only creep strains, is presented in Figure 8.14.

8.3.3. Rescaling

Data from secondary creep stages of each stress step is fitted with a second order polynomial equation, derived from the stress-strain curve relationship in EC2 (p. 35, eq. 3.17). The formula is given by:

$$\varepsilon(t) = \varepsilon_{min} + \left(1 - \left(1 - \frac{t}{t_{peak}}\right)^2\right) \times \left(\varepsilon_{peak} - \varepsilon_{min}\right) \quad (14)$$

where:

$\varepsilon(t)$	time-dependent strain
ε_{min}	strain at start of load step
ε_{max}	strain at end of load step
t_{peak}	time at end of load step
t	measured time

The difference in time between the real start of a step and the projected start time from the curve-fit is the rescaling time across which the creep curves corresponding to load steps >1 (see Figure 8.15). The secondary creep portion of each stress step is defined from the time point when the creep strain rate is less than 0.000002% (see Figure 8.16).

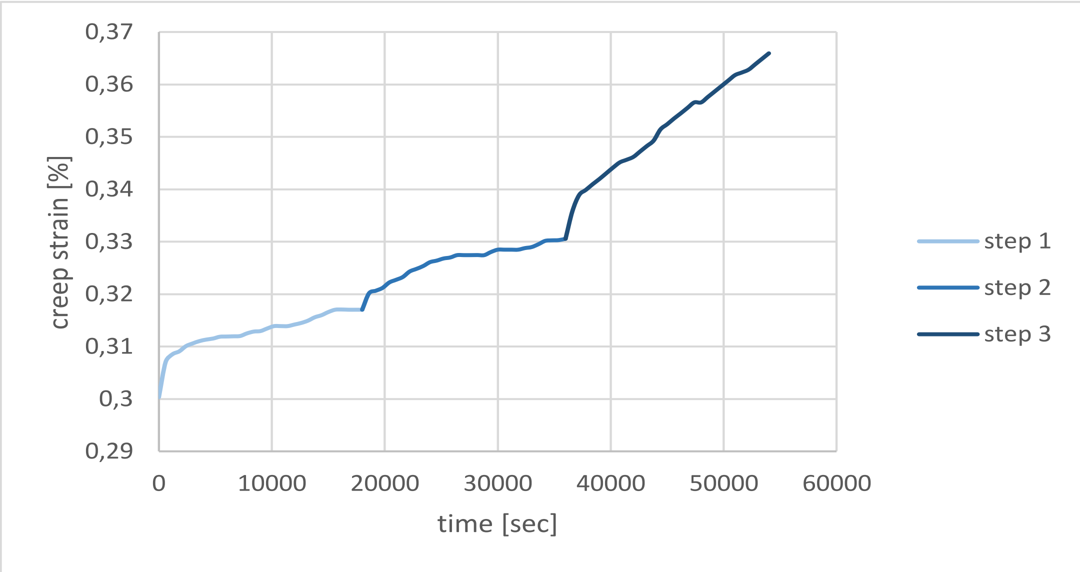

Figure 8.14 Result after vertical shifting along strain axis (result of bending creep test FC02)

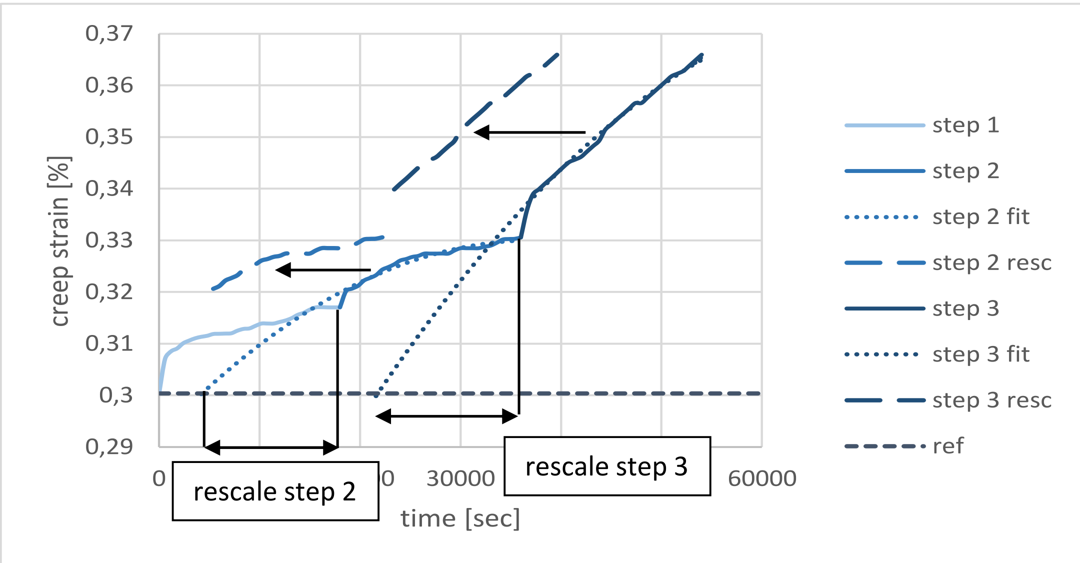

Figure 8.15 Rescaling along the linear time axis using a curve-fitting equation (result of bending creep test FC02)

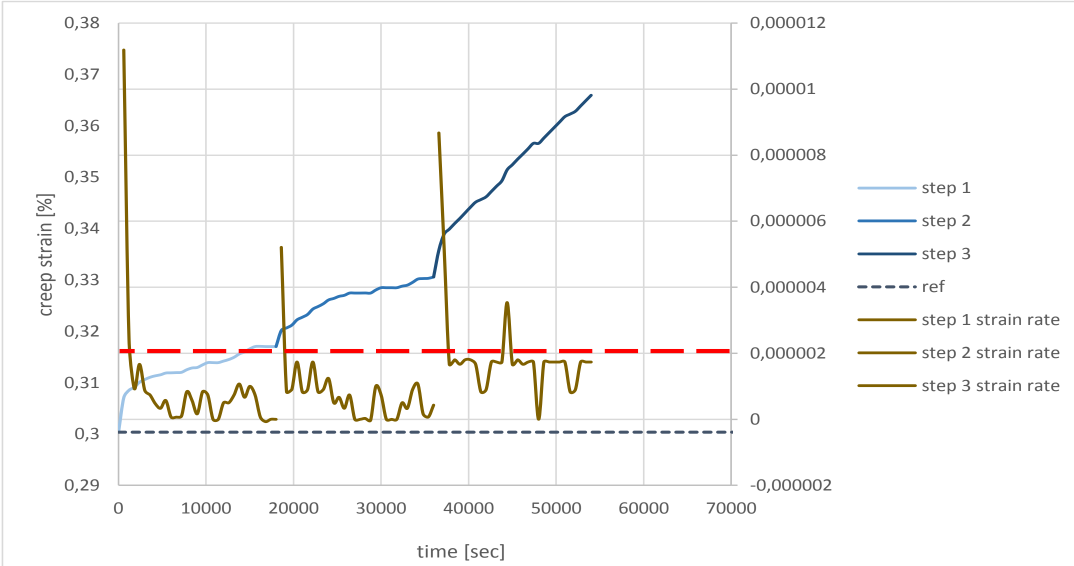

Figure 8.16 Secondary creep portions are defined from the time point when the creep strain rate is less than 0.000002% (result of bending creep test FC02)

8.3.4. Horizontal shifting

The individual creep curves that have resulted from rescaling are shifted along the logarithmic time axis (see Figure 8.17). The amount of horizontal shifting that is required for a smooth master curve is determined by the slope of the secondary creep curves obtained from rescaling. The smoothness of the final master curves was checked graphically. The linear relationship between the factors for horizontal shifting and the stress levels related to the steps in the creep tests form the same slope and overlap as much as possible (see Figure 8.18).

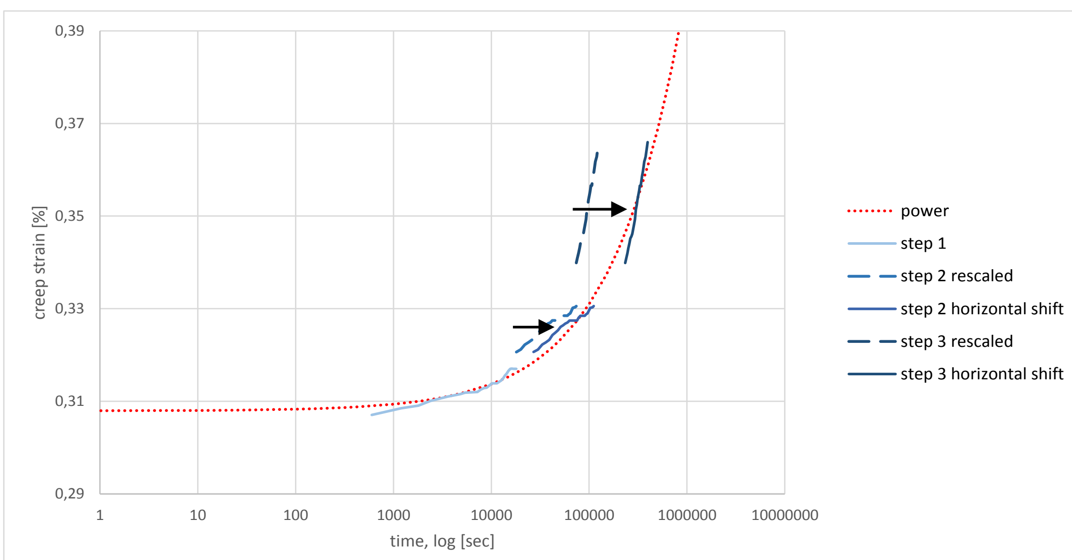

Figure 8.17 Horizontal shifting along log (time) axis (result of bending creep test FC02)

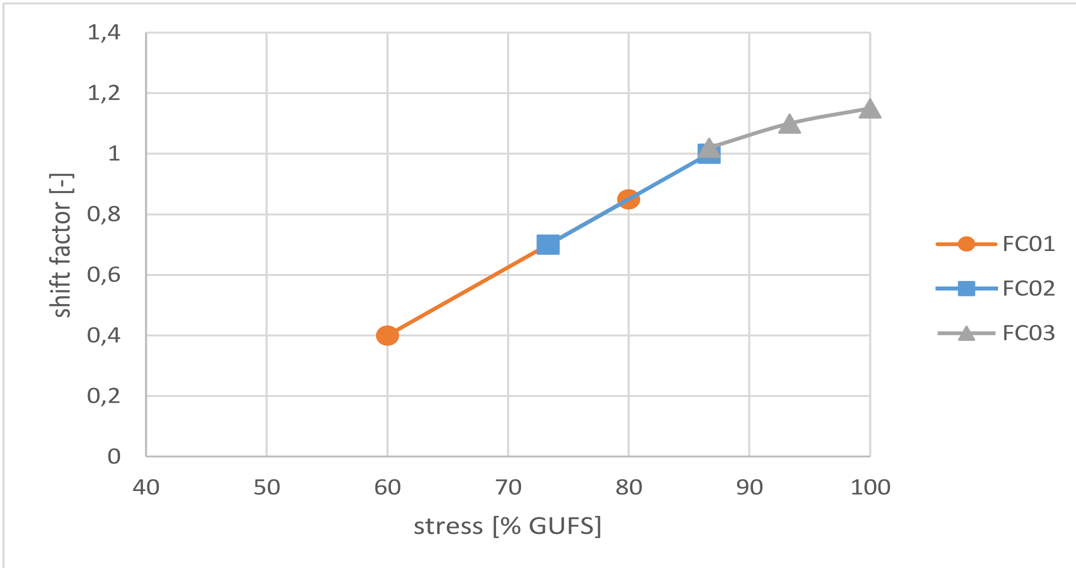

Figure 8.18 Shift factors versus stress levels of FC01-03

8.4. End results of the observations

Final creep master curves for CFRP specimens at 40%, 60%, and 80% GUFS are presented in Figure 8.19. It is remarkable that the end times that have resulted from the horizontal shifting are rather short, i.e. up to 1e6, which corresponds to ~12 days. In all three tests FC01-03, the creep strain rate increases, when the level of stress increases.

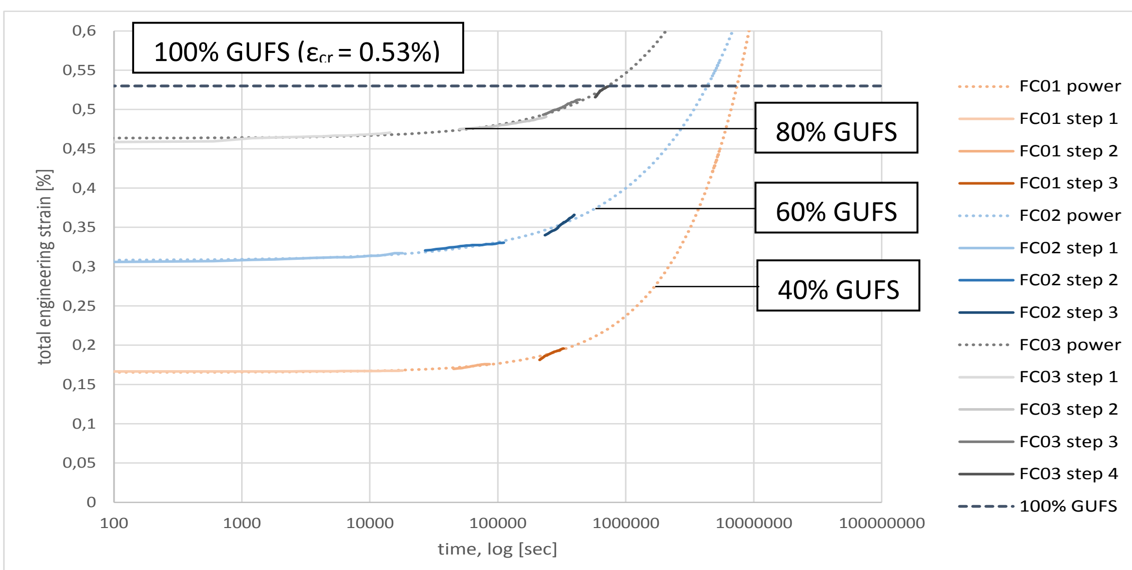

Figure 8.19 Final creep curves for CFRP specimens at 40%, 60%, and 80% GUFS

To study creep-rupture behavior of the CFRP on a long-term, the results from the stress levels at a certain reference stress are extrapolated to the value found for the average ultimate strain (ε_{ult}), using a power law equation (see Figure 8.19). The projected creep-rupture times from the curve-fit at different reference stresses are plotted in one graph, which is presented in Figure 8.20.

It was concluded that if the permanent load is 55% of the ultimate load, creep-rupture will happen in 40 days. This results does not seem realistic, as the 0.55 f_{ult} sustained stress limit from CUR96 corresponds to a service life of 50 years.

- It was concluded that out of the four steps in processing of raw test data using the SSM, rescaling is the most critical step. There is strong dependence between the rescaling step and the horizontal shifting step. The amount of horizontal shifting that is required for a smooth master curve is determined by the slope of the secondary creep curves obtained from rescaling. Figure 8.21 presents, in addition to the the creep-rupture times obtained according to the rescaling procedure as described in Section 8.3.3 (red solid line), creep-rupture times obtained from a different rescaling procedure (see Annex L). In the second case (red dashed line), the rescaling time has been taken as the difference in time between the projected start time from the EC2 curve-fit and zero time. The linear relationship between the factors for horizontal shifting and the stress levels related to the steps in the creep test do not overlap (see Annex L, Figure L1).
- It was concluded that the second order polynomial equation from EC2, used for the curve-fitting, may have resulted in improper curve-fit for the series of data points, resulting in incorrect rescaling times.
- It was concluded that in order to determine the rescaling values and corresponding horizontal shifting for the bending experiments, a corresponding conventional creep test is required as a reference test.

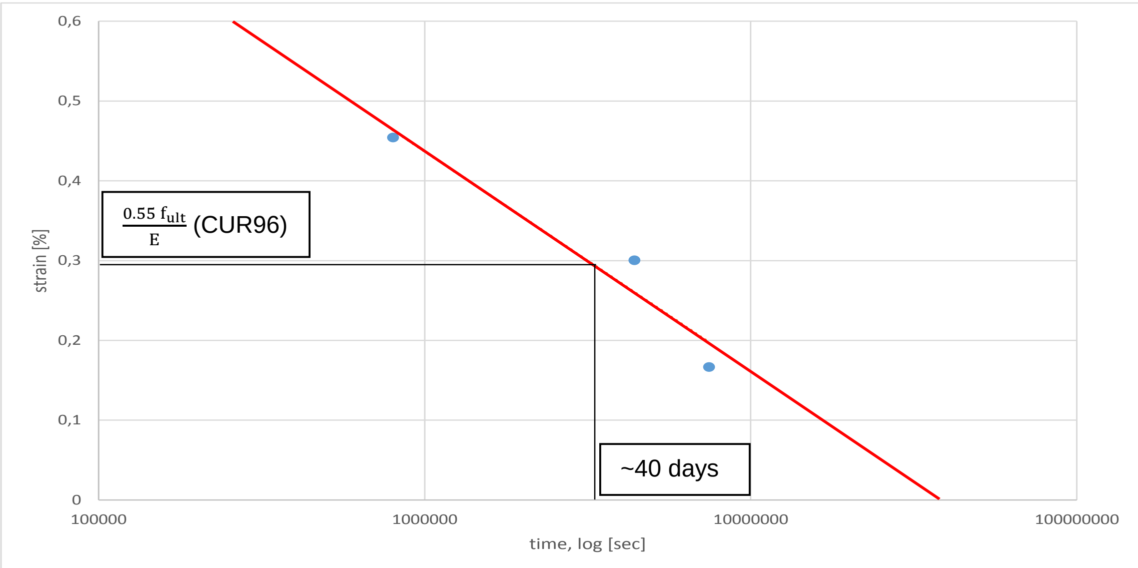

Figure 8.20 Creep-rupture times for reference stresses examined in this research

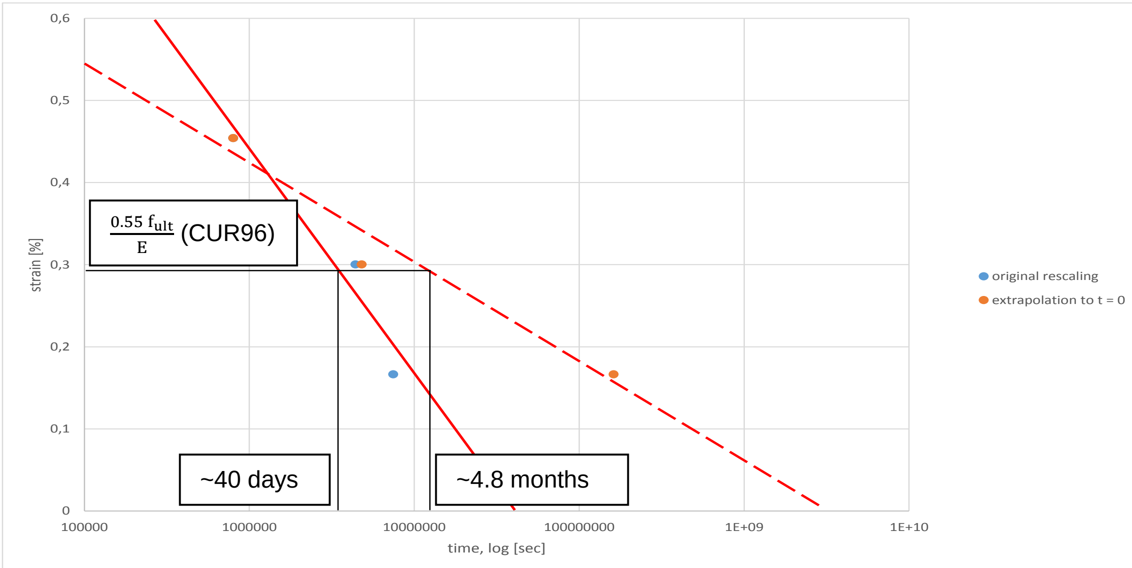

Figure 8.21 Creep-rupture times for reference stresses based on two different procedures for rescaling

9. Summary of results of creep tests using the SSM

Creep testing using the Stepped Isostress method (SSM) is performed on pultruded CFRP specimens made of Epikote epoxy and Toho Tenax STS carbon fibers (V_f = 0.65). The 30 mm x 28 mm tubular specimens are unidirectional with a winded outer layer. This chapter presents relevant effects of the creep phenomenon on specimens derived from tension (Section 9.1), compression (Section 9.2) and bending (Section 9.3) experiments.

Per load type, three creep tests were performed at different reference stresses: 40%, 60%, and 80% of the Guaranteed Ultimate Tensile Strength (GUTS), Guaranteed Ultimate Compressive Strength (GUCS), and Guaranteed Ultimate Flexural Strength (GUFS). To find the GUTS, GUCS, and GUFS of the CFRP specimens, as a percentage of their corresponding average ultimate strengths, preliminary tests were carried out in tension, compression, and bending respectively. Values found for the average ultimate tensile force ($F_{ult.mean}$), strength ($\sigma_{ult.mean}$), strain ($\varepsilon_{ult.mean}$), and modulus of elasticity (E_{mean}), from preliminary tests, are presented in Table 9.1.

property	**quantity**	**TR01-03**	**CR01-04**	**FR01-03**
$F_{ult.mean}$	kN	89.3	47.2	4.8
$\sigma_{ult.mean}$	MPa	980.3	517.7	632.6
$\varepsilon_{ult.mean}$	%	0.80	0.46	0.53
E_{mean}	GPa	119.3	117.1	118.5

Table 9.1 Results from preliminary tension (TR01-03), compression (CR01-04), and bending (FR01-03) tests

9.1. Tension creep

- The SSM requires that each specimen is tested until failure. The specimens TC01-03 failed by brittle splitting vertically along the free span. Due to brittle fracture of the specimens, it is difficult to see where the initiation of fracture occurred.

- It is remarkable that both TC02 and TC03 failed in corresponding creep tests at a final loading of 108.0 kN and 110.8 kN respectively, while the average ultimate tensile strength found was 89.3 kN. This may have been caused by:
  - The final rupture stress level, 96% GUTS, was chosen too low.
  - The specimens TC02 and TC03 may have had a higher ultimate strength than the ultimate tensile strength of TR01-03 obtained during preliminary testing. Specimens for tension testing were obtained from the producer in two tribes, which may have led to a difference in chemical composition or wall thickness of the specimens, leading to deviate response of TC02 and TC03 in SSM creep tests.

- No tertiary creep stages were obtained from test data as the specimens fractured during the jump to the final load level (TC01), or the initiation of fracture has not occurred at mid-point (TC02, TC03). Therefore predictions for creep-rupture times cannot be made according to the method described in Section 5.2.5.

- As only very little creep strains are measured (TC01 and TC02), and measured creep strains are negative (TC03), it was decided not to perform further analysis using the SSM.

9.2. Compression creep

- In a successful test of this type, the specimen fails by circumferential cracking at the center. This preferred mode of delivery for failure was observed with specimen CC02, which showed brittle fracture behavior at the mid-point. No visible damage or deformation appeared on the free span surfaces of CC01 and CC03. Both specimens did not rupture at the mid-point, but somewhere within the cup area.

- The strain-time curve in the final load level of CC02 is characterized by a stage of tertiary creep. Data from this test may be used for further analysis to predict the creep-rupture time on a long-term, according to the method described in Section 5.2.5.

- For all three tests, during the jump to the first load level, notable amount of elastic strains were measured by the laser, in contrast to the strains from the strain gauges. This may indicate the initiation of fracture, causing a decrease in length of the specimen's surface at mid-span, already occurred during the jump to the first load level.

- As almost no creep strains were measured during the SSM creep tests CC01-03, and also negative values of creep strains were measured, it was decided not to perform SSM analysis with data from strain gauges from corresponding tests.

9.3. Apparent bending creep

- The CFRP specimens used for SSM creep tests have fiber reinforcement which is not purely unidirectional. Therefore the results of the bending experiments are not representative at the material level. Results from bending experiments are used to present 'apparent' creep behavior.

- All the specimens FR01-03 and FC01-03 exhibited rupture of the CFRP at the top center, i.e. in compression. This can be grounded by the CFRP specimen being orthotropic, and having a tensile strength 1.9 times higher than compression strength. Results from top strain gauges may be used for SSM analysis to predict creep behavior in compression.

- In a successful test of this type, the specimen fails in compression, i.e. the initiation of fracture occurs at the top surface of the specimen. Specimen FC01 did not rupture precisely at the mid-point, but within the central loading span of the specimen. As the stress within the central loading span is constant in a four-point bending test, no correction has to be made.

- In a successful test of this type, the creep strain-time curve obtained from the strain gauge on top of the specimen is characterized by a stage of tertiary creep. For both FC01 and FC03 a tertiary creep stage can be observed. Predictions for creep-rupture times may be made according to the method described in Section 5.2.5.

- The end times that have resulted from the horizontal shifting are rather short, i.e. up to 1e6, which corresponds to ~12 days (see Figure 8.19).

- If the permanent load is 55% of the ultimate load, creep-rupture will happen in 40 days. This results does not seem realistic, as the 0.55 f_{ult} sustained stress limit from CUR96 corresponds to a service life of 50 years (see Figure 8.20).
    - There is strong dependence between the rescaling step and the horizontal shifting step.
    - The polynomial equation from EC2, used for the curve-fitting, may have resulted in improper curve-fit for the series of data points, resulting in incorrect rescaling times.
    - A corresponding conventional creep test is required to determine the rescaling values and corresponding horizontal shifting related to the creep tests in bending.

PART IV REPORTING

10. Conclusion and recommendations

In this chapter the results of this thesis focusing on creep characteristics of Carbon Fiber Reinforced Polymer (CFRP) in members of actively bent grid shells is presented. This chapter consists of two parts: the first part provides feedback and answers to the main- and key questions of this research as described in Section 1.2. In the second part recommendations for future research in fields where this research can be further improved and extended are presented.

10.1. Conclusion

The aim of this thesis has been defined by the following research question:

Which stress limits related to time-dependent long-term creep behavior of CFRP in members of actively bent grid shells can be defined using the Stepped Isostress Method?

To answer the main question, key questions were defined which are stated below with the drawn conclusion per question:

What are structural characteristics of actively bent grid shells?

Actively bent grid shells are curved structural surfaces made of flexible members. The application is mainly in roof structures. The members, spanning between two supports on the perimeter, are connected at their intersections by relatively simple joints, and assembled in an initially straight grid. By lifting a sufficient number of points, the straight grid is subsequently transformed into a bent shape and new geometry is preserved by fixing the supports. Finally, the surface is braced to obtain in-plain shear stiffness of the structure.

In actively bent grid shells, the main source of stress is caused by the transformation of the straight grid into a bent shape during construction. The stress in the members of the grid shells is proportional to their curvature, and the curvature is mainly due to the level of bending. From the in-plane buckling analysis of actively bent members performed with SOFiSTiK, it was concluded that the higher the amount of pre-bending, the higher the corresponding critical load. In other words, the stiffness of a member increases when the level of bending increases.

What are creep characteristics of CFRP and what are methods to study the time-dependent long-term behavior?

CFRP undergoes creep and possibly creep-rupture when subjected to a long-term permanent loading. Creep response is dominated by the polymeric resin of the FRP, and is highly dependent on the type of resin and the quality of the interface between the fibers and the resin. Other factors that have influence on creep behavior are the orientation of the fibers, the fiber volume fraction, and the form of the FRP reinforcement.

The finite element and structural analysis software SOFiSTiK may be used to study creep stress limits in actively bent grid shell design. From the creep-rupture analysis with SOFiSTiK (Section 4.4) it was concluded that if the sustained stress in GFRP and CFRP members of equal dimensions, but with different elastic modulus, is below their corresponding stress limit for creep-rupture (0.2 f_{ult} and 0.55 f_{ult} respectively, based on CUR96), the CFRP member is available for a point load at mid-span which is 11 times larger compared to the GFRP member. This might be of influence in driving the choice for using a material (e.g. CFRP over GFRP) that has better creep-rupture behavior in members of actively bent grid shells.

In addition, it was concluded that similar buckling- and creep-rupture analyses as performed in 2D, must be performed in 3D to study the importance of creep-rupture in actively bent grid shell structures as a whole.

Actively bent grid shell design may be critical for creep and creep-rupture, due to pre-stressing of the members, therefore material testing should be performed. Experimental studies have shown that accelerated creep testing using the Stepped Isothermal Method (SIM) and Stepped Isostress Method (SSM), can be performed to predict long-term creep deformation and creep-rupture times with confidence, in high-stress applications. Following from initial experimental tests, it was concluded that both methods are interesting for further investigation with respect to actively bent grid shells.

What are relevant effects of the creep phenomenon on pultruded CFRP specimens derived from SSM experiments?

From testing on pultruded tubular CFRP specimens made of Epikote epoxy and Toho Tenax STS carbon fibers it was concluded that the CFRP fails in a brittle manner. It is therefore crucially important to stay below recommended stress limits to avoid creep-rupture.

From preliminary testing it was concluded that:

- The ultimate tension strength of the CFRP specimens is 1.9 times higher than the ultimate compression strength, and 1.5 times higher than the ultimate bending strength.
- The ultimate tension strain of the CFRP specimen is 1.7 times higher than the ultimate compression strain, and 1.5 times higher than the ultimate bending strain.
- The elastic moduli corresponding to the CFRP specimens in tension, compression, and bending are 119.3, 117.1, and 118.5 GPa respectively.

From tension creep tests using the SSM it was concluded that:

- Tensile loading develops damage in the form longitudinal splitting of the CFRP.
- Additional creep testing is required to rely on test data to be processed using the SSM.

From compression creep tests using the SSM it was concluded that:

- Compression loading develops damage in the form of kink-band formation at the specimen’s center.
- Additional creep testing is necessary to explain the negative (in this case tensile strain) values of strain that were found by local strain measurements from strain gauges. In addition, additional creep testing is required to rely on test data to be processed using the SSM.

From bending creep tests using the SSM it was concluded that:

- The specimens exhibited rupture of the CFRP at the top center, i.e. in compression, due to the CFRP specimen being orthotropic, and having a tensile strength 1.9 times higher than compression strength. Results from top strain gauges may be used for SSM analysis to predict creep behavior in compression.

How to define recommendations for design stresses for CFRP in members of actively bent grid shells, based on the study of long-term creep and experiments?

According to CUR96, if the sustained stress in the CFRP is below the 0.55 f_{ult} sustained stress limit for creep-rupture, the strength of the CFRP is available for non-sustained loads over a period of 50 years. It was concluded that this limit is not applicable to all design cases, as it has resulted from creep-rupture tests performed on 6 mm diameter FRP bars that were loaded in tension. In case of design of members of actively bent grid shells, which may be critical for creep-rupture, the stress limit provided by CUR should only be used as an indication and additional material testing is required.

From SSM analysis using raw test data from bending experiments it was concluded that:

- If the permanent load is 55% of the ultimate load, creep-rupture will happen in 40 days. This result does not seem realistic, as the 0.55 f_{ult} sustained stress limit from CUR96 corresponds to a service life of 50 years.
- Out of the four steps in processing of raw test data using the SSM, rescaling is the most critical step. There is strong dependence between the rescaling step and the horizontal shifting step. The amount of horizontal shifting that is required for a smooth master curve is determined by the slope of the secondary creep curves obtained from rescaling.
- In the rescaling step, data was fitted with a second order polynomial equation, derived from the stress-strain relationship from EC2. The curve fitting may have resulted in an improper curve-fit for the series of data points, resulting in incorrect rescaling times.
- To determine the rescaling values and corresponding horizontal shifting for the bending experiments, a corresponding conventional creep test is required as a reference test.

The SSM represents a promising method for accelerated creep testing and corresponding test data analysis for CFRP in members of actively bent grid shells. Sustained stress limits derived from the SSM may be used as more realistic, i.e. less conservative stress limit values to avoid creep-rupture, compared to the values defined in CUR96, for the specific design parameters.

10.2. Recommendations

In this section, recommendations for future research in fields where this research can be further improved and extended are presented. The recommendations are summarized as follows:

- Improvement of theory and physical meaning behind het Stepped Isostress Method (SSM). It is recommended to have the primary focus on:
    - The curve-fitting procedure in the rescaling step.
    - Use of secondary creep data for the rescaling step.
    - Numerical procedure for the horizontal shifting step.

- Further investigation of application of the SSM for FRP materials that are sensitive to creep and creep-rupture behavior, as performing creep tests possibly can be done much faster than with conventional creep tests. In addition, it is recommended to perform corresponding conventional creep tests, at the same reference stress levels as used for the SSM tests.

- Investigation of the importance of creep-rupture in actively bent grid shells as a whole. Similar buckling- and creep-rupture analyses as performed in 2D in this research may be used as starting points.

- The damage mechanisms in tension, compression, and bending experiments caused brittle fracture of the CFRP without warning. To increase warning, it is recommended to investigate the use of multi-directional CFRP in the members of the grid shells.

- Investigation in the design of connections of FRP structures in general, based on the assemblies used for tension, compression, and bending experiments in this research.

- Investigation in structural redundancy; the influence of dropping out or failure of a member on corresponding structural safety and redundancy of actively bent grid shells.

Bibliography

ACI440. (2008). Guide for the Design and Construction of Externally Bonded FRP Systems for Strengthening Concrete Structures. In. Farmington Hills, U.S.A.: American Concrete Institute.

Adriaenssens, S., Block, P., Veenendaal, D., & Williams, C. (2014). *Shell structures for architecture : form finding and optimization*. In. Retrieved from Ebook Library http://public.eblib.com/choice/publicfullrecord.aspx?p=1656820

Ando, N., Matsukawa, H., Kawamura, M., Fujii, M., Miyagawa, T., & Inoue, S. (1998). EXPERIMENT AL STUDIES ON THE LONG-TERM TENSILE PROPERTIES OF FRP TENDONS.

Baverel, O., Caron, J. F., Tayeb, F., & Du Peloux, L. (2012). Gridshells in Composite Materials: Construction of a 300 m^2 Forum for the Solidays' Festival in Paris. *STRUCTURAL ENGINEERING INTERNATIONAL, 22*(3), 408-414.

Chini, S. A. A. M. A., & Wolde-Tinsae, A. M. M. A. (1988). Effect of Prestressing on Elastica Arches. *Journal of Engineering Mechanics, 114*(10), 1791-1800. Retrieved from

CNR-DT205. (2007). Guide for the Design and Construction of Structures made of FRP Pultruded Elements. In. Rome, Italy: CNR.

COURBON, J. (1984). Stabilité de l'équilibre élastique. *Techniques de l'ingénieur. Construction, 2*(C2040), C2040. 2041-C2040. 2010.

CUR96. (2017). *Vezel versterkte kunststoffen in bouwkundige en civieltechnische draagconstructies*: CUR, Civieltechnisch Centrum Uitvoering Research en Regelgeving.

D2990-01. (2001). Standard Test Methods for Tensile, Compressive, and Flexural Creep and Creep-Rupture of Plastics. In. West Conshohocken, United States: ASTM International.

Detail6. (2000). Retrieved from http://inspiration.detail.de/japanese-pavilion-at-the-expo-in-hanover-106867.html?lang=en

Douthe, C. (2007). *Etude de structures élancées précontraintes en matériaux composites, application à la comception des gridshells*. Retrieved from WorldCat.org database. Ecole des Ponts ParisTech.

Douthe, C., Caron, J. F., & Baverel, O. (2010). Gridshell structures in glass fibre reinforced polymers. *Construction and Building Materials, 24*(9), 1580-1589. doi:http://dx.doi.org/10.1016/j.conbuildmat.2010.02.037

Du Peloux, L., Tayeb, F., Caron, J.-F., & Baverel, O. (2015). *The Ephemeral Cathedral of Créteil: a 350m2 lightweight gridshell structure made of 2 kilometers of GFRP tubes.* Paper presented at the CIGOS 2015:" Innovations in Construction".

EUROCOMP. (1996). Structural Design of Polymer Composites. In. London, UK: E & FN Spon.

Fritzsche, J. C. (2013). *Gridshell efficiency optimization: optimizing efficiency form- & grid-configuration through iterative approximation and minimization strain energy.* Retrieved from Item Resolution URL https://pure.tue.nl/ws/files/46942029/761229-1.pdf WorldCat.org database.

Giannopoulos, I. P., & Burgoyne, C. J. (2009). Stress limits for aramid fibres. *Proceedings of the Institution of Civil Engineers-Structures and Buildings, 162*(4), 221-232.

Giannopoulos, I. P., & Burgoyne, C. J. (2011). Prediction of the long-term behaviour of high modulus fibres using the stepped isostress method (SSM). *Journal of materials science, 46*(24), 7660.

Gonilha, J. A., Correia, J. R., & Branco, F. A. (2013). Creep response of GFRP-concrete hybrid structures: Application to a footbridge prototype. *Composites Part B, 53*, 193-206.

Hadid, M., Guerira, B., Bahri, M., & Zouani, A. (2014). Assessment of the stepped isostress method in the prediction of long term creep of thermoplastics. *Polymer Testing, 34*, 113-119.

Happold, E., & Liddell, W. (1975). Timber lattice roof for the Mannheim Bundesgartenschau. *The structural engineer, 53*(3), 99-135.

Harris, R., Romer, J., Kelly, O., & Johnson, S. (2003). Design and construction of the Downland Gridshell. *Building Research & Information, 31*(6), 427-454.

JRC. (2016). Prospect for new guidance in design of FRP. In. Italy: L. Ascione, J.-F. Caron, P. Godonou, K. van IJselmuijden, J. Knippers, T. Mottram, M. Oppe, M. Gantriis Sorensen, J. Taby, L. Tromp.

Kotelnikova-Weiler, N. (2012). *Optimisation mécanique et énergétique d'enveloppes en matériaux composites pour les bâtiments*. Retrieved from WorldCat.org database. Université Paris-Est.

Kotelnikova-Weiler, N., Douthe, C., Hernandez, E. L., Baverel, O., Gengnagel, C., & Caron, J.-F. (2013). Materials for Actively-Bent Structures. *International Journal of Space Structures, 28*(3-4), 229-240.

Lee, L. S. (2007). 8 - Creep and time-dependent response of composites A2 - Karbhari, Vistasp M. In *Durability of Composites for Civil Structural Applications* (pp. 150-169): Woodhead Publishing.

Levien, R. (2008). The elastica: a mathematical history. *University of California, Berkeley, Technical Report No. UCB/EECS-2008-103*.

Lienhard, J. (2014). *Bending-active structures form-finding strategies using elastic deformation in static and kinetic systems and the structural potentials therein.* ITKE, Stuttgart :. Retrieved from urn:nbn:de:bsz:93-opus-94838

Mesnil, R. (2013). *Stability of elastic grid shells.* Massachusetts Institute of Technology, WorldCat.org database.

Nicholas, P., Hernandez, E. L., Gengnagel, C., th Symposium on Simulation for, A., Urban Design, S. P. o. t. S. S. M. S. t. S. o. S. f. A., & Urban Design, S. P. o. t. S. S. M. (2013). The Faraday Pavilion: Activating bending in the design and analysis of an elastic gridshell. *Simulation Series, 45*(8), 154-161

Sá, M. F., Gomes, A. M., Correia, J. R., & Silvestre, N. (2011). Creep behavior of pultruded GFRP elements - Part 2: Analytical study. *Composite Structures, 93*(9), 2409-2418.

Sá, M. r. F., Gomes, A. M., Correia, J. o. R., & Silvestre, N. (2011). Creep behavior of pultruded GFRP elements - Part 1: Literature review and experimental study. *Composite Structures, 93*(10), 2450-2459.

Tanks, J., Rader, K., Sharp, S., & Sakai, T. (2017). Accelerated creep and creep-rupture testing of transverse unidirectional carbon/epoxy lamina based on the stepped isostress method. *Composite Structures, 159*(19), 455-462.

Tayeb, F., Lefevre, B., Baverel, O., & Peloux, L. (2015). Design and realisation of composite Gridshell structures. *J. Int. Assoc. Shell Spat. Struct.(J. IASS)*, 49-59.

THINkSHELL. (2013). Gridshell Créteil 2013. Retrieved from https://www.flickr.com/photos/thinkshell/albums/72157654402636408

THINkSHELL. (2016a). CLC 2016 gridshell people 28. Retrieved from https://www.flickr.com/photos/thinkshell/32067163631/in/album-72157675194819183/

THINkSHELL. (2016b). Hybrid Structural Skin 2016 - IMGP0503. Retrieved from https://www.flickr.com/photos/thinkshell/28050044722/in/album-72157667919842984/

Van der Linden, L. P. L., Hendriks, M. A. N., Terwel, K. C., & Hofman, S. (2015). *Innovative joints for gridshells*. Retrieved from WorldCat.org database.

Yamaguchi, T., Nishimura, T., & Uomoto, T. (1998). Creep rupture of FRP rods made of aramid, carbon and glass fibers. *Structural Engineering & Construction: Tradition, Present and Future., 2*, 1331-1336.

.

APPENDICES

Annex A References of actively bent grid shells

Examples of a number of grid shells constructed over time are presented. The first three grid shells that are presented are made of timber, followed by three grid shells made of Glass Giber Reinforced Polymers (GFRP).

Project 1 **Mannheim Bundesgartenschau**

Description	Built as the first large-span grid shell
Place	Mannheimer Herzogenriedpark, Germany
Year	1975
Shape	double-curved, free-form grid shell, which does not follow geodesic paths
Size	area: 7400 m^2 height: 20 m length: 160 m width: 115 m
Material	beams: double-layer wooden slats diameter: 50 mm x 50 mm membrane: Polyester-PVC
Weight	16 kg/m
Cost	80.5 US dollar
Architect	Mutschler and Partner, Frei Otto
Engineer	Buro Happold
Form-finding	Classical way: form-finding by experimental hanging models. A constant distance (50 mm) between the nodes belonging to the same rib was assumed. Double-layer technique was used for the ribs (two overlapping laths).
Construction	The grid shell was built flat on the ground, as a two-way mat of straight continuous rods, and then raised into position. Additional bracing elements (thin 6 mm cables) were added to enhance the in-plane shear stiffness.
Connections	More than 33.000 unique joints were used, able to freely rotate. Each node has four laths crossing at a single point
Features	First large-span grid shell.
Drawbacks	long construction time: one year. Lots of complex and expensive joints.

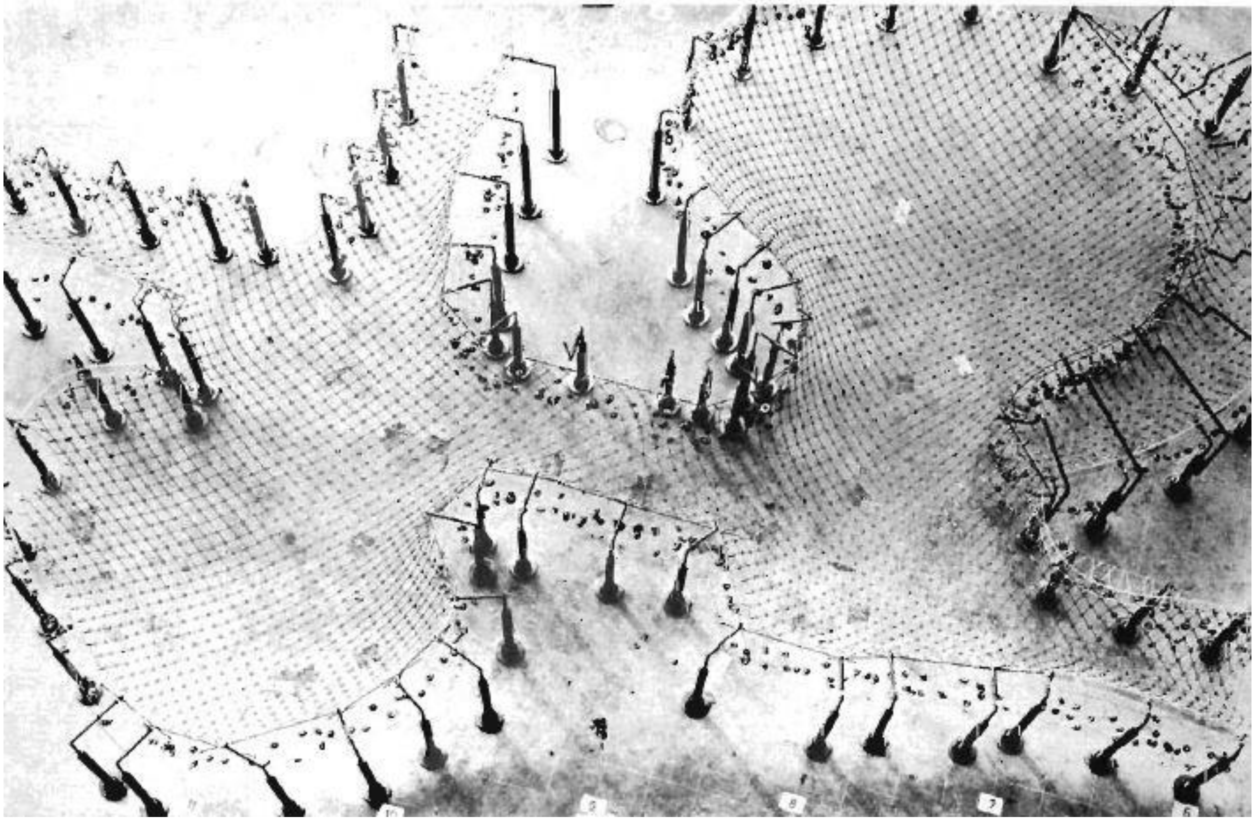

Figure A1 Hanging chain model of the Mannheim grid shell (Happold & Liddell, 1975)

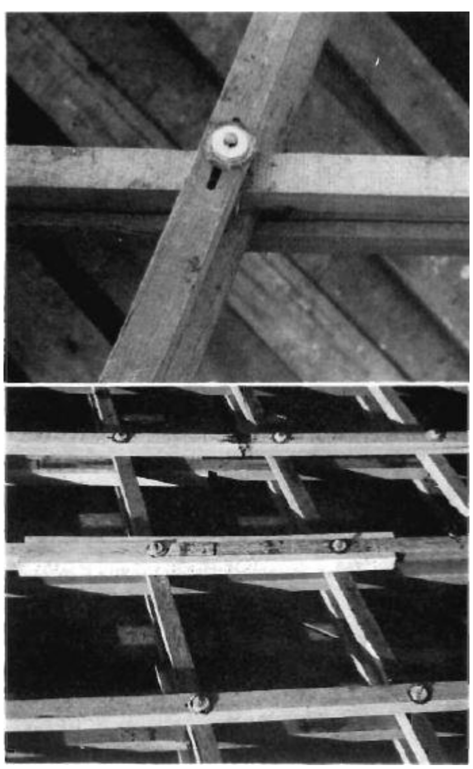

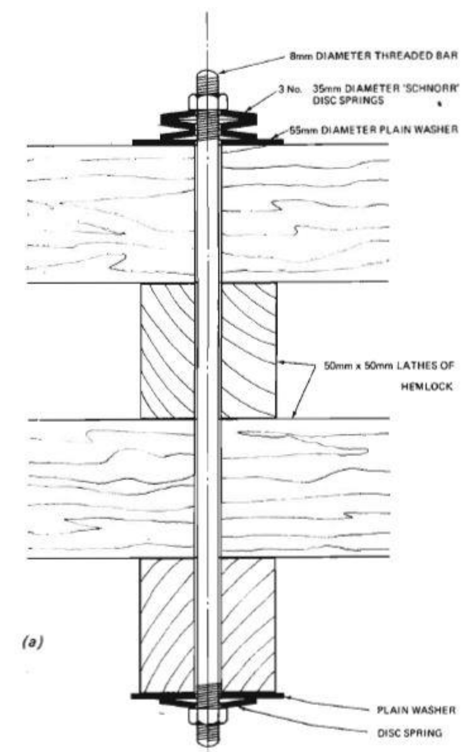

Figures A2, A3 Node joints (Happold & Liddell, 1975)

Project 2 Japanese pavilion for the Hannover Expo 2000

Description	Built for the Hannover World EXPO 2000
Place	Hannover, Germany
Year	2000
Shape	double-curved grid shell following geodesic paths
Size	area: 3600 m^2 height: 15,9 m length: 73,8 m width: 25 m
Material	beams: Cardboard tubes length: up to 40 m diameter: 12.5 cm membrane: impregnated textile and paper fabric
Architect	Shigeru Ban
Engineer	Buro Happold
Form-finding	Classical way: form-finding by experimental hanging models. Planks composing the rig are only subjected to torsion and bending around the weak axis, while the ‘allowable’ width of the cross-section of the planks is enhanced.
Construction	The grid is laid flat on the ground and then lifted and bent into the given geometry using the elasticity of timber. The final geometry is obtained by a scaffolding system and stiff border element at its perimeter edge.
Connections	Cardboard tubes tied together with polyester strips. Bracing by timber ladder elements.
Features	Short construction time: tree weeks. Sustainable materials used.
Drawbacks	Fire regulations

Figure A4 Exterior view of the Japan pavilion (Detail6, 2000)

Figure A5 Interior view of the Japan pavilion (Detail6, 2000)

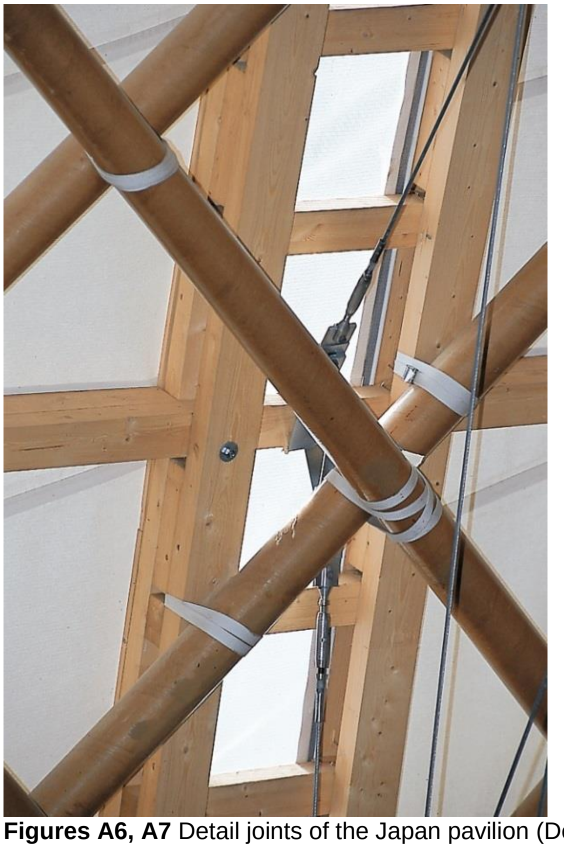

Figures A6, A7 Detail joints of the Japan pavilion (Detail6, 2000)

Project 3 **Carpenter hall of the Weald and Downland Museum**

Description	Built to host the Weald and Downland museum
Place	Sussex, England
Year	2002
Shape	double-curved grid shell following geodesic paths
Size	height: 7- 11 m length: 50 m width: 24 m grid-configuration: mesh geometry of grid does not follow geodesic paths
Material	beams: Oak sourced from Normandy length: up to 40 m diameter: 12.5 cm membrane: impregnated textile and paper fabric
Weight	total: 6000 kg
Cost	approx.: 430 euro/m^2
Architect	E. Cullinan
Engineer	Buro Happold
Form-finding	Classical and modern way: form-finding by experimental- and computer models
Construction	The grid shell was built on a raised platform and bending was induced via gravity and the structure's own weight.
Connections	Four timber laths are clamped together with steel plates on either side with four steel bolts.
Features	Use of new construction methods for grid shells
Drawbacks	long construction time: eight months. Lots of complex and expensive joints

Figure A8 Interior view of the Downland grid shell (Harris, Romer, Kelly, & Johnson, 2003)

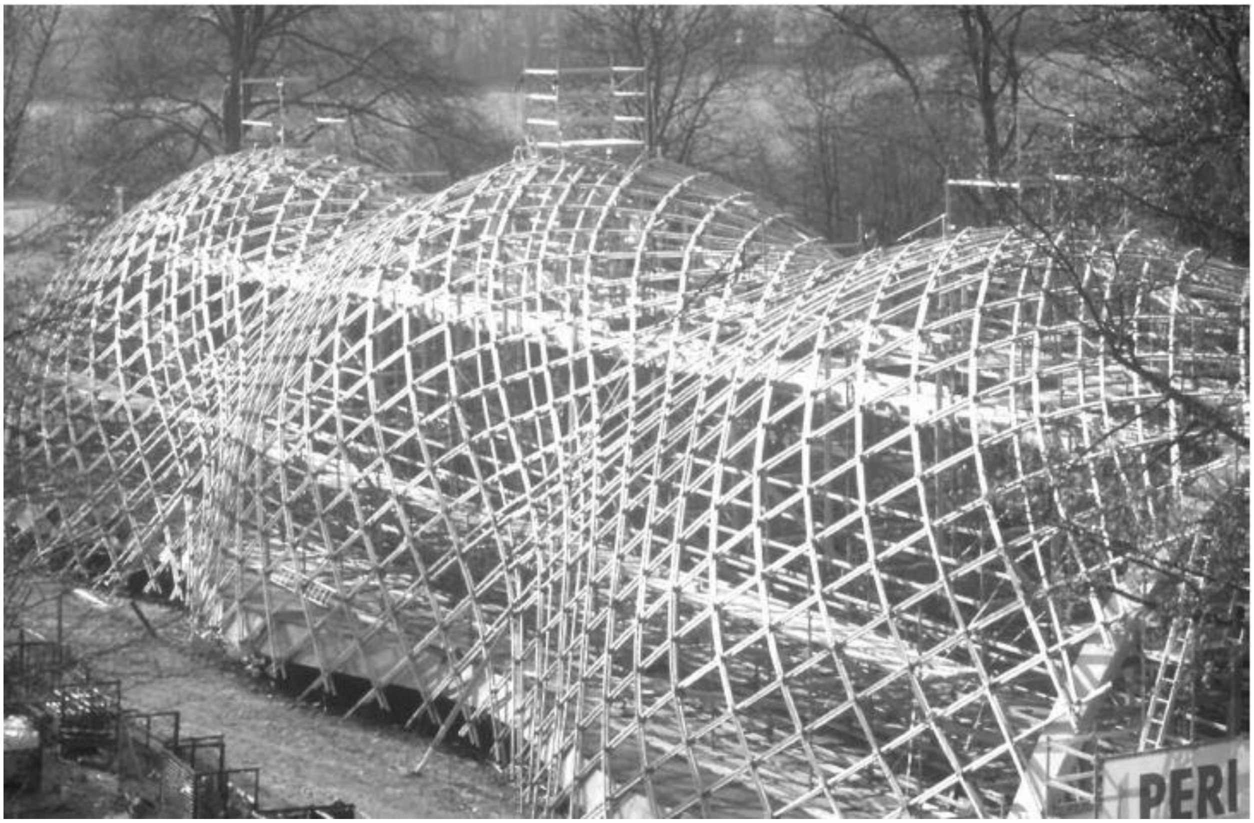

Figure A9 Final shape of the Downland grid shell (Harris et al., 2003)


Figure A10 Gable end strapping system (Harris et al., 2003)


Figure A11 Detail joint

Project 4 **Soliday's Festival Pavilion**

Description	Built to house up to 500 visitors at the Solidays' festival
Place	Longchamp, Paris, France
Year	24 – 26 June 2011
Shape	A half peanut (two domes)
Size	area: 280 m^2 height: 7 m length: 26 m width: 15 m grid-configuration: mesh size: 1 m
Material	Tubes: pultruded unidirectional GFRP Young's modulus: 25 GPa, limit stress: 400 MPa, length: 13,4 m (total: 1600 m) diameter: 41,7 mm wall thickness: 3 mm Membrane: polypropylene PVC coated canvas (500m^2)
Weight	5 kg/m^2
Cost	materials: approximately 150 euro/m^2, whole grid shell: 45.000 euro
Architect	Navier research unit
Engineer	T/E/S/S
Form-finding	Modern way: form-finding by computer models Steps in form finding: First, choice on geometry. Second, design of geometrical grid shell according to the compass method. Third, relaxation of grid shell according to dynamic relaxation (automatic generation). Fourth, non-linear structural analysis with real mechanical properties. Structural analysis: method based on dynamic relaxation.
Construction	Main building steps: the grid of continuous bars was built flat on the ground; the elements pinned together to prevent in-plane shear stiffness and allow for large-scale deformations during erection. Then, the grid was erected by two cranes and attached on anchorages to obtain its final shape. Then, a third layer of beams was installed with the use of new scaffolding elements to let the structure behave like a shell. Final, positioning and stretching of the membrane.
Connections	For major structural details: standard swivel scaffolding elements allowing rotation around their axis to connect tubes, steel sleeves connecting composite tubes, ground anchorages fixing the grid shell to the composite slab, edge beam lacing the fabric
Features	Short construction time: few hours for about ten people (two cranes).
Drawbacks	Several cracks in the continuous beam due to disadvantageous load combination: bending + local transverse concentrated forces through other beams. The scaffolding connectors damages the canvas.

Figure A12 Exterior view of the peanut shaped pavilion (Baverel, Caron, Tayeb, & Du Peloux, 2012)

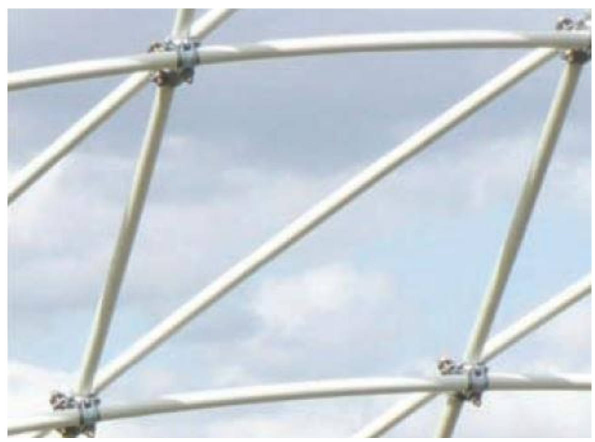

Figures A13, A14 Mesh of the grid before and after bracing (Baverel et al., 2012)

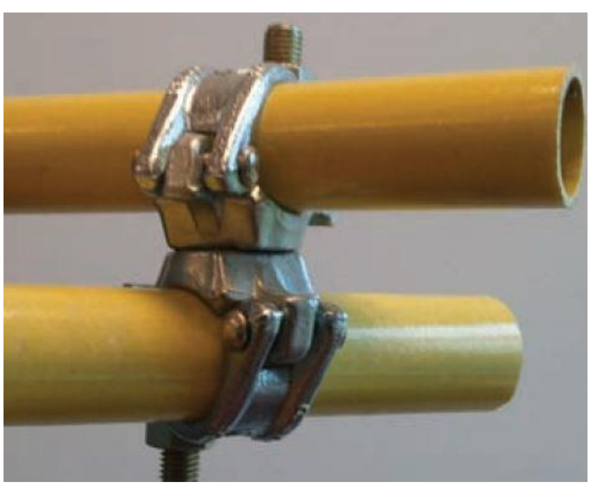

Figure A15, A16 Swivel coupler and cracks on the continuous beam (Baverel et al., 2012)

Project 5 **Faraday pavilion**

Description	Built as a seating and relaxation space for the 2012 Roskilde festival
Place	Roskilde, Denmark
Year	2012
Shape	Three domes
Size	area: approximately 30 m x 40 m height: 4 m length: 10 m width: 10 m grid-configuration: irregular grid topology
Material	Tubes: pultruded unidirectional GFRP Young's modulus: 25 GPa limit stress: length: (total: diameter: 40 mm wall thickness: 3 mm Membrane: PVC coated (500 m^2)
Weight	5 kg/m^2
Cost	materials: 150 $euro/m^2$, total: 45.000 euro
Architect	Navier research unit, School of civil engineering
Engineer	T/E/S/S

Form-finding Modern way: form-finding by computer models

Steps in form-finding: extended dynamic relaxation with bending included. Shell form and grid topology (not pre-described) are determined by simulation.
Structural analysis: different calculative models relating to material behavior, element and structure are solved and synthesized. Non-linear, three-dimensional models was created within the FEM-package sofistik.

Construction The radial elements were bent first and diagonal struts were used as lateral bracing. Then transverse elements were bent and connected to the radials with rotating scaffolding joints.

Connections Rotating swivel couplers to connect the elements of the grid (1,5 kg per connection)

Features Unique grid-configuration.
Drawbacks Lack of reinforcement at grid shells edges resulted in maximum deformations at border profiles.

Figure A17 Faraday Pavilion (Nicholas et al., 2013)

Project 6 **Ephemeral Cathedral in Paris**

Description	Built to replace the Creteil cathedral during its renovation, lasting at least two years.
Place	Creteil, Paris, France
Year	2013
Shape	Stretched dome
Size	area: 350 m^2 height: 7 m length: 25 m width: 15 m. grid-configuration: mesh size: 1 m.
Material	Tubes: approx. 2 kilometers of pultruded unidirectional GFRP from Topglass (Owens Corning glass fibers, polyester resin from DSM). Young's modulus: 25 GPa limit stress: 400 MPa length: 13,4 m (total: 1775 m) diameter: 41,7 mm wall thickness: 3,5 mm Membrane: polypropylene PVC coated canvas with transparent strips for daylight (opaque: 530 m^2, transparent: 25 x 0,5 = 12,5 m^2).
Weight	5 kg/m^2
Cost	400k euro
Architect	Navier research unit
Engineer	T/E/S/S
Form-finding	Modern way: form-finding by computer models. Steps in form-finding: first, a continuous shape with curvatures homogeneous as possible was defined. Then, the geometric properties of the beam were chosen, with the outer radius as the most important parameter. Then, determination of the grid-configuration using the compass method. Then, computation of the resulting shape. Then, the bracing layer was modelled and a full structural analysis was performed using two numerical models. Structural analysis according to Eurocomp. 1st numerical model: based on dynamic relaxation, taking axial stress and bending moments into account. Relevant for beams with orthotropic cross-section. 2nd numerical model: based on dynamic relaxation, taking also torsion into account. Relevant for beams with anisotropic cross-section. (Result: to create beam structures with original shapes, beams with oblong sections could be used).
Construction	Main building steps: the grid of continuous bars was built flat on the ground; the elements pinned together to prevent in-plane shear stiffness and allow for large-scale deformations during erection. Then, the grid was erected by two cranes and attached on anchorages to obtain its final shape. Then, a third layer of beams was installed with the use of new scaffolding elements to let the structure behave like a shell. Final, positioning and stretching of the membrane.
Connections	For major structural details: standard swivel scaffolding elements allowing rotation around their axis to connect tubes (1130u), steel sleeves connecting composite tubes (125u), ground anchorages fixing the grid shell to the composite slab (123u), edge beam lacing the fabric.
Features	Short construction time; few hours for about ten people.
Drawbacks	To extend the lifespan of the GFRP tubes, their long-term behavior should be better characterized.

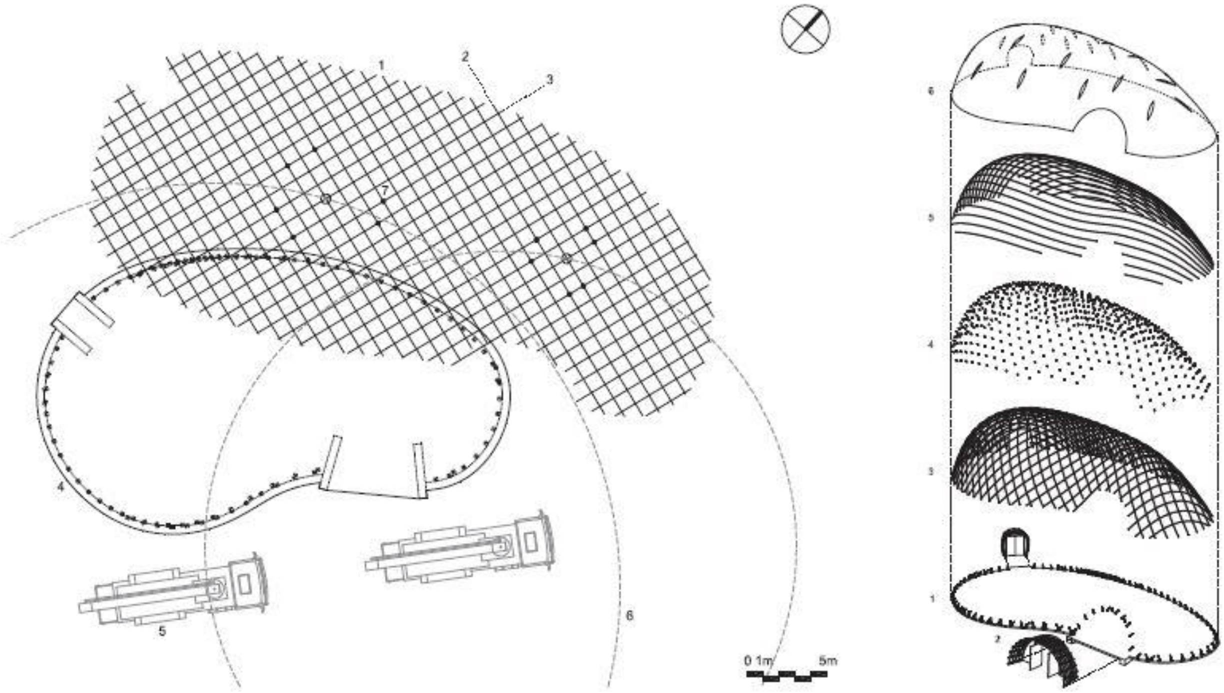

Figure A18 Construction plan and stages (Du Peloux, Tayeb, Caron, & Baverel, 2015)

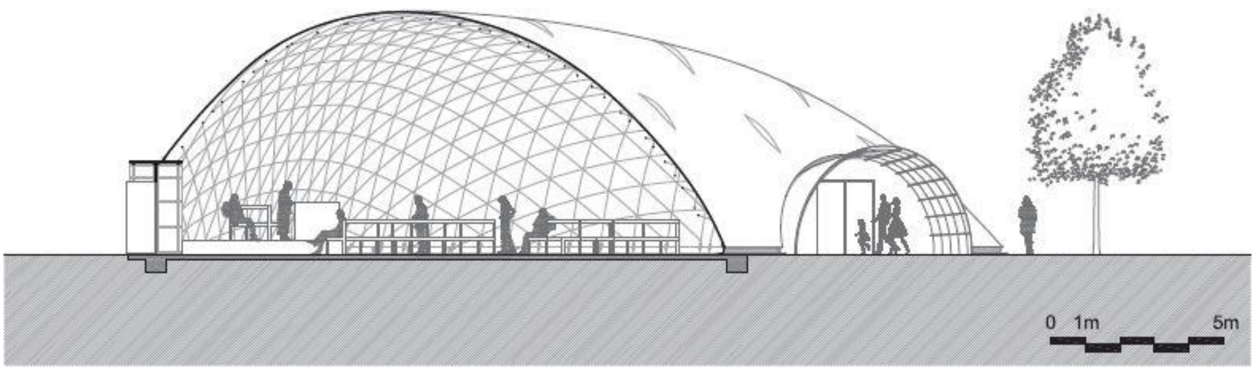

Figure A19 Interior view of the Ephemeral Cathedral (Du Peloux et al., 2015)

Figure A20 GFRP tubes, steel door, grid, and coated fabric PVC (Du Peloux et al., 2015)

Annex B Structural principles of shells, pre-formed grid shells, and non-linear beam theory

Shells

Shells are generalizations of isotropic homogeneous plates. In order to understand the structural behavior of shells, the structural behavior of plates is studied first. Subsequently, the translation from these flat surfaces to curved surfaces is made (Adriaenssens, Block, Veenendaal, & Williams, 2014).

A. Flat plates and plane stress

A flat plate can be loaded by forces in its two main directions: in its own plane or out of plane. In-plane loading of a flat plate is defined by the term ‘plane-stress’ or ‘membrane-stress’ (Figure B1). Loading out of plane results in bending and torsion of the plate (Figure B2). The membrane stress in the plane of a flat plate is an important concept in theory of shells and can be compared to the axial stresses in an arch. It’s components are presented in Figure B1 where (Adriaenssens et al., 2014):

σ_x the normal stress in x-direction
σ_y the normal stress in y-direction
τ_{xy} the shear stress in the x-direction perpendicular to the y-direction
τ_{yx} the shear stress in the y-direction perpendicular to the x-direction

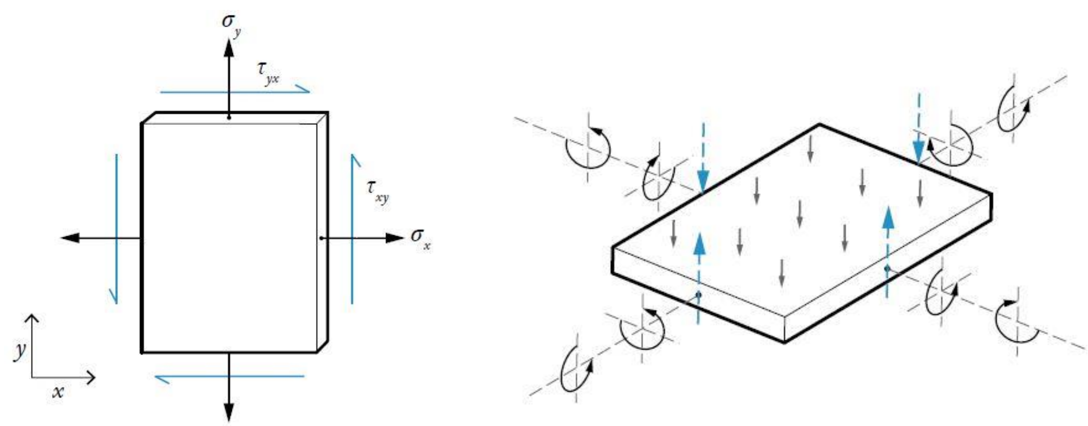

Figure B1, B2 Plane stress, bending of the plate (Adriaenssens, 2014)

B. Membrane behavior

In contrast to a flat plate, a shell is a structure defined by a three-dimensional curved surface. Due to this curvature, shells are able to carry out-of-plane loads by in-plane shear and normal forces. This behavior of shells is also called membrane behavior and is described by the membrane theory of shells.

Just like in the case of the in-plane stress of flat plates, there are three components of membrane stress in membrane theory of shells. The difference with in-plane stress is that, instead of two corresponding equilibrium equations, there are three equilibrium equations. Two of those equations correspond to the same directions as in the case of the plane stress, namely in direction tangent to the surface of the shell. The third equation corresponds to direction perpendicular to the tangent-plane of the shell. The load is in balance due to the multiplication of the membrane stresses by the curvature (Adriaenssens et al., 2014).

The fact that there are three stresses that are unknown and three equilibrium equations, indicates that shells should be statically determinate. However, it is often impossible to determine if a solution of those equations exist or not. Solutions depend on the boundary conditions and the geometry of the shell.

C. Bending behavior

In regions where out-of-plane loads cannot be fully carried by in-plane shell forces, bending moments are introduced in the system to compensate for this shortcoming. This bending action is required to prevent buckling of shells and possible modes of inextensible deformation. The behavior of shells under bending moments is also called bending behavior and is described by the bending theory of shells.

Typical regions of a shell which cannot be solved by pure membrane behavior are (Van der Linden, Hendriks, Terwel, & Hofman, 2015):

- at the supports of the shell structure
- at the position of a concentrated force
- at the position the shell makes a sudden change in geometry

Superposition of the equations from membrane and bending theory of shells, result in the equations of shell theory. Hereby the structural behavior of shells can be described.

Pre-formed grid shells

The structural principles of grid shells correspond to the structural principles of shells. The main difference between grid shells and shells is that grid shells are made of individual members in a grid instead of a continuous surface. The grid can contain more than one layer, but its thickness is significantly smaller compared to the dimensions of the two other directions.

A. Membrane behavior

Grid shells transfer in-plane loads in the direction of their elements, whereas shells carry these loads in all directions. Grid shells contain therefore a limited number of load paths, in contrast to the infinite number of load paths of shells. Pre-formed grid shells are constructed from prefabricated sub-frames, which form a rigid structural surface. These sub-frames carry out-of-plane loads by in-plane stresses.

B. Bending behavior

As with shells, in regions of grid shells where out-of-plane loads cannot be fully carried by in-plane shear forces, bending moments are introduced in the system. In contrast to shells, grid shells resist these bending moments through their cross-sections

Non-linear beam theory

This section introduces the basics of bending, which is based on the analysis of beams (Lienhard, 2014). The Euler-Bernoulli (BE) beam theory, or the classical beam theory, is used to calculate load-carrying and deflection characteristics of beams. The simplified differential equation of bending is given by:

$$y''(x) = \frac{M(x)}{EI} \tag{15}$$

where:
$y''(x)$ the second derivative of the out of plane displacement
M(x) the moment in the beam
EI the bending stiffness of the beam

The BE beam theory has also formulated a second order nonlinear differential equation, which takes large displacements into account. The equation is used for long slender beams and is given by:

$$\frac{1}{r(x)} = \frac{y''(x)}{\left[1 + \left(y'(x)\right)^2\right]^{2/3}} \tag{16}$$

where:
$\frac{1}{r(x)}$ the curvature of the beam
$y'(x)$ the first derivative of the out of plane displacement
$y''(x)$ the second derivative of the out of plane displacement

From this equation it can be noticed that the bending moment is always proportional to the change in curvature due to the applied load.

Derivation of the moment curvature relation

A relationship between the curvature due to bending and bending moment of a beam can be described, which is independent of the beam theory (Lienhard, 2014). For a segment with height t, which is presented in Figure B3, holds:

$$\frac{r(x_0)}{dx} = \frac{t}{\Delta dx} \tag{17}$$

where:
$r(x_0)$ radius of curvature
t height of the beam

Introduction of Hooke's law ($\sigma = E \times \varepsilon$) gives:

$$\frac{t}{r(x_0)} = \frac{\Delta dx}{dx} = \varepsilon = \frac{\sigma}{E} = \frac{M(x_0) \times t}{EI} \tag{18}$$

where:
$\frac{1}{r(x_0)}$ curvature
t height of the beam
$M(x_0)$ moment at x = 0
ε bending strain

σ	bending stress
E	elastic modulus
EI	bending stiffness

Then, according to a permissible stress, the minimum bending radius is given by:

$$r_{min}(x_0) = \frac{E \times t}{2 \times \sigma_{Rd}} \tag{19}$$

where:

$r_{min}(x_0)$	minimum bending radius
E	elastic modulus
t	height of the beam
σ_{Rd}	permissible stress

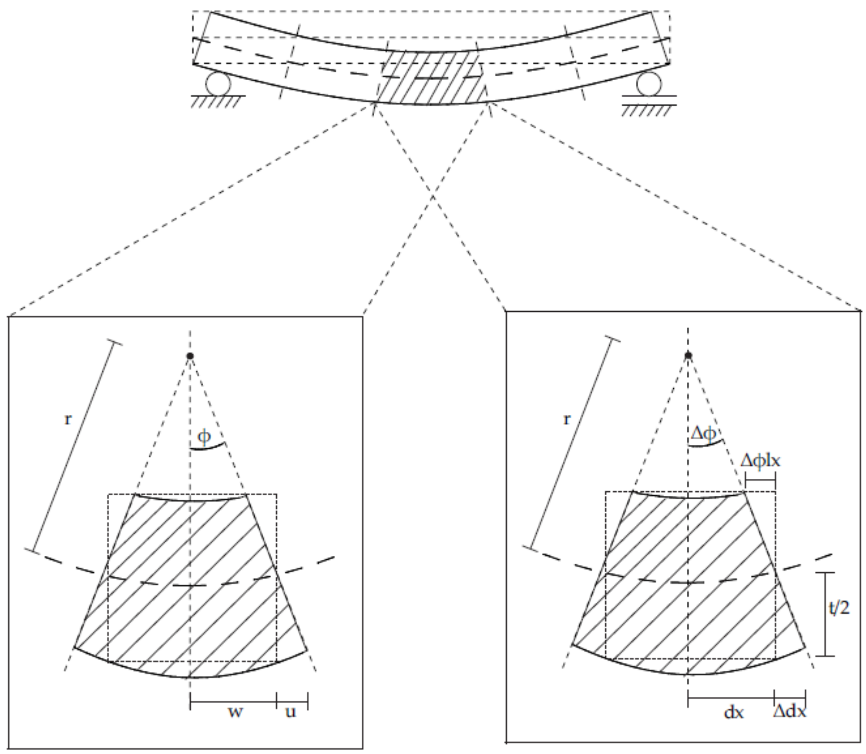

Figure B3 Geometrical relationships in a beam with large deflection (Lienhard, 2014)

Annex C Design verifications according to CUR96

Actively bent grid shells should be verified to both the serviceability limit states (SLS) and the ultimate limit states (ULS). For these verifications, where different design situations are considered, different partial safety and conversion factors have to be used. This Annex presents the material properties, partial safety and conversion factors to be used, considering creep as the aspect to be verified.

A. Material parameters

The actively bent members of the grid shells are produced by the process of pultrusion. The members, spanning between two supports on the perimeter, are pultruded CFRP laminates made up from unidirectional (UD) plies. As all plies are equal and lie in the same direction, the fiber direction is the only principal direction of the laminate. Elastic properties of FRP laminates can be obtained from Classical Laminate Theory[2] (CLT).

The elastic behavior of UD plies can be described by four parameters, abbreviated to E_1, E_2, G_{12}, v_{12}. Subsequently, v_{21} can be derived from E_1, E_2, and v_{12}, (JRC, 2016):

$$E_1 = [E_R + (E_{F1} - E_R) \times V_f] \times \varphi_{UD} \tag{20}$$

$$E_2 = \left[\frac{(1 + \xi_2 \eta_2 V_f)}{(1 - \eta_2 V_f)} \times E_R\right] \times \varphi_{UD} \tag{21}$$

$$G_{12} = \left[\frac{(1 + \xi_G \eta_G V_f)}{(1 - \eta_G V_f)} \times G_R\right] \times \varphi_{UD} \tag{22}$$

$$\nu_{12} = \nu_R - (\nu_R - \nu_F) \times V_{f,} \qquad \nu_{21} = \nu_{12} \times \frac{E_2}{E_1} \tag{23}$$

where:

E_1	the stiffness in fiber direction, i.e. longitudinal direction
E_2	the stiffness perpendicular to fiber direction, i.e. transverse direction
G_{12}	the longitudinal shear stiffness
v_{12}, v_{21}	the Poisson's ratios in longitudinal and transverse direction

B. Partial safety factors

A method to obtain design values is to divide the characteristic value of the material at the prescribed design life by a partial safety factor. For verifications of ULS for a FRP laminate or structure, the material partial factor γ_M should be calculated from (JRC, 2016):

$$\gamma_M = \gamma_{M1} \times \gamma_{M2} \tag{24}$$

where:

γ_M	the material partial factor
γ_{M1}	the material partial factor representing uncertainties in material properties.
γ_{M2}	the material partial factor depending on the production process and nature of the constituent parts

For verifications of SLS, the material partial factors γ_1 and γ_2 are 1.0.

C. Conversion factors

For verifications of ULS and SLS for a FRP laminate or structure, applicable conversion factors for every given situation should be determined. The total conversion factor η_c is calculated from (JRC, 2016):

$$\eta_c = \eta_{ct} \times \eta_{cm} \times \eta_{cv} \times \eta_{cf} \quad (25)$$

where:

η_{ct}	the conversion factor for temperature effects
η_{cm}	the conversion factor for humidity effects
η_{cv}	the conversion factor considering creep effects
η_{cf}	the conversion factor considering fatigue effects

The conversion factors to be taken into account for different limit states, are presented in Table E.1. The conversion factor for creep η_{cv} should be used for verifications of strength (ULS), stability (ULS), creep (SLS), and damage (SLS).

	Aspect being verified						
Influencing factor	Strength (ULS)	Stability (ULS)	Fatigue (ULS)	Creep (SLS)	Momentary deformation (SLS)	Comfort (vibrations) (SLS)	Damage (SLS)
η_{ct}	√	√	√	√	√	√	√
η_{cm}	√	√	√	√	√	√	√
η_{cv}	√	√		√			√
η_{cf}		√		√	√	√	√

Table E.1 Conversion factors to be considered for ULS and SLS verifications (JRC, 2016)

The creep conversion factor η_{cv} is calculated from (CUR, 2017):

$$\eta_{cv} = 1/\Delta\varepsilon_v \times t^n \quad (26)$$

where:

$\Delta\varepsilon_v$	the increase in strain rate of the considered UD ply
t	the duration of the load(s) in hours
n	an exponent depending on the fiber type. In case the fibers lie in the direction of the long term load[1]:

- n = 0,01 for an UD ply;
- n = 0,04 for a woven ply;
- n = 0,10 for a mat-ply;

[1]These factors are derived for GFRP. For CFRP these factors are conservative.

According to CUR (2017), for laminates with different fiber orientations, the conversion factor η_{cv} should be determined according to the method described in Section 2.4.5.4 of CUR, or the Theory of Findley (Section X).

a. Strength (ULS)

For ULS verifications for FRP structures subjected to (quasi-) permanent loads, creep-rupture should be considered. The partial safety factor for creep effects should be used. In

CNR-DT (2007), a partial safety factor of 1.5 is proposed. The conversion factor for creep should only be used in case of long-term loads.

CUR (2017) proposes a 0,2% conservative assumption for design value of maximum strain in structural members subjected to (quasi-) permanent loads. The use of other values is allowed if determined by testing.

To avoid creep-rupture under (quasi-)permanent loads, the following stress limits, defined by ACI (2008) may be used as an indication (CUR, 2017):

GFRP	0,2 $f_{x,Rd}$[3]
CFRP	0,55 $f_{x,Rd}$
AFRP	0,3 $f_{x,Rd}$

[3] $f_{x,Rd}$ is the characteristic value of the initial ultimate strength.

The total partial safety factor for strength verifications in SLS $\gamma_{m,s}$, is calculated from (see Section 1.3.2):

$$\gamma_{M.s} = \gamma_{M1} \times \gamma_{M2} \tag{27}$$

The influence of creep is obtained considering the duration of the load: permanent, long or medium (6 months) loads.

The reference value of the creep conversion factors for 20 years, $\eta_{cv.20.L}$ and $\eta_{cv.20.T}$, are calculated, taking into account the design situation, manufacturing process and direction of the loading (see Tables 10.1 and 10.2 in JRC2016). The reference creep factor for strength verifications in ULS of pultruded profiles loaded in the direction of pultrusion is calculated from:

$$\eta_{cv.20} = \frac{1}{1.8 - \delta} \tag{28}$$

where:

δ	the mass portion of fibers, which is calculated from:

$$\delta = \frac{1}{1 + \frac{\frac{1}{V_f} - 1}{\frac{\gamma_f}{\gamma_r}}} \tag{29}$$

where:

V_f	the fiber volume fraction
γ_f	the fiber density
γ_r	the resin density

Subsequently, the reference creep conversion factors for 20 years, $\eta_{cv.20.L}$ and $\eta_{cv.20.T}$, are transformed in the logarithmic scale (see Figure 2.1 in JRC2016) to the period of 6 years.

The total conversion factors for strength verification in ULS in longitudinal and transverse direction, $\eta_{c.s.L}$ and $\eta_{c.s.T}$, are calculated from below equations:

$$\eta_{c.s.L} = \eta_{ct} \times \eta_{cm} \times \eta_{cv.L} \tag{30}$$

$$\eta_{c.s.T} = \eta_{ct} \times \eta_{cm} \times \eta_{cv.T} \quad (31)$$

where:

η_{ct}	the conversion factor for temperature effects
η_{cm}	the conversion factor for humidity effects
$\eta_{cv,L}$, $\eta_{cv,T}$	the conversion factors for creep effects to the period of 6 months

b. Stability (ULS)

For stability verifications of structural elements, the effects of creep on the structure's deformation should be taken into account. Considering stability, creep does not influence the stiffness of the structure, but could lead to larger eccentricities in case of long-term loads. In other words, the conversion factor for creep effects η_{cv} for stability verifications should be applied to determine the deformed state for the purpose of eccentricity.

The total partial safety factor for stability verifications in ULS, $\gamma_{m,b}$, is calculated from:

$$\gamma_{M.b} = \gamma_{M1} \times \gamma_{M2} \quad (32)$$

The total conversion factors for stability verification in ULS in longitudinal and transverse direction, $\eta_{c.b.L}$ and $\eta_{c.b.T}$, are calculated from below equations. The influence of creep is the same as in case of strength ULS.

$$\eta_{c.b.L} = \eta_{ct} \times \eta_{cm} \times \boldsymbol{\eta_{cvL}} \times \eta_{cf} \quad (33)$$

$$\eta_{c.b.T} = \eta_{ct} \times \eta_{cm} \times \boldsymbol{\eta_{cvT}} \times \eta_{cf} \quad (34)$$

where:

$\eta_{c.b.L}$	the total conversion factor for the stability in longitudinal direction;
$\eta_{c.b.T}$	the total conversion factor for the stability in transverse direction;
η_{cf}	the conversion factor for fatigue effects;

c. Creep (SLS)

For creep verifications in SLS, the material partial factors γ_1 and γ_2 are 1.0. The total conversion factor η_c is calculated from:

$$\eta_c = \eta_{ct} \times \eta_{cm} \times \eta_{cv} \times \eta_{cf} \quad (35)$$

where:

η_{ct}	the conversion factor for temperature effects
η_{cm}	the conversion factor for humidity effects
η_{cv}	the conversion factor for creep effects
η_{cf}	the conversion factor for fatigue effects

The influence of the creep conversion factor, η_{cv}, should be assessed regarding (quasi-)permanent loads. For the determination of η_{cv} is referred to Section a.

d. Damage (SLS)

For damage verifications in SLS, the material partial factors γ_1 and γ_2 are 1.0. The calculation of the total conversion factor η_c is the same as for creep verifications in SLS (see Section c).

Annex D Analytical models for creep of FRP on a long-term

Actively bent grid shells use the bending capability of long and slender members within their specific construction process. It is therefore particularly interesting to study the long-term creep behavior of CFRP members which are subjected to bending. An description of existing analytical models to study the long-term creep behavior of FRP is presented in presented in this annex.

Over the past years, several studies have determined the time-dependent creep behavior of FRP structural elements (Sá, Gomes, Correia, & Silvestre, 2011). However, only few of these studies examined the flexural creep behavior of FRP elements in bending. In the paper of (Sá et al., 2011), a summary of different studies that investigated flexural creep behavior is presented. Aspects related to the constitution of the materials, the scale of elements, the types of loading, and the duration of tests are compared. From this summary it was concluded that most flexural creep testing has focused on short-durations with small specimen, rather than long-duration with full size structural elements.

Besides this experimental study, the paper of (Sá et al., 2011) presents an analytical study of the flexural creep behavior of laminated FRP material and pultruded GFRP profiles. In this particular study, existing analytical models to simulate the creep behavior of both laminated specimens and FRP profiles, namely Findley's power law, Bruger-Kelvin model, and Proni-Dirichlet series, were investigated. The author of the paper concludes that for the prediction of the long-term creep behavior of pultruded GFRP elements, Findley's power law coupled with experimental data is the best approach (Sá et al., 2011).

A. Findley's Power Law

Findley's power law is an empirical model based on experimental tests to predict the viscoelastic behavior of FRP. The law provides a formula for the time-dependent flexural elastic modulus, for SLS verifications of applications in Civil Engineering (Sá et al, 2011).

The original form of Findley's power law considers elements in compression or tension and is presented below. This original form can be extended to other specific forms if the FRP elements are subjected to different loading, e.g. axial, shear or torsion (Sá, Gomes, Correia, & Silvestre, 2011):

$$\varepsilon(\mathrm{t}) = \varepsilon_0 + \mathrm{m} \times (\mathrm{t}/\tau_0)^{\mathrm{n}} \tag{36}$$

where:

$\varepsilon(t)$	the time-dependent creep strain (or deflection – $v(t)$)
ε_0	the initial elastic strain which is both stress- and temperature-dependent (or initial elastic deflection – v_0)
m	a coefficient which is both stress- and temperature-dependent
n	a material constant which is stress-independent and may be a dependent on temperature or moisture content
t	the time after loading
τ_0	the reference unit time

Both parameters m and n need to be determined by creep test data to characterize Findley's power law. Principles are described in the paper of (Sá et al., 2011).

For low stress levels, both the initial elastic strain ε_0, and the coefficient m may be expressed as follows:

$$\varepsilon_0 = \varepsilon_0' \times \sinh\left(\frac{\sigma}{\sigma_\varepsilon}\right), \qquad \mathrm{m} = \mathrm{m}' \times \sinh\left(\frac{\sigma}{\sigma_\mathrm{m}}\right) \tag{37}$$

where:

σ the applied stress

σ_ε, ε_0', m', σ_m material constants to be determined from creep tests at several applied stress levels

In the work of (Sá et al., 2011), it is recommended that the loads applied in SLS should not exceed 40% of the ultimate stress in bending.

B. Prediction of the time-dependent flexural elastic modulus (Findley + test data)

If both parameters m and n of the Finley's power law are determined, the reduction in stiffness of FRP at a given time t can be predicted. In order to determine the time-dependent flexural elastic modulus, E(t), the following equation may be used (Sá et al., 2011):

$$\varepsilon(t) \approx \frac{\sigma}{E(t)} \qquad E(t) = \frac{E_0 \times E_t}{E_t + E_0 \times t^n} \tag{38}$$

where:

E(t) the time-dependent flexural elastic modulus (also known as viscoelastic modulus)

E_0 the initial elastic modulus

E_t the creep elastic modulus

The initial elasticity moduli, E_0, and creep moduli, E_t, can be determined from:

$$E_0 = \frac{\sigma_\varepsilon}{\varepsilon_0'}, \qquad E_t = \frac{\sigma_m}{m'} \tag{39}$$

where:

σ_ε, ε_0', m', σ_m are material constants to be determined from creep tests at several applied stress levels.

C. Practice design formulation for the time-dependent flexural elastic modulus

For SLS verifications, in long-term behavior, the time-dependent flexural elastic modulus, E(t), also known as viscoelastic modulus, can be considered by design equation of the following well-known form (Sá et al, 2011):

$$E(t) = E_0 \times \chi(t) \tag{40}$$

where:

χ(t) a reduction factor which is time-dependent and can be obtained from:

$$\chi(t) = \left(1 + \frac{E_0}{E_t} \times t^n\right)^{-1}, \qquad \chi(t) = \left(1 + \frac{1}{\beta} \times t^n\right)^{-1} \tag{41}$$

where:

$\beta = E_t/E_0$ the ratio of creep elastic modulus over initial elastic modulus

β can be determined from the prediction model described in the paper of Sá et al (2011), and is based on creep test results obtained from short-duration tests.

As an alternative, the reduction factor $\chi(t)$ can also be considered by the following equation:

$$\chi(t) = [1 + \phi(t)]^{-1}. \qquad \phi(t) = \frac{1}{\beta} \times t^n \tag{42}$$

where:

$\phi(t)$ a viscosity coefficient due to longitudinal deformations, which is time-dependent, and depends on β and t (in hours).

The Technical Recommendation of the Italian National Research Council (CNR-DT205, 2007), presents values for viscosity coefficients, $\phi(t)$, due to longitudinal deformations $\phi_E(t)$, and shear deformations $\phi_G(t)$ of pultruded GFRP elements. These coefficients for GFRP, and corresponding equations to obtain the longitudinal and transverse elastic moduli, $E_L(t)$ and $G_{LT}(t)$, are presented in Figure D.1.

t (elapsed time)	$\phi_E(t)$	$\phi_G(t)$
1 year	0.26	0.57
5 years	0.42	0.98
10 years	0.50	1.23
30 years	0.60	1.76
50 years	0.66	2.09

$$E_L(t) = \frac{E_L}{1+\phi_E(t)},$$

$$G_{LT}(t) = \frac{G_{LT}}{1+\phi_G(t)}.$$

Figure D.1 Coefficients of viscosity due to longitudinal and shear deformations and corresponding elastic moduli equations (CNR-DT205, 2007)

Based on the equations of Findley's power law and the time-dependent flexural elastic modulus, Bank (2006) proposes general creep models for GFRP pultruded profiles in compression and in bending. Figure D.2 presents parameters of Bank's creep model for flexure and shear in flexure (Gonilha, Correia, & Branco, 2013).

Sustained loading type	E_t (GPa)	G_t (GPa)	n
Flexure	1241.06	186.16	0.3

Figure D.2 Parameters of Bank's GFRP creep model (Gonilha et al., 2013)

EUROCOMP (1996) presents data on the time-dependent elasticity moduli for unidirectional FRP in tension and in shear. As the members of the actively bent grid shells investigated in this thesis are primarily subjected to bending, the general equation from EUROCOMP (1996) describing creep is not relevant for this research.

Annex E Input data SOFiSTiK model of an actively bent member

Chapter 4 presents a two-dimensional in-plane buckling analysis of an actively bent member with constant cross-section. This finite element and analysis software SOFiSTiK has been used for numerical calculations. This annex presents the input data (TEDDY) that has been used to define the SOFiSTiK model of an actively bent member.

```
+prog aqua urs:1
head material and sections
echo full yes
mat 1 e 25e6 mue 0.32
tube 1 D 40 t 3 mno 1 $tube section
end

+PROG SOFIMSHA urs:2
HEAD beam structure
echo full no
syst spac gdiv 1000
page unii 0 unio 0
node 1 0 0 0 fix pymxpz
node 50 3[m] 0 0 fix py
node 100 6[m] 0 0 fix pxpymxpz
grp 0
beam mesh 1 50 div 10 ncs 1
beam mesh 50 100 div 10 ncs 1
grp 1
spri na 1 dx 1 cp 100000
END

+prog sofiload urs:5.1
head load definition
page unii 0 unio 0
lc 1 $lateral load at the middle
node 50 type pzz -0.003
loop#i 20
lc 2+#i $axial compression force at both ends
node 1 type wxx 38*(1+#i)
endloop
lc 99 $distributed load
node 50 type pzz 1.4
end

+prog ase urs:5.2
head prebend
syst prob th3
echo full no
echo load yes
grp 1 off
lc 101
lcc 1
end

+prog ase urs:5.3
head bend 1
```

```
syst prob th3 plc 101
echo full no
echo load yes
CTRL WARN 183
CTRL ITER 3 V2 1
grp 1 off
lc 102
lcc 2
end

+prog ase urs:5.4
loop#i 19
let#n #i+3
head bend #n
syst prob th3 plc 99+#n
echo full no
echo load yes
grp 1 off
lc 100+#n
lcc #n
end
endloop
end

+prog ase urs:3
head "central load"
syst prob th3 plc 121
echo full no
echo load yes
CTRL WARN 183
CTRL ITER 3 V2 1
grp 1 off
lc 200
lcc 121
lcc 99
end
endloop
end

+prog ase urs:4
head "imperfection"
syst prob th3
obli lc 121 facv 1
lc 300 dlz 0.000001
end
endloop
end

+prog ase urs:5
head "imperfection"
syst prob th3 plc 300
grp 0,1 yes
lc 301
lcc 99
end
endloop, end
```

Annex F Preliminary tension tests with acrylic and epoxy adhesive bonded assemblies

A. Tensile testing with acrylic versus epoxy adhesive

Tensile creep testing using the SSM will be performed with CFRP pultruded (+ winding & braiding) specimens with a diameter of 30 mm, wall thickness of 1 mm, and a nominal length of 600 mm. The composite contains of 0.65 volume fraction Toho Tenax STS fibers in a Epikote epoxy resin. According to the producer, the material has 2300 MPa tensile strength, 130 GPa elastic modulus, and a glass transition temperature of 65°C. Based on preliminary calculations, it is expected that the specimens tested will fail at 210 kN of force at 1,77% strain.

Materials and specimens

M27 rods measuring 300 mm in length will be used as fitting between the specimens and the testing machine. One side of this rod will be adhesive bonded into the specimen over 200 mm height. The other end will be prepared in the testing machine, wherefore it's diameter will be reduced to 24 mm.

The behavior of the bonded assembly using two different adhesives was tested: a 406E/17 acrylic adhesive (MMA) with 16 – 23 N/mm^2 capacity and a 320/310B epoxy adhesive with 16 – 20 N/mm^2 (capacity see Figure F1 and F2). The threaded rods were bonded to the specimens with adhesives that were cured for 24 hours at room temperature.

Experimental procedure

To test the behavior of both adhesives in the bonded assemblies, tensile tests were carried out with two specimens, which were prepared with the different adhesives. Tensile testing was performed on a MTS 647 Hydraulic Wedge Grip with 250 kN capacity (see Figure F3). The specimens were prepared with two LVDTs (gauge length = 130 mm) and three strain gauges, to measure displacement and strain respectively.

The specimens were loaded at room temperature at a constant load rate of 0.001 mm/sec. Tensile responses of CFRP specimens prepared with the adhesives in bonded assemblies are presented in Figures F4-7.

Figure F1 CFRP specimen prepared with 320/310B epoxy and 604E/17 acrylic adhesive in bonded assembly

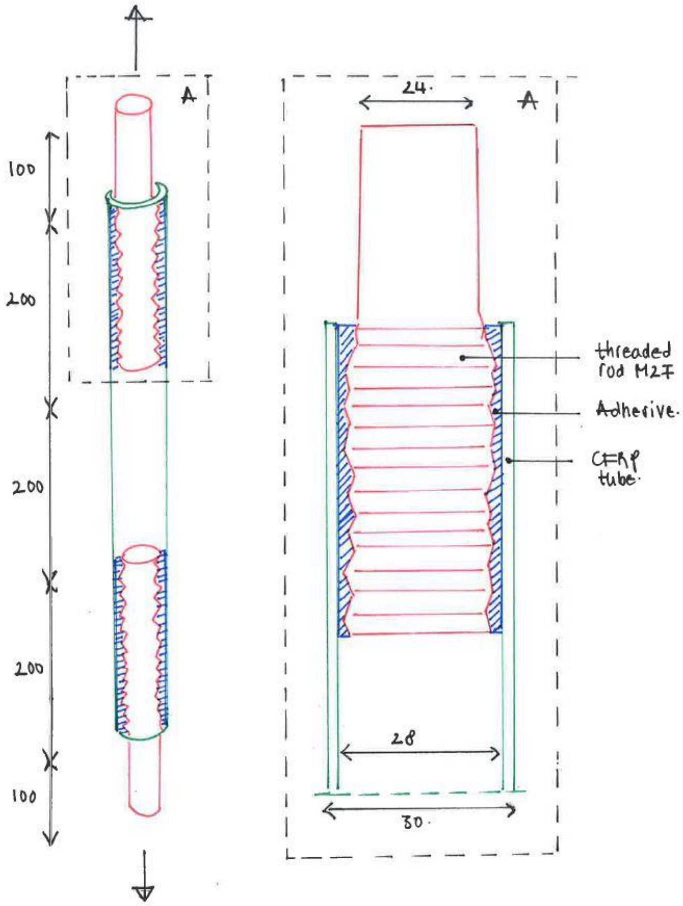

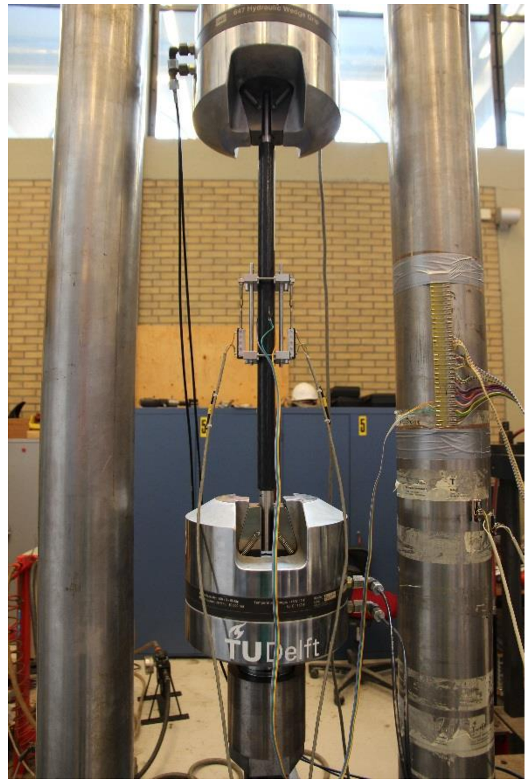

Figure F2 Detail bonded assembly for tensile creep tests

Figure F3 CFRP test specimen and MTS 647 test rig

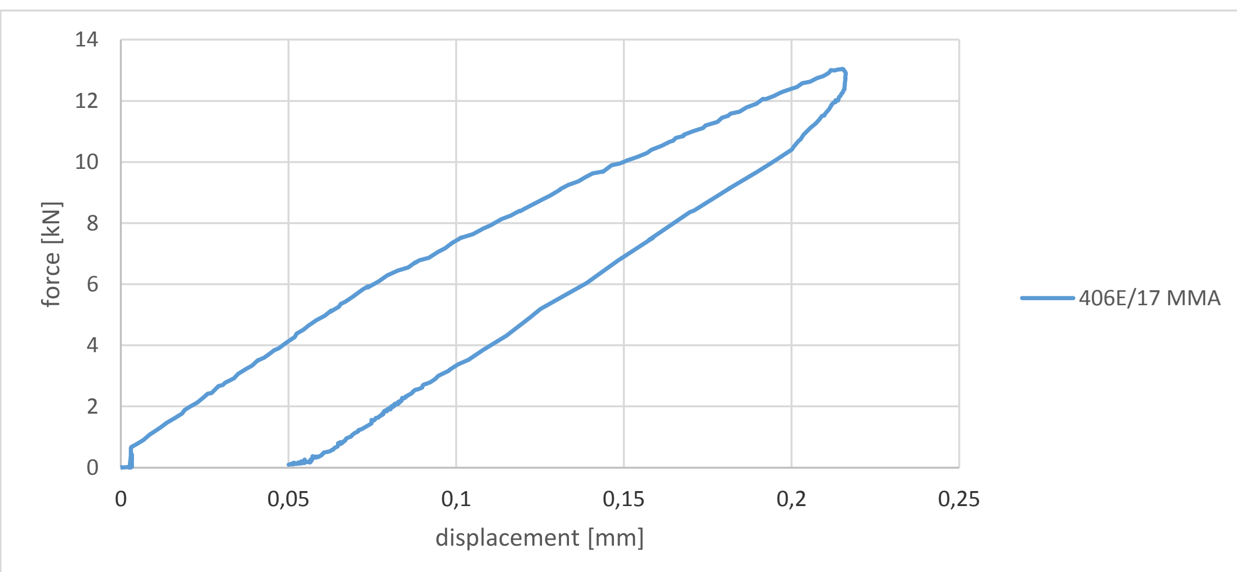

Figure F4 Tensile response of CFRP specimen prepared with 406E/17 MMA in bonded assembly

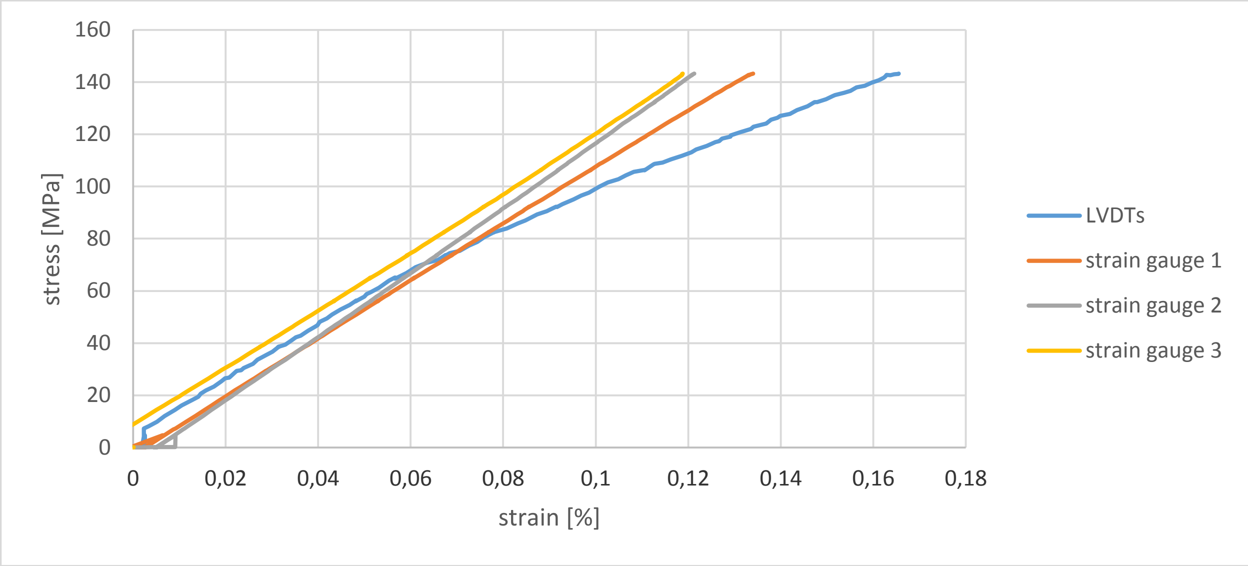

Figure F5 Tensile response of CFRP specimen prepared with 406E/17 MMA in bonded assembly

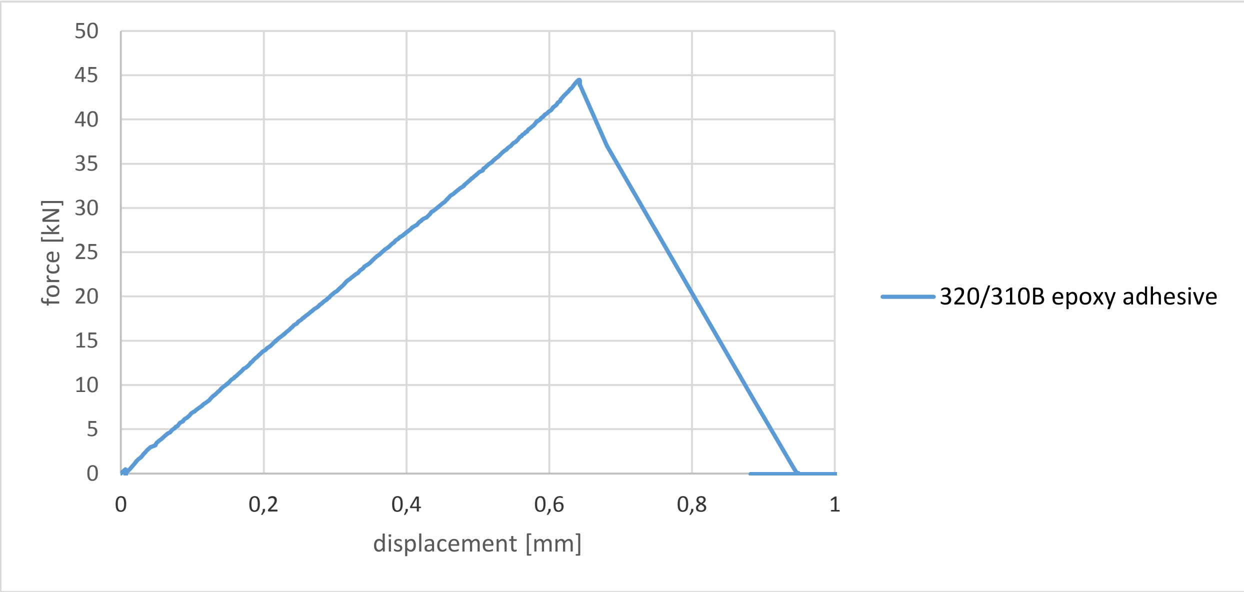

Figure F6 Tensile response of CFRP specimen prepared with 320/310B epoxy adhesive in bonded assembly

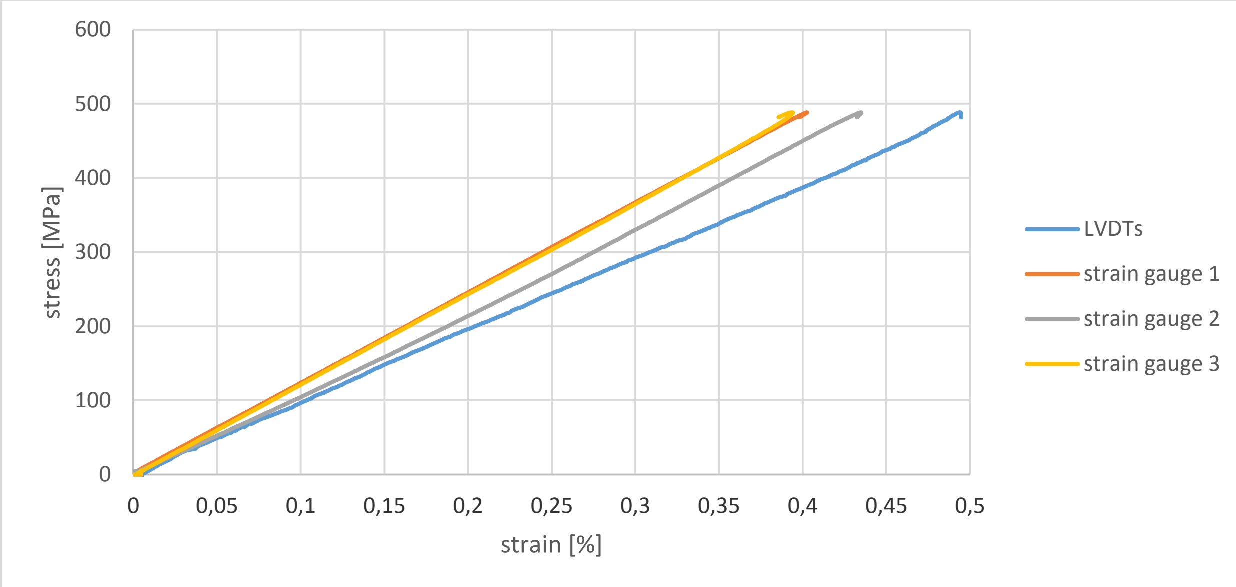

Figure F7 Tensile response of CFRP specimen prepared with 320/310B epoxy adhesive in bonded assembly

Initial results and observations

The bonded assembly using the acrylic interface between CFRP and rod failed at 13.1 kN of force at 0.22 mm displacement, after 115 sec. of increasing stress. The threaded rod prepared with the top head of the testing rig, was pulled out entirely from the specimen. No damage mechanism was observed on the specimen itself. It appeared that the 406E/17 acrylic adhesive had not cured properly; the substance was still wet (see Figure F8).

The cause of this phenomenon could be the presence of oxygen during the gluing process. In general, the 406E/17 acrylic adhesive is suitable for bonding of areas where no oxygen is present. During the adhesive bonding of the rod into the specimen, air has entered the specimen.

The specimen tested with the epoxy bonded interface between CFRP and rod failed at 43.9 kN of force at 0.64 mm displacement, after about 270 sec. of increasing stress. The damage mechanism observed on the specimen is presented in Figure F9. A crack has propagated along the length of the specimen near position of the rods, over a height of 120 mm.

It was observed that there was insufficient adhesion between the 320/310B epoxy adhesive and the specimen. This may be caused by the inside of the specimen not being cleaned properly. Adhesion improvement between the epoxy adhesive and the inside of the CFRP tube may be obtained by improving the solving-sanding-solving process before the adhesive bonding of the rod into the specimen.

From Figure F7 it can be seen that the strain gauges have measured differences in strain in the CFRP specimen. Radial stresses appeared to have occurred at the specimen, which may have been influenced by joint eccentricities of differences in Poisson’s ratio.

From the slope of the initial linear portion of the stress-strain curves in Figure F7 – the elastic region – a material Young’s modulus of about 100 GPa was calculated. This value of Young’s modulus is smaller than the 130 GPa according to the producer.

Figure F8 M27 rod with 406E/17 acrylic adhesive after tensile test

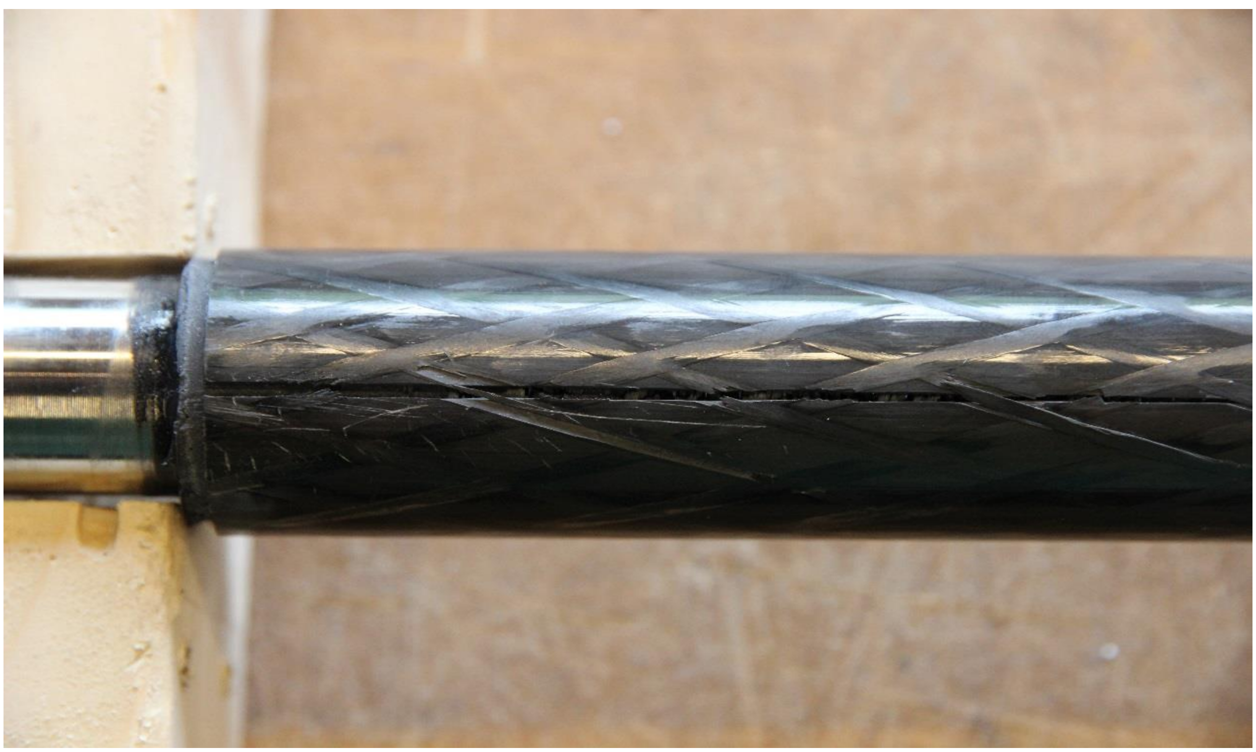

Figure F9 Damage mechanism observed on CFRP specimen prepared with 320/310B epoxy adhesive

Conclusions

The behavior of the bonded assemblies using two different adhesives was tested: a 406E/17 acrylic adhesive and a 320/310B epoxy adhesive. Both assemblies using the acrylic and epoxy adhesive failed at 13.1 kN and 43.9 kN of force respectively. Based on preliminary calculations it was expected that the specimens themselves would fail at 210 kN of force, instead of modes of failure occur in the bonded assemblies.

Based on the observed failure modes, it was concluded that the 320/310B epoxy adhesive works the best for the assembly concerned. The behavior of this adhesive will therefore be further investigated. To improve adhesion between the epoxy adhesive and the specimen, the solving-sanding-solving process will be performed more conscientiously. To avoid crack propagation along the length of the specimen near the rods, further testing will be done with steel tubes which are adhesive bonded to the exterior of the specimens.

B. Tensile testing with epoxy adhesive bonded assembly

Tensile creep testing using the SSM will be performed with CFRP pultruded (+ winding & braiding) specimens with a diameter of 30 mm, wall thickness of 1 mm, and a nominal length of 600 mm. Based on preliminary calculations, it is expected that the specimens will fail at ~210 kN of force at 1,77% strain.

Materials and specimens

M27 rods measuring 300 mm in length were used as fitting between the specimens and the testing machine. One side of this rod was adhesive bonded into the specimen over 200 mm height with a Lord 320/310B epoxy adhesive. To fit the other end in the testing machine, the rod's diameter was locally reduced to 24 mm. In addition, aluminum tubes measuring 200 mm in length were adhesive bonded to the exterior of the specimens ends with the Lord 320/310B epoxy adhesive.

Experimental procedure

A tensile tests was performed to find the average ultimate strength of the CFRP. 600 mm long 30 mm x 28 mm CFRP tubes were prepared with M27 rods and aluminum tubes, leaving a free length of 200 mm (see Figure F10).

Tensile testing was performed on a MTS 647 Hydraulic Wedge Grip with 250 kN capacity (see Figure F11). Displacement was measured with two LVDTs (gauge length = 130 mm). Strain was measured with three strain gauges, prepared with the center of the tube.

The specimen was loaded at room temperature at a constant load rate of 0.01 mm/sec. Tensile responses of the CFRP adhesively bonded assembly are presented in Figures F12 and F13.

Initial results and observations

The CFRP adhesively bonded assembly failed at 39,0 kN of force at 0,52 mm displacement, after 290 sec. of increasing stress. The threaded rod prepared with the top head of the test rig, was pulled out entirely from the specimen. No damage mechanism was observed on the specimen itself. It was observed that there was no adhesion between the Lord 320/310B epoxy adhesive and the inside of the tube see Figure F14). From the slope of the initial linear portion of the stress-strain curve (LVDTs) in Figure F13, a material Young's modulus of 110 GPA was calculated (GPA).

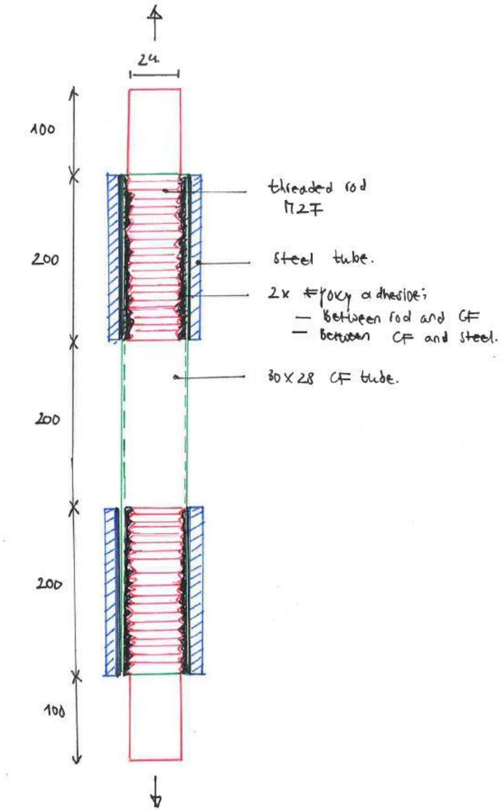

Figure F10 Detail of CFRP adhesively bonded assembly

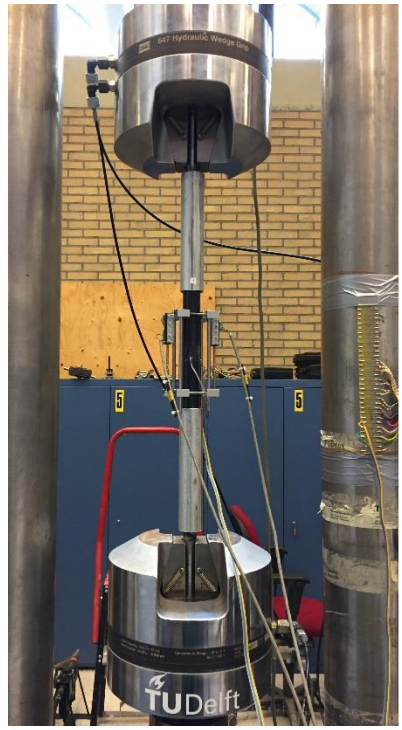

Figure F11 CFRP test specimen in MTS 647 test rig

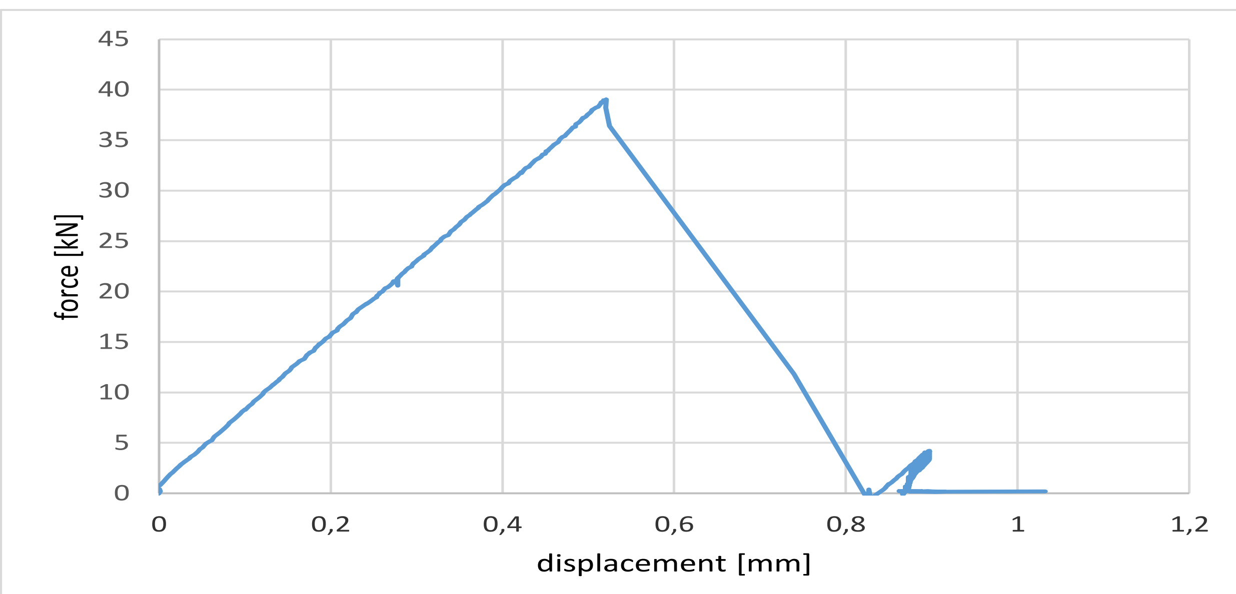

Figure F12 Tensile response of CFRP adhesively bonded assembly

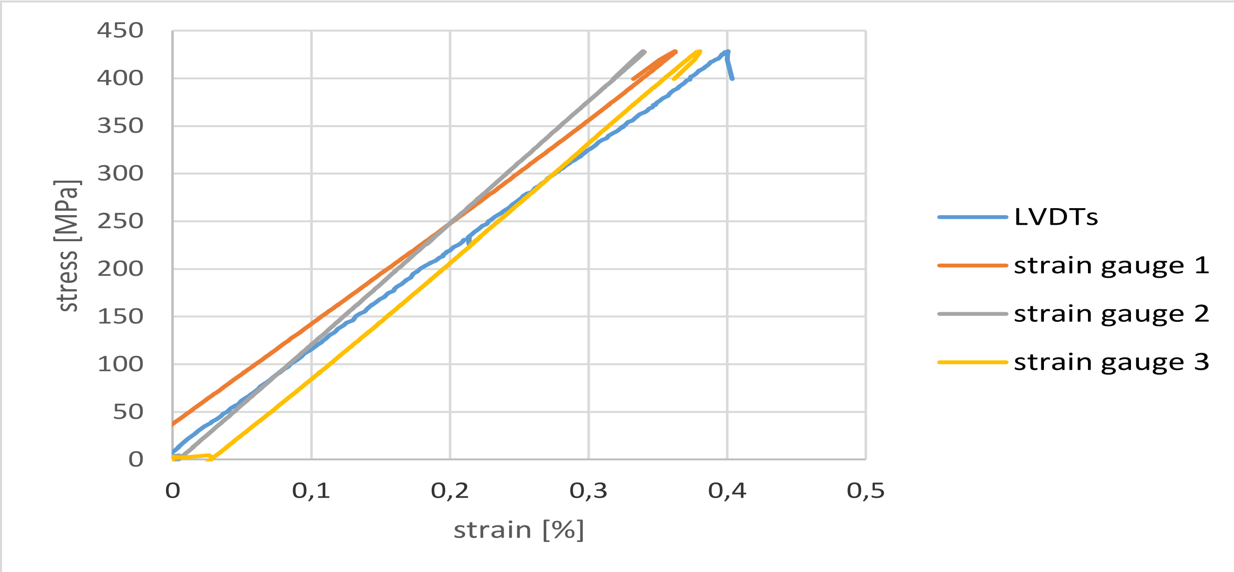

Figure F13 Tensile response of CFRP adhesively bonded assembly

Conclusions

A tensile test with a CFRP adhesively bonded assembly was performed to find the average ultimate strength of the CFRP. The assembly using an 320/310B epoxy adhesive failed at 39,0 kN of force, where the rod prepared with the top head of the test rig was pulled out entirely from the specimen. Lack of adhesion between the epoxy adhesive and the inside of the tube may be caused due to mould release agent being present at the inside of the tube. To improve adhesion between epoxy adhesive and the specimen, all mould release agent should be removed from the specimen before the adhesive is applied. Based on preliminary calculations it is expected that the CFRP specimen will fail at ~210 kN of force. Further testing will be performed with CFRP specimen prepared with steel clamping devices, without using adhesives (see Chapter 6).

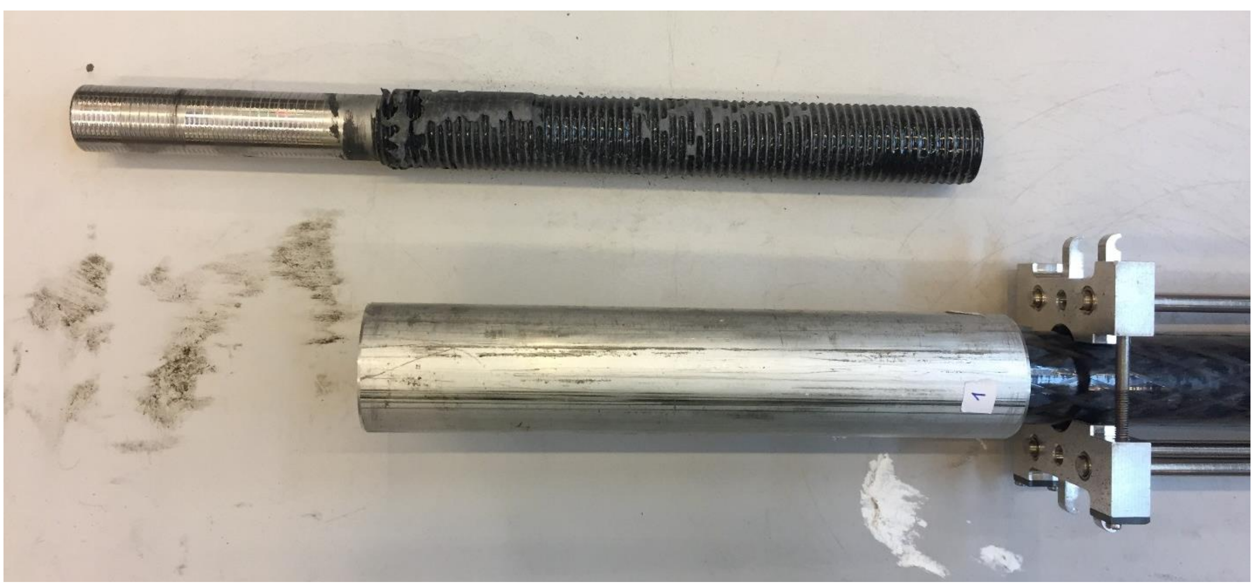

Figure F14 M27 rod with 320/310B epoxy adhesive pulled out entirely from the CFRP specimen

Annex G Details of clamping device for tensile tests and adhesive bonded assembly for compression tests

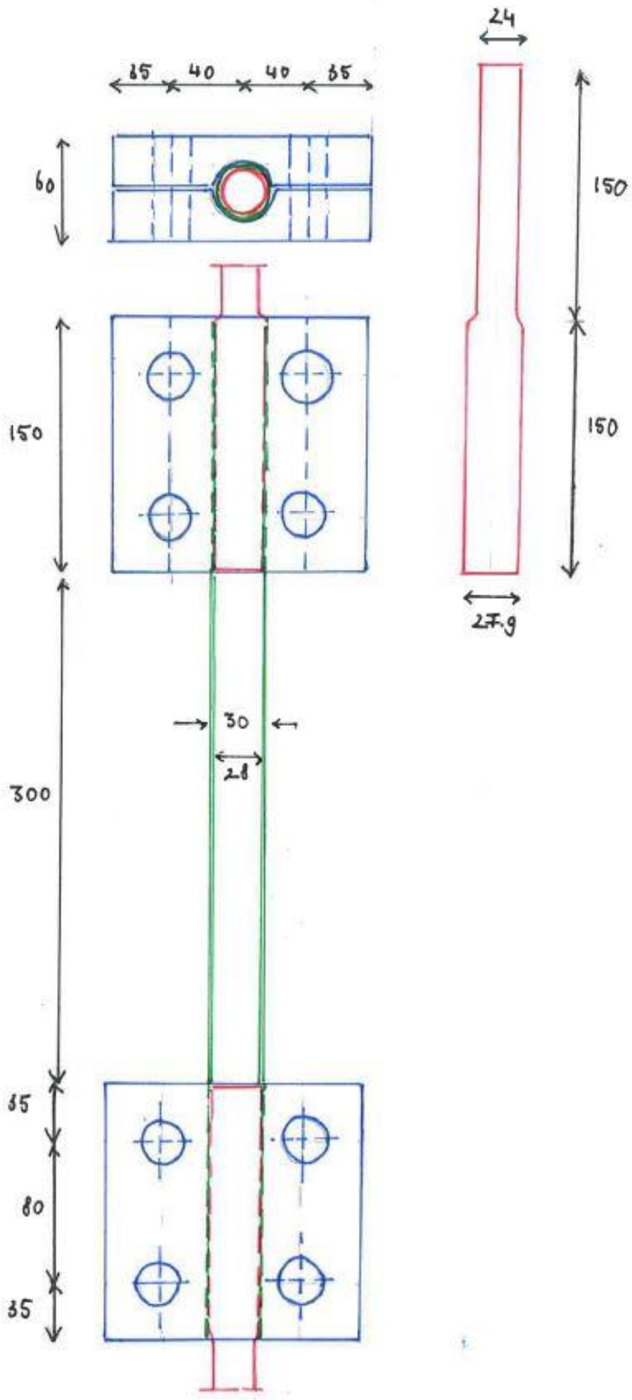

Figure G1 Detail clamping device tension tests

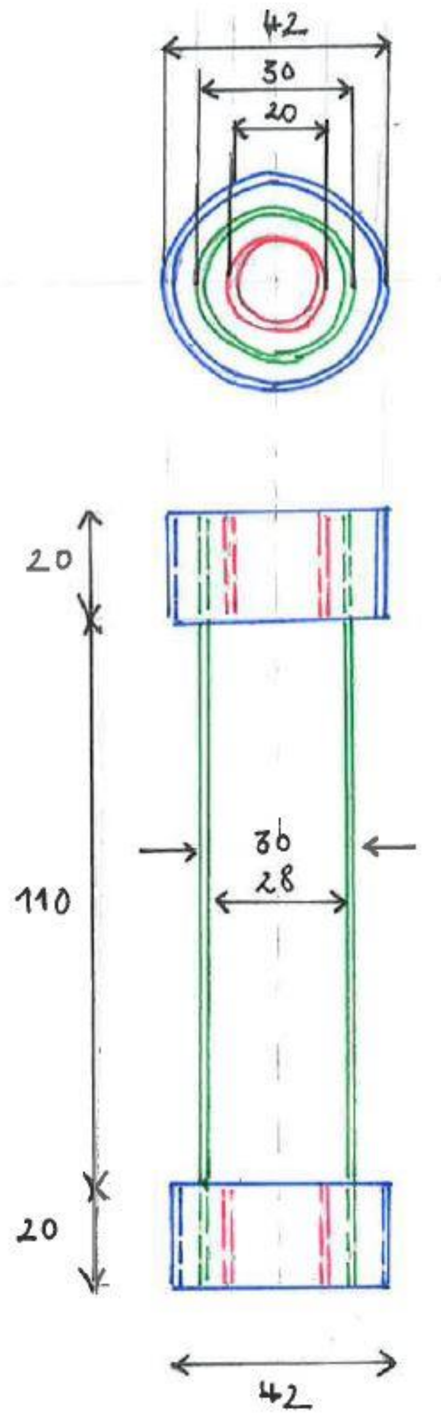

Figure G2 detail adhesive bonded assembly compression tests

Annex H Results and observations SSM tension creep tests TC01-03

A. Results and observations SSM creep test TC01

- The CFRP specimen tested at a reference stress of 40% GUTS ruptured after a few seconds in the fourth load step (see Figure H2). The specimen failed by brittle splitting vertically along the free span (see Figure H1). Due to the brittle failure, it is difficult to see where the initiation of fracture occurred.

- Strains from strain gauges and LVDTs just before rupture of the specimen are presented in Figures H3-4. A sudden increase in strains from LVDTs happened about 20 seconds before a sudden increase in strains from strain gauges. At failure of the specimen, the resulting strain is characterized by a decrease in length of the specimen's center surface (see Figure H4). Rupture of the specimen did not start at the mid-point – position of the strain gauges.

- Creep strains from strain gauges and LVDTs of different load levels are presented in Figures H5-6 and Table H1. Only little creep strains were measured during TC01.

- Elastic strains from strain gauges and LVDTs of different load levels are presented in Figures H7-8 and Table H2. The proportion of measured strains from the different strain gauges and laser is similar to each other in each increase in stress, with the exception of the high strains from LVDTs measured during the jump from the third to the fourth load step. Probably rupture has started during this jump.

- In a successful SSM test of this type, the creep strain-time curve of the final load level is characterized by a stage of tertiary creep. In this test, no tertiary creep stage was observed as the specimen fractured during the jump to the final load level following the rupture of the CFRP.

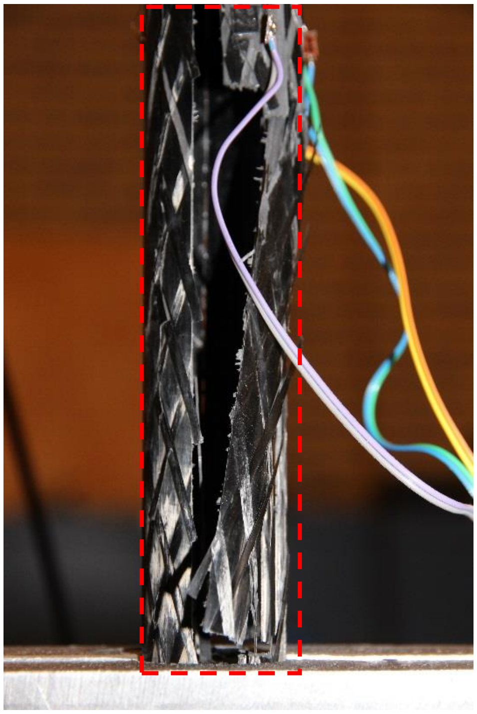

Figure H1 Rupture of CFRP specimen TC01

Total strains

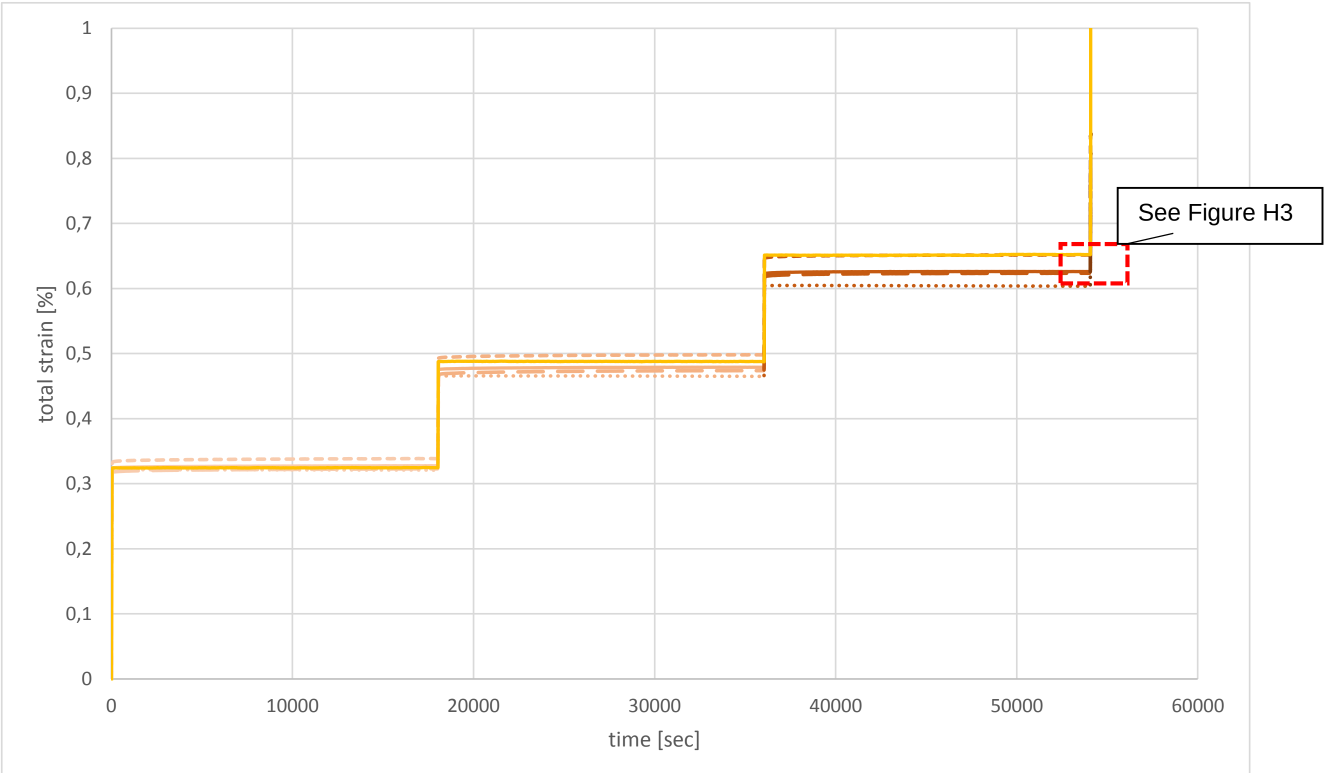

Figure H2 Total strains from strain gauges (orange) and LVDTs (yellow) versus time of TC01

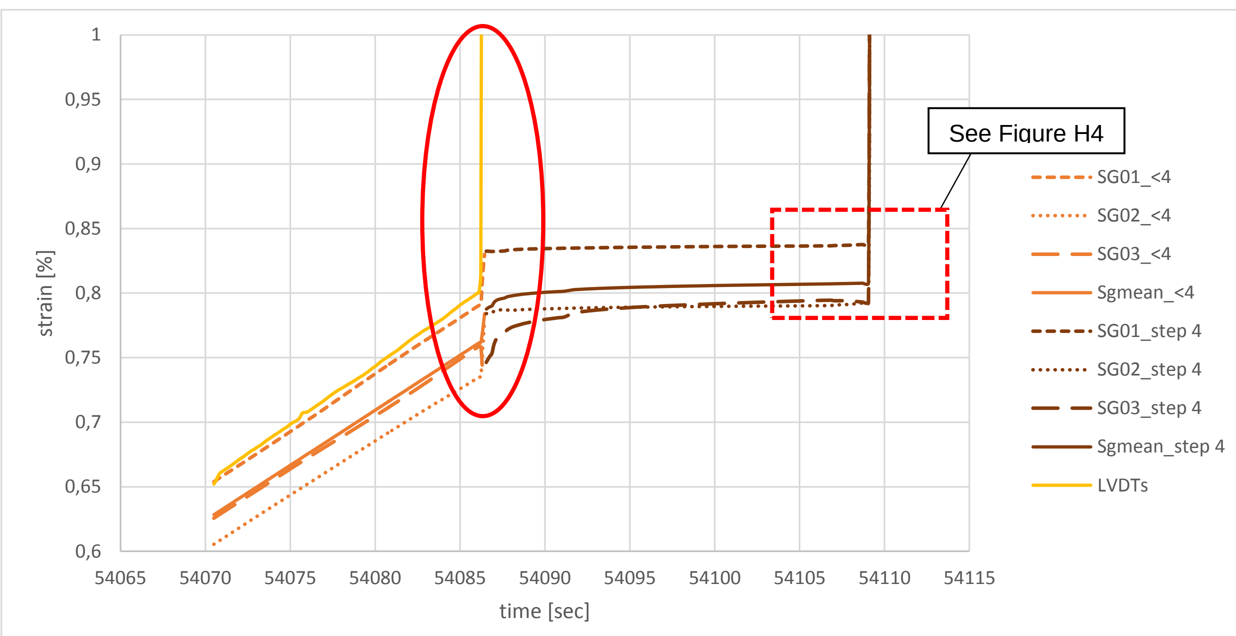

Figure H3 Strains from strain gauges and LVDTs just before rupture of the specimen

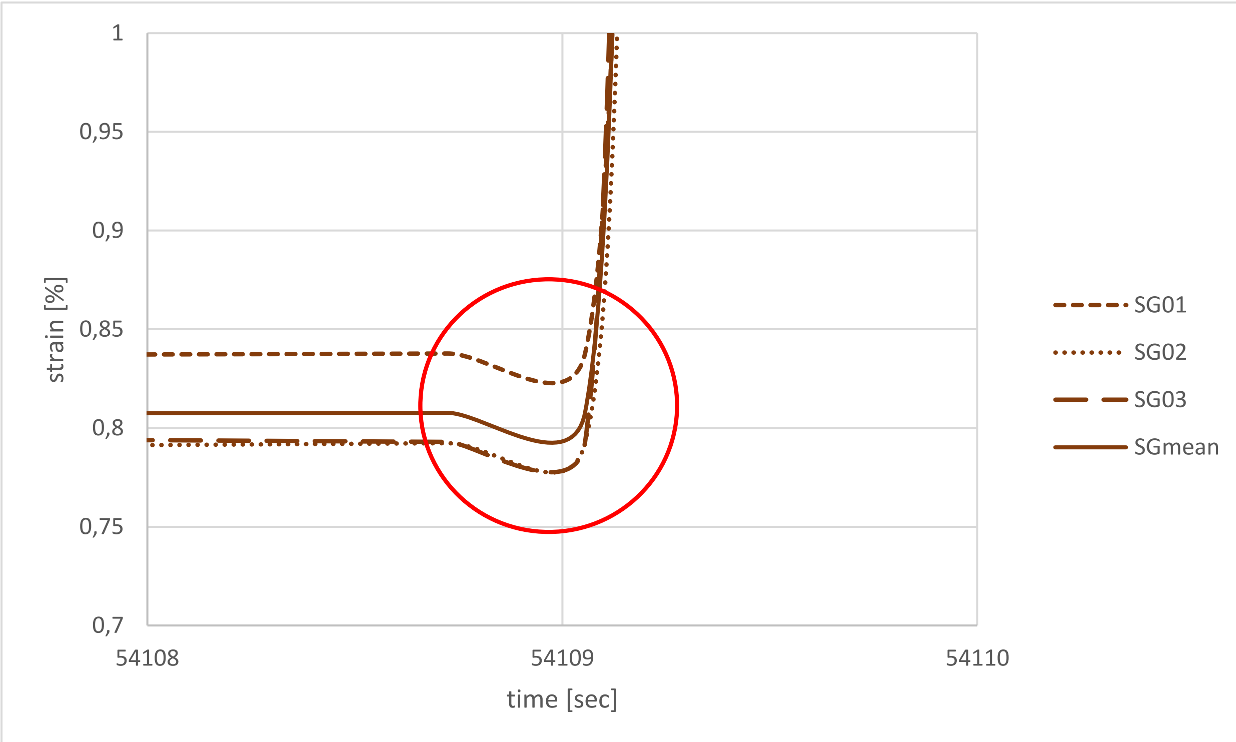

Figure H4 Creep strains from strain gauges in final load level – at rupture of the CFRP specimen

Creep strains

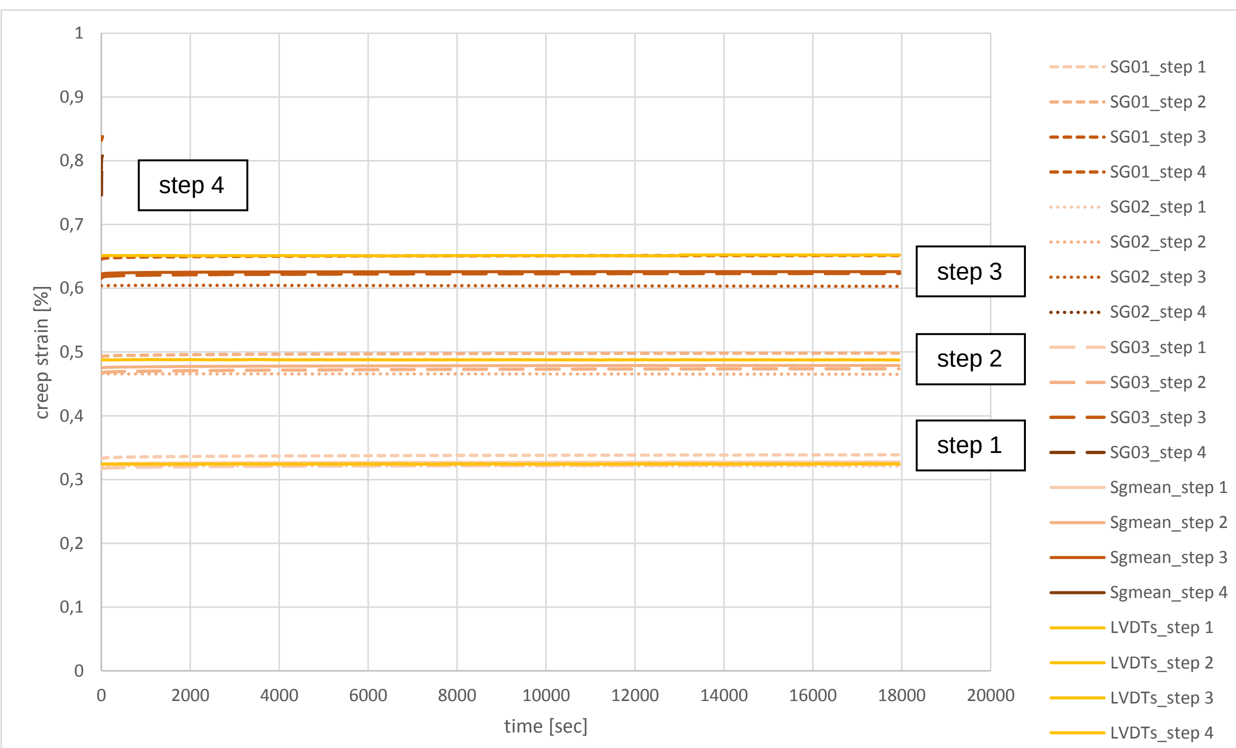

Figure H5 Comparison of creep strains from strain gauges and LVDTs between load levels

name	reference stress			step parameters	load step			
test	% GUTS	% UTS	MPa		1	2	3	4
TC01	40	39,3	385,0	stress level [MPa]	385,0	564,6	744,3	923,9
				step duration [hr]	5	5	5	0,01
				Δε_SG01 [%]	0,005	0,005	0,005	0,005
				Δε_SG02 [%]	0,000	-0,001	-0,001	0,008
				Δε_SG03[%]	0,005	0,006	0,008	0,047
				Δε_SGmean [%]	0,003	0,004	0,004	0,020
				Δε_LVDTs [%]	0,000	0,000	0,001	1,321

Table H1 Creep strains from strain gauges and LVDTs of TC01

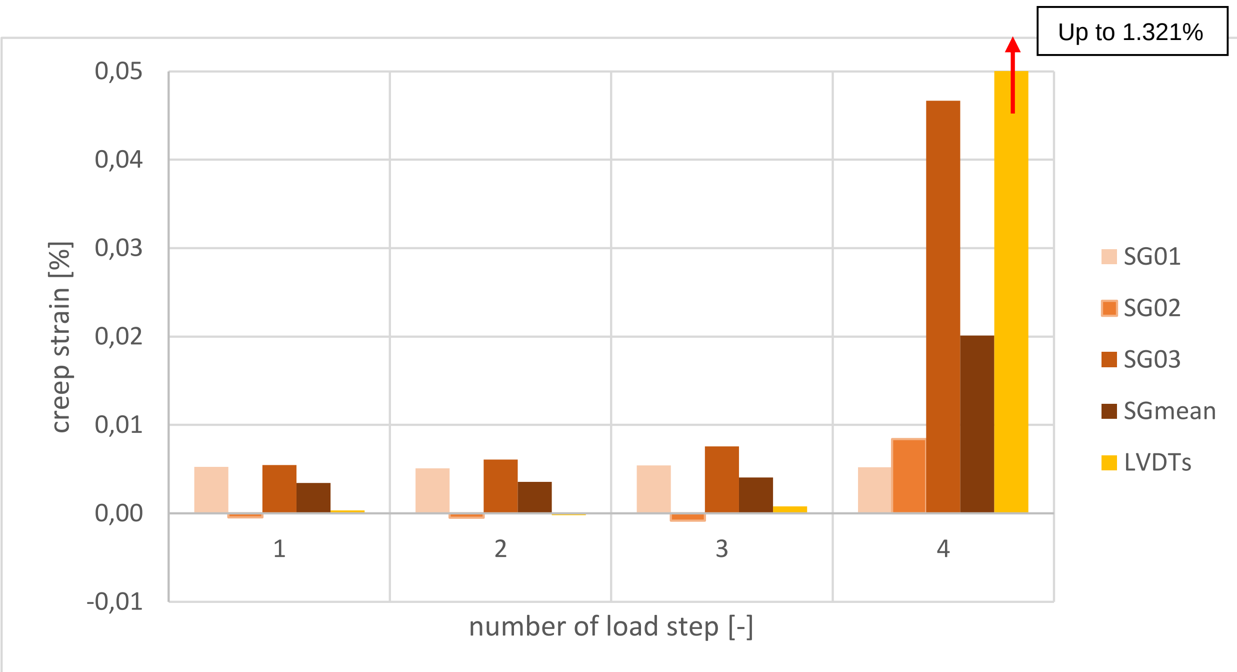

Figure H6 Comparison (Δ between start and end of load step) of creep strains between load levels

Elastic strains

name	reference stress			jump parameters	jump			
test	% GUTS	% UTS	MPa		0 to 1	1 to 2	2 to 3	3 to 4
TC01	40	39,3	385,0	stress increase [MPa]	385,0	179,7	179,7	179,7
				duration [sec]	35	16	16	16
				Δε_SG01 [%]	0,331	0,148	0,146	0,176
				Δε_SG02 [%]	0,321	0,140	0,137	0,174
				Δε_SG03[%]	0,317	0,138	0,140	0,117
				Δε_SGmean [%]	0,323	0,142	0,141	0,156
				Δε_LVDTs [%]	0,368	0,163	0,162	1,828

Table H2 Elastic strains from strain gauges and LVDTs of TC01

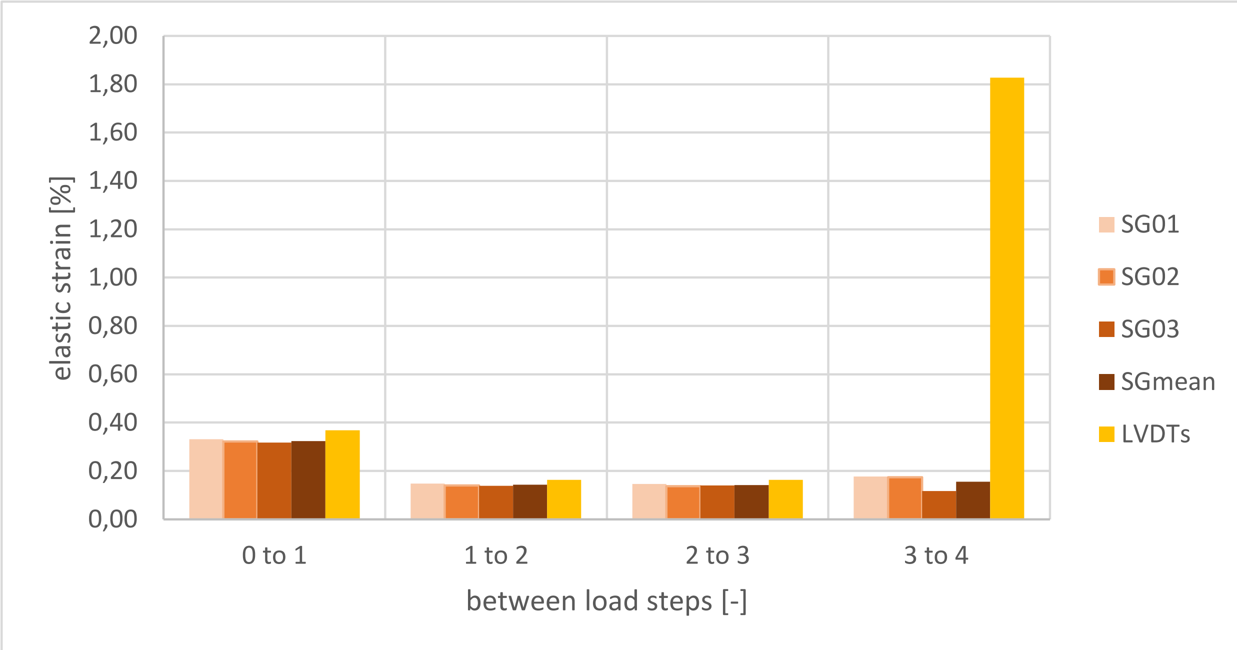

Figure H7 Comparison (Δ between start and end of load step) of elastic strains between each increase in stress

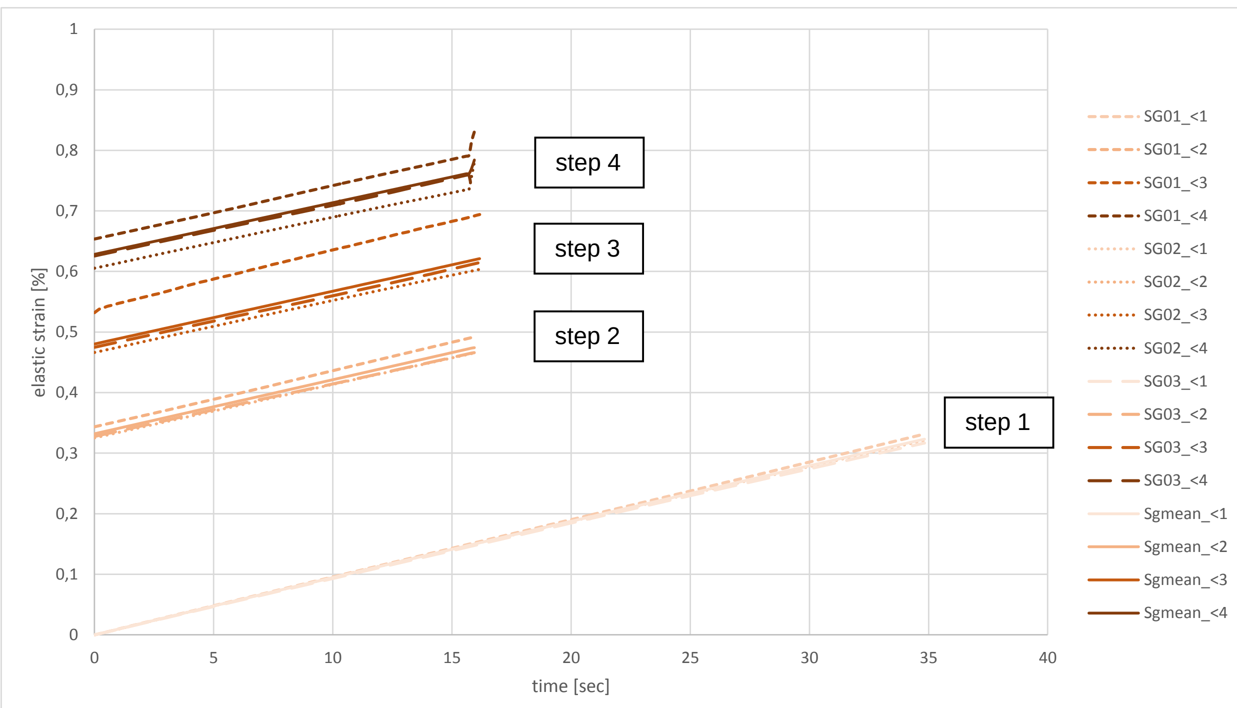

Figure H8 Comparison of elastic strains from strain gauges between each increase in stress

B. Results and observations SSM creep test TC02

- The CFRP specimen tested at a reference stress of 60% GUTS still had not ruptured after 103.5 hours in the final load step (see Figure H10), therefore it was decided to break down the experiment. The specimen was subjected to increasing amount of tensile loading and finally failed at 108 kN of force (see Figure H9). Due to brittle failure, it is difficult to see where the initiation of fracture occurred.

- Strains from strain gauges and LVDTs just before rupture of the specimen are presented in Figures H11-12. The resulting strain is characterized by a decrease in length of the specimen's center surface and an increase in length of the specimen's surface captured by LVDTs (130 mm length at the center). Fracture of the specimen following the rupture of the CFRP has not started at the mid-point.

- Elastic strains from strain gauges and LVDTs of different load levels are presented in Figures H16-17 and Table H6. The proportion of measured strains from the different strain gauges and LVDTs is similar to each other in each increase in stress.

- In a successful SSM test of this type, the creep strain-time curve of the final load level is characterized by a stage of tertiary creep. In this test, no tertiary creep stage was obtained from the strain gauges as the specimen as the initiation of fracture has not occurred at mid-point.

Figure H9 Rupture of CFRP specimen TC02

Total strains

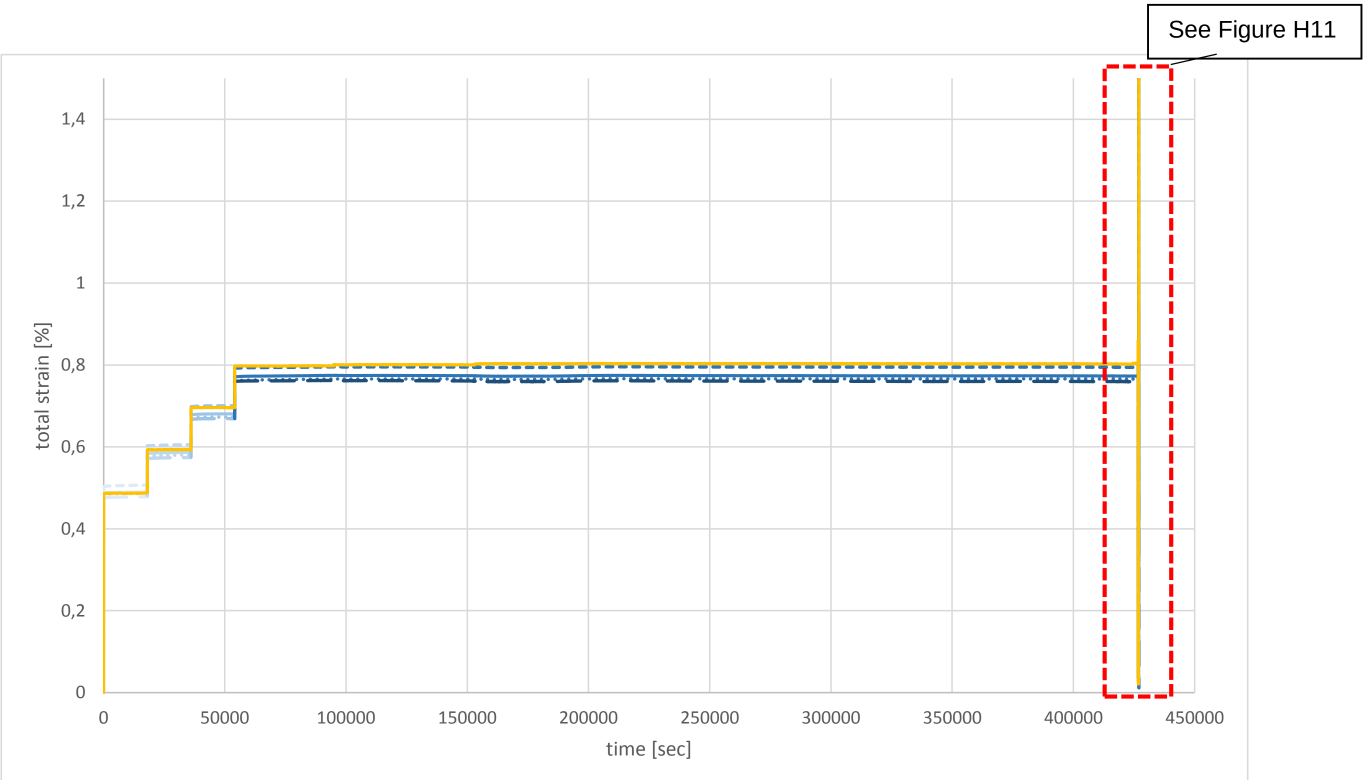

Figure H10 Total strains from strain gauges (blue) and LVDTs (yellow) versus time of TC02

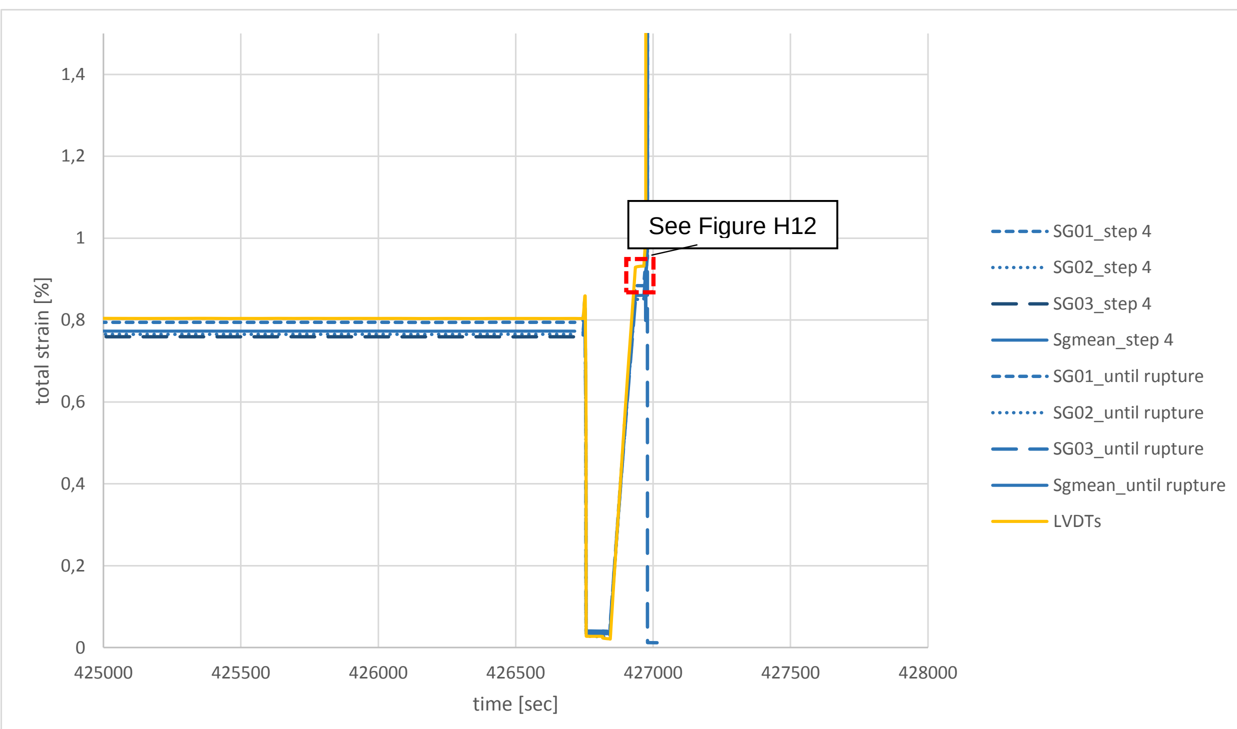

Figure H11 Strain from strain gauges and LVDTs just before rupture of the specimen

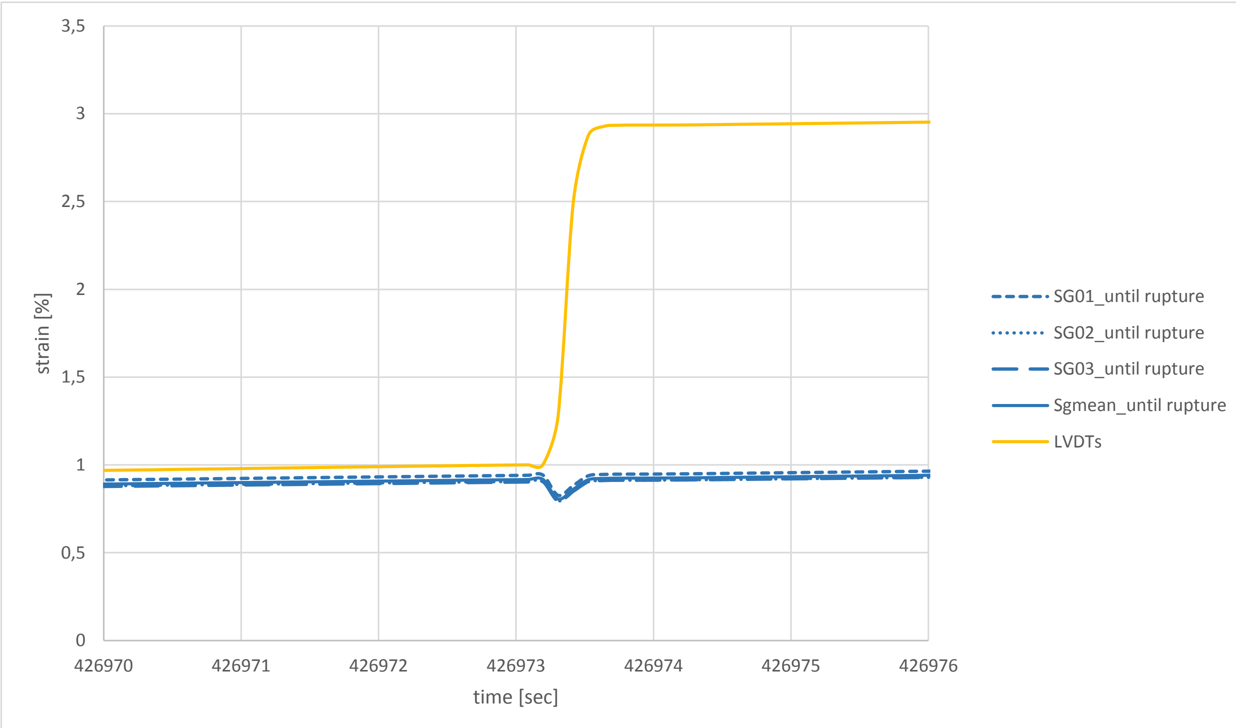

Figure H12 Strain is characterized by a decrease in length of the specimen's center surface, and an increase in length of the specimen's surface captured by LVDTs (130 mm)

Creep strains

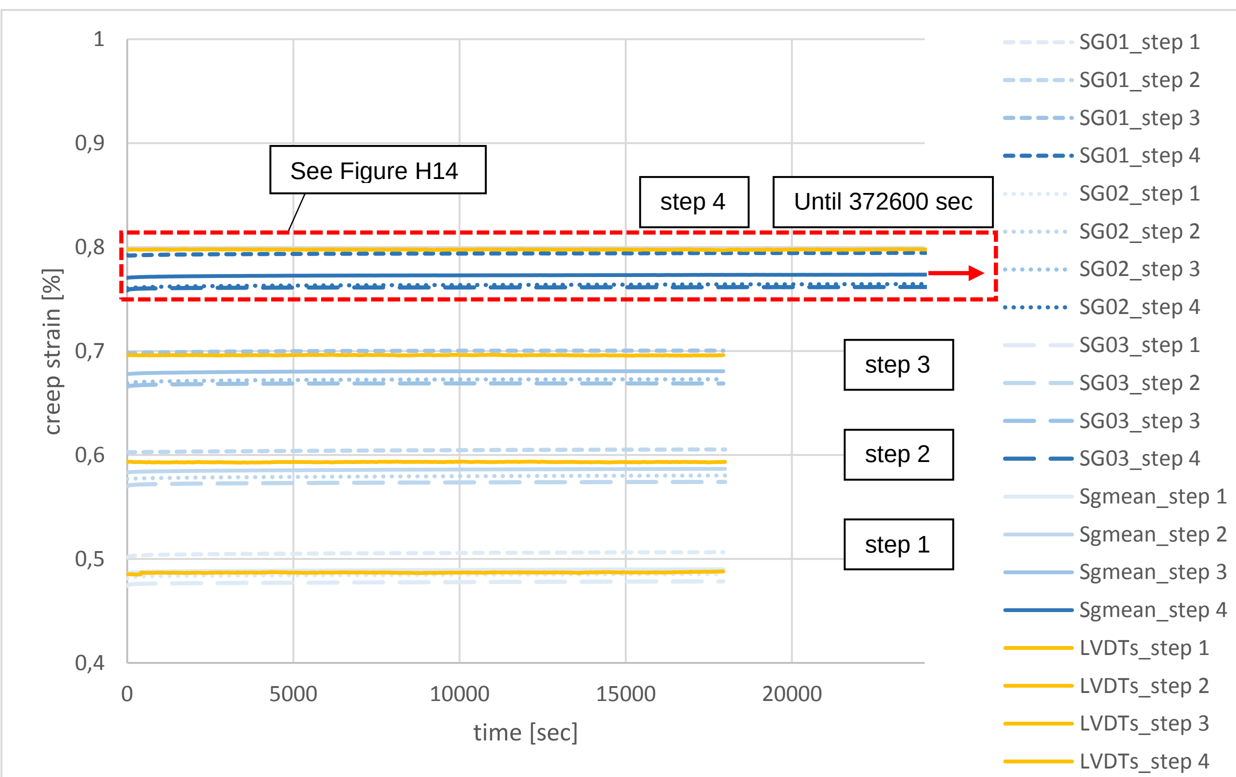

Figure H13 Comparison of creep strains from strain gauges and LVDTs between load levels

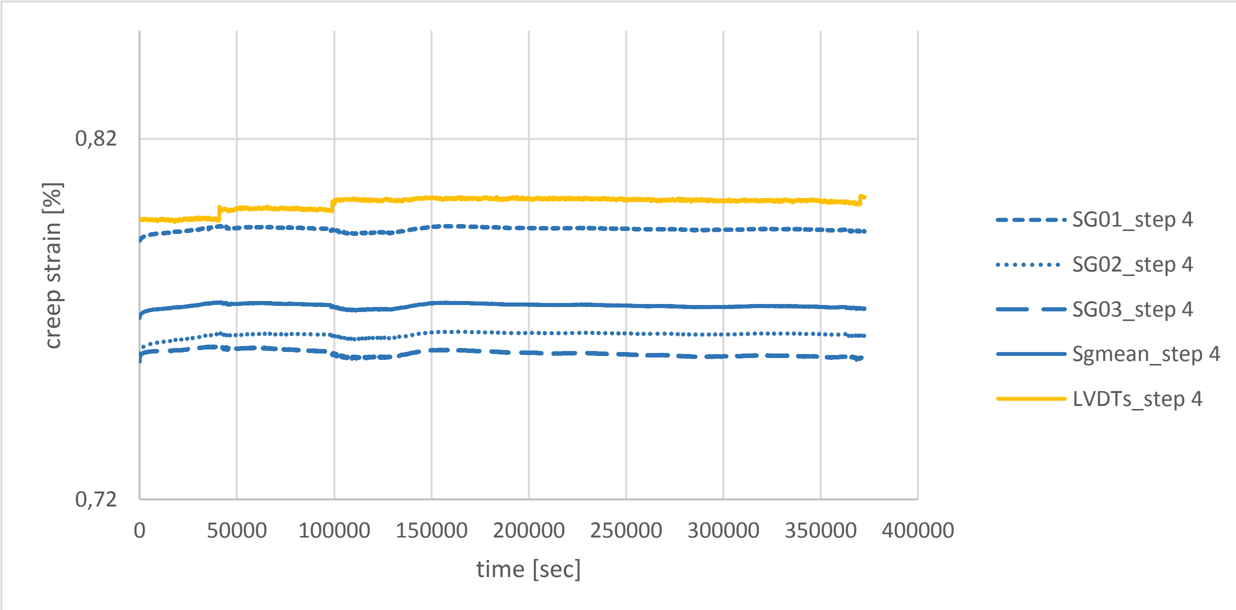

Figure H14 Creep strains from strain gauges and LVDTs in final load level

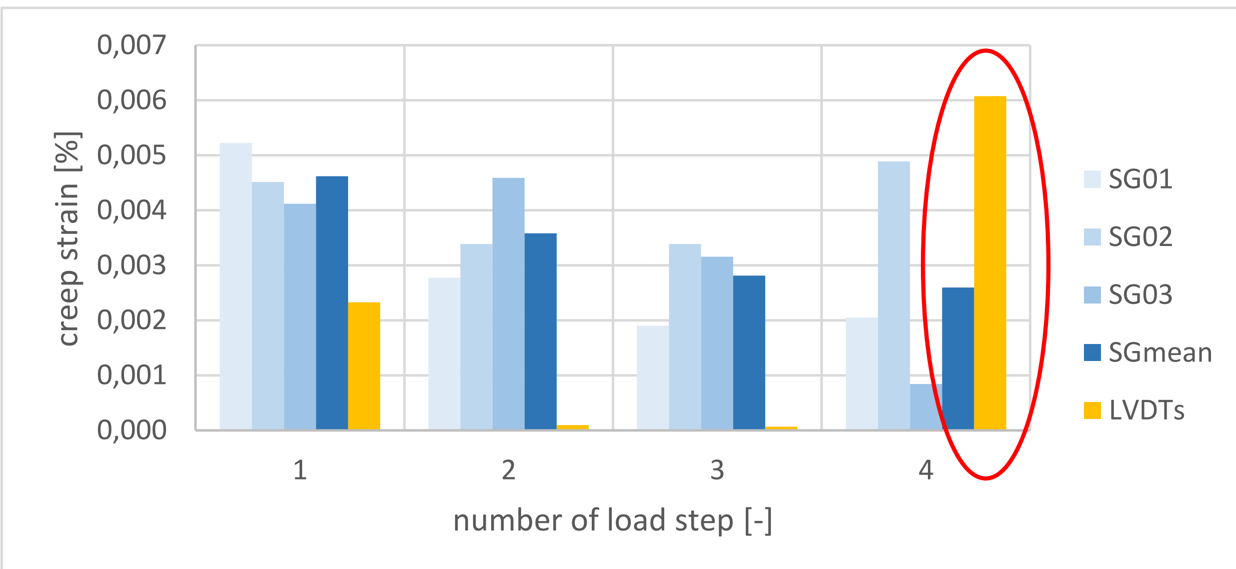

Figure H15 Comparison (Δ between start and end of load step) between load levels

name	reference stress			**step parameters**	**load step**			
test	% GUTS	% UTS	MPa		1	2	3	4
TC02	60	58,9	577,5	stress level [MPa]	577,5	693,0	808,4	923,9
				step duration [hr]	5	5	5	103,5
				Δε_SG01 [%]	0,005	0,003	0,002	0,002
				Δε_SG02 [%]	0,005	0,003	0,003	0,005
				Δε_SG03[%]	0,004	0,005	0,003	0,001
				Δε_SGmean [%]	0,005	0,004	0,003	0,003
				Δε_LVDTs [%]	0,002	0,000	0,000	0,006

Table H3 Creep strains from strain gauges and LVDTs of TC02

Elastic strains

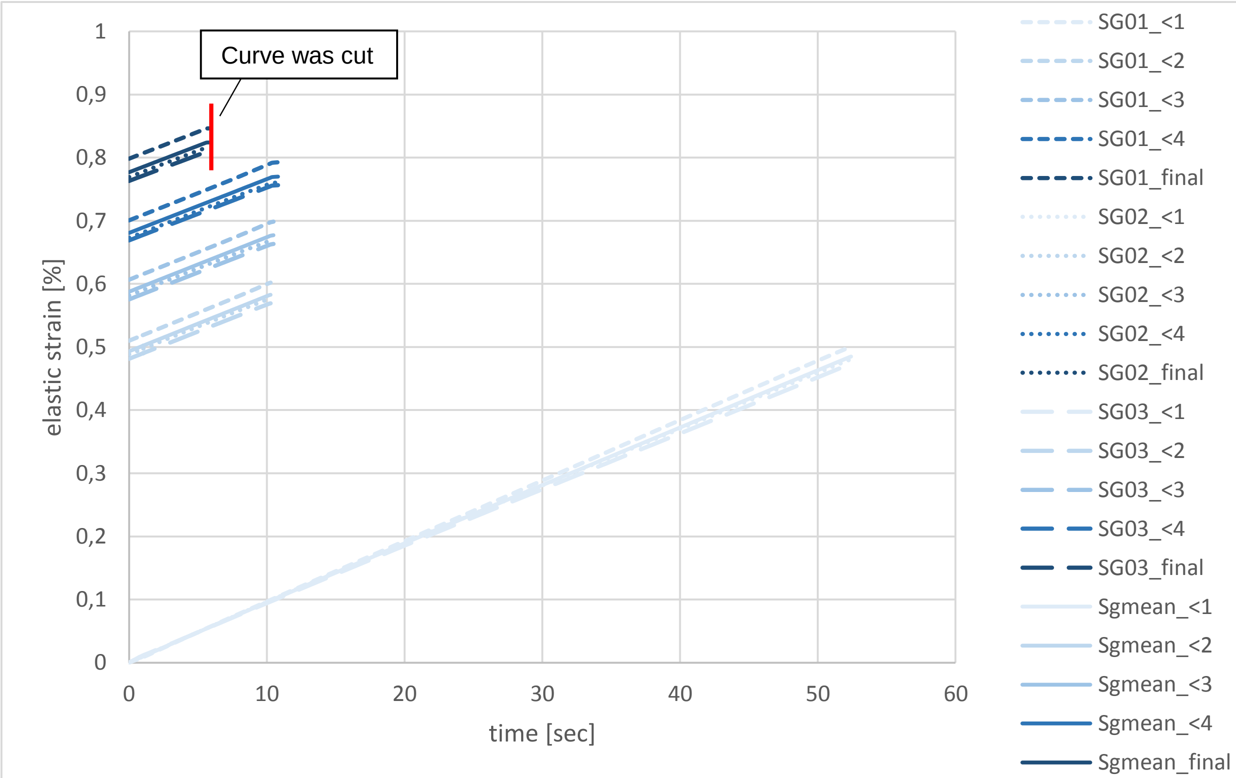

Figure H16 Comparison of elastic strains from strain gauges between each increase in stress

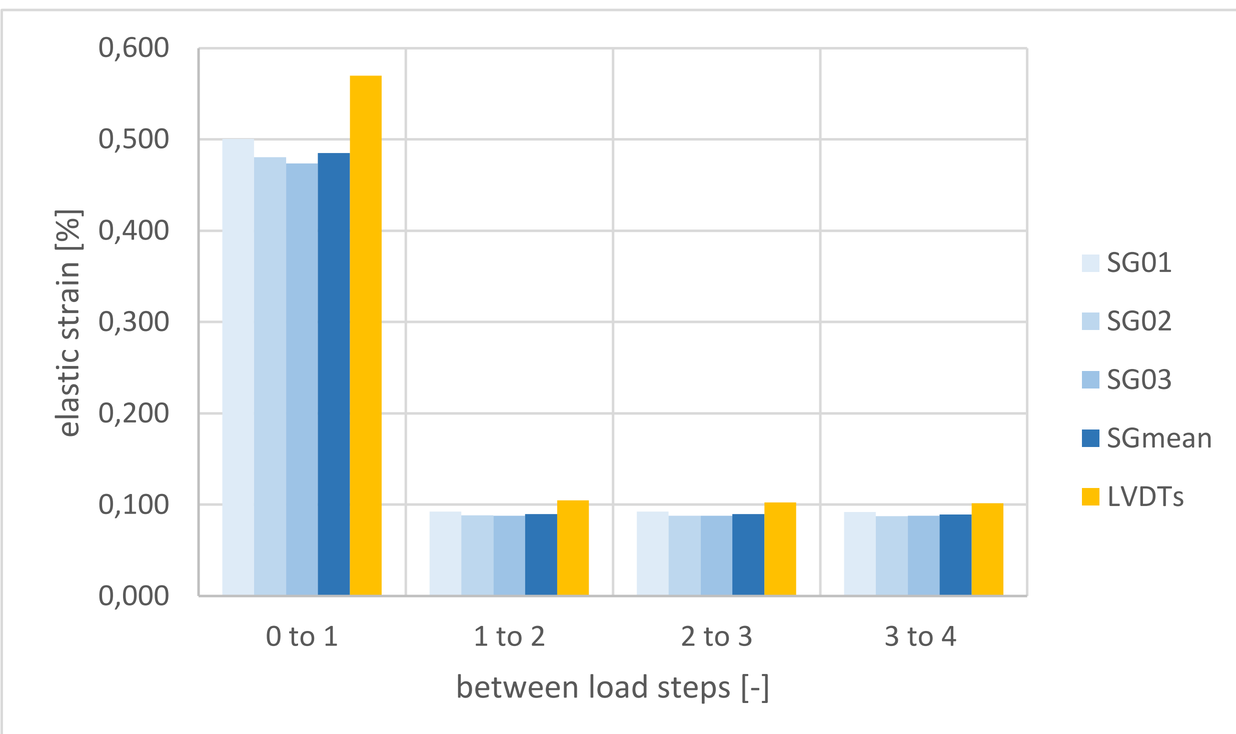

Figure H17 Comparison (Δ between start and end of load step) of elastic strains between each increase in stress

name	reference stress			jump parameters	jump			
test	% GUTS	% UTS	MPa		0 to 1	1 to 2	2 to 3	3 to 4
TC02	60	58,9	577,5	stress increase [MPa]	577,5	115,5	115,5	115,5
				duration [sec]	52	10	10	11
				Δε_SG01 [%]	0,501	0,092	0,092	0,092
				Δε_SG02 [%]	0,481	0,088	0,088	0,088
				Δε_SG03[%]	0,473	0,088	0,088	0,088
				Δε_SGmean [%]	0,485	0,090	0,090	0,089
				Δε_LVDTs [%]	0,570	0,105	0,103	0,101

Table H4 Elastic strains from strain gauges and LVDTs of TC02

C. Results and observations SSM creep test TC03

- The CFRP specimen tested at a reference stress of 80% GUTS still had not failed after 37.7 hours in the final load step, and it was decided to increase the loading with one step (step 5). After 21.6 hours it was decided to increase the loading with another step (step 6), and finally to break down the experiment. The specimen was subjected to increasing amount of tensile loading, and finally failed at 110.8 kN of force (see Figure H18).

- Figure H19 and H20 show creep strains from strain gauges and LVDTs which are not displayed as smooth curves. This may be caused by a change of temperature in the Lab during the SSM creep test influencing the test. Analysis of TC03 results and Lab temperatures is required to investigate this possibly cause. Creep strains from LVDTs may be affected by the LVDTs which possibly were not firmly attached to the specimen.

- Figure H21 and Table H5 show the difference in creep strains between the start and end of the load levels, measured by strain gauges and LVDTs. It is remarkable that of both load levels 1 and 2 the difference is negative. Possible causes: the CFRP specimen has crept at a cross-section different from its center part / the strain gauges were attached incorrectly to the specimen.

- Figure H22 and H23 show the elastic strains from strain gauges (Figure H22 and H23) and LVDTs (Figure H23) obtained during each increase in stress. As with Figure H20, strains from LVDTs are not displayed as smooth curves. At the final breaking force (110.8 kN) of the specimen, no increase or decrease of elastic strains was measured by both the strain gauges and LVDTs. This may be caused by failure of the specimen at a different location.

Total strains

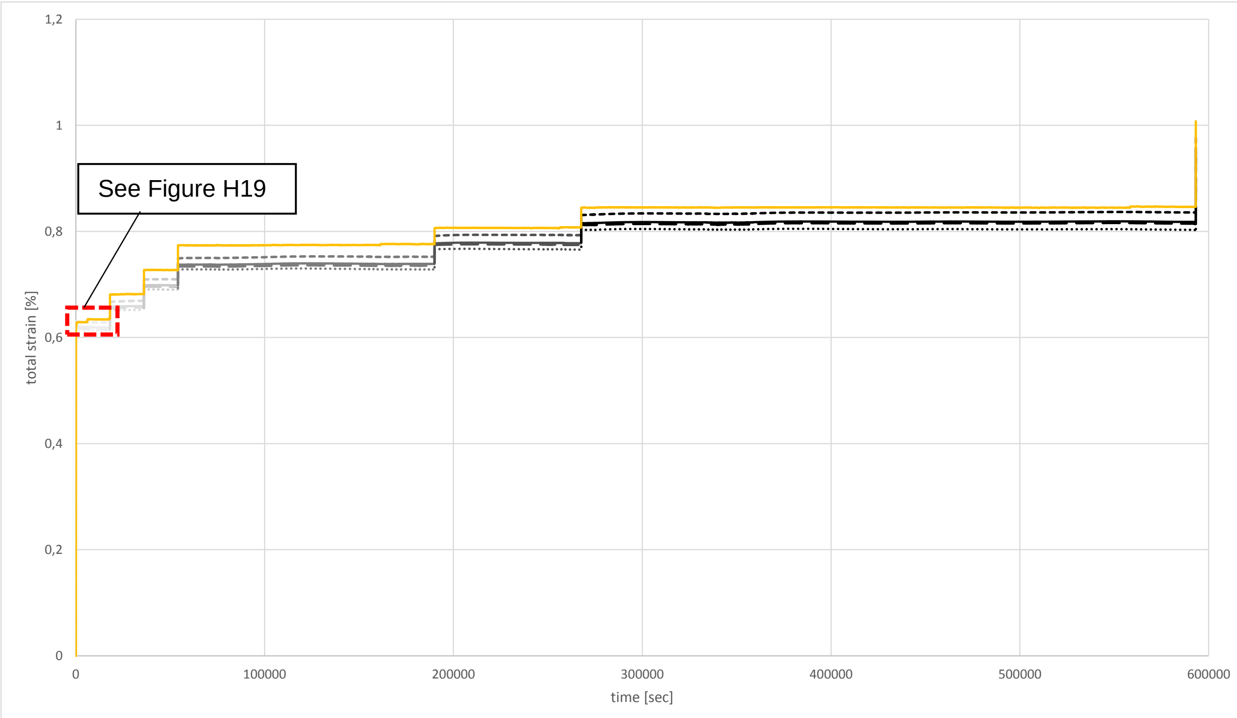

Figure H18 Total strain measured by strain gauges (grey) and LVDTs (yellow) versus time of TC03 results

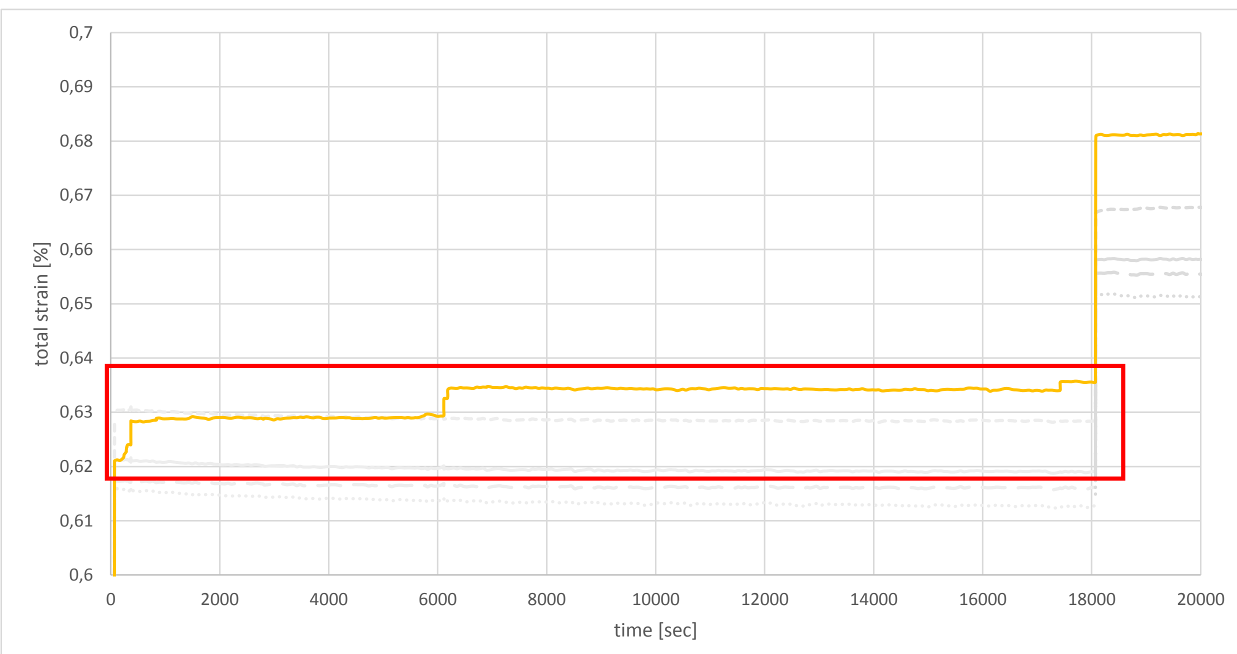

Figure H19 Strains from strain gauges and LVDTs in load step 1

Creep strains

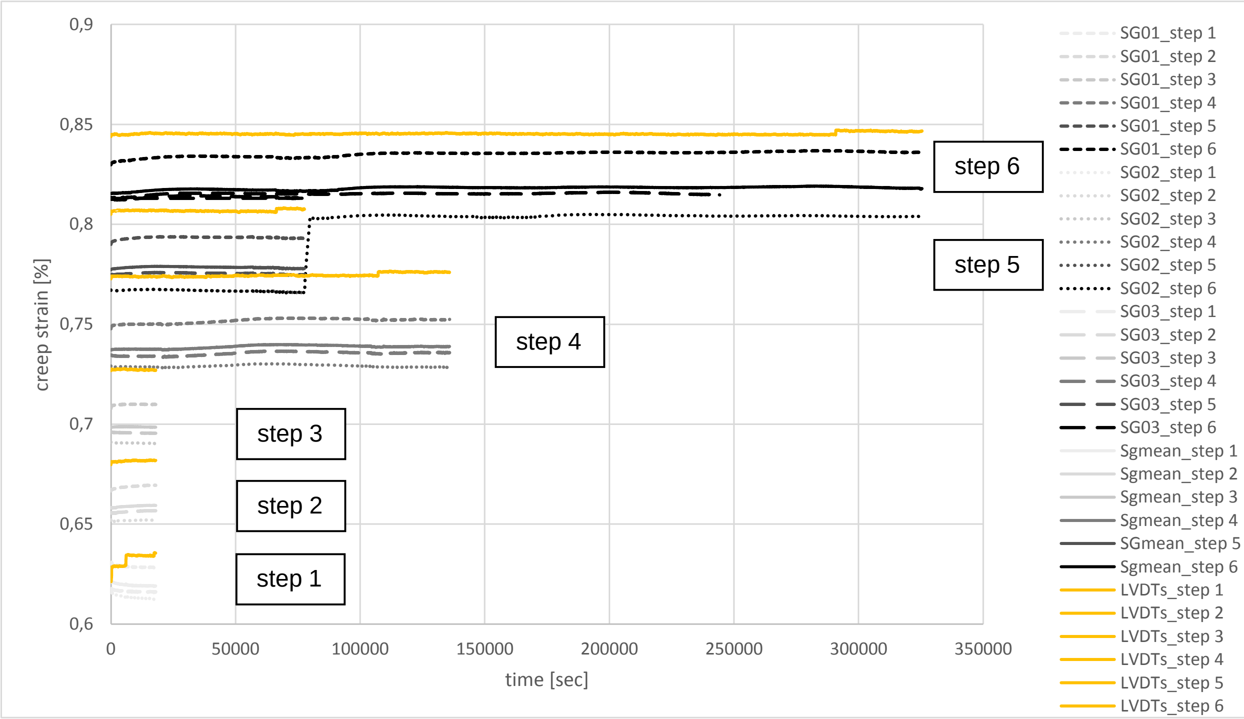

Figure H20 Comparison of creep strains from strain gauges and LVDTs between load levels

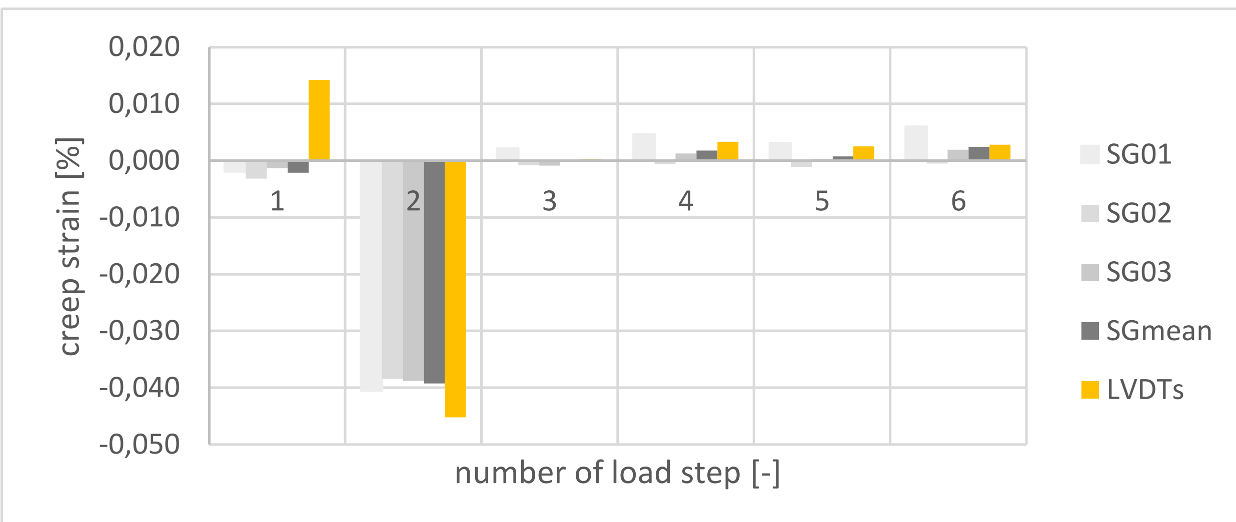

Figure H21 Comparison (Δ start and end of load step) of creep strains between different strain gauges and LVDTs

name	reference stress			step parameters	load step					
test	% GUTS	% UTS	MPa		1	2	3	4	5	6
TC03	80	78,5	769,9	stress level [MPa]	769,9	821,3	872,6	923,9	976,340136	1026,87105
				step duration [hr]	5	5	5	37,7	21,6	90,4
				Δε_SG01 [%]	-0,002	-0,041	0,002	0,005	0,003	0,006
				Δε_SG02 [%]	-0,003	-0,038	-0,001	-0,001	-0,001	-0,001
				Δε_SG03[%]	-0,001	-0,039	-0,001	0,001	0,000	0,002
				Δε_SGmean [%]	-0,002	-0,039	0,000	0,002	0,001	0,002
				Δε_LVDTs [%]	0,014	-0,045	0,000	0,003	0,003	0,003

Table H5 Creep strains from strain gauges and LVDTs of TC03

Elastic strains

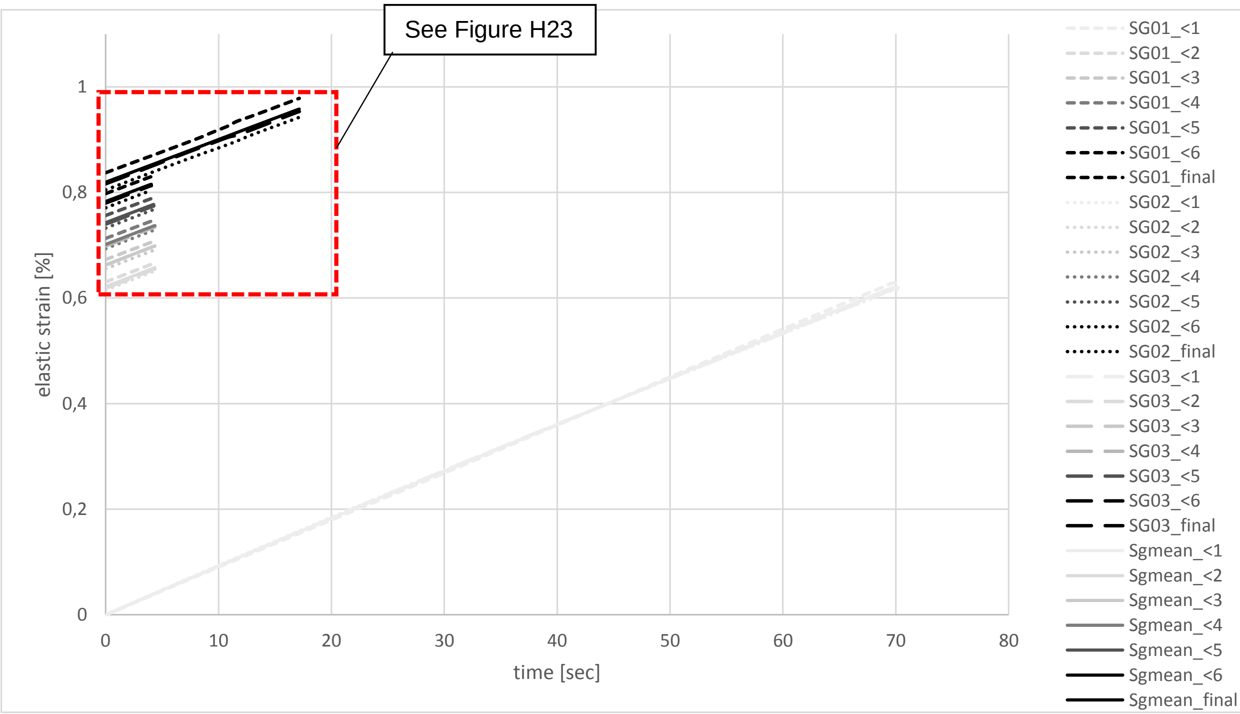

Figure H22 Elastic strains from strain gauges obtained during each increase in stress

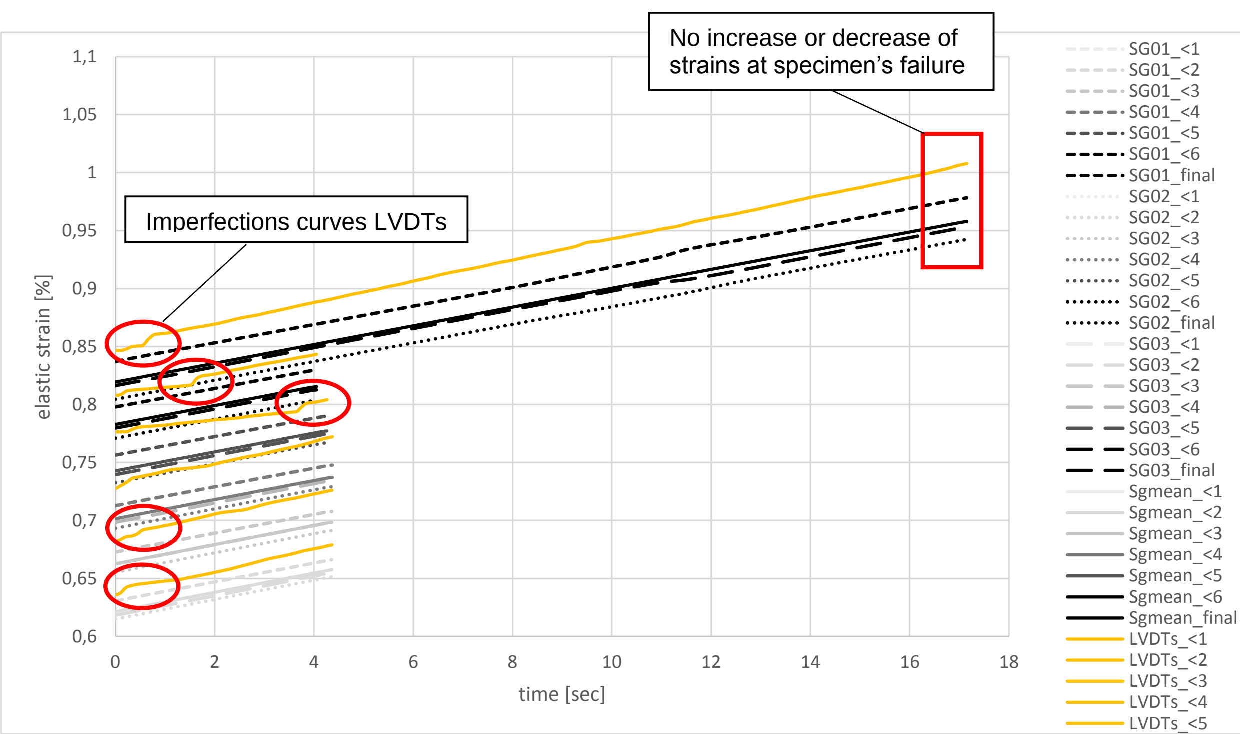

Figure H23 Elastic strains from strain gauges and LVDTs obtained during each increase in stress

Annex I Results and observations SSM compression creep tests CC01-03

A. Results and observations SSM creep test CC01

- The CFRP specimen tested at a reference stress of 40% GUCS ruptured after 8.8 hours in the fourth load step (see Figure I2). The specimens were prepared with metal cups, leaving a free span of 110 mm. No visible damage or deformation appeared on the free span' surface. The specimen did not rupture at the mid-point, but somewhere within the cup area (see Figure I1).

- At failure of the specimen, the resulting strain from the laser is characterized by a decrease in length of the specimen's surface somewhere along its length (see Figure I3).

- Creep strains from strain gauges and laser of different load levels are presented in Figures I4-5 and Table I1. The difference of creep strains measured by the laser is significantly higher compared to the (negative) difference of creep strains measured by the strain gauges (see Figure I5). This may indicate creep occurred at another location than midpoint, causing decrease in length of the specimen's surface at mid-point.

- Small decreases in length of the specimen's surface at mid-point in the first jump are presented in Figure I6.

- A remarkable difference of elastic strains from strain gauges and laser between the first jump in stress and the following jumps is presented in Figure I7 and Table I2. During the jump to the first load level, notable amount of elastic strains are measured by the laser, in contrast to the strains from strain gauges. This may indicate the initiation of fracture has already occurred during the jump to the first load level (somewhere within the cup area).

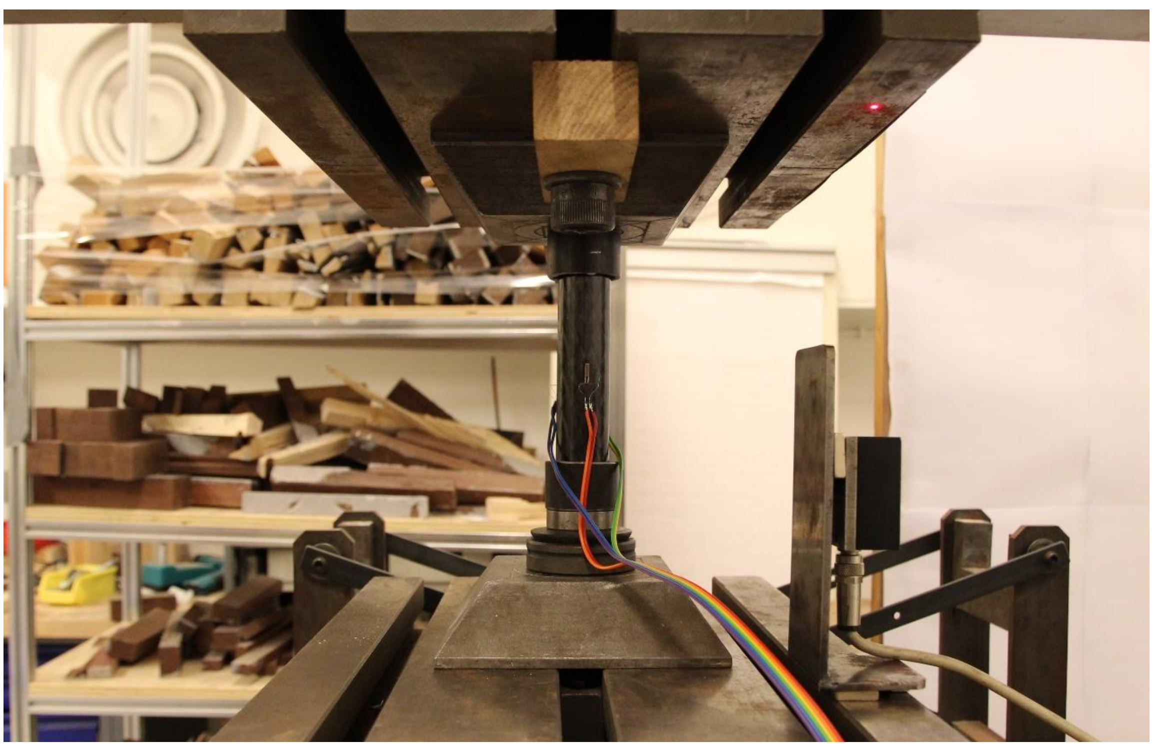

Figure I1 Compression test set-up with CFRP specimen CC01 (no visible damage or deformation appeared)

Total strains

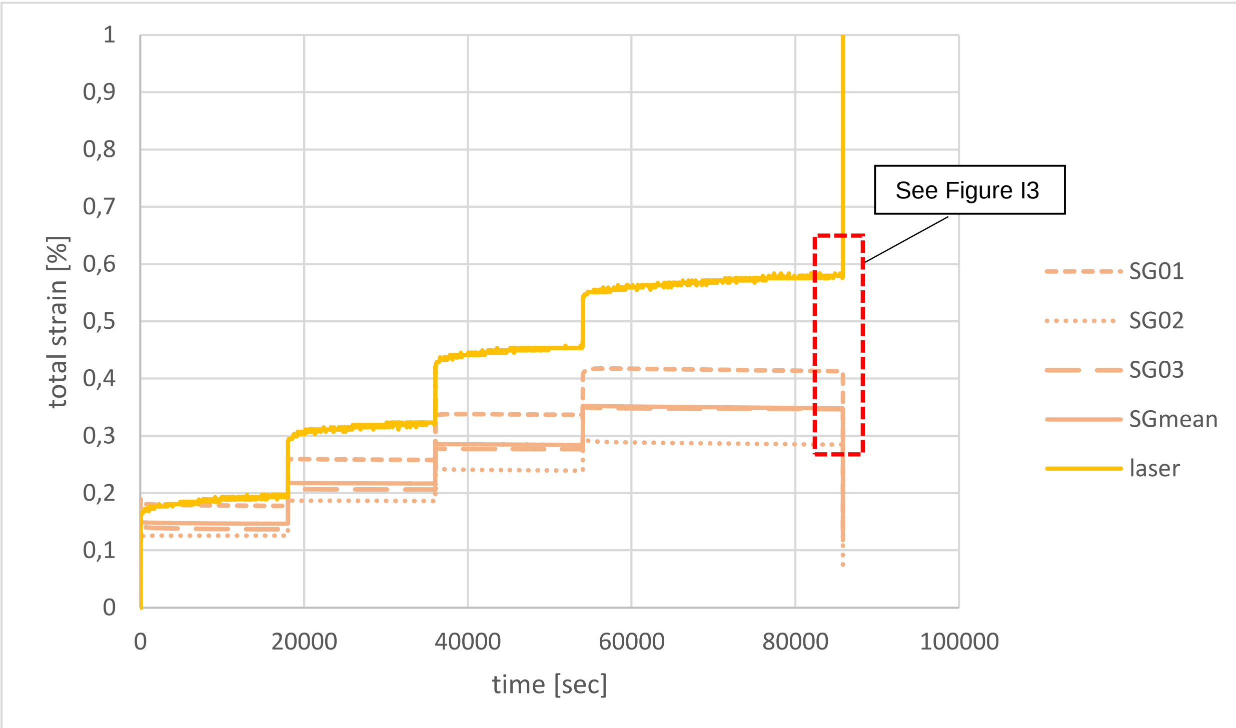

Figure I2 Total strains from strain gauges and laser of CC01

Figure I3 Strains from strain gauges and laser just before rupture of the specimen

Creep strains

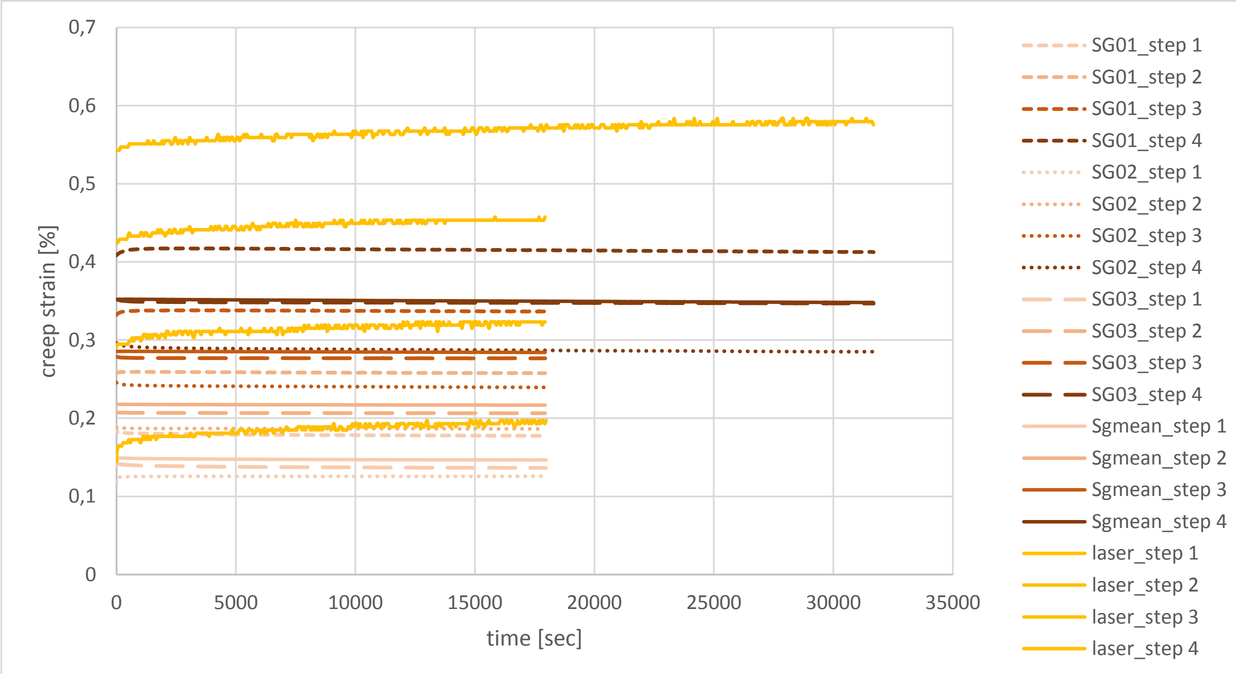

Figure I4 Comparison of creep strains from strain gauges and laser between load levels

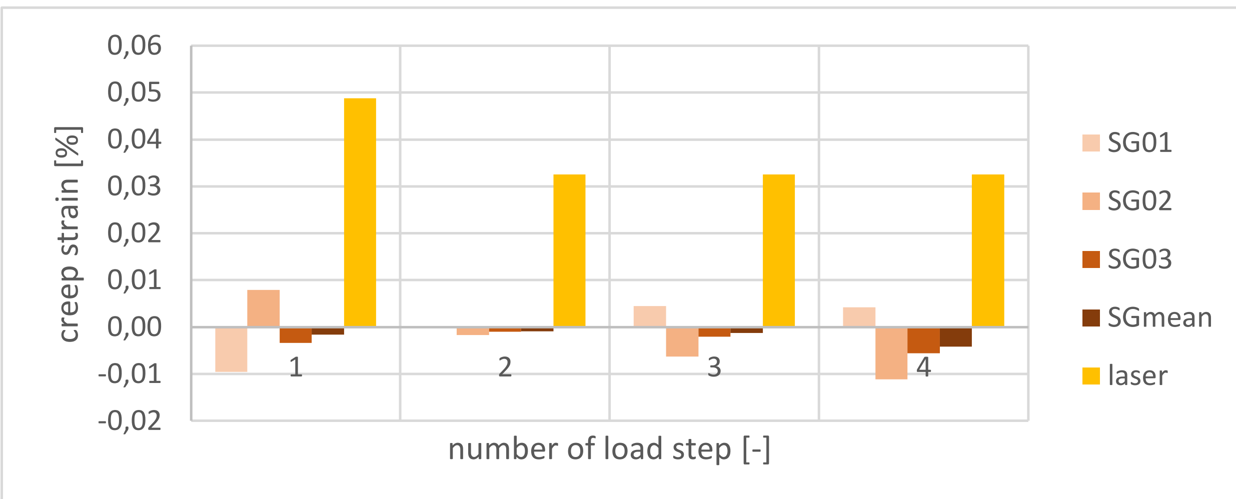

Figure I5 Comparison (Δ between start and end of load step) of creep strains between load levels

name	reference stress			**step parameters**	**load step**			
test	% GUTS	% UTS	MPa		1	2	3	4
CC01	40	34,7	179,9	stress level [MPa]	179,9	260,8	341,7	422,7
				step duration [hr]	5	5	5	8,8
				Δε_SG01 [%]	-0,010	0,000	0,004	0,004
				Δε_SG02 [%]	0,008	-0,002	-0,006	-0,011
				Δε_SG03[%]	-0,003	-0,001	-0,002	-0,006
				Δε_SGmean [%]	-0,002	-0,001	-0,001	-0,004
				Δε_laser [%]	0,049	0,033	0,033	0,033

Table I1 Creep strains from strain gauges and laser of CC01

Elastic strains

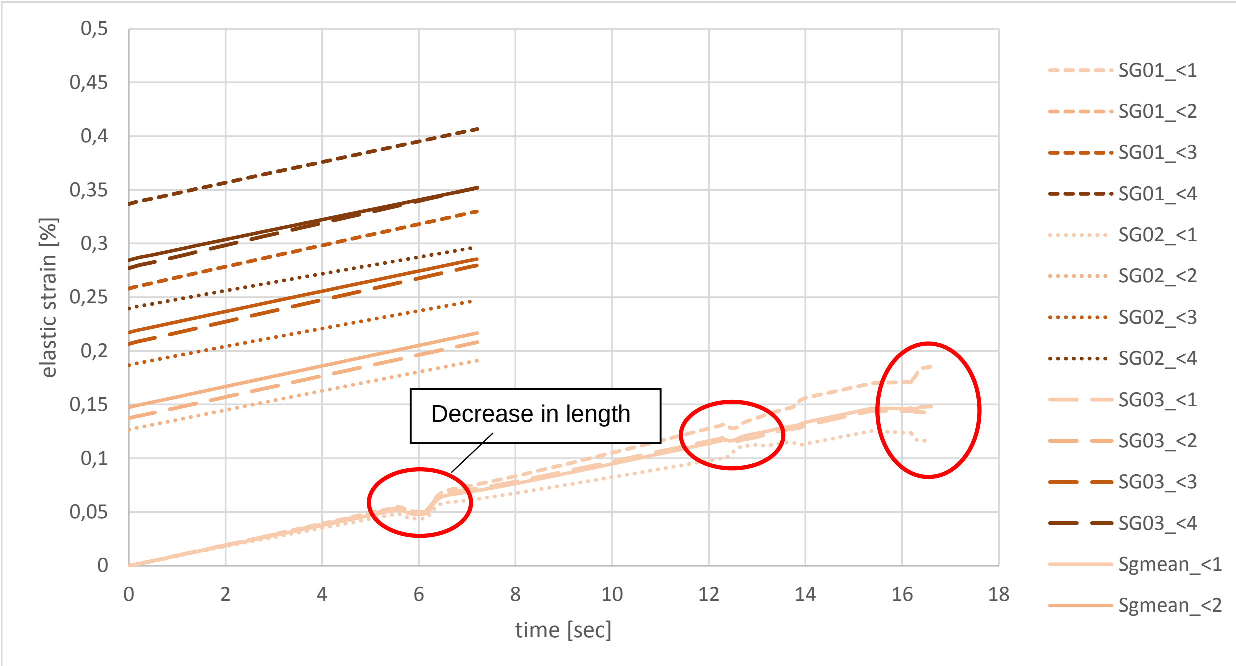

Figure I6 Comparison of elastic strains from strain gauges and laser between each increase in stress

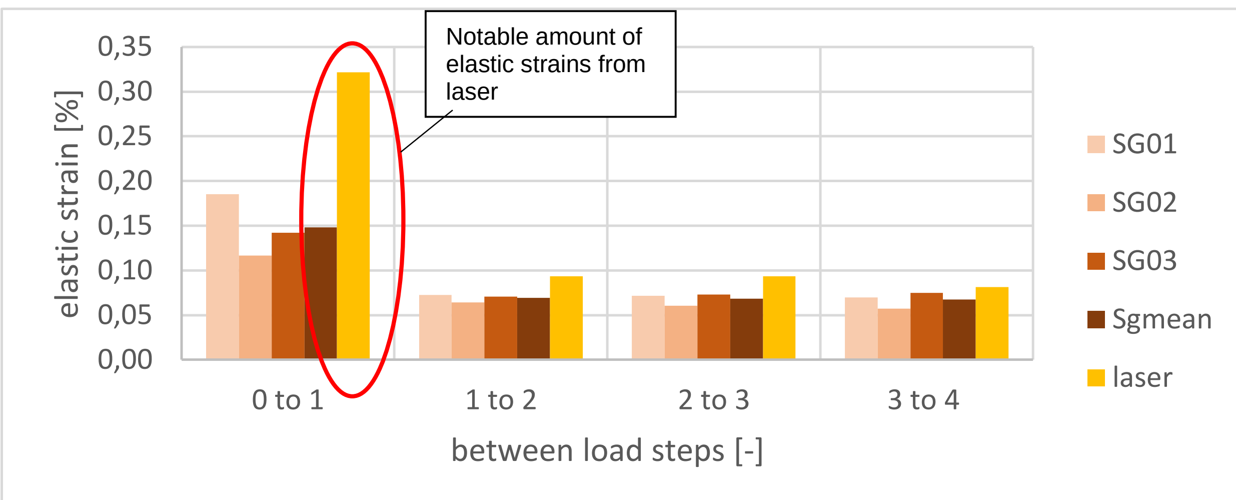

Figure I7 Comparison (Δ between start and end of load step) of elastic strains between each increase in stress

name	reference stress			jump parameters	jump			
test	% GUTS	% UTS	MPa		0 to 1	1 to 2	2 to 3	3 to 4
CC01	40	34,7	179,9	stress increase [MPa]	179,9	80,9	80,9	80,9
				duration [sec]	17	7	7	7
				Δε_SG01 [%]	0,185	0,073	0,072	0,070
				Δε_SG02 [%]	0,117	0,064	0,060	0,057
				Δε_SG03[%]	0,142	0,071	0,073	0,075
				Δε_SGmean [%]	0,148	0,069	0,068	0,067
				Δε_laser [%]	0,321	0,094	0,094	0,081

Table I2 Elastic strains from strain gauges and laser of CC01

B. Results and observations SSM creep test CC02

- The CFRP specimen tested at a reference stress of 60% GUCS still had not failed after 11.3 hours in the final load step, and it was decided to increase the loading with a fifth step (see Figure I8). After 2.7 hours the specimen failed by brittle circumferential cracking at the center, the preferred mode of delivery for failure in a successful SSM test of this type (see Figure I9).

- Creep strains from strain gauges and laser of different load levels are presented in Figures I10-12. More strain was measured by the laser indicating deformation not only occurred at mid-point. At failure of the specimen, the resulting strain in characterized by a decrease in length of the specimen's surface at the areas of strain gauges 1-3 and 5, and an increase in length of the specimen's surface at the areas of strain gauges 4 and 6. Tertiary creep stage observed.

- A comparison (difference between start and end of load step) of creep strains between load levels is presented in Figure I13 and Table I3. Positive and negative creep strains are measured in the final load level showing the brittle fracture behavior of the CFRP.

- Small decreases in length of the specimen's surface at mid-point in the first jump are presented in Figure I14.

- Elastic strains from strain gauges and laser of different load levels are presented in Figures I14-15 and Table I4. During the jump to the first load level, notable amount of elastic strains are measured by the laser, in contrast to the trans from strain gauges. This may indicate the initiation of fracture has already occurred during the jump to the first load level. During the second-fifth jump in stress, less strains are measured by the laser than by the strain gauges, which is expected for brittle fracture at the center.

- Strains from strain gauges in the final load level cannot be used for SSM analysis to predict creep deformations on a long-term as they contain negative values.

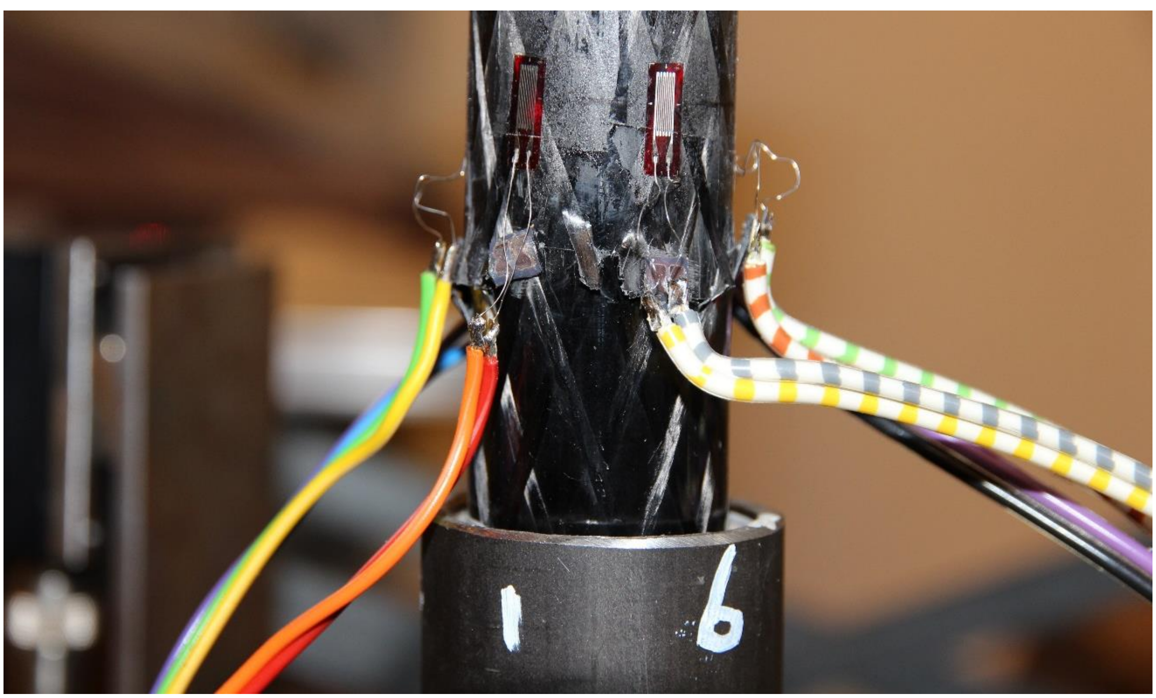

Figure I8 Rupture of the CFRP specimen CC02

Total strains

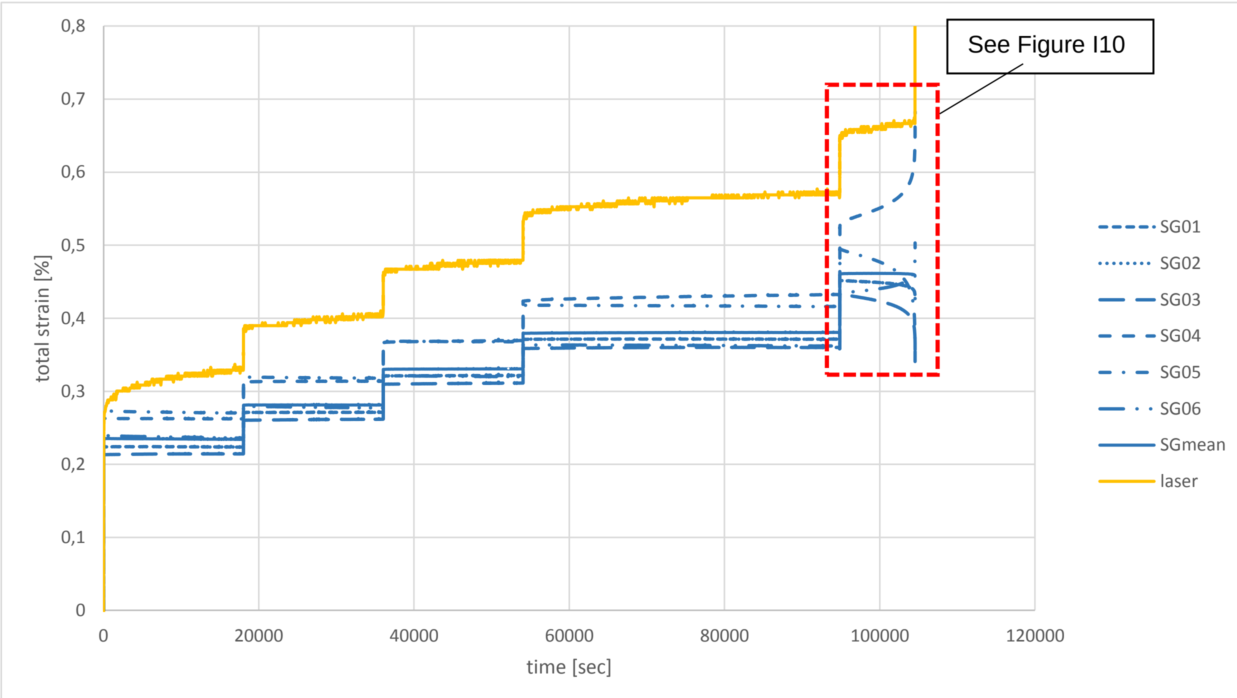

Figure I9 Total strains from strain gauges and laser of CC01

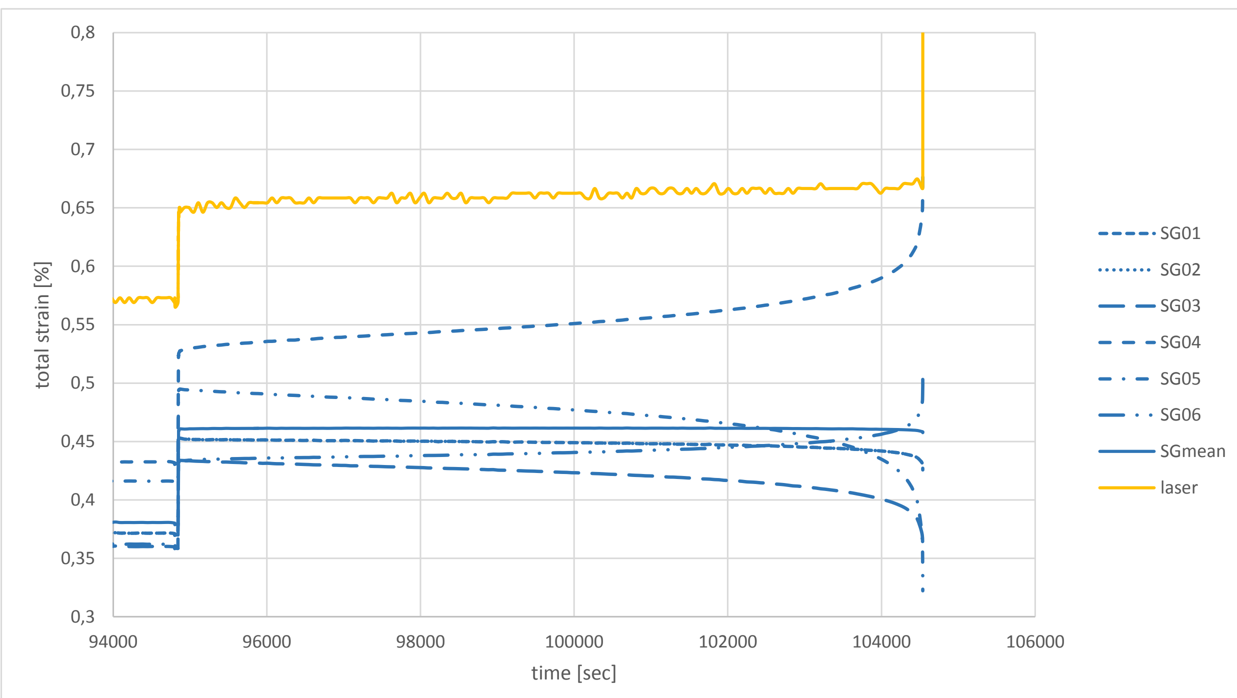

Figure I10 Strains from strain gauges and laser in final load level

Creep strains

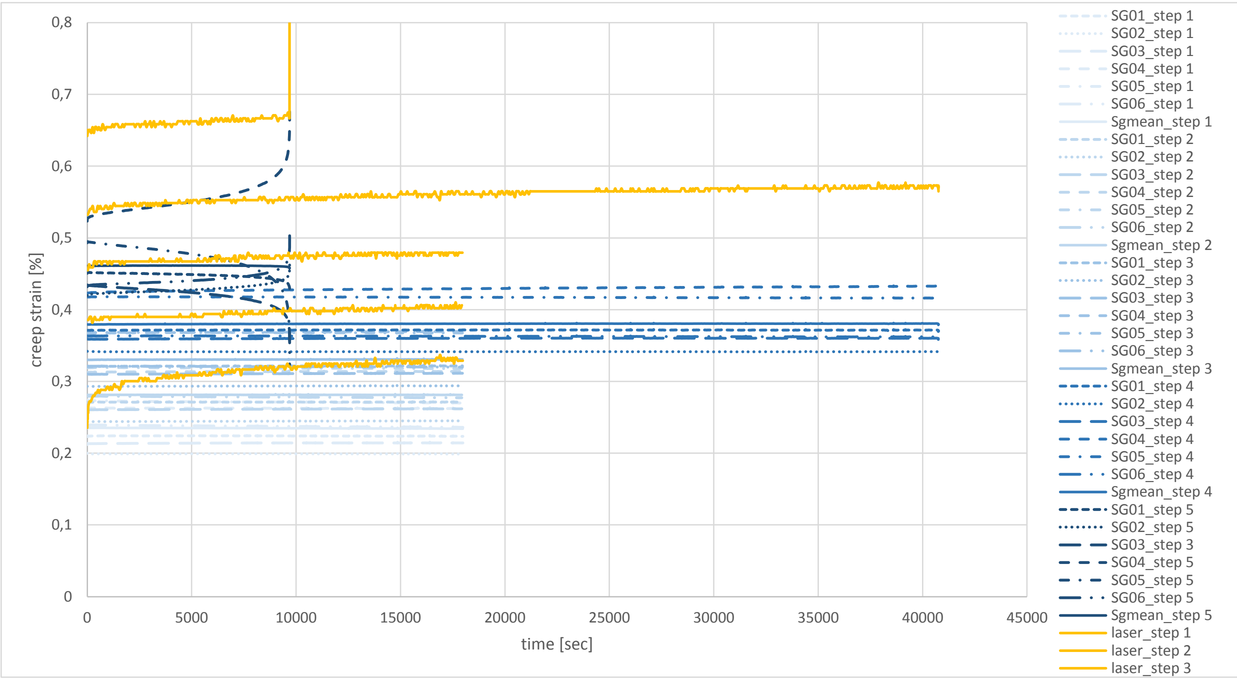

Figure I11 Comparison of creep strains from strain gauges and laser between load levels

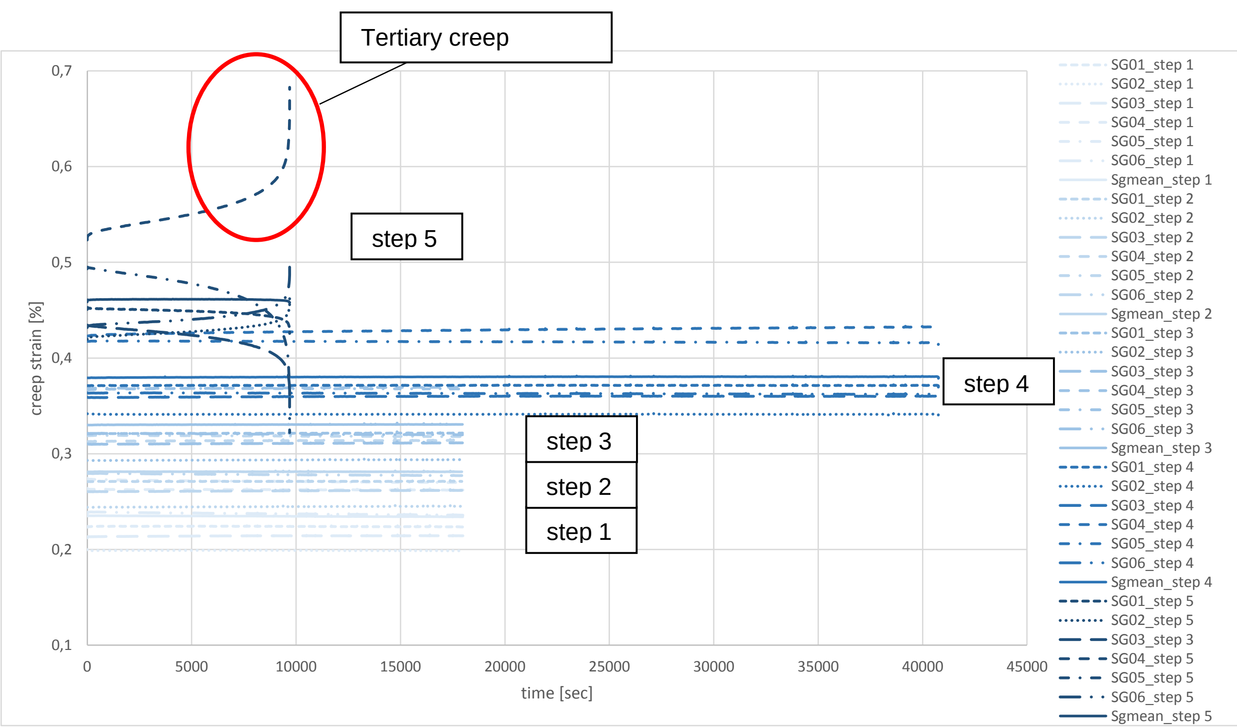

Figure I12 Comparison of creep strains from strain gauges between load levels

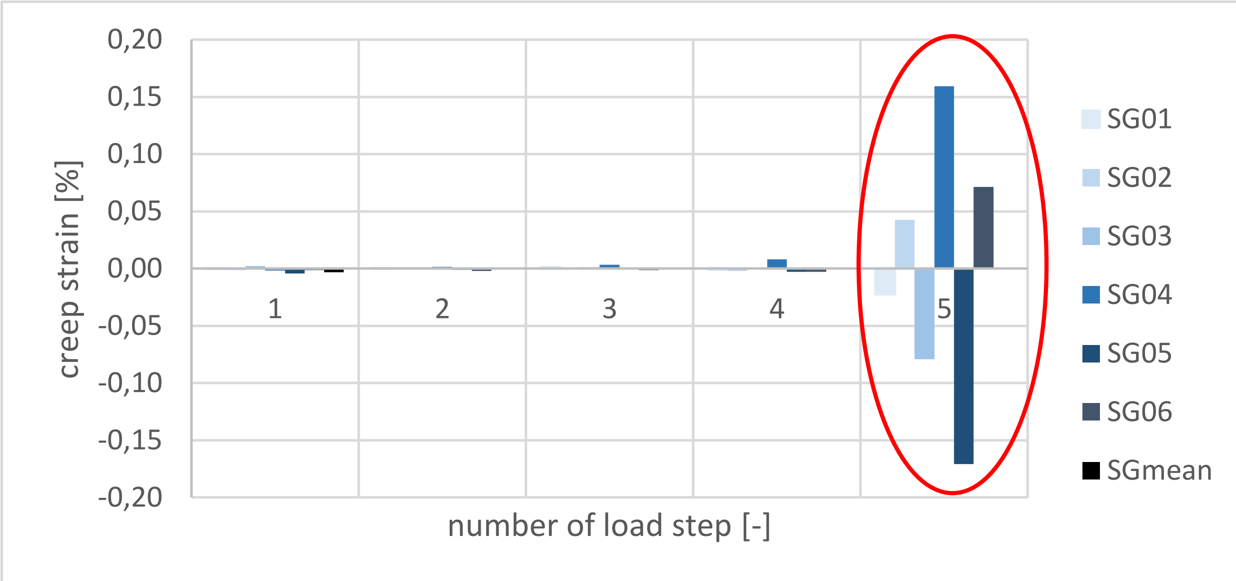

Figure I13 Comparison (Δ between start and end of load step) of creep strains between load levels

name	reference stress			step parameters	load step				
test	% GUTS	% UTS	MPa		1	2	3	4	5
CC02	60	52,1	269,8	stress level [MPa]	269,8	320,8	371,7	422,7	503,5
				step duration [hr]	5	5	5	11,3	2,7
				Δε_SG01 [%]	0,000	0,000	0,001	-0,001	-0,023
				Δε_SG02 [%]	-0,001	0,001	0,001	-0,002	0,042
				Δε_SG03[%]	0,002	0,001	0,001	-0,001	-0,079
				Δε_SG04 [%]	-0,002	0,001	0,003	0,008	0,160
				Δε_SG05 [%]	-0,004	-0,001	0,000	-0,003	-0,171
				Δε_SG06 [%]	-0,001	-0,002	-0,001	-0,003	0,071
				Δε_SGmean [%]	-0,003	0,000	0,001	0,000	0,000
				Δε_laser [%]	0,094	0,020	0,024	0,033	1,257

Table I3 Creep strains from strain gauges and laser of CC02

Elastic strains

name									
test	reference stress			jump parameters	jump				
	% GUTS	% UTS	MPa		0 to 1	1 to 2	2 to 3	3 to 4	4 to 5
CC02	60	52,1	269,8	stress increase [MPa]	269,8	51,0	51,0	51,0	80,8
				duration [sec]	24	4	5	5	7,4
				Δε_SG01 [%]	0,223	0,046	0,049	0,050	0,082
				Δε_SG02 [%]	0,200	0,045	0,047	0,048	0,080
				Δε_SG03[%]	0,212	0,046	0,048	0,048	0,075
				Δε_SG04 [%]	0,265	0,048	0,051	0,053	0,093
				Δε_SG05 [%]	0,275	0,048	0,049	0,050	0,079
				Δε_SG06[%]	0,237	0,042	0,043	0,044	0,071
				Δε_SGmean [%]	0,235	0,046	0,048	0,049	0,080
				Δε_laser [%]	0,411	0,045	0,045	0,049	0,077

Table I4 Elastic strains from strain gauges and laser of CC02

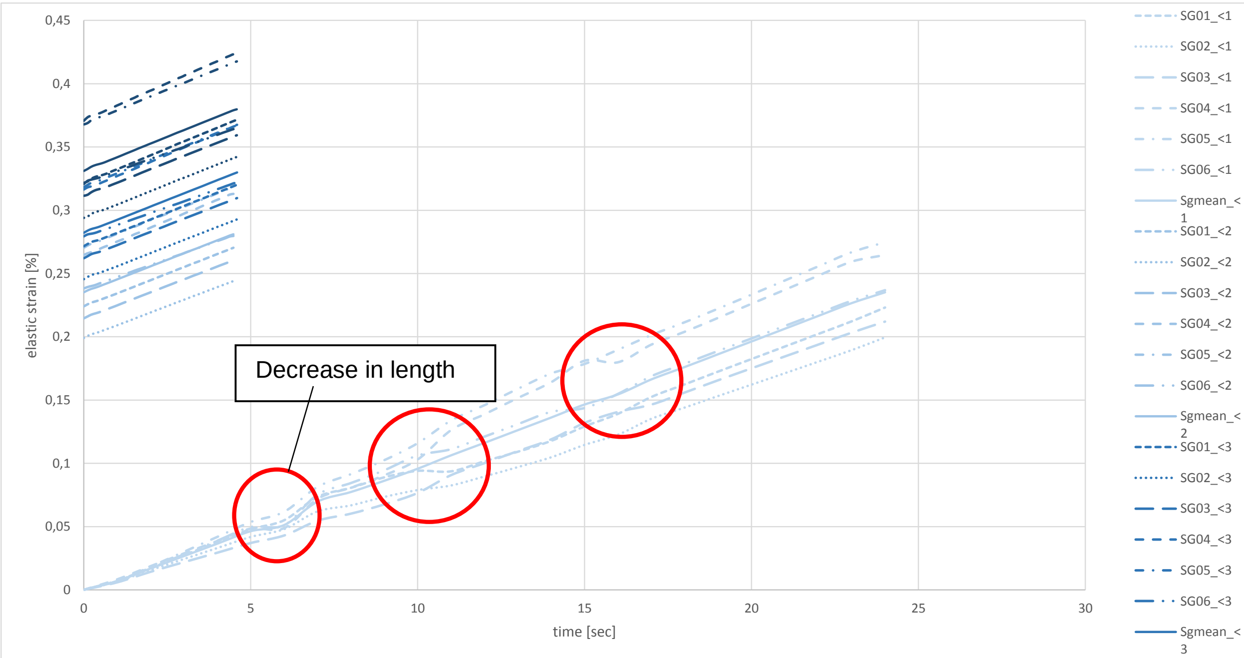

Figure I14 Comparison of elastic strains from strain gauges and laser between each increase in stress

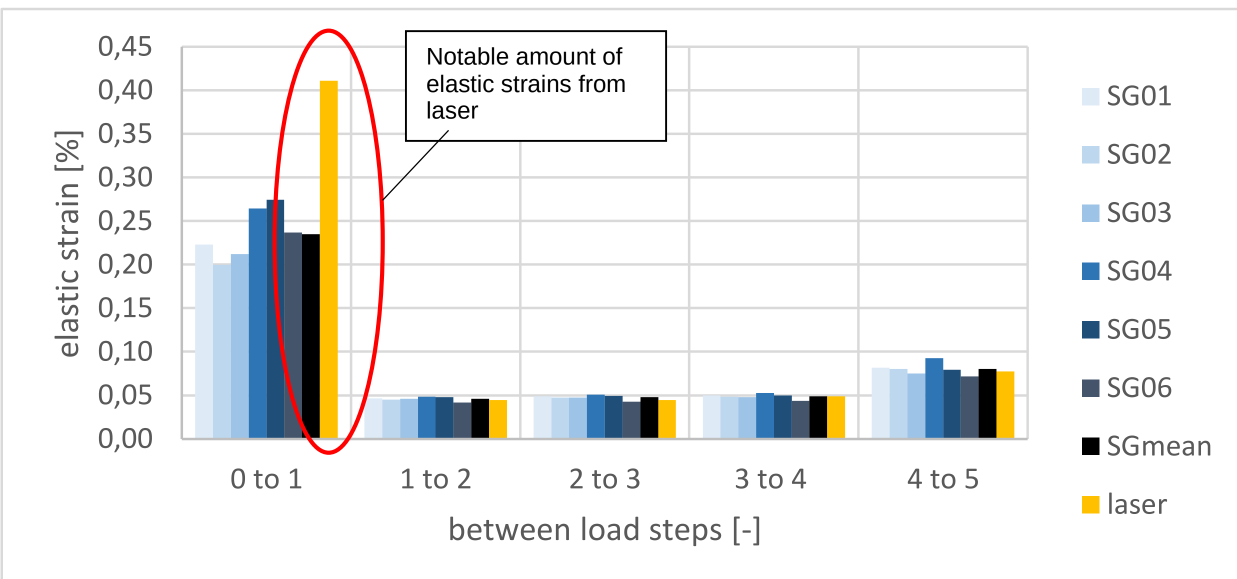

Figure I15 Comparison (Δ between start and end of load step) of elastic strains between strain gauges and laser

C. Results and observations SSM creep test CC03

- The CFRP specimen tested at a reference stress of 80% GUCS failed during the jump from the third to the fourth load step. No visible damage or deformation appeared on the free span' surface. The specimen did not rupture at mid-point, but somewhere within the cup area (see Figure I16). As a large number of points was measured in the third load step, measurements from strain gauges and laser were stopped after 3.7 hours (see Figures I17-18).

- Total strains from strain gauges and laser are presented in Figure I17. Significant more strains are measured by the laser than by the strain gauges. This may indicate creep occurred at another location than mid-point.

- The resulting strains from strain gauges are characterized by various increases and decreases in length of the specimen's surface at mid-point (see Figure I18). It is concluded that data cannot be used for further analysis using the SSM.

- Elastic strains from strain gauges are presented in Figure I19. Similar to CC01 and CC02, small decreases in length of the specimen's surface at mid-point in the first jump are obtained

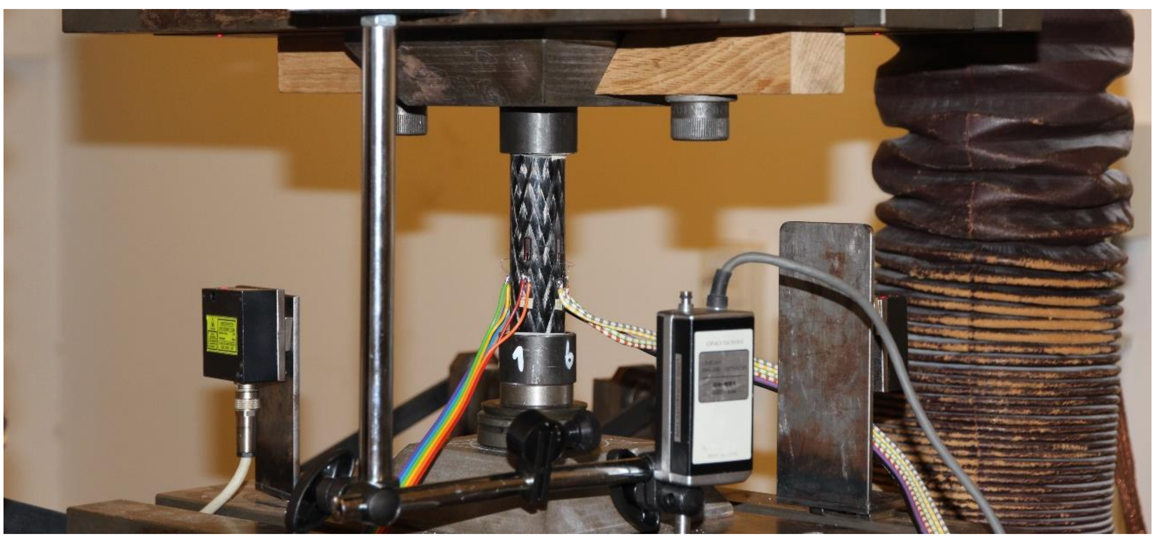

Figure I16 Compression test set-up with CFRP specimen CC03 (no visible damage or deformation appeared)

Total strains

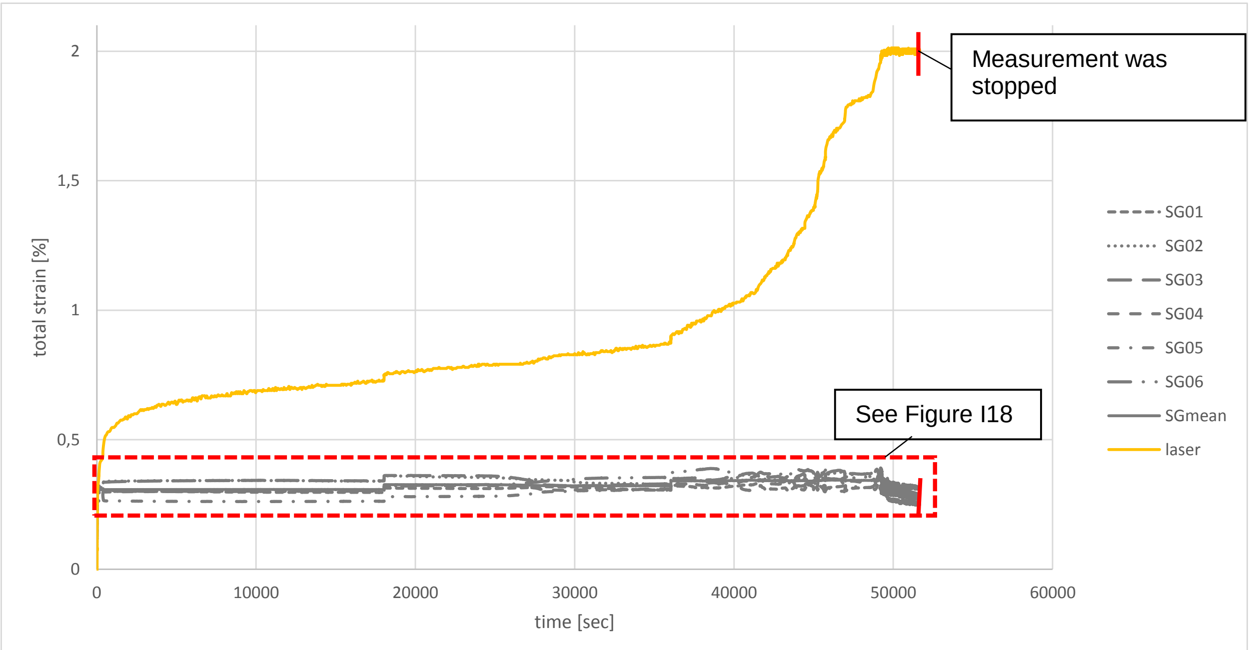

Figure I17 Total strains measured by strain gauges and laser versus time of CC03

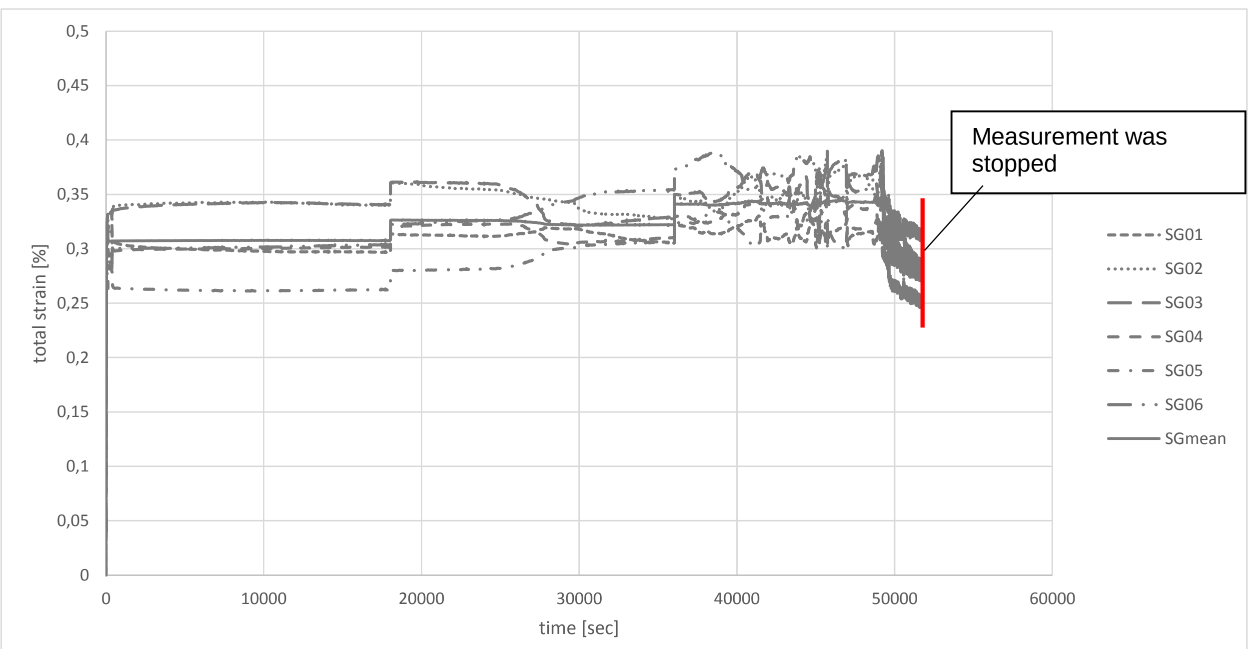

Figure I18 Strains from strain gauges versus time of CC03

Elastic strains

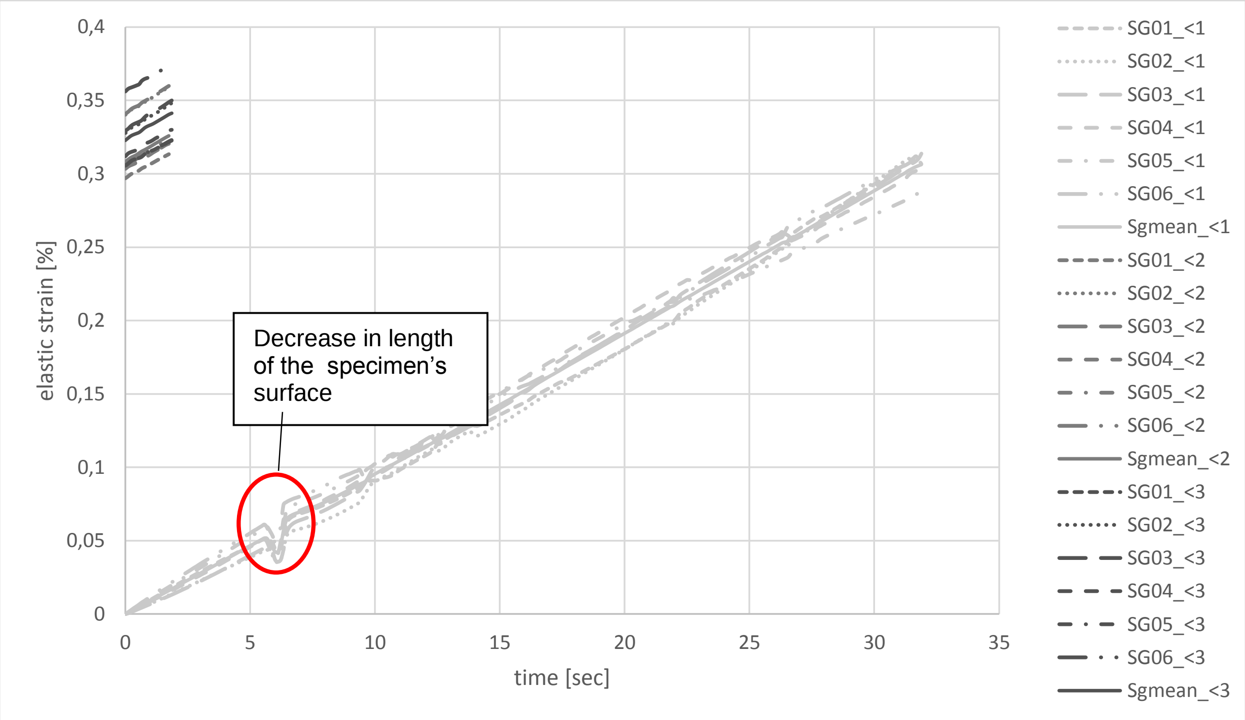

Figure I19 Elastic strains from strain gauges obtained during each increase in stress

Annex J Results and observations SSM bending creep tests FC01-03

A. Results and observations SSM creep test FC01

- The CFRP specimen tested at a reference stress of 40% GUFS ruptured after 0.3 hours in the fourth load step (see Figure J2). The specimen did not rupture precisely at the mid-point, but within the central loading span of the specimen (see Figure J1). As the stress within the central loading span is constant in a four-point bending test, no correction has to be made.

- In the SSM creep test FC01, a little too much stress was applied by the test rig during each increase in stress. Resulting imperfections in the total strain-time curves (see Figure J2) were removed from the curves. It cannot be relied on the creep strains at the beginning of each load step.

- Creep strains from strain gauges and laser of different load levels are presented in Figures J3-6 and Table J1. Figure J5 shows the brittle fracture behavior of the CFRP. At failure of the specimen, the resulting strain is characterized by a decrease in length of the specimen's top surface (strain gauge top – SGT) and an increase in length of the specimen's bottom surface (strain gauge bottom – SGB).

- In a successful test of this type, the creep strain-time curve obtained from the strain gauge on top of the specimen (SGT) is characterized by a stage of tertiary creep. For FC01 a tertiary creep stage is observed.

- Elastic strains from strain gauges and laser of different load levels are presented in Figures J7-8 and Table J2. The proportion of measured strains from the different strain gauges and laser is similar to each other in each increase in stress (see Figure J8).

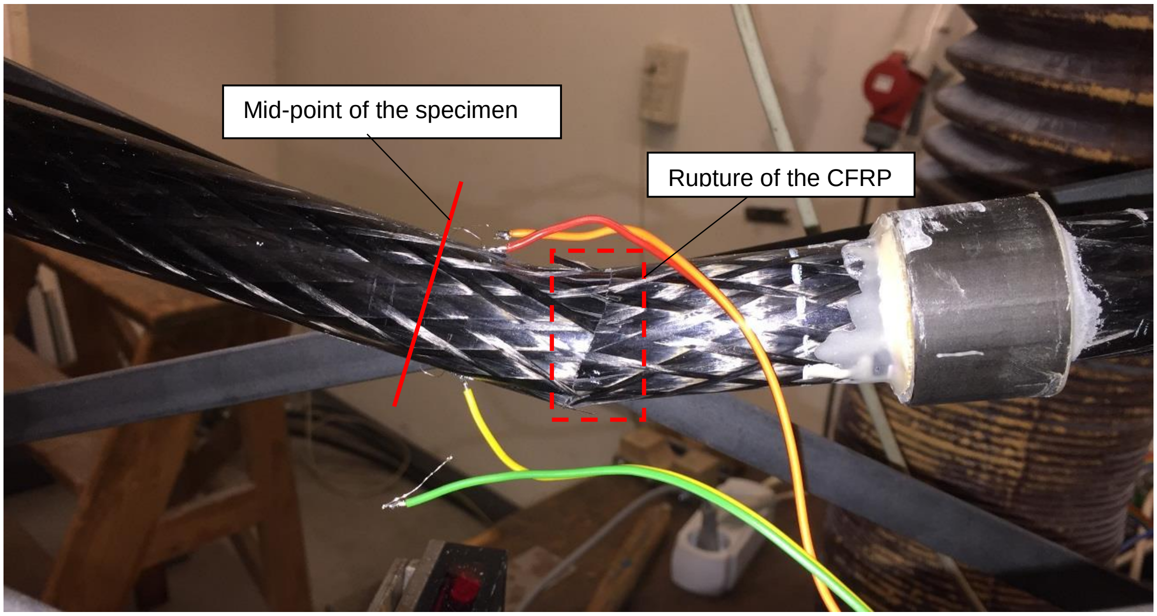

Figure J1 Rupture of CFRP specimen FC01

Total strains

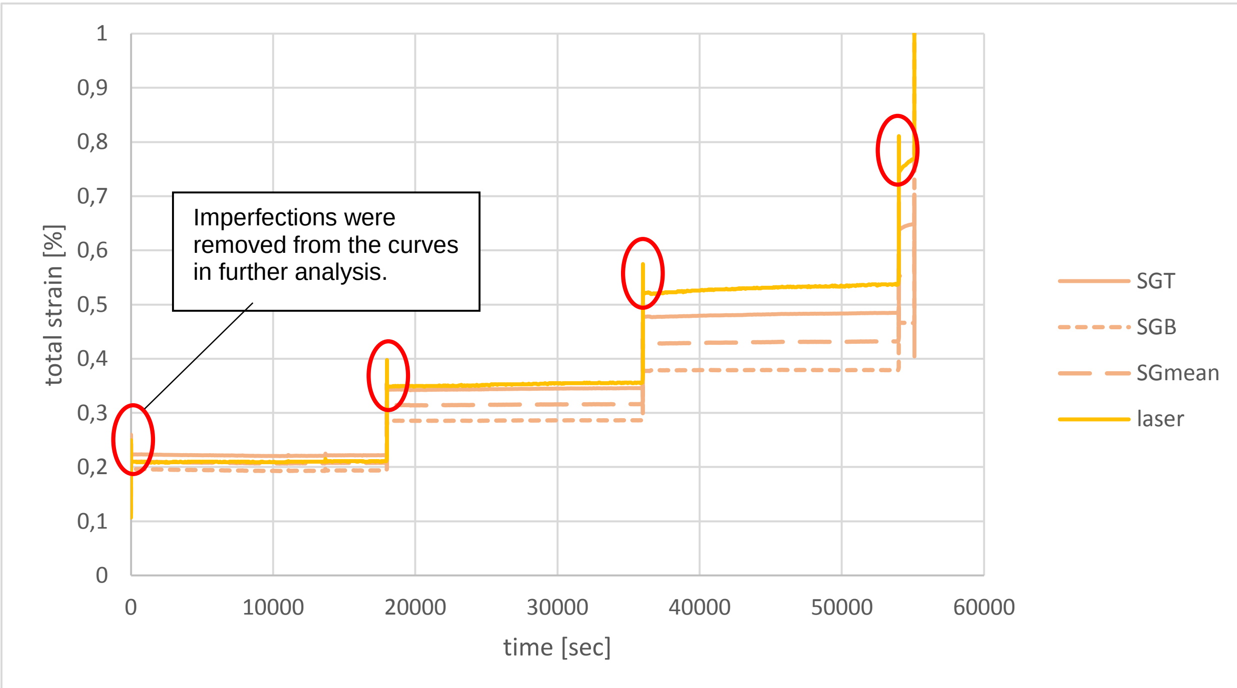

Figure J2 Total strains from strain gauges and laser versus time of FC01

Creep strains

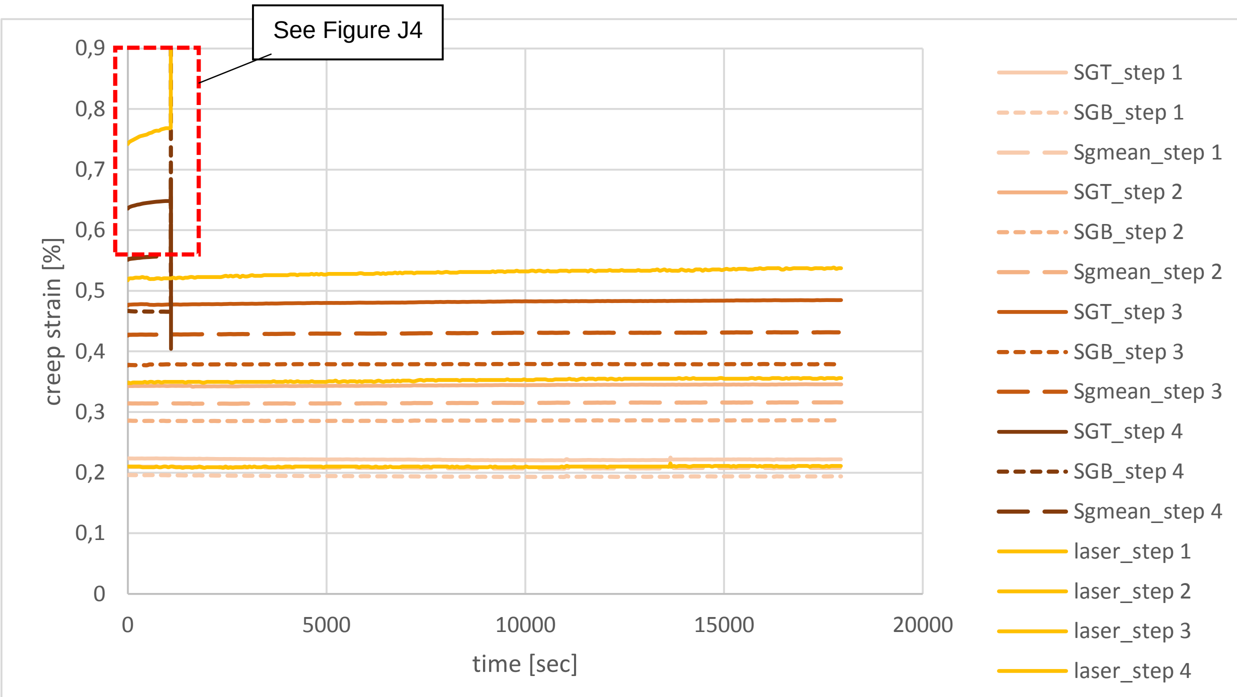

Figure J3 Comparison of creep strains from strain gauges and laser between load levels

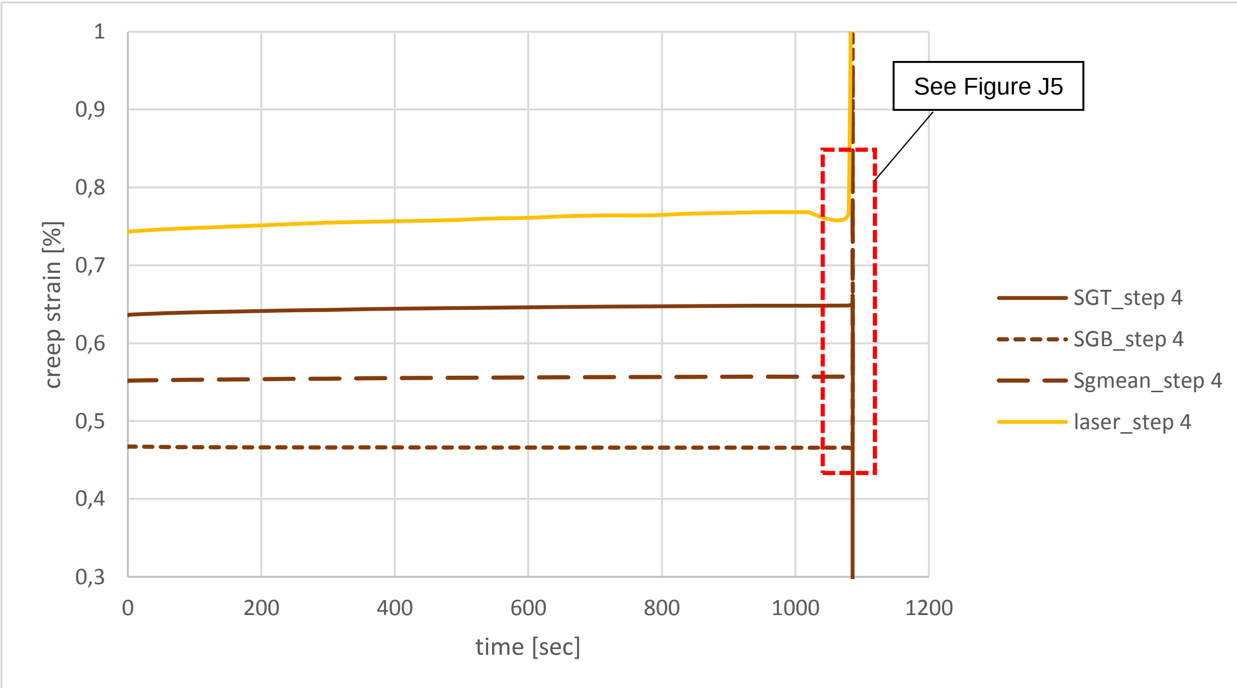

Figure J4 Creep strains from strain gauges and laser in final load level

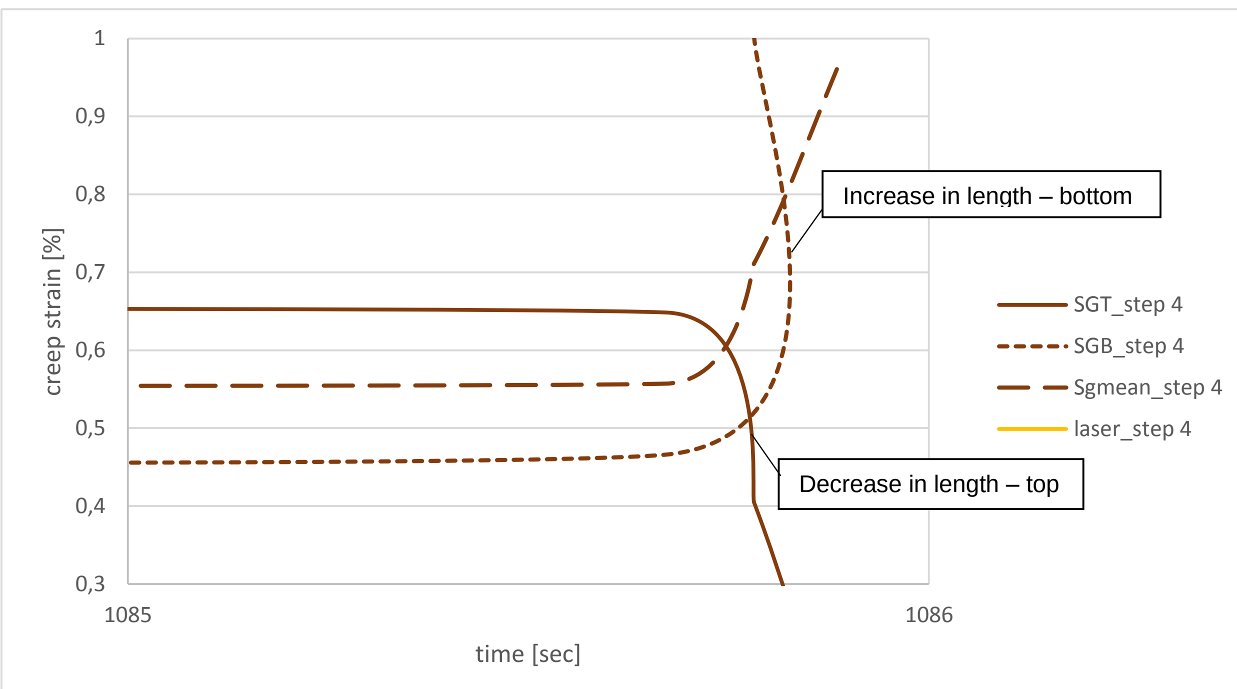

Figure J5 Creep strains from strain gauges in final load level – at rupture of the CFRP specimen

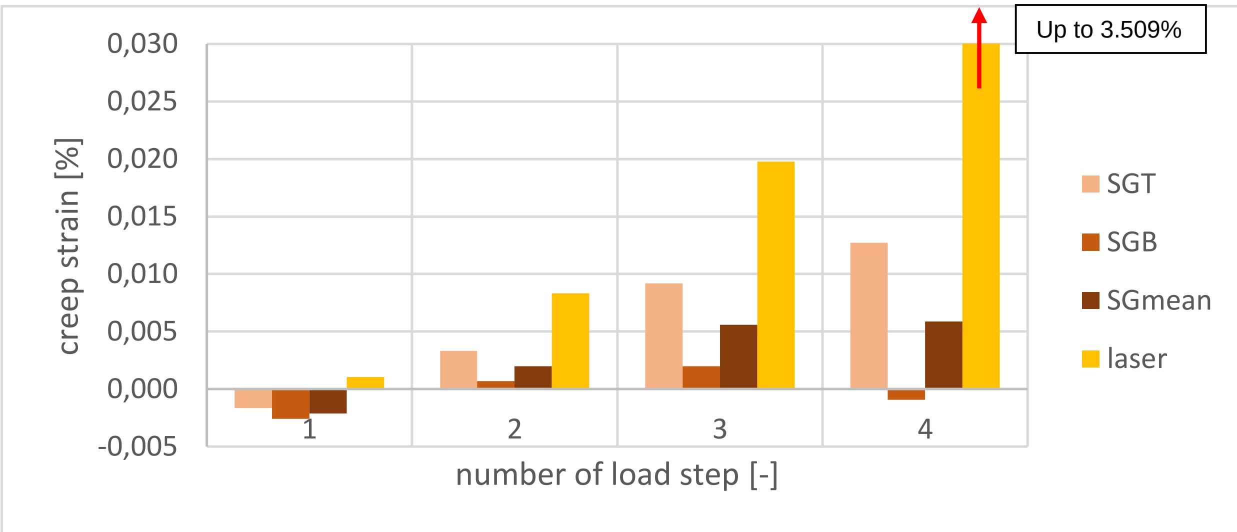

Figure J6 Comparison (Δ between start and end of load step) of creep strains between load levels

name	reference stress			step parameters	load step			
test	% GUFS	% UFS	MPa		1	2	3	4
FC01	40	37,4	236,8	stress level [MPa]	236,8	355,2	473,7	592,1
				step duration [hr]	5	5	5	0,3
				Δε_SGT [%]	-0,002	0,003	0,009	0,013
				Δε_SGB [%]	-0,003	0,001	0,002	-0,001
				Δε_SGmean [%]	-0,002	0,002	0,006	0,006
				Δε_laser [%]	0,001	0,008	0,020	3,509

Table J1 Creep strains from strain gauges and laser of FC01

Elastic strains

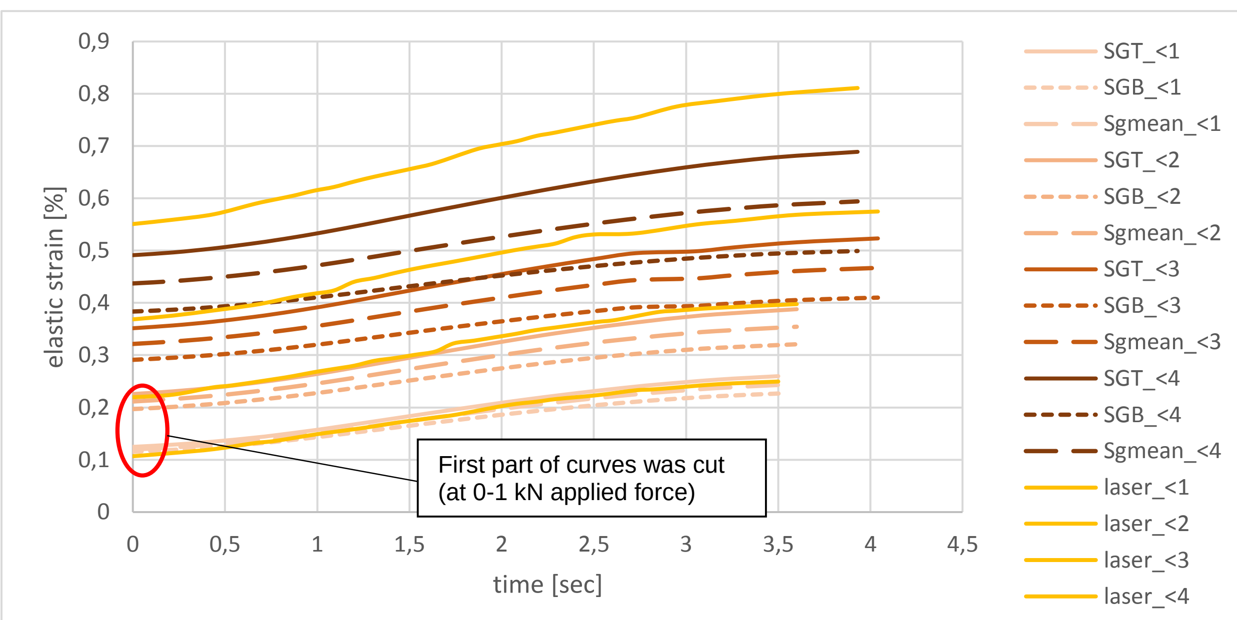

Figure J7 Comparison of elastic strains from strain gauges and laser between each increase in stress

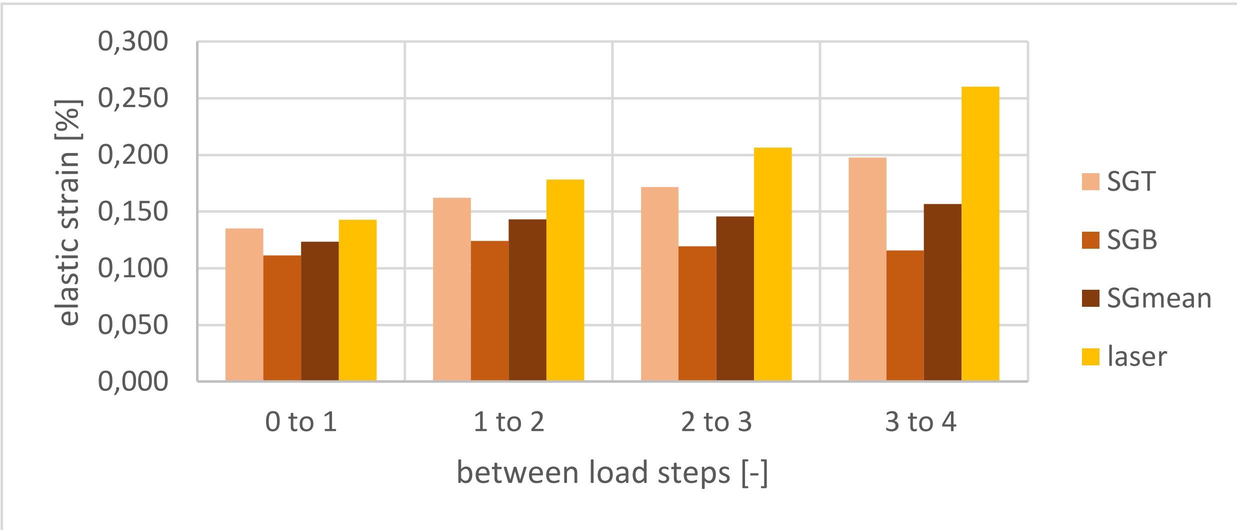

Figure J8 Comparison (Δ between start and end of load step) of elastic strains between each increase in stress

name	reference stress			**jump parameters**	**jump**			
test	% GUCS	% UCS	MPa		0 to 1	1 to 2	2 to 3	3 to 4
FC01	40	37,4	236,8	stress level [MPa]	236,8	355,2	473,7	592,1
				duration [sec]	4	4	4	4
				Δε_SGT [%]	0,135	0,162	0,172	0,198
				Δε_SGB [%]	0,111	0,124	0,119	0,116
				Δε_SGmean [%]	0,123	0,143	0,146	0,157
				Δε_laser [%]	0,143	0,178	0,206	0,260

Table J2 Elastic strains from strain gauges and laser of FC01

B. Results and observations SSM creep test FC02

- The CFRP specimen tested at a reference stress of 60% GUFS ruptured during the jump from the third to the fourth load level (see Figure J10). The specimen did rupture precisely at the mid-point – at the positions of the strain gauges (see Figure J9).

- Creep strains from strain gauges and laser of different load levels are presented in Figures J11-12 and Table J3. Figure J12 presents a comparison (Δ between start and end of load step) of creep strains between load levels. A positive difference was measured by the strain gauge on top of the specimen (SGT), in contrast to a negative difference measured by the strain gauge at the bottom side (SGB).

- In a successful test of this type, the creep strain-time curve obtained from the strain gauge on top of the specimen (SGT) is characterized by a stage of tertiary creep. As the specimen ruptured during the jump from the third to the fourth load level, no stage of tertiary creep is observed in Figure J10.

- Elastic strains from strain gauges and laser of different load levels are presented in Figures J13-15 and Table J4. The proportion of measured strains from the different strain gauges and laser in similar to each other in each increase in stress (see Figure J15). Figure J14 shows brittle fracture of the CFRP.

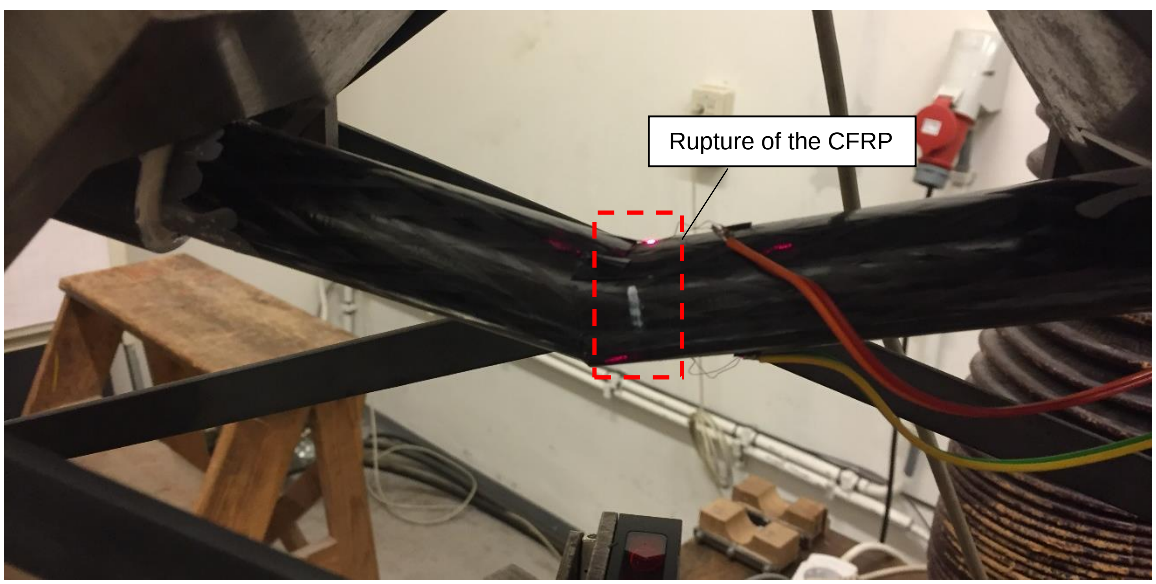

Figure J9 Rupture of CFRP specimen FC02

Total strains

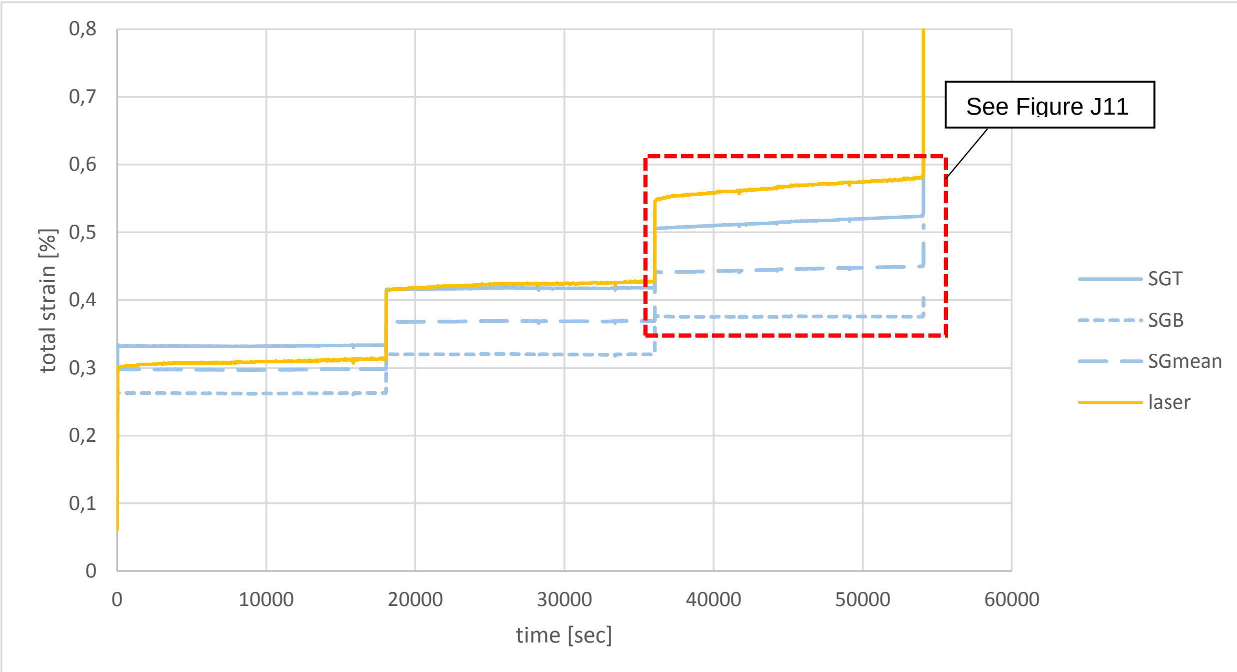

Figure J10 Total strains from strain gauges and laser versus time of FC02

Creep strains

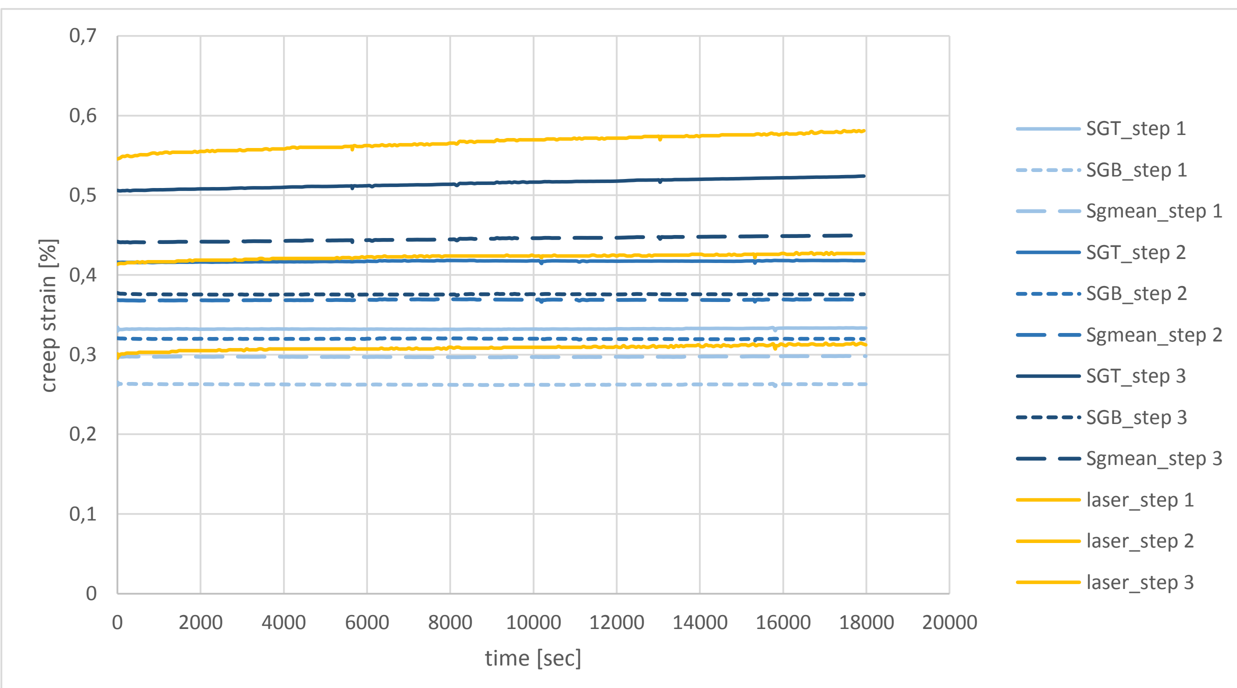

Figure J11 Comparison of creep strains from strain gauges and laser between load levels

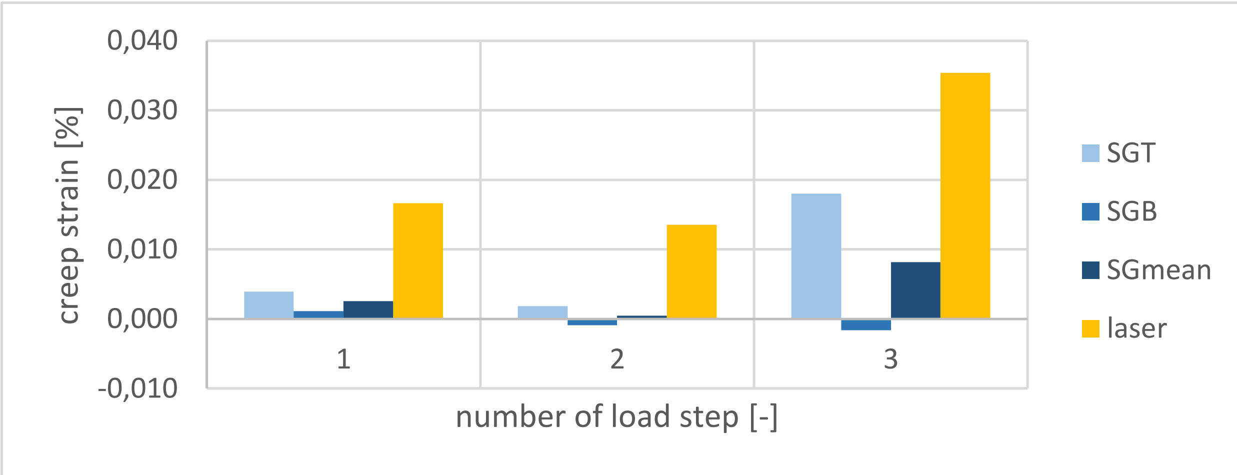

Figure J12 Comparison (Δ between start and end of load step) of creep strains between load levels

name	reference stress			step parameters	load step			
test	% GUFS	% UFS	MPa		1	2	3	4
FC02	60	56,2	355,2	stress level [MPa]	355,2	434,2	513,1	592,1
				step duration [hr]	5	5	5	-
				Δε_SGT [%]	0,004	0,002	0,018	-
				Δε_SGB [%]	0,001	-0,001	-0,002	-
				Δε_SGmean [%]	0,003	0,000	0,008	-
				Δε_laser [%]	0,017	0,014	0,035	-

Table J3 Creep strains from strain gauges and laser of FC02

Elastic strains

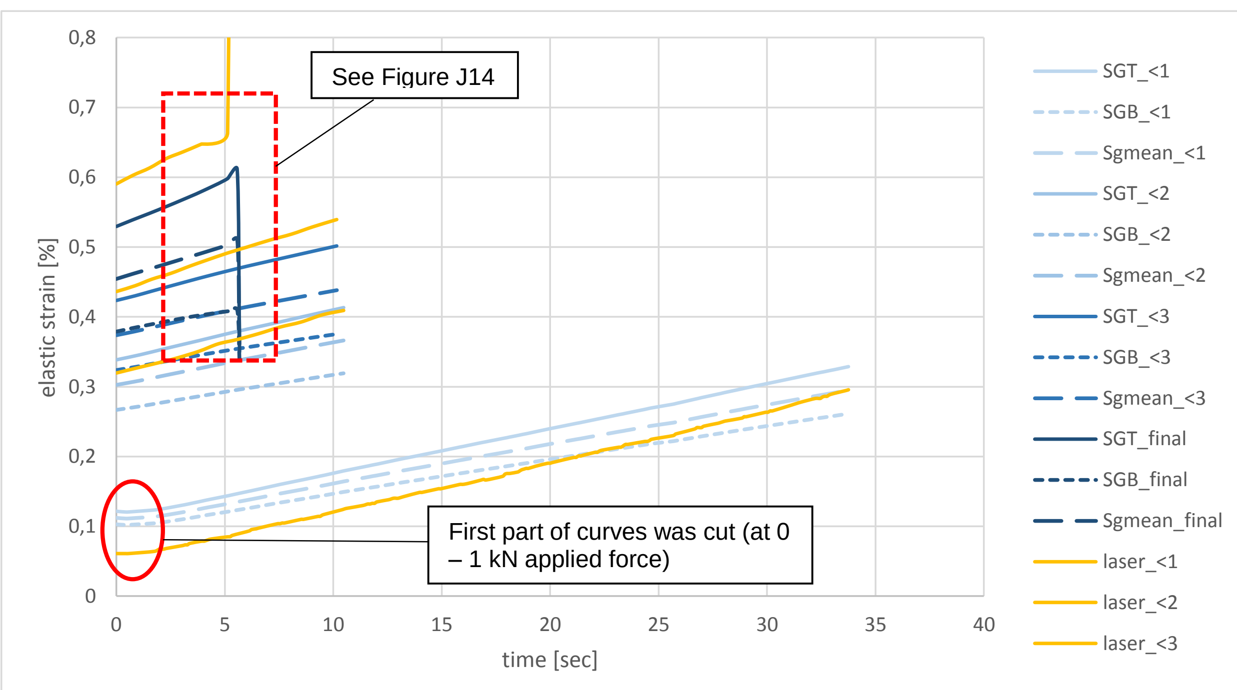

Figure J13 Comparison of elastic strains from strain gauges and laser between each increase in stress

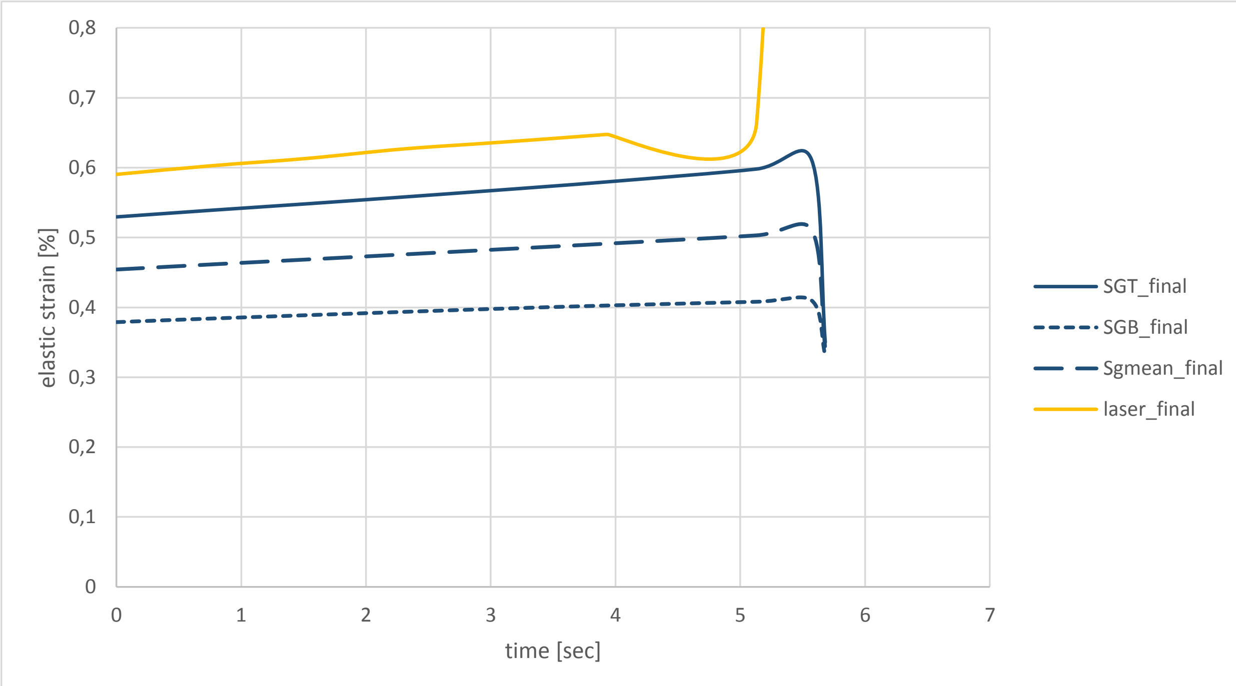

Figure J14 Elastic strains from strain gauges and laser during jump from the third to the fourth load level – at rupture of the CFRP specimen

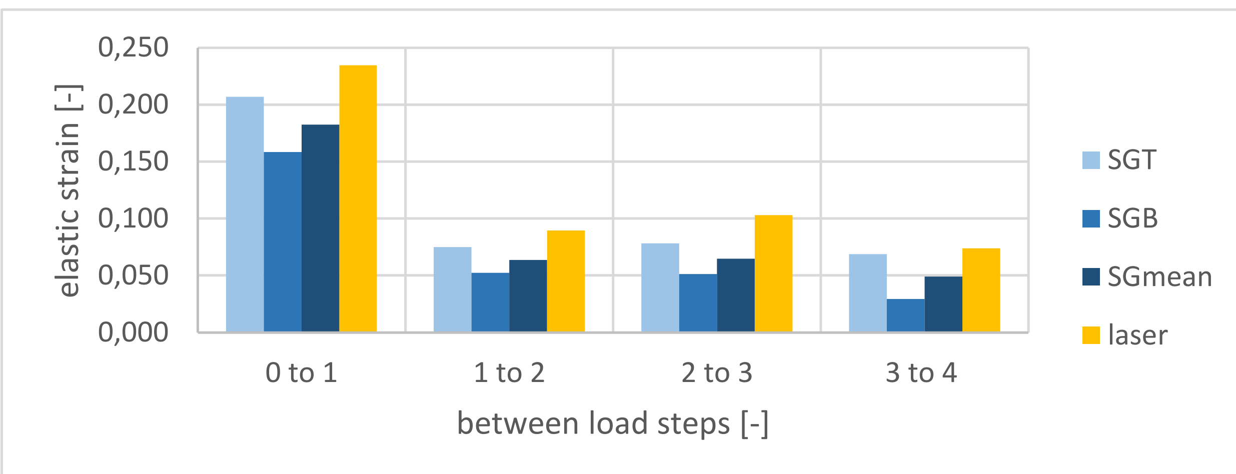

Figure J15 Comparison (Δ between start and end of load step) of elastic strains between each increase in stress

name	reference stress			jump parameters	jump			
test	% GUFS	% UFS	MPa		0 to 1	1 to 2	2 to 3	3 to 4
FC02	60	56,2	355,2	stress level [MPa]	355,2	78,9	78,9	78,9
				duration [sec]	3	10	10	5
				Δε_SGT [%]	0,207	0,075	0,078	0,069
				Δε_SGB [%]	0,158	0,052	0,051	0,029
				Δε_SGmean [%]	0,183	0,064	0,065	0,049
				Δε_laser [%]	0,235	0,090	0,103	0,074

Table J4 Elastic strains from strain gauges and laser of FC02

C. Results and observations SSM creep test FC03

- The CFRP specimen tested at a reference stress of 40% GUFS ruptured after 3.4 hours in the fourth load level (see Figure J17). The specimen did rupture precisely at the mid-point – at the positions of the strain gauges (see Figure 16).

- Creep strains from strain gauges and laser of different load levels are presented in Figures J18-21 and Table J5. From Figure J20 can be seen that the initiation of fracture occurred at the top surface of the specimen, following the rupture of the CFRP. The creep strain-time curve obtained from the strain gauge at the specimen's top surface is characterized by a stage of tertiary creep.

- Elastic strains from strain gauges and laser of different load levels are presented in Figures J22-23 and Table J6. The proportion of measured strains from the different strain gauges and laser is similar to each other in each increase in stress (see Figure J23).

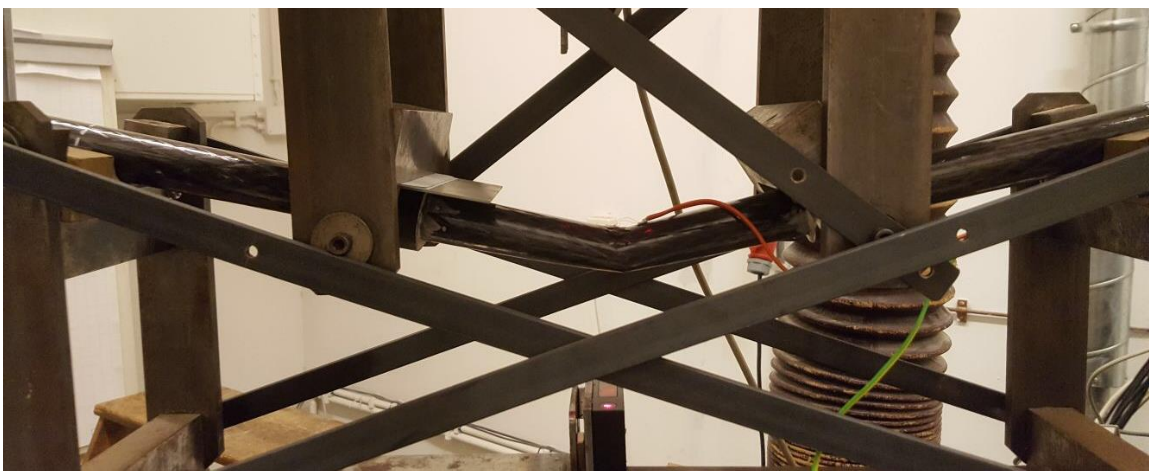

Figure J16 Rupture of CFRP specimen FC03

Total strains

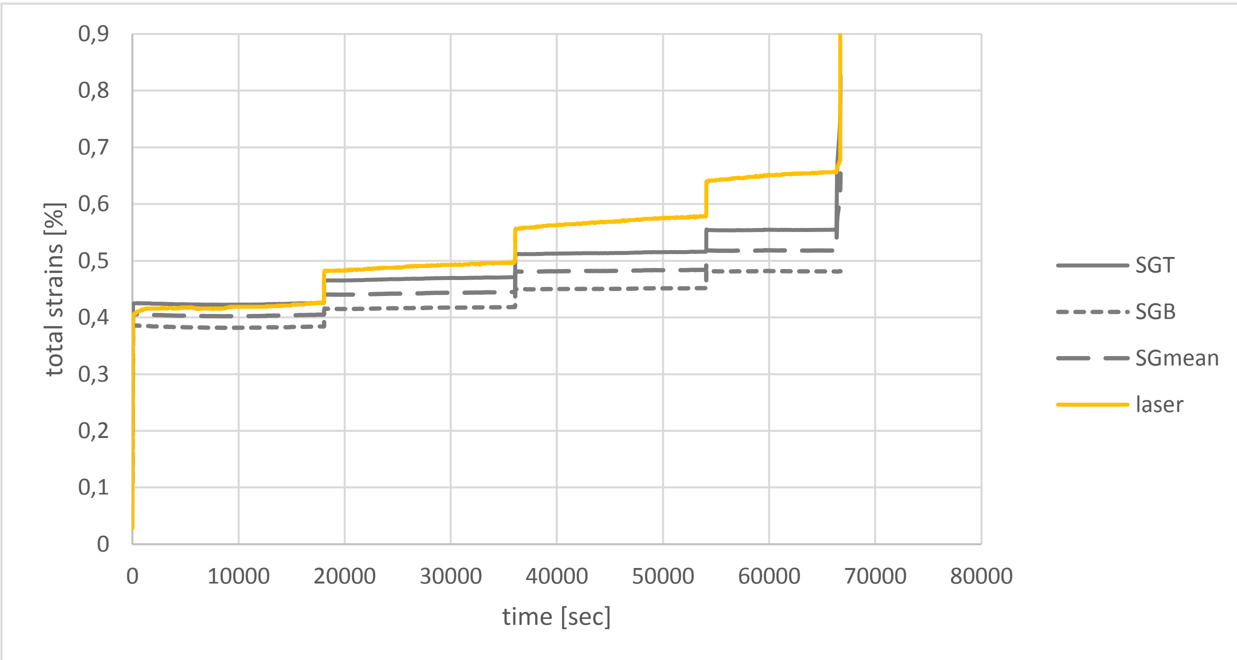

Figure J17 Total strains from strain gauges and laser versus time of FC03

Creep strains

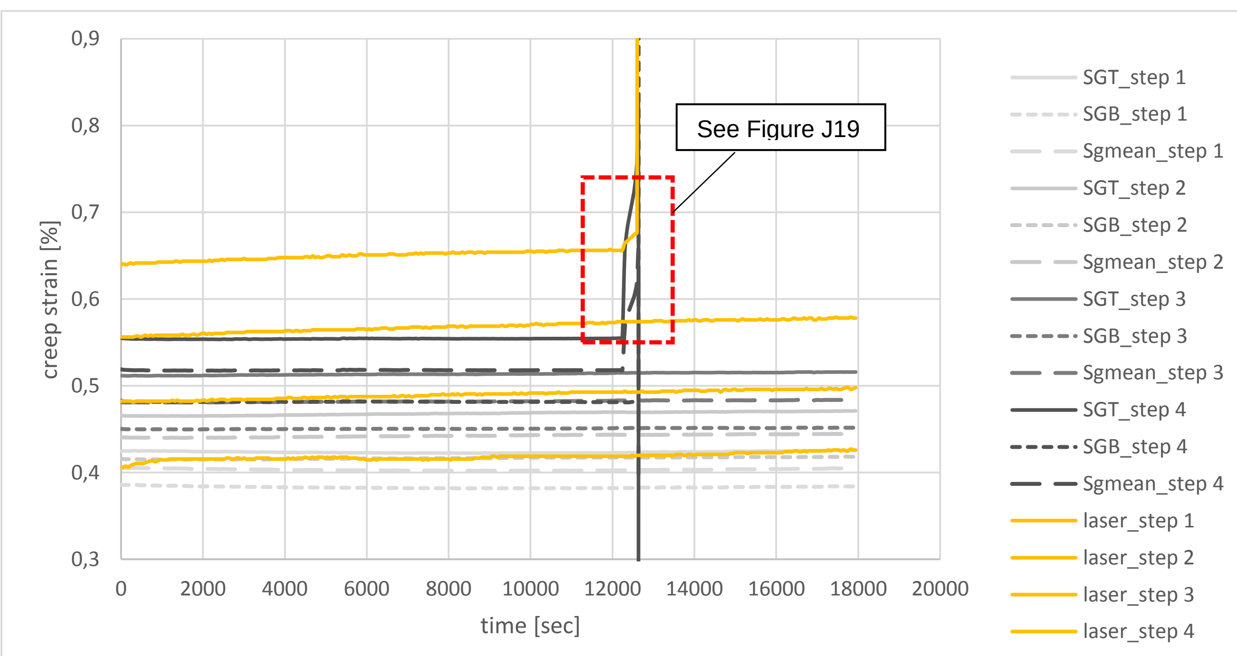

Figure J18 Comparison of creep strains from strain gauges and laser between load levels

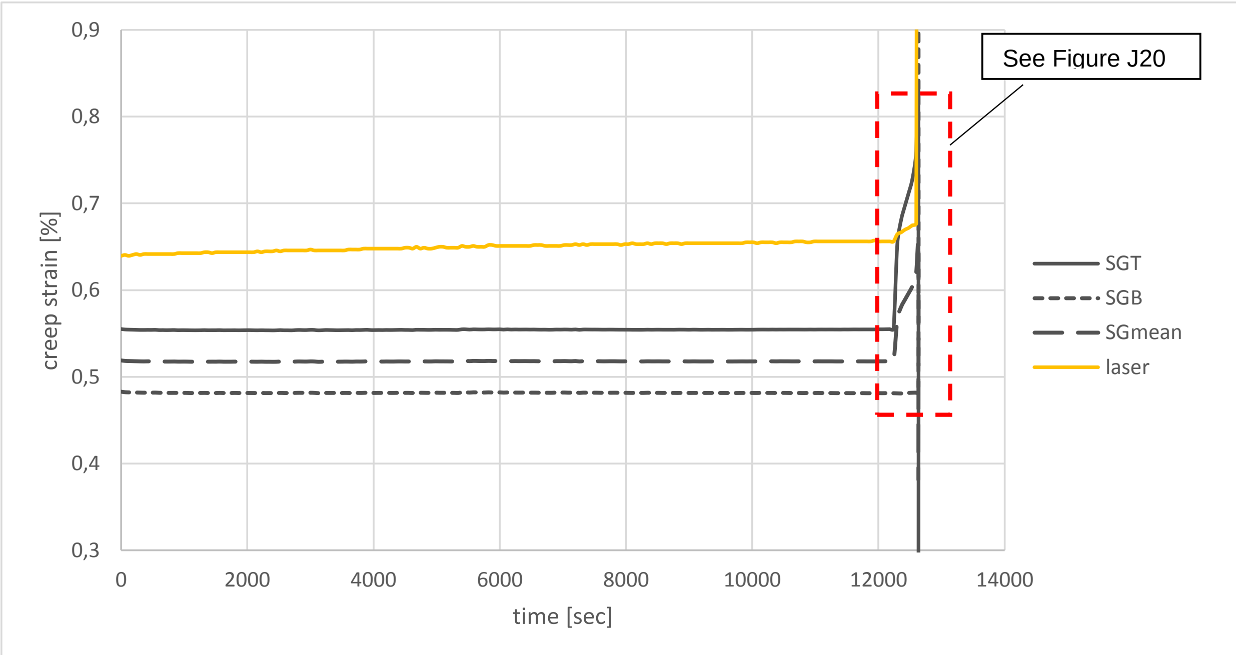

Figure J19 Creep strains from strain gauges and laser in final load level

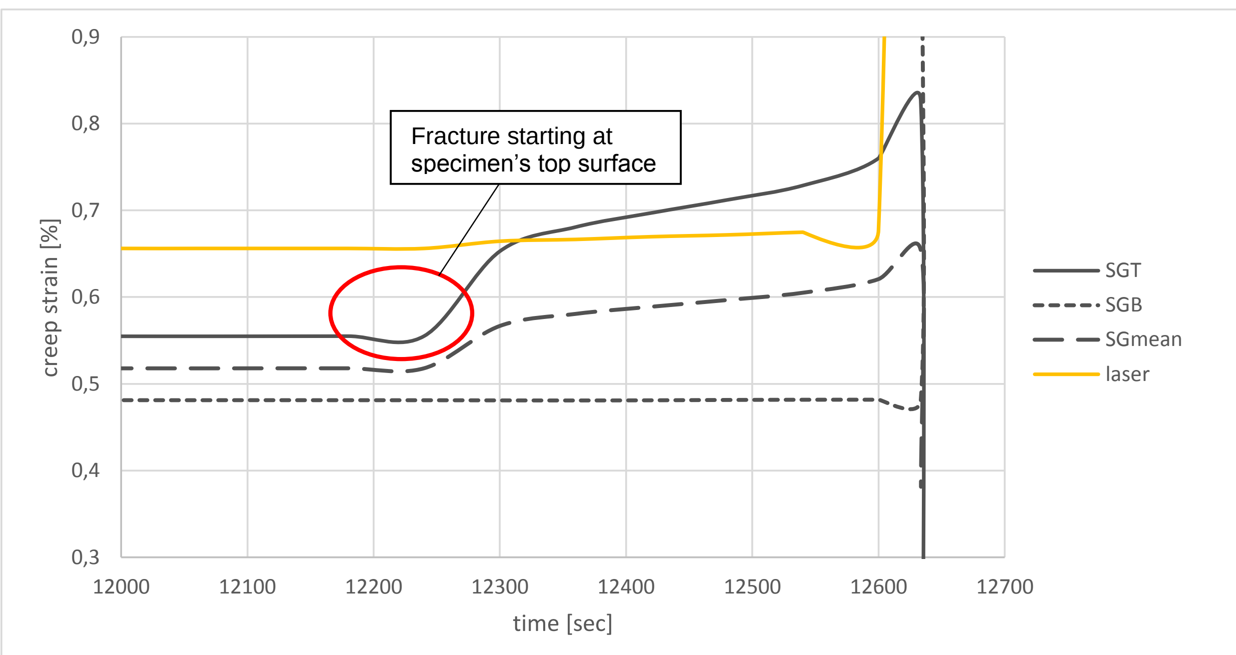

Figure J20 Creep strains from strain gauges and laser in final load level – at rupture of the CFRP specimen

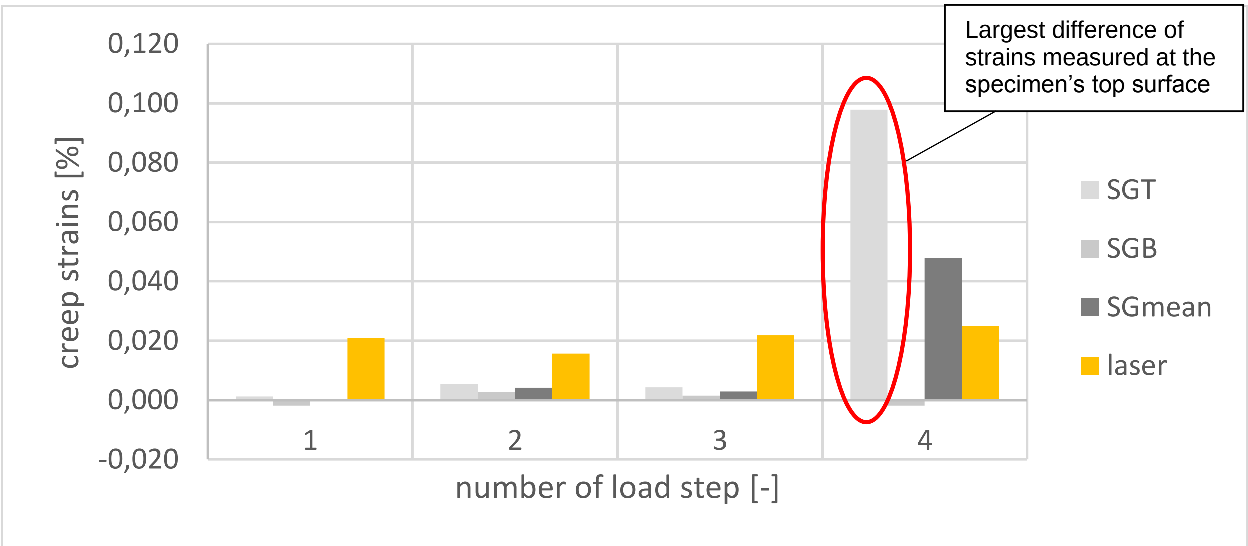

Figure J21 Comparison (Δ between start and end of load step) of creep strains between load levels

name	reference stress			**step parameters**	**load step**			
test	% GUFS	% UFS	MPa		1	2	3	4
FC03	80	74,9	473,7	stress level [MPa]	473,7	513,1	552,6	592,1
				step duration [hr]	5	5	5	3,4
				Δε_SGT [%]	0,001	0,005	0,004	0,098
				Δε_SGB [%]	-0,002	0,003	0,001	-0,002
				Δε_SGmean [%]	0,000	0,004	0,003	0,048
				Δε_laser [%]	0,021	0,016	0,022	0,025

Table J5 Creep strains from strain gauges and laser of FC03

Elastic strains

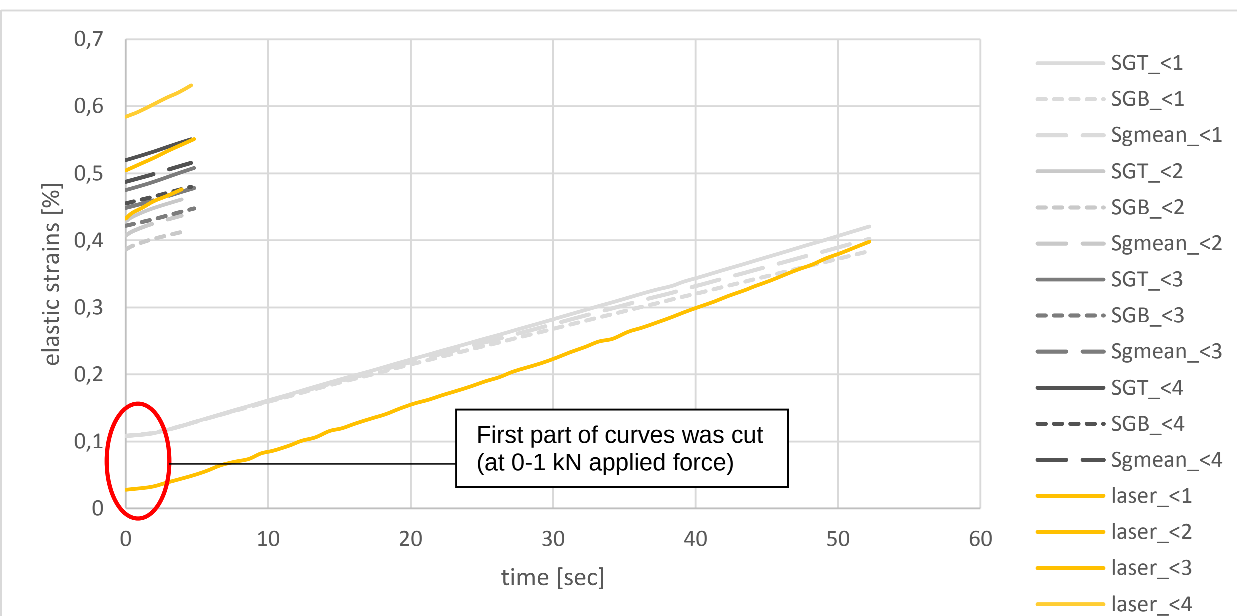

Figure J22 Comparison of elastic strains from strain gauges and laser between each increase in stress

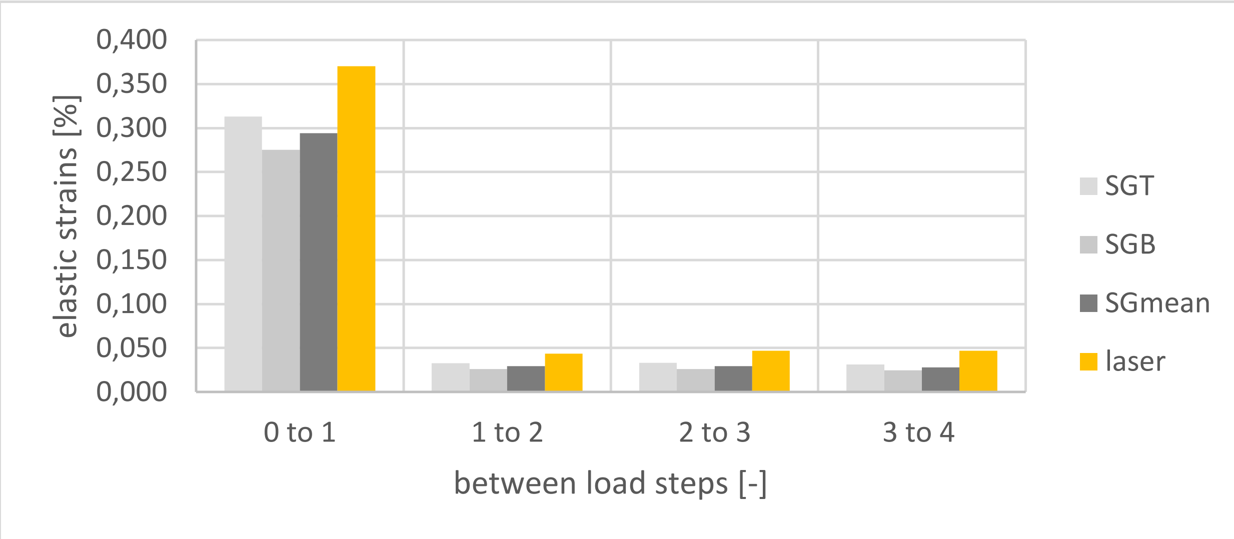

Figure J23 Comparison (Δ between start and end of load step) of elastic strains between each increase in stress

name	reference stress			jump parameters	jump			
test	% GUFS	% UFS	MPa		0 to 1	1 to 2	2 to 3	3 to 4
FC03	80	74,9	473,7	stress level [MPa]	473,7	513,1	552,6	592,1
				duration [sec]	52	4	5	5
				Δε_SGT [%]	0,313	0,033	0,033	0,031
				Δε_SGB [%]	0,275	0,026	0,026	0,025
				Δε_SGmean [%]	0,294	0,029	0,029	0,028
				Δε_laser [%]	0,370	0,044	0,047	0,047

Table J6 Elastic strains from strain gauges and laser of FC03

Annex K Mechanical scheme and preliminary calculations bending (corresponding to Chapter 8)

Mechanical scheme

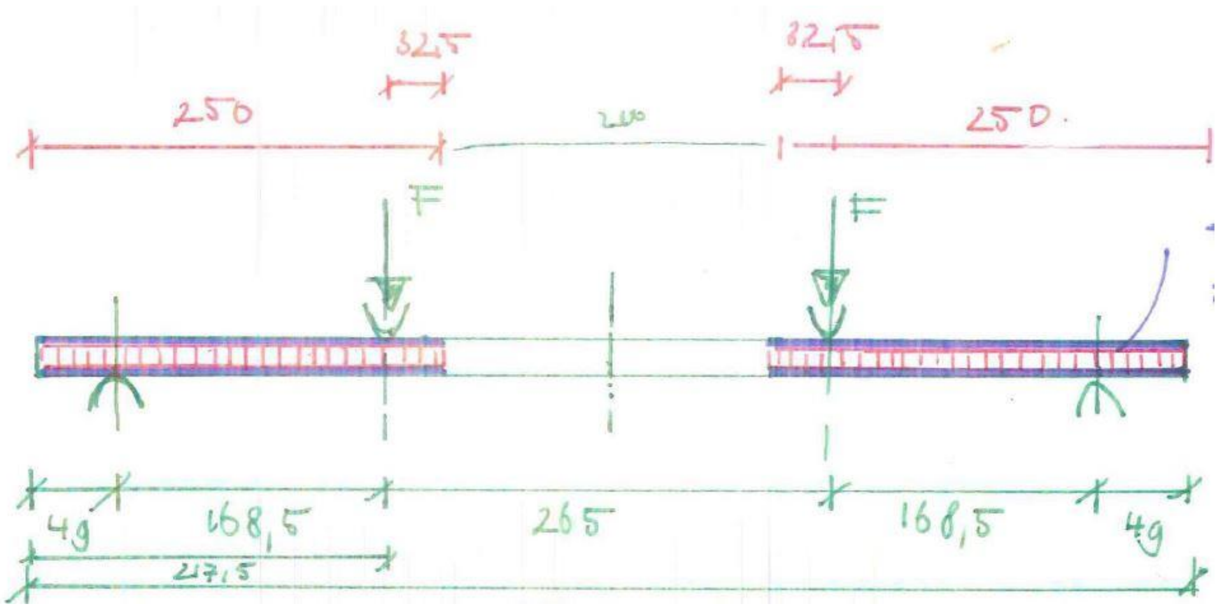

Figure K1 Mechanical scheme bending tests

Preliminary calculations bending testing

Preliminary calculations were made with the purpose of predicting the average ultimate bending force ($F_{B.ult}$), deflection at mid-span ($\delta_{B.ult}$), and strains ($\varepsilon_{B.ult}$), that would result from preliminary bending tests. It was expected that the specimens loaded in bending would show compression failure. Therefore the average ultimate compression strength (σ_{C}.ult) and elastic modulus (E_C) obtained from preliminary compression tests were used in the preliminary calculations corresponding to the bending tests.

The elastic bending moment is calculated from:

$$M_{el} = W_{el} \times \sigma_{C.ult} \quad (43)$$

where:

M_{el}	**elastic bending moment**	**0.33 kNm**
W_{el}	elastic section modulus	639 mm^3
$\sigma_{c.ult}$	compression strength	518 MPa

The ultimate bending moment is calculated from:

$$M_{ult} = M_{el} \times C \quad (44)$$

where:

M_{ult}	**ultimate bending moment**	**0.43 kNm**
M_{el}	elastic bending moment	0.33 kNm

C	factor approximation	1.3

The ultimate bending force is calculated from:

$$F_{B.ult} = \frac{2\ M_{ult}}{½(L - a)} \tag{45}$$

where:

$F_{B.ult}$	**ultimate bending force**	**5.1 kN**
M_{ult}	ultimate bending moment	0.43 kNm
L	span	602 mm
a	distance between the load introduction points	265 mm

The ultimate deflection is calculated from:

$$\delta_{ULT} = \frac{F_{B.ult}\ L^2\ b\left(3 - 4\frac{b^2}{L^2}\right)}{48\ E_C I} \tag{46}$$

where:

$\delta_{B.ult}$	**ultimate deflection**	**15.5 mm**
$F_{B.ult}$	ultimate bending force	5.1 kN
L	span	602 mm
b	distance from support to load introduction point	168.5 mm
$E_C I$	bending stiffness	1122863255 Nmm^2

The ultimate strain is calculated from:

$$\varepsilon_{B.ult} = \frac{M_{ult}\ y}{E_c I} \times 100 \tag{47}$$

where:

$\varepsilon_{B.ult}$	**ultimate strain**	**0.57 %**
M_{ult}	ultimate bending moment	0.43 kNm
y	outer radius of specimen	15 mm
$E_C I$	bending stiffness	1122863255 Nmm^2

Laser I measuring downwards to the top of the specimens was used to calculate strains. From the measured deflections, the radius of curvature of the specimens was calculated, followed by the strains. The calculated strains were compared to the measurements from strain gauges. The radius of curvature is calculated from:

$$R = \left(\frac{\delta_{(x=½L)}}{2}\right) + \left(\frac{a^2}{8\ \delta_{(x=½L)}}\right) \tag{48}$$

where:

R	**radius of curvature**
$\delta_{(x=½L)}$	measured deflection

Accompanying strains are calculated from:

$$\varepsilon_{laser\ I} = \frac{y}{R} \tag{49}$$

where:
$\varepsilon_{laser\ I}$ **calculated strains from laser I**
y outer radius of specimen
R radius of curvature

Laser II measuring upwards to the bottom of the specimen was used for measurement of the total deflection of the specimen and to calculate the modulus of elasticity. The bending moment is calculated from:

$$M = F \times ½\, b \tag{50}$$

where:
M **calculated bending moment**
F applied load
b distance from support to load introduction point

The bending strength equal to the stress in the outer layer of the specimen is calculated from:

$$\sigma_B = \frac{M\, y}{I} \tag{51}$$

where:
σ_B **bending strength**
M calculated bending moment
Y outer radius of specimen
I moment of inertia

The bending stiffness is calculated from:

$$EI = \frac{F}{\delta_{(x=½L)}} \frac{L^2\, b\, \left(3 - 4\, \frac{b^2}{L^2}\right)}{48} \tag{52}$$

where:
EI bending stiffness
F applied load
$\delta_{(x=½L)}$ measured deflection
L span
b distance from support to load introduction point

Annex L Final creep curves for CFRP specimens with the projected start time from the curve-fit at t=0 (corresponding to Section 8.4)

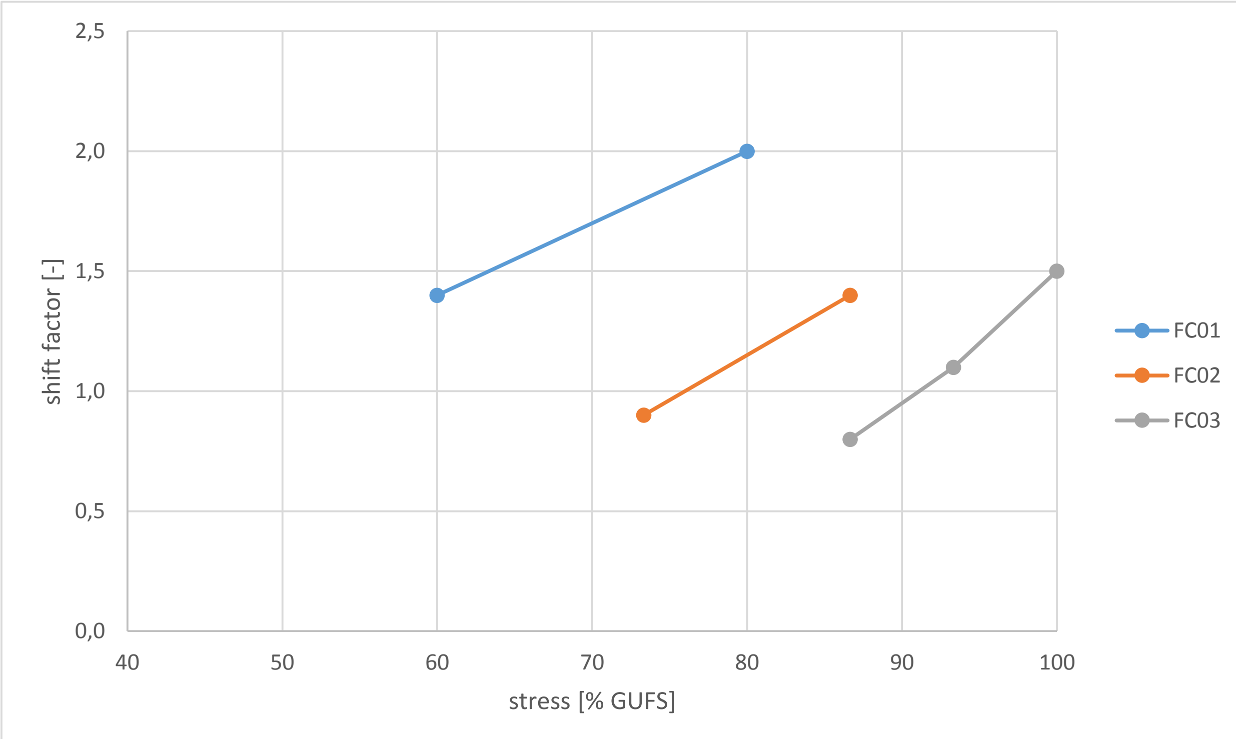

Figure L1 Shift factors versus stress levels of FC01-03 – projected start time from the curve fit at t=0

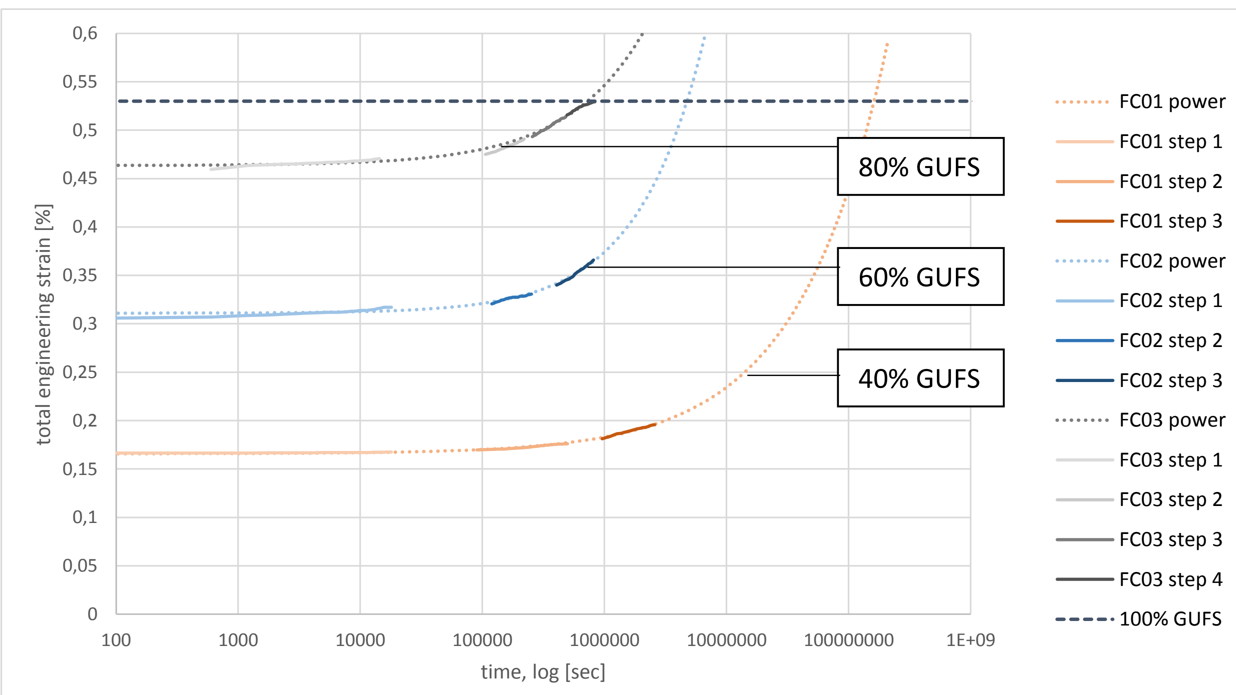

Figure L2 Final creep curves of CFRP specimens at 40%, 60%, and 80% GUFS – projected start time from the curve fit at t=0

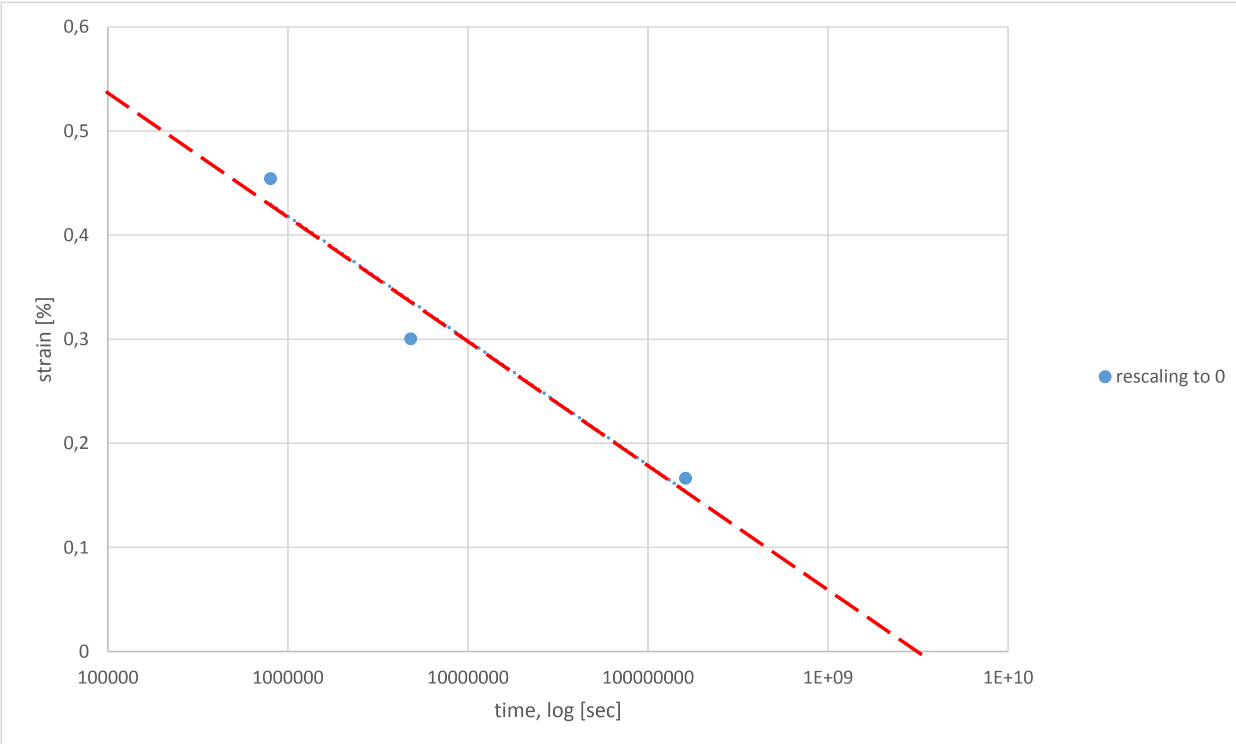

Figure L3 Creep-rupture time for reference strains – projected start time from the curve fit at t=0